Injectable calcium phosphate-based bone replacement cements

Injizierbare calciumphosphat-basierte Knochenersatzzemente

Doctoral thesis for a doctoral degree

at the Graduate School of Life Sciences,

Julius-Maximilians-Universität Würzburg,

Section: Biomedicine

Submitted by

Jan Lukas Weichhold

From Fürth

"Science is not about big words. It's not about lab coats and safety goggles, and it's definitely not about trying to make yourself sound fancy. Science is not an end in itself, but a path. It's a method to help you discover the underlying order of the world around you and to use those discoveries to help you predict how things will behave in the future."

— J. Kenji López-Alt,
scientist, cook, author, inspiration

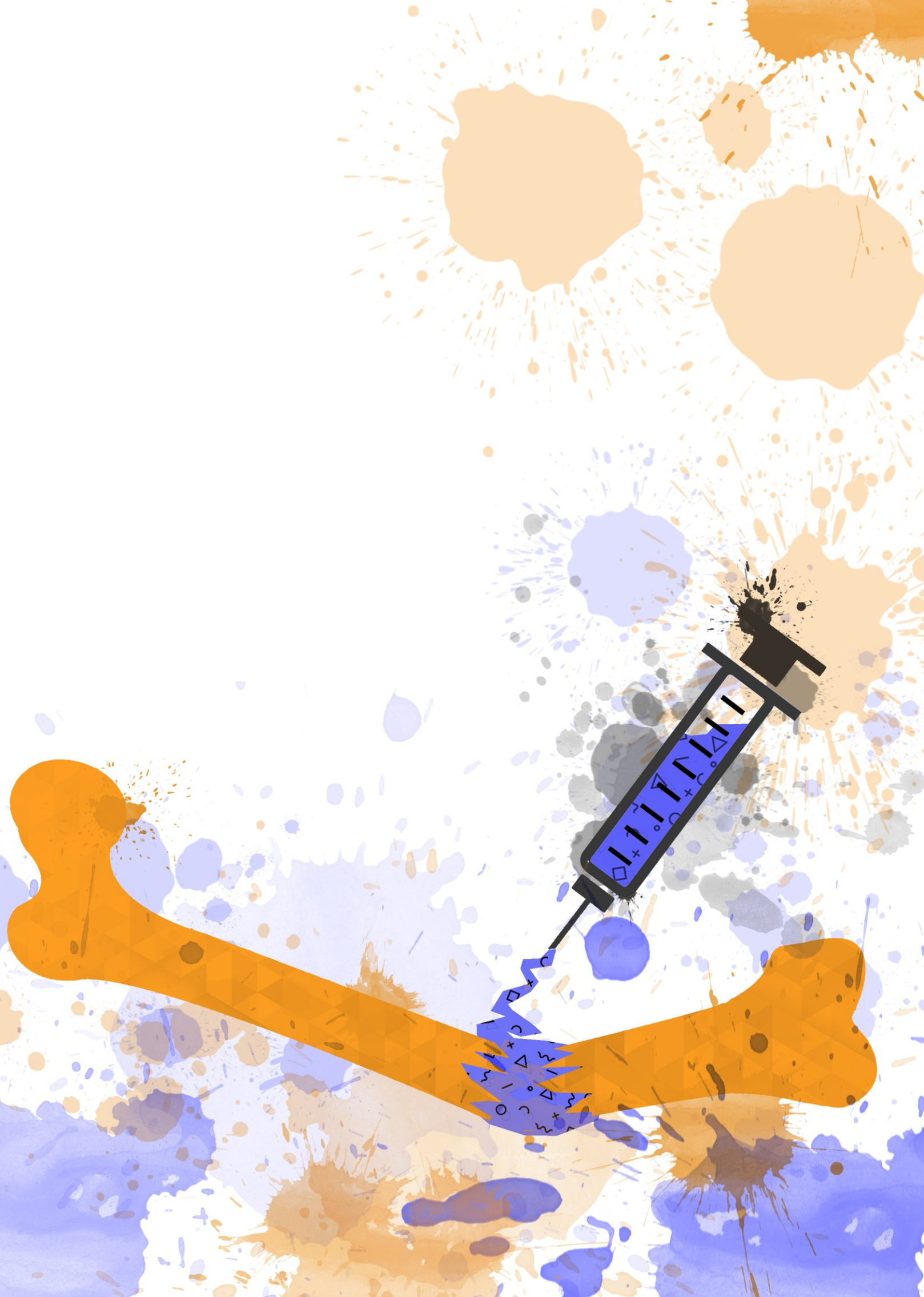

Submitted on: _____

Members of the Thesis Committee

Supervisor (primary): Prof. Dr. Uwe Gbureck

Supervisor (second): Prof. Dr. Jürgen Groll

Supervisor (third): Dr. Katrin Hurle

Supervisor (forth): Prof. Dr. Torsten Blunk

Chairperson: Prof. Dr. Christoph Sotriffer

Date of Public Defense: _____

Date of Receipt of Certificates: _____

Table of contents

1 AIMS AND MOTIVATION 1

2 STATE OF KNOWLEDGE 9

2.1 CALCIUM PHOSPHATES 11

2.1.1 Natural occurrences 13

2.1.2 The CaO-P_2O_5 system 16

2.1.3 Minerals of the CaO-P_2O_5-H_2O System 17

2.2 CEMENT SYSTEMS 30

2.2.1 Calcium phosphate cement (CPC) systems 32

2.2.2 Cement properties 38

2.2.3 Cement modifications 47

2.2.4 Bone cement applications 50

3 SETTING MECHANISM OF A CDHA FORMING ALPHA-TCP CEMENT MODIFIED WITH SODIUM PHYTATE FOR IMPROVED INJECTABILITY 53

3.1 ABSTRACT 56

3.2 INTRODUCTION 57

3.3 RESULTS 59

3.3.1 Characterization of Powder Samples 59

3.3.2 Cement Paste Characterization 62

3.3.3 Hydration Reaction 64

3.3.4 Characterization of Hydration Products 69

3.4 DISCUSSION 78

3.5 CONCLUSIONS 85

4 HYDRATION MECHANISM OF A CALCIUM PHOSPHATE CEMENT MODIFIED WITH PHYTIC ACID 87

4.1 ABSTRACT 89

4.2 INTRODUCTION 91

4.3 RESULTS 92

4.3.1 Characterization of powder samples 92

4.3.2 Material properties during setting 93

4.3.3 Characterization of hardened samples 103

4.4 DISCUSSION 106

4.5 CONCLUSION 111

5 PYROPHOSPHATE IONS INHIBIT CALCIUM PHOSPHATE CEMENT REACTION AND ENABLE STORAGE OF PREMIXED PASTES WITH A CONTROLLED ACTIVATION BY ORTHOPHOSPHATE ADDITION 113

5.1 ABSTRACT 116
5.2 INTRODUCTION 117
5.3 RESULTS 119
5.3.1 Powder characterization 119
5.3.2 Cement paste characterization 119
5.3.3 Setting characterization 125
5.3.4 Characterization of hardened cement 133
5.4 DISCUSSION 136
5.5 CONCLUSION 140

6 CONCLUDING DISCUSSION AND PERSPECTIVES 141

7 SUMMARY | ZUSAMMENFASSUNG 153

8 METHODOLOGY 163

8.1 POWDER FABRICATION 165
8.1.1 Alpha Tricalcium Phosphate (α-TCP) 165
8.1.2 Beta Tricalcium Phosphate (β-TCP) 165
8.1.3 Calciumdeficient Hydroxyapatite (CDHA) 166
8.2 PARTICLE SIZE DISTRIBUTION AND SPECIFIC SURFACE AREA 167
8.2.1 α-TCP 167
8.2.2 β-TCP 167
8.3 QUANTITATIVE PHASE COMPOSITION 168
8.3.1 α-TCP 168
8.3.2 β-TCP 168
8.3.3 Quantity calculations 170
8.4 ZETA POTENTIAL 171
8.5 PASTE AND SAMPLE COMPOSITION 172
8.6 RHEOLOGY 174
8.7 INJECTABILITY 175
8.8 HEAT FLOW CALORIMETRY 176
8.9 IN-SITU XRD 178
8.10 STORAGE STABILITY OF CEMENT PASTES 181
8.11 PORE WATER ANALYSIS DURING STORAGE 182
8.12 PH DEVELOPMENT 183
8.13 1H NMR 183
8.14 3D PRINTING 184
8.15 XRD OF HARDENED SAMPLES 185

8.16 CONTROLLED SETTING 186
8.17 IMETER 187
8.18 COMPRESSIVE STRENGTH 188
8.19 POROSITY 189
8.20 SEM IMAGING AND LIGHT MICROSCOPY 190
8.21 STATISTICS 190

9 APPENDIX 191

9.1 CIRCULUM VITAE 192
9.2 PUBLICATIONS AND CONFERENCE CONTRIBUTIONS 194
9.3 AFFIDAVIT 196
9.4 EIDESSTATTLICHE ERKLÄRUNG 197
9.6 CONTRIBUTION TO FIGURES AND TABLES 198
9.7 ACKNOWLEDGEMENT | DANKSAGUNG 208

10 REFERENCES 213

***Figure 1**. General structure of a mammalian bone. Reprinted from [155] under the terms of the Creative Commons Attribution 4.0 International License (CC BY 4.0) 15*

***Figure 2**. **a)** Binary phase diagram in the system of CaO (C) and P_2O_5 (P) and **b)** highlight of the region around the relevant composition of HAp. Reprinted with permission from [169]. 16*

***Figure 3**. Unit cell of α-TCP shown from the **a)** a-axis, **b)** b-axis and **c)** c-axis. Created with Vesta Ver. 3.5.7 [187]; Ca^{2+}: red orbs, PO_4^{3-}: green tetrahedrons with blue dots(O^2).....18*

***Figure 4**. Unit cell of β-TCP shown from the **a)** a-axis, **b)** b-axis and **c)** c-axis. Created with Vesta Ver. 3.5.7 [187]; Ca^{2+}: red orbs, PO_4^{3-}: green (P^{5+}) tetrahedrons with blue dots(O^{2-}**).**.....20*

***Figure 5**. Crystal structure of hydroxyapatite (HAp, $Ca_{10}(PO4)_6(OH)_2$) presented from **a)** the top (c-axis) and **b)** the side; Ca^{2+}: green orbs, PO_4^{3-}: pink tetrahedrons, OH^-: red and white tablets. Reprinted with permission from [214]. 20*

***Figure 6**. Crystal structure of octacalcium phosphate (OCP, $Ca_8(HPO_4)_2(PO_4)_4{\cdot}5H_2O$) oriented along the c-axis. Ca^{2+}: green orbs, PO_4^{3-}: light blue tetrahedrons, H_2O: red and white sticks. Reprinted and modified from [248] under the terms of the Creative Commons Attribution 4.0 International License (CC BY 4.0).....24*

***Figure 7**. Crystal structures of **a)** Brushite (DCPD, $CaHPO_4{\cdot}2H_2O$) along its a-axis **(top)** and its b-axis **(bottom), b)** Dicalcium phosphate monohydrate (DCPM, $CaHPO_4{\cdot}H_2O$) along its c-axis **(top)** and its a-axis **(bottom)** and **c)** Monetite (DCPA, $CaHPO_4$) along its c-axis (top) and its b-axis (bottom); Ca^{2+}: green orbs, PO_4^{3-}: pink tetrahedrons, O of H_2O: blue orbs. Reprinted and modified from [174] under the terms of the Creative Commons Attribution 4.0 International License (CC BY 4.0).....24*

***Figure 8.** Theoretical compositions in the ternary system of CaO, P_2O_5 and H_2O. Reprinted with permission from [345]. Values are presented in wt%.....32*

***Figure 9.** Solubility phase diagrams dependent on the pH value for the ternary system, $Ca(OH)_2$–H_3PO_4–H_2O, at 25 °C, showing the solubility isotherms of $CaHPO_4$ (DCPA), $CaHPO_4{\cdot}2H_2O$ (DCPD), $Ca_8H_2(PO_4)_6{\cdot}5H_2O$ (OCP), α-$Ca_3(PO_4)_2$ (α-TCP), β-$Ca_3(PO_4)_2$ (β-TCP), $Ca_4(PO_4)_2O$ (TTCP), and $Ca_{10}(PO_4)_6{\cdot}(OH)_2$ (HA). **a)** Reprinted with permission from [384] and **b)** from [385] under the terms of the Open Archive TOULOUSE Archive Ouverte (OATAO).....35*

***Figure 10.** Experimental setup of an injectability test. 41*

***Figure 11.** Particle network dependant on the particle size and distribution shown as a schematic of mono-dispersed particles **(A and E)** and transitional bi-dispersed particles **(B, C and D)**. Reprinted with permission from [438].....43*

***Figure 12.** Graphical description of the **a)** Derjaguin, Verway, Landau and Overbeek (DVLO) theory. [557, 558] and **b)** the electrical double layer (EDL) including the stern layer, potential, the diffuse layer and the zeta (ζ) potential. Reprinted with permission from [439] 49*

***Figure 13**. Particle size distribution of α–TCP and CDHA, determined by laser diffraction using isopropyl alcohol as a lubricant; the means of three independently prepared measurements are presented; the error bars represent the standard deviation. 60*

***Figure 14**. Surface charge of α-TCP, CDHA and a α-TCP/ CDHA mixture in water and a 0.002 M sodium phytate solution determined by the zeta potential measurement. Every powder was prepared independently three times, and the error bars represent the standard deviation. 61*

Figure 15. *The paste viscosity development of the samples Phy_0.25 (**black**) and Phy_1.00 (**blue**) at 23 °C (**line**) and 37 °C (**dotted line**). The reference Phy_0.00 was not measurable. Every sample was prepared three times independently, and one representative curve is shown.* *62*

Figure 16. *Injectability of all five paste formulations (Phy_0.00 – Phy_1.00) 2, 5 and 10 min after the powder and liquid mixing. Every sample has been prepared three times, and the error bars represent the standard deviation.* *63*

Figure 17. *The calorimetry results of the samples composed of α–TCP and CDHA (weight ratio 9:1) with different amounts of sodium phytate; a 0.2 M Na_2HPO_4 solution was used as the mixing liquid with an L/P of 0.3 ml/g_{Powder}. The measurements were performed at (**a**) T = 23 °C and (**b**) T = 37 °C; three independent measurements were run for each sample; one representative curve is shown for Phy_0.75 at T = 23 °C and for Phy_0.50, Phy_0.75 and Phy_1.00 at 37 °C, and for the other samples the mean of three independent measurements is presented.* *65*

Figure 18. *The pH measurements of (**a**) 0.2 M Na_2HPO_4 aqueous solutions containing variable amounts of sodium phytate (wt.% related to the powder content of the corresponding cement pastes) and (**b**) cements composed of α–TCP and CDHA (weight ratio 9:1) with 0 and 0.25 wt.% sodium phytate; a 0.2 M Na_2HPO_4 aqueous solution was used as the mixing liquid with an L/P of 1.2 ml/g_{Powder}. The measurements were performed at T = 37 °C; three independent measurements were run for each sample, and the error bars represent the standard deviation.* *66*

Figure 19. *The quantitative in-situ XRD results of samples composed of α–TCP and CDHA (weight ratio 9:1) with different amounts of sodium phytate; a 0.2 M Na_2HPO_4 aqueous solution was used as the mixing liquid with an L/P of 0.3 ml/g_{Powder}. The measurements were performed at T = 37 °C; three independent measurements were run for each sample, and the error bars represent the standard deviation; the data were corrected for the water loss occurring during the measurement.* *68*

Figure 20. *The quantitative in-situ XRD results of samples composed of α–TCP and CDHA (weight ratio 9:1) with different amounts of sodium phytate; a 0.2 M Na_2HPO_4 aqueous solution was used as the mixing liquid with an L/P of 0.3 ml/g_{Powder}. The measurements were performed at T = 23 °C; three independent measurements were run for each sample, and the error bars represent the standard deviation.* *68*

Figure 21. *The compressive strength of all five paste formulations (0.00–1.00) after 1 d and 7 d at 37 °C and 100% humidity. Every sample has been prepared independently at least 9 times, and the error bars represent the standard deviation.* *74*

Figure 22. *The pore diameter distribution and total porosity of all mixtures after (**left**) 1 d and (**right**) 7 d of hydration at 37 °C and 100% humidity. The sample Phy_1.00 was not hardened after 1 d, so it was not possible to measure the pores.* *77*

Figure 23. *CDHA crystals of the mixtures Phy_0.00, Phy_0.25, Phy_0.50 and Phy_1.00 grown for 1 d and 7 d at 37 °C and 100% humidity, visualized with the SEM. All samples have been observed on different areas, and representative images were selected for presentation.* *78*

Figure 24*. Changes in the zeta potential ζ of β-TCP depending on the amount of added phytic acid (IP6)* *92*

Figure 25*. Injectability of different cement pastes as the amount injected in percent after 5 and 10 min setting time at room temperature and a L/P of 0.83 ml/g; the reference is not presented, since it was not injectable.* *93*

***Figure 26**. **a)** Viscosity development of the different mixtures during the first 20 minutes of the hydration reaction at 20 °C and s = 250 Pa, **b)** the mixtures' storage and loss moduli over the course of the reaction is shown 2 min after the mixing until 22 min, at 20 °C, x = 1 rad/s and c = 0.04%. The reference is not depicted as it set to fast for the measurement. Samples were measured 3 times, one representative curve is shown for each sample. 94*

***Figure 27**. Calorimetry curves of b-TCP mixed with H_3PO_4 solution and variable concentrations of IP6 respectively 0.5 M citric acid monohydrate (reference IP6_0) at **a)** T = 23 °C; **b)** T = 37 °C; one representative curve was shown for each sample; w/c = 0.5 ml/g. 95*

***Figure 28**. Development of quantitative phase content determined by in-situ XRD and G-factor quantification in β-TCP mixed with a solution of H_3PO_4 (molar ratio 1:1) and **a)** 0.5 M citric acid monohydrate; T = 23 °C, **b)** 10 wt% IP6 related to the β-TCP content; T = 23 °C, **c)** 10 wt% IP6 related to the β-TCP content; T = 37 °C, **d)** 20 wt% IP6 related to the β-TCP content; T = 37 °C; the means of three measurements were shown (b: two measurements); w/c = 0.5 ml/g; violet diamonds: β-TCP ; cross: β-TCP initial; red square: brushite; green triangle: Monetite violet circle: MCPM; violet triangle: unassigned phase. 97*

***Figure 29.** Diffraction pattern of β-TCP mixed with a solution of H_3PO_4 (molar ratio 1:1) and 10 wt% IP6 related to the β-TCP content, recorded after **a)** 24 h and **b)** 1 h; T = 23 °C; w/c = 0.5 ml/g; the background contributions of Kapton film and water were subtracted from the measured pattern for better presentation; the diffraction patterns of the crystalline phases presented were calculated with software TOPAS 4.2 (Bruker AXS, Karlsruhe). 98*

***Figure 30**. In-situ ^1H NMR results of β-TCP mixed with a solution of H_3PO_4 (molar ratio 1:1) and 10 wt% IP6 related to the β-TCP content; w/c = 0.5 ml/g; T = 23 °C; **a)** quantities of ^1H fraction; **b)** development of the relaxation times T2. .....101*

***Figure 31**. pH profile of the setting reaction of cements composed of β-TCP and 0, 5, 10, 12.5, 15 or 20 wt.% IP6 containing phosphoric acid solution at a L/P of 0.83 mL/g. 102*

***Figure 32.** Brushite and monetite content in β-TCP mixed with a solution of H_3PO_4 (molar ratio 1:1) and different wt% of IP6 related to the β-TCP content, the reference with 0 wt.% IP6 contained 0.5 M citric acid monohydrate solution; the quantities were normalized to the sum of the contents of monetite and brushite; means of three independently prepared measurements were shown; w/c = 0.5 ml/g; T = 23 °C. 103*

***Figure 33**. Compressive strength **a)** and corresponding selected stress-strain-curves **b)** of cuboidal cement specimens composed of β-TCP and 0, 5, 10, 12.5, 15 or 20 wt% IP6 containing phosphoric acid solution at a L/P of 0.83 mL/g after 2, 4, 8 and 24 h of setting at 37 °C and 100% humidity.....104*

***Figure 34**. Scanning electron micrographs of fracture surfaces from cement specimens composed of β-TCP and 0 **(a, A)**, 10 **(b, B)**, or 20 wt.% **(c, C)** IP6 containing phosphoric acid solution at a L/P of 0.83 mL/g after 2 (small letter) and 24 h (capital letter) of setting at 37 °C and 100% humidity.....105*

***Figure 35.** pH values of the raw solutions **(stars)** mixed into the cement powder **(squares)** and the development during hardening after activation with 20.8 % Na_2/Na **(triangles)** for the samples containing no PP **(black)** and 0.05 wt% PP **(blue)**; n=3. .....120*

***Figure 36**. Zeta potential of alpha-TCP against water and different solutions of sodium pyrophosphate or sodium orthophosphate. A one way Anova was applied, **: p<0.001. .....121*

***Figure 37**. XRD analysis of the pastes PP0 to PP02 after storage at 25 °C for 1, 3, 7, and 14 d, presented as one representative curve out of three measurements and a cut out comparison of the angle range between 25° and 40° 2ϑ after 14 d of storage **(right side)**. The samples have been measured between 7-70° 2ϑ CuK_α with a step size of 0.022° and an integration time of 4s. 122*

***Figure 38**. Injectability of the pastes PP0, PP005, PP01 and PP02 activated with Na21. (*: $p < 0.05$) 125*

***Figure 39.** Storage and loss modulus development during the first 30 minutes after the activation with Na21 for all PP concentrations. γ = 0.1%, ω = 5 rad/s, Ø = 5 cm, d = 0.6 mm. Representative curves for each sample group have been chosen; n = 3. ..... 126*

***Figure 40**. Images of the four different Na21 pastes directly after the application onto the rheometer measurement area. 127*

***Figure 41**. Isothermal calorimetry of samples composed of α-TCP mixed with PP solutions of variable concentrations and addition of 20.8 vol% Na_2/Na solution related to the volume of the PP solution; T = 37 °C, L/P = 0.4 ml/g in the prefabricated paste; each measurement was reproduced three times; one representative curve is presented for each sample. 128*

***Figure 42.** Isothermal calorimetry of samples composed of α-TCP mixed with 0.05 wt.% PP solution and addition of Na2/Na solution in different vol% related to the volume of PP solution; T = 37 °C, L/P = 0.4 ml/g in the prefabricated paste; each measurement was reproduced three times; one representative curve is presented for each sample. 130*

***Figure 43**. In-situ XRD results of samples composed of α-TCP, PP solution in different concentrations and addition of 20.8 vol% Na2/Na solution; T = 37 °C, L/P = 0.4 ml/g in the prefabricated paste; the means of three independent measurements are presented, error bars represent the standard deviation. 132*

***Figure 44. a)** Quantitative XRD results and **b)** degree of hydration of storage samples composed of α-TCP, PP solution in different concentrations and addition of 20.8 vol% Na_2/Na solution; T = 37 °C, L/P = 0.4 ml/g in the prefabricated paste; the means of three independent measurements are presented, error bars represent the standard deviation. 133*

***Figure 45.** Compressive strength dependent on the amount of PP (0 - 0.2 wt% in the solution) in the stabilized paste and on the amount of Na_2/Na (10 – 42 wt% relative to the liquid fraction) solution used to activate the setting process sorted by prioritising the PP amount after 1d **(A)** and 7d **(B)** of hardening in 100% humidity and 37°C (Two way Anova; * : $p < 0.03$; ** : $p < 0.001$). 134*

***Figure 46**. Total porosity **(left y-axis** and **line graph)** and relative pore volume **(right y-axis** and **histogram)** by pore diameter of Na21_PP0-PP02 after 1d of hardening at 100% humidity and 37°C. 135*

***Figure 47**. Stored pastes in 5 ml falcon tubes composed of α-TCP and hyaluronic acid solution with a range of Mw from 8-15 kDa to 2-2.5 MDa after one day of storage **(top)** and 21 days of storage **(bottom)**. (n=3, one representative has been selected) Reprinted and adjusted with permission from the bachelor thesis of Maximilian Pfeiffle [738]. 147*

***Figure 48**. One layer scaffold of the 1 wt.% 2-2.5 MDa paste printed in air and hardened in Na_2/Na solution afterwards. Overview image **(left)** and detailed intersection **(right)**. Reprinted with permission from the bachelor thesis of Maximilian Pfeiffle [738]. 149*

***Figure 49**. One layer scaffold of the 1wt.% 2-2.5 MDa paste printed directly in Na_2/Na solution. Overview image **(left)** and detailed intersection **(right)**. Reprinted with permission from the bachelor thesis of Maximilian Pfeiffle [738]. 149*

***Figure 50**. Printed sample for compressive strength tests in top view **(A)** and side view **(B)**, **(C)** representative compressive strength test curves of the cast cement sample (light blue) and the printed sample (dark blue). Reprinted and adjusted with permission from the bachelor thesis of Maximilian Pfeiffle [738].....150*

***Figure 51**. Schematic depicting the custom syringe mount used for all injectability measurements.....175*

***Figure 52**.**(A)** Utensils used to store, mix and inject the cement paste: metal cannula (Ø: 2 mm), syringe with cap filled with the stabilized paste (5 ml, top, green cap), syringe with cap filled with the Na_2/Na solution (3 ml, bottom, blue cap) and the Luer lock connector. **(B)** shows the configuration of the two syringes for the mixing process.....186*

List of Tables

***Table 1**. Summary of existing orthophosphates and important characteristics [87, 155, 171-174]. 17*

***Table 2**. Minerals in the NH_4-MgO-P_2O_5 system, their corresponding solubility product constants and solubilites calculated at 25 °C, Reprinted and modified with permission from [290]. 28*

***Table 3.** D_V values obtained by laser diffraction and BET surface areas of α–TCP and CDHA; the values are the means of three independent preparations, while for the laser diffraction ten measurement runs were performed for each preparation; the errors represent the standard deviations of the three preparations. 60*

***Table 4.** The quantitative phase composition and degree of hydration of samples composed of α–TCP and CDHA (weight ratio 9:1) with different amounts of sodium phytate after 1 d and 7 d of hydration; a 0.2 M Na_2HPO_4 aqueous solution was used as the mixing liquid with an L/P of 0.3 ml/g_{Powder}; the samples were stored at 37 °C. 70*

***Table 5.** True CS and aspect ratio rz/rx of CDHA crystallites in storage samples after 1 d and 7 d of hydration; a 0.2 M Na_2HPO_4 solution was used as the mixing liquid with an L/P of 0.3 ml/g_{Powder}; the samples were stored at 37 °C. 71*

***Table 6.** The quantitative phase composition of samples composed of α–TCP and CDHA (weight ratio 9:1) with different amounts of sodium phytate after 1 d, 2 d, 4 d and 7 d of hydration; a 0.2 M Na_2HPO_4 aqueous solution was used as the mixing liquid with an L/P of 0.3 ml/g_{Powder}; the samples were stored at 23 °C. 72*

***Table 7.** The degree of hydration of samples composed of α–TCP and CDHA (weight ratio 9:1) with different amounts of sodium phytate after 1 d, 2 d, 4 d and 7 d of hydration; a 0.2 M Na_2HPO_4 aqueous solution was used as the mixing liquid with an L/P of 0.3 ml/g_{Powder}; the samples were stored at 23 °C. 72*

***Table 8.** True CS and aspect ratio rz/rx of CDHA crystallites in the storage samples after 1 d, 2 d, 4 d and 7 d of hydration; a 0.2 M Na_2HPO_4 solution was used as the mixing liquid with an L/P of 0.3 ml/g_{Powder}; the samples were stored at 37 °C. 73*

***Table 9.** The total pore volume, porosity and average pore size of all samples stored for 1 d and 7 d at 37 °C and 100% humidity, measured by Hg-porosimetry. 76*

***Table 10.** DV values of the α-TCP starting powder, determined by laser diffraction; the means of three independent preparations are presented (10 measurement runs per preparation), the errors represent the standard deviation. 119*

***Table 11.** pH values of solutions used for cement paste preparation; the means of three measurements are shown, the error is derived from measurements of buffers with defined pH (7 and 9). 119*

***Table 12.** Ion concentration of Ca and P determined by pore water analysis via ICP-MS after the storage of α-TCP mixed with H_2O for 1, 3, 7 and 14 d at 4 °C; measurements were performed once, an error of ± 0.1 mmol/l can be assumed. 123*

***Table 13**. Concentration of Na, P and Ca in pore water after storage of prefabricated cement pastes for 7 d at 4 °C; measured values are means of two independently prepared measurements, the error represents deviation from the mean; the theoretical values for PP005 and PP05 are calculated from the PP concentrations of the corresponding solutions. 124*

***Table 14.** Qualitative evaluation of extrudability **(color** red: bad, yellow: acceptable, green: good**)** and shape fidelity **(words)** of the cement pastes with 1 wt% of HyAc and a Mw range from 8-15 kDa to 2-2.5 MDa and*

pastes with a concentration range of 1 to 5 wt% of HyAc with a Mw of 2-2.5 MDa. Reprinted with permission from the bachelor thesis of Maximilian Pfeiffle [738]. *148*

***Table 15**. recipes of all IP6 solutions used in **Chapter 4**. * This solution is a 0.5 M citric acid solution and functions as a reference as a classical setting retarder.* *173*

***Table 16.** Operating conditions for ICP-MS measurements.* *182*

***Table 17.** Qualitative contributions for Manuscript 1 used in **Chapter 3**.* *198*

***Table 18**. Qualitative contributions for Manuscript 2 used in **Chapter 4**.* *199*

***Table 19**. Qualitative contributions for Manuscript 3 used in **Chapter 5**.* *200*

***Table 20**. Qualitative contributions for Manuscript 4 used in **Chapter 6**.* *201*

Table 21**. Qualitative contributions for Manuscript 1 used in **Chapter 3 ..... *202*

Table 22**. Qualitative contributions for Manuscript 1 used in **Chapter 4 ..... *203*

Table 23**. Qualitative contributions for Manuscript 1 used in **Chapter 5 ..... *204*

Table 24**. Qualitative contributions for Manuscript 1 used in **Chapter 6 ..... *205*

Chapter 1

Aims and Motivation

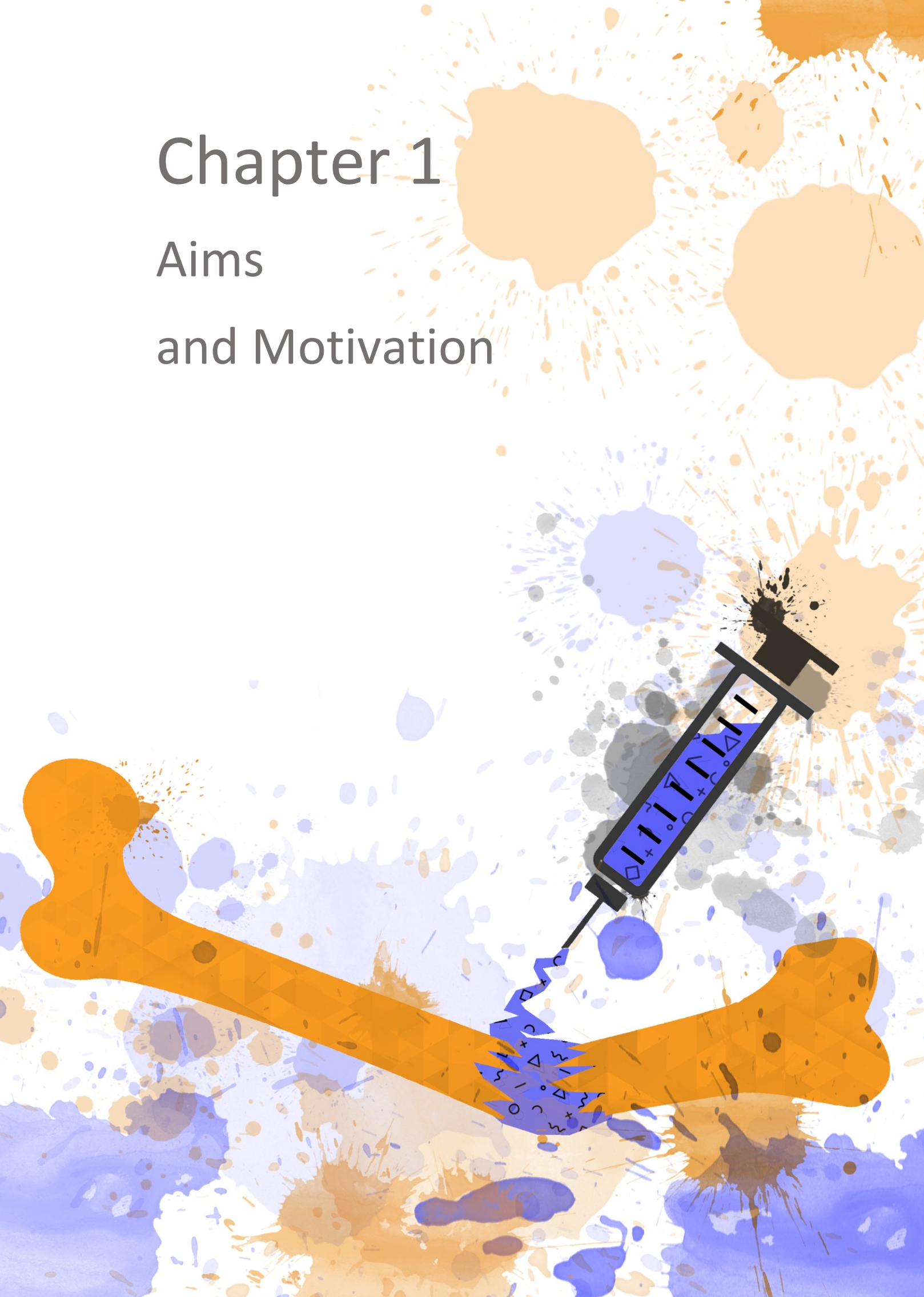

Chapter 1

Aims and Motivation

Humans have a natural urge for self-preservation. [1, 2] Living organisms like the human body are equipped with several tools and mechanisms to preserve its integrity by self-healing, but they are not invincible and still have limitation. [3-8] This urge, and limitation inevitably lead to the development of medicine as a means to preserve and prolong one's life by treating diseases and injuries. [9, 10] The main structural and mechanical framework of the human body is the skeleton. [11, 12] If this framework is compromised several mechanisms activate to regenerate the skeleton at the site of fracture, but some defects may be too big a task. Mostly when the defect size is too big (defect size < 2.5cm [13]) the body cannot fully bridge and restore the missing bone. [14, 15] To be able to treat such defects above the critical defect size, researchers, and clinicians developed bone replacements. As for the origin of these replacements there are three different options: autologous (autograft), allogenic (allograft) and xenogenic (xenograft). [16-21] These were already reported in skeletal remains of prehistoric people such as Aztecs, Egyptians and Khurits. [19, 22] In 1668 Jacob van Meekeren described the first bone grafting procedure. He transplanted a xenograft from a dog calvarium to a soldiers skull. [23] A further documented surgery was an allograft transplant performed in 1882 by William MacEwen. [17] At the start of the 1920's bone grafting was an established surgical technique. [18]

Autografts are bone replacements from the same organism. Here a donor site, most frequently the ilia crest due to its quality and volume, gets selected inside the patient's body and the necessary bone size and shape gets extracted from there to be placed into the defect. [24-26] The same is true for allografts, but the body of origin is not the patient's body but a different donor body. A xenograft does not come from a human body but is from an animal body or manufactured completely outside of one and is then introduced into the defect like an implant.

The first two have the advantage of a high biocompatibility being the same material (bone mineral and collagen) as the one that needs to be replaced. This offers a high osteoconductivity, growth factors (non-collagenous bone matrix proteins) for osteoinduction,

and progenitor stem cells for osteogenesis. [16, 24] First of all the availability and compatibility (possibility for transfer of contaminants, toxins, or infections from the donor) of an allograft makes it very hard to rely on it. [27-29] Allografts can be processed before implantation to minimize the risk of a pathogenic transfer, but this may degrade the transplant biologically and impair the mechanical properties. [28, 29] Autografts circumvent the compatibility problem by using the same body as the origin, but that also means first an additional surgery is needed to extract the graft that lengthens the surgery but is limited by supply, iatrogenic complications secondary to graft procurement. [30] Additionally a high donor site morbidity is reported which makes it less attractive. [31-34] Nevertheless autografts are still the gold standard. [35, 36] But because this method has drawbacks for the patient and is limited by the defect size and available donor sites, researchers strive to develop materials for xenografts, that can supersede autografts as the gold standard. [37]

For xenografts several material properties, that come naturally with auto- and allografts, must be taken into account. A material that is supposed to be used as a bone replacement should be at least bio-inert like titanium for example. But important properties to compete with natural materials are cytocompatibility, osteogenesis, osteo-conductivity, structural support [38] and a benefit would be osteo-inductivity. [27, 39] Besides metal and polymer based implants also implants with a composition closer to actual bone are of great interest. [40] Here a separation is made between sintered ceramic implants and mineral bone cements. [41] Both materials are prepared by mixing a powder with a liquid (water or organic binder) and shaping them into the desired form. The distinction between sintered ceramics and cements is made in the next step. While cements just set over time and develop mechanical strength on their own, sintered ceramics need to be treated thermally to evaporate the liquid and enable a reaction in the powder component. Bioinert sintered ceramics can be of alumina, zirconia or mixed origin, while bioactive sintered ceramics can be bioactive glasses, mainly based on a doped SiO_2 glass, but also calcium phosphate ceramics. [41] The latter composition is also found as the main group of mineral bone cements.

Calcium phosphate cements (CPC) find application in a wide variety of formulations and forms. However, they are far from perfect. [42] They offer the general material properties mentioned above, but cements require elevated attention to specific characteristics. These requirements are the ability to sterilize the cement educts without altering their behaviour during application. Further, these cements need to develop a sufficient mechanical strength to be suitable for a bone replacement even for low load-bearing defects. Also the degradability or resorbability of the set cement is of high interest as it is one of the main advantages of these

types of materials over e.g. metal or polymer-based implants. A big unique selling point of cements is the ability to mould them into a defect specific shape during application as these materials transition from a liquid pasty consistency to a sturdy hardened implant shortly after the application. This transition behaviour and the time that it takes for the cement can be utilized to achieve minimal invasive application methods via the injection through a syringe. This adds the injectability of a cement paste to the list of highly interesting characteristics of such materials.

Additionally, from a clinicians point of view there is a demand for higher resorption rates and better physical properties. [43] For self-setting formulations also an improvement in cement viscosity is of high demand to prevent separation during injection. [44-47] The paste cohesion is often even more important for the cement's behaviour after injection to prevent leakage and spreading of the paste into undesired areas next to the defect site. [48] As these cements start setting as soon as the educts are combined there is not only the need for a quick application, but also for the cement to be mixed on site in the operating theatre. This can cause problems of deviation between applications by the operation theatre staff and poses the risk of contamination as they usually need to be prepared in an open container and then transferred into the syringe. [49-54]

It becomes clear, these injectable cements are amongst the CPCs most in need of improvements. Here problems such as filter pressing, phase separation and overall bad injectability hold them off from a broad application by surgeons. Modifications to the cement's viscosity and setting behaviour are the most promising starting points. However, this is often detrimental to the overall injectability, when focussing only on paste cohesiveness. [55, 56] The field of self-setting calcium orthophosphate cements is of great potential.

Therefore this work aims to address several important characteristics for both major CPC systems (apatite and brushite forming cements). The goal was to investigate the possibility to use new setting retarder like sodium phytate (IP6) to not only control the setting time and behaviour but also create a paste that shows improved injectability due to the newly introduced modification. Furthermore, a system that can be stored as a premixed paste based on the modification of an apatite-forming cement modified with sodium pyrophosphate (PP) should be developed.

The need for a development into this direction is supported by extensive reviews on these materials. These proposed some important topics that have to be addressed to further develop this material class for both brushite and apatite forming cements. [57-59]

i. Fully Injectable formulations [60]
ii. Open microporous formulations for optimized osteoconductivity [60]
iii. Drug / hormone loaded cements for treatment of diseases [61-63]
iv. Incorporation of autologous or allogenic osteoprogenitor cells [64-66]
v. Premixed calcium phosphate cements [67-74]
vi. Patient or defect specific grafts fabricated via novel 3D printing techniques [75]

In **Chapter 2** an overview of all relevant topics for this work is given. The start from natural occurrences of calcium phosphates, both geologically and biologically, transitioning into the specifics of the relevant calcium phosphate minerals and their characteristics serves as an introduction to the topic. Further into the chapter this fundamental information gets set into context with the mechanisms of cement systems. Here after the explanation of each system also the relevant properties a calcium phosphate cement (CPC) must exhibit are presented and possible modifications are proposed. This proposal directly leads to applications of these materials, but also to current limitations. Some of these limitations may be overcome by further research in their direction. This thesis aims to address the property of injectability by manipulation of the cements setting time and interparticle interactions affection the viscosity. Referring to the proposed improvements above**, Chapter 3** and **4** address mainly point (i) and to a lower extend point (ii) and **Chapter 5** focusses mainly on point (v).

In **Chapter 3** and **Chapter 4** commonly known apatite forming and brushite forming CPC systems of α-TCP or β-TCP as starting powder respectively are modified by the addition of sodium phytate to the liquid. This addition tackles the problem of fast setting time by retarding the setting reaction to reach a time applicable for the desired surgical window. The addition of these phytate ions into the liquid also alters the particles surface charge and therefore influences their particle-particle interaction leading to a better injectability via an increased viscosity.

While the retarding effect of phytate in **Chapters 3** and **4** enabled a good injectability and application within an appropriate amount of setting time. The goal of the work presented in **Chapter 5** was to produce a water-based cement paste that can be stored as a premixed paste without reacting. To stop the setting reaction once the powder and liquid is combined completely and rather introduce a mechanism to store the now premixed paste, the inhibitory effect of sodium pyrophosphate on CPCs is utilized. This paste is then activated once the reaction is needed via a secondary water-based solution containing a high concentration of sodium orthophosphate salts. The possibility to premix a paste and then store it until it is

needed introduces a way to control the composition more precisely from the manufacturer side. Common uncertainties in the preparation of the CPC in different operation theatres are eliminated.

Chapter 6 the concluding discussion and outlook is based on additional work outside of this thesis with the materials presented in the previous chapters **Chapter 3**, **4** and **5**. The materials from **Chapter 3** and **4** have been evaluated concerning their cell compatibility with osteosarcoma cell line MG63 for the osteoblastic cells and RAW 264.7 for the osteoclastic cells. These tests have been done by a dental student (Valentin Steinacker) in coordination with Jan Weichhold.

Chapter 5 shows possible other material scientific options to use a CPC paste modified in the presented way. Here not yet published work on a 3D printer ink composed of the system presented in **Chapter 5** and further adjusted in terms of viscosity by the addition hyaluronic acid (HyAc) shows a promising future to tackle point (vi).

Chapter 2

State of Knowledge

Chapter 2

State of Knowledge

2.1 Calcium phosphates

The group of calcium phosphates (CaPs) has many representatives in nature. Some are in form of inorganic mineral ores, while some are found in the form of skeletal part in living organisms such as bones or teeth. As humans are composed of 3-7 wt% of bone mass this chemical group is of high interest. [76-78] There have been extensive studies of calcium phosphates over a wide range of years and topics. [76-84]

The group of calcium phosphates is made up of minerals consisting of mainly calcium cations (Ca^{2+}) and phosphate group anions (PO_4^{3-}). Depending on the circumstances during formation a varying degree of hydrogen ions (as OH^-, HPO_4^{2-}, $H_2PO_4^-$ or H_2O) are integrated. [85] Due to the vast amount of combination possibilities of calcium and phosphorous oxides with and without H_2O the supergroup of calcium phosphates needs to be subdivided into several chemically similar smaller sections. This is done through the differentiation by phosphate anions and leads to the suffixes ortho- (for PO_4^{3-}), meta- (for PO_3^-), pyro- (for $P_2O_7^{4-}$) and poly- (for $(PO_3)_n^{n-}$). For ortho- and pyrophosphates the individual members of the respective subgroup can further be categorized by their calcium ion substitution. Here a numerical labelling approach leads to mono-, di-, tri- and tetra-calcium phosphates. [86-88].

Orthophosphates can contain a wide range of dopants both introduced intentionally in a lab setting, to control its properties, and due to the chemical composition of the surrounding environment during natural formation. Here calcium ions (Ca^{2+}) in the crystal lattice can be partially replaced by Sr^{2+}, Ba^{2+}, Mg^{2+}, Mn^{2+}, K^+, Na^+ or $Fe^{2/3+}$ ions. In the case of naturally formed apatites the fluoride is sometimes swapped out for hydroxide, chloride, and bromide. [89] Lastly the orthophosphate ions can be substituted to form carbonate variants (CO_3^{2-}), but also vanadate (VO_4^{3-}) and arsenate (AsO_4^{3-}) ions can be incorporated. [90] These substitutions normally don't exceed trace concentrations, except for F^- and OH^- where complete solid

solutions can be achieved. As with almost all crystalline material aside from substitutions also imperfections in the form of missing ions in the lattice are a common alteration, leading to non-stochiometric minerals. Non substituted calcium phosphates exhibit a clear white colour, but this can change drastically with different substitutions.

This work will mostly concentrate on orthophosphates as the main subject of research with the exception of a pyrophosphate salt as an optional additive. The main representatives of this mineral group relevant for this work are the chemically equal but crystallographic different tricalcium phosphate (TCP, $Ca_3(PO_4)_2$) polymorphs α-TCP and β-TCP. Additionally the main water containing calcium phosphate minerals are brushite (Bru, DCPD, $CaHPO_4{\cdot}2H_2O$) and hydroxyapatite (HAp, $Ca_{10}(PO_4)_6(OH)_2$) or rather its variant calcium deficient Hydroxyapatite (CDHA, $Ca_{10-x}(PO_4)_{6-x}(HPO_4)_x(OH)_{2-x}$; x=1 mostly).

2.1.1 Natural occurrences

Geological occurrences

While some of these minerals and variants have not been found formed under natural conditions most of them are. The aforementioned calcium deficient hydroxyapatite was found in an ion-substituted form. [91] Others form deposits in igneous rocks , but also in sedimentary rocks as phosphorites. [92-95] These are formed as metabolites of various sulfur bacteria, consisting of mainly francolite (carbonate-fluorine apatite, $Ca_5[(F,OH,CO_2)/(PO_4)_3]$) and can be found all over the world in Morocco, Florida, Tunisia, Estonia, Algeria and Germany (Leipzig). [94, 96-100] This mineral francolite has a variation that is also of a biological origin but then found in geological context. Collophane is a cryptocrystalline mineral that was discovered as early as 1870.[101, 102] All natural phosphorites consist mainly of these minerals, but can also contain other minerals from the calcium phosphate group. These include a monoclinic analogue to hydroxyapatite named clinohydroxyapatite [103], staffelite, which is formed in environments high in carbon [104], and also brushite. [105, 106]

Aside from these occurrences where the calcium phosphates are the main component of the rock deposit, they can also be found in smaller quantities throughout a variety of geological sites. To be economically usable as a source for calcium phosphates a rock must have at least over 15 % apatite. These rocks serve as sources for the elements to be further used in industrial production. To achieve this, they are broken up and refined to fit their purpose, but nature also holds minerals that are found in industrial products. On the far end of the Ca/P spectrum (=2.0) is tetracalcium phosphate or hilgenstockite [107], which was found naturally in Hörde (Westphalia. GER). Its trivial name is used but does not serve as its official mineral name. [108] The β-polymorph of TCP can be found in its natural form of whitlockite or Ca-whitlockite in New Hampshire (USA) and is a highly ion substituted variant of the stochiometric TCP. [108-111]

Biological occurrences

Calcium phosphates are also a common find in a biological context. The described phosphorites are partially made up of minerals of bacterial origin, but also bigger organisms like isolated cells, invertebrates and vertebrates synthesize them. [112] The ability to store and regulate essential elements like calcium or phosphorous, through the synthesis of CaPs in the form of ACP near the mitochondria, enables the control of element concentrations inside basic organisms. [113] Vertebrates use CaPs as the main inorganic component of their skeletal parts e.g., bones, teeth, fish enameloid and antlers), but they can also form pathological calcifications

like dental and urinary calculus/stones. [114-119] CaPs can even precipitate in the brain as so-called brain sand.[120] Focussing on the human body, with the exception of some parts of the inner ear all hard tissue is made up of sodium, potassium, magnesium or carbonate substituted CDHA called "biological apatite" [121-125], also called by its mineral name dahlite. [126, 127] Human bone is not 100% CaP. Only about 60-70% is CaP accompanied by 20-30% collagen and water as the rest. [120, 128, 129] It can also be found dissolved in body fluids such as blood serum [130], urine [131], sweat [132] and milk. [133, 134]

Bone

The term skeleton summarizes all osseous tissue of a single animal or human. It has a variety of functions including the protection of organs, serving as the support structure for the whole body and facilitate movement. [135] From a material science point of view the material known as bone is a complex composite of inorganic crystalline phases (calcium phosphate minerals) intertwined with bioorganic phases (collagen). [136-140] This composite has been "used" by nature for a long time. Already dinosaur fossils were found to be of CaP composition. [141-146] Most fossils can be found of a diagenetic fracolite composition. [147] Francolite is a variation of fluorapatite and is characterized by a wide variety of substitutions ranging from magnesium, strontium or sodium for the calcium position to sulphate or carbonate for the phosphate position depending on the chemical composition of the surroundings where the fossil was sedimented. [148-150]

In this work mostly the inorganic parts, which make up about 25-75% (dry weight) and 35-65% (volume) of bone, are of interest. The high range of these values is a result of drastically different compositions not only between different mammalians, but also between various locations in the same organism. The ratio of collagen to inorganic compound can adjust its mechanical properties. A higher mineral content leads to a more pronounced brittle behaviour [151-153], whereas a larger amount of collagen enables a much more flexible nature. [154] Further bone can be divided into two types. The dense outer layer is called compact or cortical bone, which encases a much more porous (avg. 75-97% porosity) inner bone mesh called cancellous, trabecular or spongious bone. (**Figure 1**)

As it is of much higher density (~1.80 g/cm^3), cortical bone accounts for a bigger part of the weight of the skeleton. On the other hand, the porous foam-like shape of cancellous bone makes up the majority of volume. [86, 116, 138, 139]

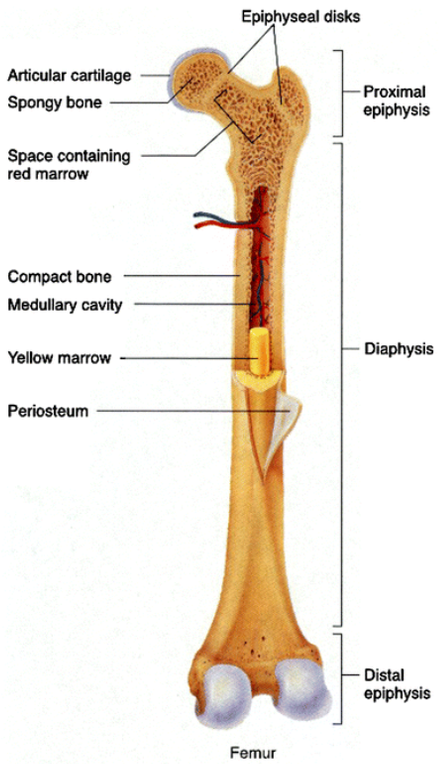

***Figure 1**. General structure of a mammalian bone. Reprinted from [155] under the terms of the Creative Commons Attribution 4.0 International License (CC BY 4.0) .*

As stated above the inorganic part of bone consists of biological apatite like ion substituted CDHA, but with a deficiency in hydroxyl groups. [156-158] Even though the composition of bone is known and investigated to a good degree, there is no agreement yet on the formation mechanism. Generally, the formation is divided in two biomineralization processes in literature. The active, or (organic) matrix mediated, way is described as a formation process where the mineral deposits are directed to form in a way not recognised in simple supersaturated solutions. Here individual nano sized biological apatite crystals are assembled into bones through the activity of cells like osteoblasts. [159, 160] On the other hand the passive, also called biologically induced, way of mineralization is similar to the precipitation from a supersaturated solution. No cells are required to guide the process and the nucleation may happen on all thermodynamically suitable nuclei. [114, 140, 161-166] Bone is not only formed in human bodies but can also be used in medicine to heal them. This happens in form of bone substitutes as allografts [167] from cadavers and xenografts. [168]

2.1.2 The $CaO-P_2O_5$ system

All CaPs can be categorized and named by their chemical compositions as described above, but there are some key characteristics that help to group them also by their behaviour. As seen below (**Figure 2 a)** the main factor to influence the mineral composition of a calcium phosphate mixture is the relation of available calcium oxide to phosphor oxide or easier the ratio of Ca/P. Small variations can lead to a biphasic material composition during synthesis.

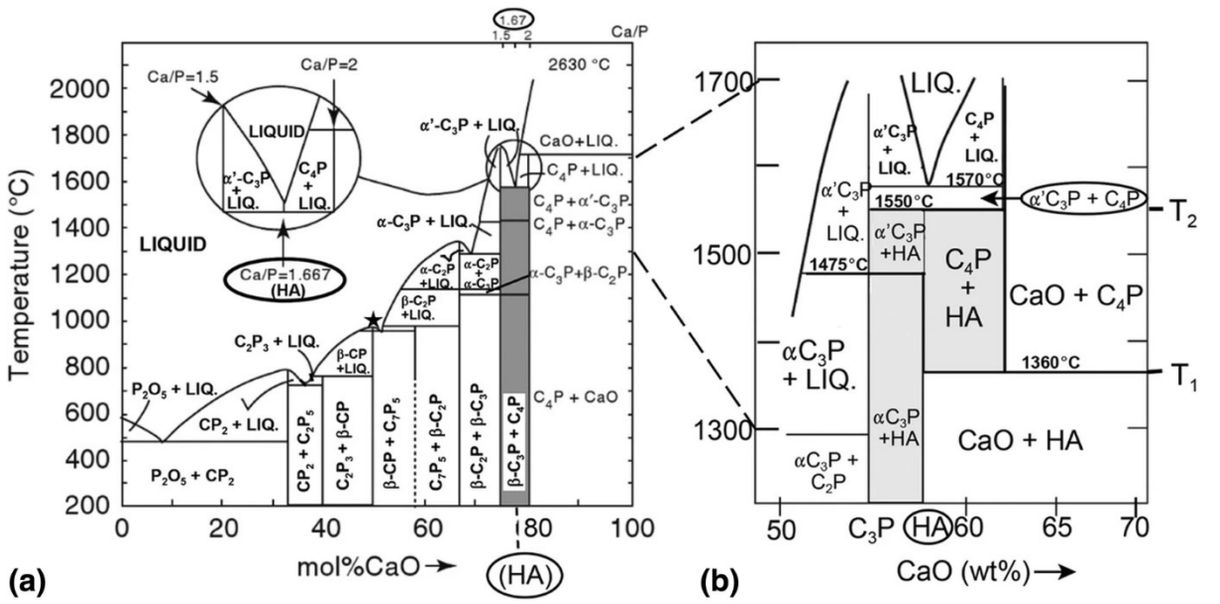

***Figure 2**. **a)** Binary phase diagram in the system of CaO (C) and P_2O_5 (P) and **b)** highlight of the region around the relevant composition of HAp. Reprinted with permission from [169].*

This ratio ranges from 0.5 for monocalcium phosphate anhydrous/monohydrate (MCPA/MCPM, $Ca(H_2PO_4)_2/\cdot H_2O$) to 2.0 for tetracalcium phosphate (TTCP, $Ca_4(PO_4)_2O$) with the range of the highest interest at 1 for Brushite (DCPD) and Monetite (DCPA) over 1.5 for α- and β-TCP to 1.5-1.67 for CDHA and HAp.(**Table 1**) In the system of $CaO-P_2O_5$ there are no studies in the recent past showing the existence of solid solutions. [170]

Acidity/basicity and solubility are directly dependant on the Ca/P ratio, where minerals of higher Ca/P ratio exhibit more basicity and are therefore less soluble. [86-88] This means it is possible for CaPs to be dissolved as a highly soluble mineral with lower Ca/P ratio and then subsequently be precipitated elsewhere after being transported with the solvent. This is the main mechanism of hydraulic cements.

***Table 1**. Summary of existing orthophosphates and important characteristics [87, 155, 171-174].*

Ca/P	Compound	Abbr.	Formula	Solubility at 25°C [g/l]	Space group	Density [g/cm³]
0.5	Monocalcium phosphate monohydrate	MCPM	$Ca(H_2PO_4)_2{\cdot}H_2O$	~18	Triclinic P $\bar{1}$	2.23
0.5	Monocalcium phosphate anhydrous	MCPA	$Ca(H_2PO_4)_2$	~17	Triclinic P $\bar{1}$	2.58
1.0	Brushite, Dicalcium phosphate dihydrate	DCPD	$CaHPO_4{\cdot}2H_2O$	~0.088	Monoclinic 1a	2.32
1.0	Dicalcium phosphate monohydrate	DCPM	$CaHPO_4{\cdot}H_2O$	-	Monoclinic $P2_1/c$	-
1.0	Monetite, Dicalcium phosphate anhydrous	DCPA	$CaHPO_4$	~0.048	Triclinic P $\bar{1}$	2.89
1.33	Octacalcium phosphate	OCP	$Ca_8(HPO_4)_2(PO_4)_4{\cdot}5H_2O$	~0.0081	Triclinic $\bar{1}$	2.61
1.5	α-Tricalcium phosphate	α-TCP	$\alpha\text{-}Ca_3(PO_4)2$	~0.0025	Monoclinic $P2_1/a$	2.86
1.5	β-Tricalcium phosphate	β-TCP	$\beta\text{-}Ca_3(PO_4)$	~0.0005	Hexagonal R3c	3.08
1.2-2.2	Amorphous calcium phosphate	ACP	$Ca_xH_y(PO_4)_z{\cdot}nH_2O$ n=3-4.5	-	-	-
1.5-1.67	Calcium- deficient hydroxyapatite	CDHA	$Ca_{10-x}(PO4)_{6-x}(HPO_4)_x(OH)_{2-x}$ (0<x<1)	~0.0094	Monoclinic $P2_1/b$ or hexagonal $P6_3/m$	3,13
1.67	Hydroxyapatite	HA, HAp	$Ca_{10}(PO4)_6(OH)_2$	~0.0003	Monoclinic $P2_1/b$ or hexagonal $P6_3/m$	3.16
2,0	Tetracalcium phosphate	TTCP	$Ca_4(PO_4)_2O$	~0.0007	Monoclinic $P2_1$	3.05

2.1.3 Minerals of the $CaO\text{-}P_2O_5\text{-}H_2O$ System

Alpha tricalcium phosphate (α-TCP)

The alpha polymorph of TCP ($Ca_3(PO_4)_2$) is known as a unique phase since 1932. [175, 176] It is obtained by heating CDHA or a mixture of $CaCO_3$ and MCPM with a Ca/P ratio of 1.5

above ~1125°C as here the transition of β-TCP to α-TCP starts. (**Figure 2**) [177] Hence it is a high temperature phase of the CaP group. Other sources report transitioning temperatures from 1100°C [178], over 1155°C [170, 179, 180] up to 1350°C [181]. Due to the higher temperatures and its metastability at ambient conditions [182] it is considered to be the high temperature polymorph of β-TCP. But studies show it to be obtainable at 800-1000°C, when doped with silica [183] and is therefore called "silica stabilized α-TCP". [184-186] Being a polymorph it shares the same chemical composition as other TCPs, but differentiates itself by solubility and crystal structure. (**Table 1**)

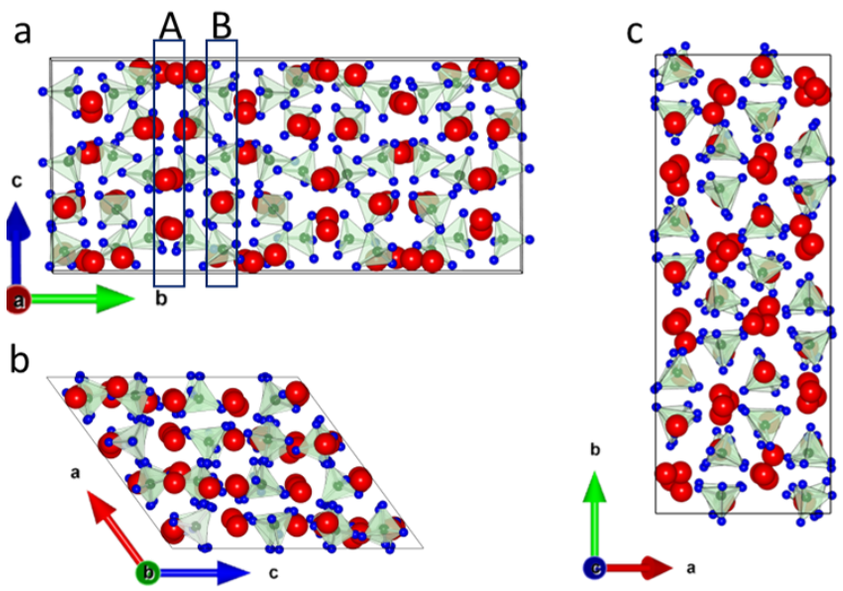

***Figure 3**. Unit cell of α-TCP shown from the **a)** a-axis, **b)** b-axis and **c)** c-axis. Created with Vesta Ver. 3.5.7 [187]; Ca^{2+}: red orbs, PO_4^{3-}: green tetrahedrons with blue dots(O^2).*

The crystals of α-TCP consist of tightly bonded PO_4 tetrahedrons (green and blue) bound by Ca^{2+} ions (red orbs).(**Figure 3**) It is of monoclinic structure made up of 24 formula units containing 312 atoms in the space group $P2_1/a$. [188-190] Simplified it consists of two repeating and alternating columns aligned along (0 1 0) where one only has Ca^{2+} ions (A) and the other one is a combination of calcium and phosphate ions (B).

Due to its higher solubility and lower stability compared to its β polymorph, it exhibits higher reactivity in aqueous systems. [182] The hydrolysis of α-TCP with water yields CDHA. [191-193] Its reactivity can be increased by milling the powder. [194].

In medicine it finds use case as a component of self-setting CPCs. [195, 196] On its own it is resorbed faster than new bone can be formed [197] and normally converts to the less degradable CDHA. This TCP variant of particular interest has been studied extensively. [198]

Beta tricalcium phosphate (β-TCP)

The other common polymorph of TCP ($Ca_3(PO_4)_2$) besides α-TCP is β-TCP. [175, 176] Just like the other high temperature polymorph it may also not be precipitated from aqueous solution but can be prepared similarly to α-TCP by heating mixtures of calcium and phosphate salts with a Ca/P ratio of 1.5 across the mixture. As it starts to transition to its α-polymorph above 1125°C the temperature is to be kept between 800°C and 1100°C to obtain pure β-TCP. Phase purity can be aided by the addition of Mg^{2+} ions. [199] This is then closer to the substituted variant Whitlockite (β-TCMP, β-$(Ca, Mg)_3(PO_4)_2$) that can be found in nature. [109] Although being called a high temperature variant it may also be obtained at around 150°C by precipitation from water free ethylene glycol. [200, 201] It shows a higher symmetry compared to α-TCP and crystallizes in the hexagonal system with the space group R3c.(**Figure 4**)

Its unit cell contains 21 formula units with 273 atoms. Six Ca^{2+} sites (red orbs) are only half occupied (half-filled red and white orbs) to maintain charge neutrality per unit cell. These vacancies can also be distributed differently over the six sites. [189, 190, 199]

The magnesium substituted β-TCMP is less soluble than pure β-TCP [202] so β-TCMP can be formed in nature. This is as e.g., dental calculi, urinary stones, dentinal caries, salivary stones, arthritic cartilage and sometimes in soft-tissue deposits. [86, 115, 203-206] Just like α-TCP also the β polymorph is used in medicine. Here it is part of self-setting CPC formulations [57] or in different grafts. [197, 207-212].

β-TCP has not only medicinal use. One interesting usage is in food industry. Here the additive known also as E341 prepared from calcium hydroxide and phosphoric acid is used as an improver for bakery and helps prevent clumping of powders (flour, milk, dried cream, cocoa powder) through its hygroscopic properties. It might also be added as a supplement. [213]

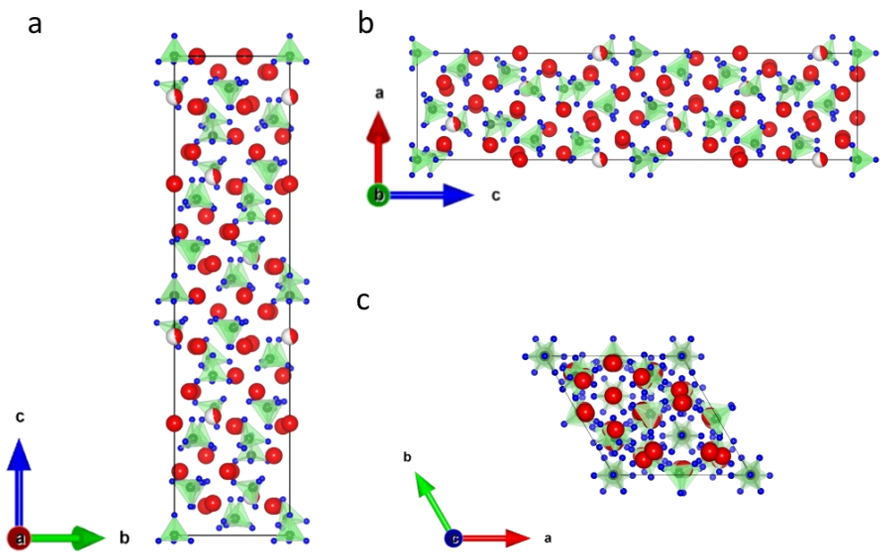

***Figure 4**. Unit cell of β-TCP shown from the **a)** a-axis, **b)** b-axis and **c)** c-axis. Created with Vesta Ver. 3.5.7 [187]; Ca^{2+}: red orbs, PO_4^{3-}: green (P^{5+}) tetrahedrons with blue dots(O^{2-}).*

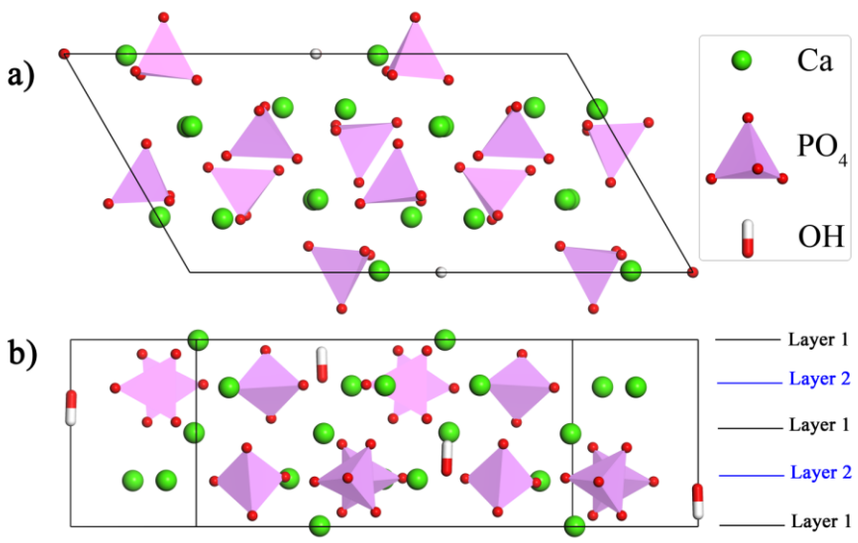

***Figure 5**. Crystal structure of hydroxyapatite (HAp, $Ca_{10}(PO_4)_6(OH)_2$) presented from **a)** the top (c-axis) and **b)** the side; Ca^{2+}: green orbs, PO_4^{3-}: pink tetrahedrons, OH^-: red and white tablets. Reprinted with permission from [214].*

Hydroxyapatite (HA or HAp)

Hydroxyapatite is usually written as $Ca_{10}(PO_4)_6(OH)_2$ even though it can be shortened to $Ca_5(PO_4)_3(OH)$, but as its unit cell contains two formula units this is ignored.(**Figure 5**) It is the second most stable CaP after fluorapatite and the least soluble.(**Table 1**) HAp is composed of two different kinds of layers that repeat along the c-axis. Layer 1 (**Figure 5**) only contains calcium ions, whereas Layer 2 contains both calcium and phosphate ions. Between these layers the OH^- ions can be found. [215-218]

Its crystal structure shows monoclinic symmetry in the space group $P2_1/b$ [218, 219], which is transformed to the hexagonal space group $P6_3/m$ above ~250°C. [173, 218, 220, 221] During this transition only the orientation of the OH^- inside the crystal lattice changes. The hexagonal variant is not stable as the shift of the OH^- ions may induce strain into the lattice. This strain can be compensated by vacancies or substitutions. This is also the reason why hexagonal HAp is mostly substituted and very rarely stochiometric at ambient temperature.

HAp can be synthesized in ambient conditions through wet methods and from solid-state reactions. [222] Wet methods include hydrothermal synthesis, precipitation and hydrolysis of other CaPs like α-TCP. As with previous CaPs the Ca/P ratio is crucial. To obtain phase pure HAp it has to be exactly 1.67.(**Figure 2**, **Table 1**) But even then, as described earlier, HAp seldomly precipitates stochiometrically. This implies the formation of precursors like the non-crystalline amorphous calcium phosphate (ACP) or the calcium deficient hydroxyapatite (CDHA). This can be prevented in high pH (10-11) and higher temperature (>90°C). [223]

Though HAp is never pure in a biological setting, it is commonly used as a component in medical application, be it as coatings, dental implants [224-226] or bioceramics. [227-229] Aside from biomedical usage HAp has a wide variety of applications across a large field.

Calcium deficient hydroxyapatite (CDHA)

This non stochiometric HAp also called calcium deficient hydroxyapatite, due to the lack of one calcium ion compared to HAp, with the formula $Ca_{10-x}(PO_4)_{6-x}(HPO_4)_x(OH)_{2-x}$ ($0<x<1$) is known to literature since the 1770s. [230, 231] The crystal structure of CDHA not only shows Ca vacancies but also OH vacancies. This is accompanied by protonation of some PO_4 groups leading to further vacancies. [232] These vacancies may be compensated by substitution of OH^- with neutral H_2O. [233]

It can be prepared similarly to the wet methods for HAp, but the Ca/P ratio may vary between 1.5 and 1.67 influencing the degree of deficiency. A common method is to boil a calcium and phosphate rich solution for several hours and subsequently precipitate CDHA. [234, 235] The easiest way of synthesis is the hydrolysis of α-TCP. [191-193] Like HAp, the precipitation pathway of CDHA initially forms ACP as a precursor phase, which transforms then to the crystalline and stable CDHA. CDHA exhibits a poorly crystalline structure, when precipitated. As mentioned previously it can be converted to β-TCP above ~700°C when the Ca/P ratio equals 1.5. Otherwise it is a biphasic mixture of HAp and β-TCP. [236]

In a biological context CDHA is always doped with a variety of ions: Na^+, K^+, Mg^{2+}, Sr^{2+} substitute Ca^{2+}, CO_3^{2-} substitutes PO_4^{3-} or HPO_4^{2-} and F^- or Cl^- replace OH^-. Together with some water this forms the main inorganic component of human and animal normal and pathological calcifications. [86, 113, 115] Hence, CDHA is one of the most important materials for bone replacement applications. [237]

Amorphous calcium phosphate (ACP)

This member of the CaP group is the only non-crystalline phase with variable composition. It was first described in 1845 [238] and for the longest time viewed as a unique CaP, when it is more the amorphous state of all members in the CaP group. [239] There are two groups of ACPs as all other CaPs can also be divided into low-temperature (precipitation) or high temperature (solid state synthesis). [239] ACP was earlier described as a precursor to HAp or CDHA during hydrolysis. This happens in the form of low-temperature ACPs ($Ca_xH_y(PO_4)_z{\cdot}nH_2O$ n=3-4.5) precipitating in supersaturated solutions of calcium and orthophosphate salts [218] in the form of spherical particles in the diameter range of 200-1200 Å. The size decreases with higher pH and increases with the temperature. [240] These ACP spheres subsequently recrystallize as more stable crystalline CaPs like CDHA [218]

ACPs find application in self-setting CPCs [57], as a component in bioactive composites [239, 241] and in surgery [239, 242]. Apart from medical applications ACPs also have a use e.g., in food industry as clearing for syrups.

Octacalcium phosphate (OCP)

The CaP with the highest water content, Octacalcium phosphate (OCP, $Ca_8(HPO_4)_2(PO_4)_4{\cdot}5H_2O$), is, just like ACP, found to be a transitional stage during the hydrolysis of one better soluble CaP to a less soluble. It is known since 1843 [243] and can be prepared through a variety of pathways. [244-247] Similarly to ACP and other low-temperature CaPs it can be precipitated from supersaturated solutions containing Ca and PO_4 ions, as long as the Ca/P ratio equals 1.33. OCP forms very small plate-like crystals. Its crystal structure is triclinic with the space group $P\bar{1}$. [248] Its unit cell has an apatite layer with a similar composition as HAp enclosed by two hydrated layers.(**Figure 6**) [249] The transition from OCP to HAp happens by the elimination of the described hydrated layers.

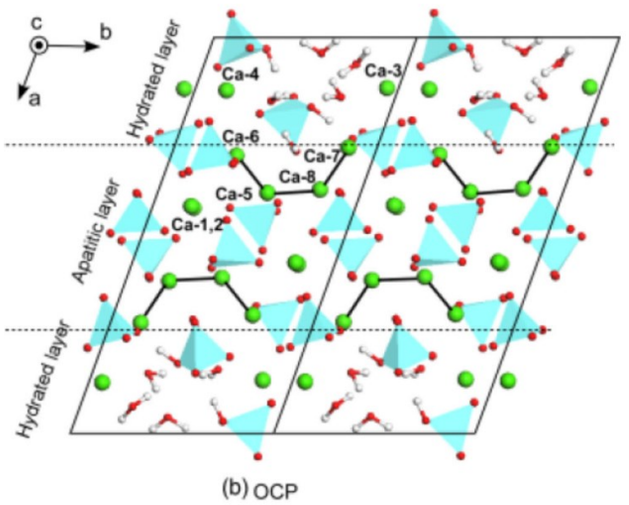

***Figure 6**. Crystal structure of octacalcium phosphate (OCP, $Ca_8(HPO_4)_2(PO_4)_4{\cdot}5H_2O$) oriented along the c-axis. Ca^{2+}: green orbs, PO_4^{3-}: light blue tetrahedrons, H_2O: red and white sticks. Reprinted and modified from [248] under the terms of the Creative Commons Attribution 4.0 International License (CC BY 4.0).*

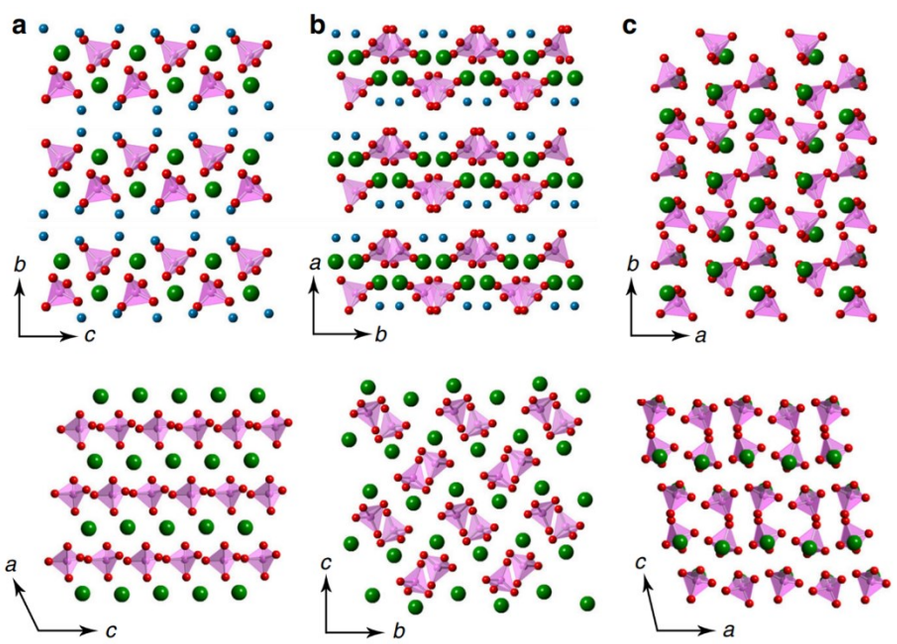

***Figure 7**. Crystal structures of **a)** Brushite (DCPD, $CaHPO_4{\cdot}2H_2O$) along its a-axis **(top)** and its b-axis **(bottom), b)** Dicalcium phosphate monohydrate (DCPM, $CaHPO_4{\cdot}H_2O$) along its c-axis **(top)** and its a-axis **(bottom)** and **c)** Monetite (DCPA, $CaHPO_4$) along its c-axis (top) and its b-axis (bottom); Ca^{2+}: green orbs, PO_4^{3-}: pink tetrahedrons, O of H_2O: blue orbs. Reprinted and modified from [174] under the terms of the Creative Commons Attribution 4.0 International License (CC BY 4.0).*

Brushite (DCPD), Monetite (DCPA) and DCPM

The mineral known as brushite is also abbreviated DCPD in the context of CaPs and is known since 1804.[250] As a natural mineral it was discovered in guano on Avis Island (Caribbean).[251] Its synthesis is like most other CaPs a precipitation of crystals from a supersaturated solution containing calcium and phosphate ions. The important factors are again the Ca/P ratio equalling 1, while the pH is in the range from 2.0 to 6.5. [252] It may also be prepared by neutralization of phosphoric acid or MCPM solutions with a calcium source. This source is commonly CaO, $CaCO_3$ or a basic CaP. As the name states, DCPD contains two water molecules per formula unit. This water is stored in layers between calcium and phosphate layers. (**Figure 7 a**; blue water layers between green and pink layers) These layers alternate along the b-axis of the monoclinic crystal lattice. [253]

This crystal water is lost at temperatures above ~80°C and leads to a ~11% volume decrease during the transformation to the triclinic anhydrous Monetite (DPCA) (**Figure 7 b**). [254] The anhydrous DCPA was not known until 1879 [255] and described as the mineral monetite before 1882 found in Puerto Rico. [256] As a result of the absence of water in the crystal lattice, it is less soluble than brushite (**Table 1**). Just like its water containing counterpart DPCD it can be precipitated under the same conditions but at elevated temperatures (>90°C). Its formation can also be favoured, if the availability of water is limited or no water is present at all. This is achieved in gels [257], ethanol [258] and in water-oil/oil-water systems. [259]

In contrast to DCPA, DCPD can be found in pathological calcifications. [86, 115, 116] Nevertheless both DCPD and DCPA are used in medicine as components of self-setting CPC formulations. [57] DCPA also gets implanted as a bioceramic. [260]

In line with other CaPs, DCPA and DCPD also find usage in the food industry. DCPD can be used as a calcium supplement in food. Further it is used to adjust texture, help in bakery and serve as a water retention additive. Lastly dairy industry uses it as a mineral supplement. Also DPCA finds usage as nutritional supplement in cereals or noodle products and as a dough conditioner. [195]

DCPM was only recently discovered in 2020 [174] and is not yet fully established as a cement phase. In water it is reported to be stable for half an hour and then transform into poorly crystallized HAp within the next 30 minutes. It can be stabilized in water by the addition of citrate salts for at least 2h or even longer when adding sodium polyacrylate. The solution pH of a DCPM solution can reach values of 8.2, which makes it the highest among the DCPX variations. They also report it having the highest solubility among the DCPX variations, but no definitive value is known yet. Another noteworthy property of DCPM is its high adsorption capacity for different drugs like ibuprofen. This might make it a suitable material for drug delivery applications.

Bi- and Tri-phasic CaPs

Briefly, all mentioned CaPs might also be fabricated in a mixture of two or more different minerals. The minerals phases can either be of the same Ca/P ratio (e.g., α- and β-TCP) or of different values (e.g., HAp and β-TCP). The resulting multiphase formulations can further be specified by their preparation conditions. A difference is made between heating a compound of non-stochiometric ACP [261-263] or CDHA above ~700°C or bringing stochiometric compositions up to a temperature of above 1300°C. [236]

These material mixtures offer more flexibility and adjustment possibilities in their properties (bioactivity, bioresorbability, osteoconductivity and osteoinductivity), as two CaPs can behave different in the same environment. As an example, in a mixture of HAp with a TCP [185, 264-267] the apatite is less soluble, therefore an increasing amount of it leads to a slower resorption and vice versa. [236]

Magnesium (MgP), Calcium Magnesium (CaMgP) Phosphate and Calcium Silicate (CaSi) minerals

Aside from CaP based mineral bone cements also magnesium phosphate (MgP, MgO - P_2O_5), calcium magnesium phosphate (CaMgP, CaO – MgO - P_2O_5) and calcium silicate (CaSi, CaO - SiO_2) cements are used. The difference of minerals from these classes to the aforementioned CaP minerals is first of all the lower amount of research done for an application as biomaterials. Most relevant MgPs show a Mg/P ratio between 1 and 1.5 similar to the Ca/P ratio found in brushite, monetite, DCPM, and the TCP variants (**Table 2**). An equivalent to HAp with a ratio of 1.67 is not present in the MgP system. Compared to the CaP counterparts the MgP phases show an increased amount of crystal water and can be precipitated from aqueous solution. [268, 269] Except for Newberyite ($MgHPO_4 \cdot 3H_2O$), all other MgPs dissolve incongruent. [268] Through high temperature calcination the water containing MgPs can be converted into magnesium pyrophosphate ($Mg_2P_2O_7$) or the TCP equivalent orthophosphate farringtonite ($Mg_3(PO_4)_2$). [270, 271] Just like CaPs, MgPs can incorporate several cations in their crystal structure like Na^+, K^+ or NH_4^+. [270, 272-275] The latter is of special interest for MgPs as the incorporation of ammonium ions into the MgP crystal allows for the precipitation of another group of minerals not present in the CaP system. Dittmarite (dimagnesium ammonium phosphate monohydrate, $MgNH_4PO_4 \cdot H_2O$), schertelite (dimagnesium ammonium phosphate tetrahydrate, $MgNH_4PO_4 \cdot 4H_2O$), struvite (dimagnesium ammonium phosphate hexahydrate, $MgNH_4PO_4 \cdot 6H_2O$) [276] and hannayite ($(NH_4)_2Mg_3(HPO_4)_4 \cdot 8H_2O$) [277] are the most common representatives of this group.

While these were pure MgPs or ammonium substituted MgPs, also magnesium substitution for CaPs (CaMgP) can be of interest. The presence of Mg^{2+} ions can inhibit the crystallization of CaP phases and promote the formation of amorphous phases. This is an effect of the active growth sites being blocked by the Mg^{2+} ions. [278-284] This retardig effect is discussed further in the section about cement modification. As already mentioned above, β-TCP can be stabilized with Mg^{2+} even >1125 °C and prevent the phase conversion to its α variant resulting in a particular dense monolith. [285, 286] Here up to 14 mol% Mg^{2+} can be incorporated which then leads to formation of the mineral whitlockite. [287, 288] The magnesium doping leads to a decreased solubility, but improves the mechanical behaviour, of the tricalcium phosphate. [289]

***Table 2**. Minerals in the NH_4-MgO-P_2O_5 system, their corresponding solubility product constants and solubilites calculated at 25 °C, Reprinted and modified with permission from [290].*

Mg/P ratio	MgP compound	Chemical formula	Solubility -log(K_{sp})	Solubility mg/l
-	Magnesium oxide	MgO	25.0	$1.27 \cdot 10^{-8}$
-	Brucite	$Mg(OH)_2$	11.2	6.79
0.5	Schertelite	$(NH_4)_2Mg(HPO_4)_2 \cdot 4H_2O$	-	-
0.75	Hannayite	$(NH_4)_2Mg(HPO_4)_2 \cdot 8H_2O$	-	-
1	Newberyite	$MgHPO_4 \cdot 3H_2O$	5-51-5-82	$(1.69\text{-}2.54) \cdot 10^3$
1	Struvite	$NH_4MgPO_4 \cdot 6H_2O$	9.94-13.4	8.38-119
1	K-Struvite	$KMgPO_4 \cdot 6H_2O$	10.6	78.0
1	Dittmarite	$NH_4MgPO_4 \cdot H_2O$	-	-
1.5	Farringtonite	$Mg_3(PO_4)_2$	23.4	2.15
1.5	Bobierrite	$Mg_3(PO_4)_2 \cdot 8H_2O$	25.2	1.46
1.5	Catiite	$Mg_3(PO_4)_2 \cdot 22H_2O$	23.1	6.2

Also, HAp can have a tenth of its calcium substituted by magnesium. [291, 292] As magnesium has a smaller ion radius this leads to a reduction of lattice parameters [293] and crystallinity of HAp. [291, 292] The doping of HAp increases its solubility compared to non-doped stochiometric HAp probably as a result of the reduced crystallinity and/or an increased surface hydration. [293, 294] On the other side of the CaP spectrum is brushite, which can also be substituted with magnesium. Here the substitution enables brushite to be stable under physiological conditions without converting to HAp. [295]

Apart from these phosphates also silicates are of interest for a biomedical application. Relevant representatives of this group are tricalcium silicate (alite, Ca_3SiO_5, C_3S) and dicalcium silicate (belite, Ca_2SiO_5, C_2S). [296-298] These calcium silicates make up about 75% of the fully set portland cement. [299] The main active component of the clinker is alite (C_3S), which is responsible for the strength development up to 28 days after starting the setting reaction. [300-302] It has a nesosilicate structure, meaning it contains $[SiO_4]^{4-}$ tretrahedrons which can bond with metal ions such as calcium, magnesium, iron and more. [303] Like the TCPs also alite shows a polymorphism dependend on the temperature and impurities. From lower to higher temperature alite can crystallize in the triclinic (T alite), monoclinic (M alite) and rhombohedral (R alite) crystal system. Here the symmetry increases with the temperature, but the unit cell size decreases. [304-307] Belite (C_2S) is the second most important clinker phase.

In contrast to alite it has a slow reactivity in the early stages of the setting, but accounts for the main compressive strength of the set cement. Aside from that it also improves the durability of the cement in terms of resistance to drying, shrinkage or chemical attack. [308] As with alite and the TCPs also belite shows polymorphism. Here the potential crystal structures also change with the temperature and impurities and range from monoclinic (β belite), orthorhombic (α' belite) to hexagonal (α belite) with increased synthesis temperature. There is also the possibility for a γ belite at temperatures between β and α' belite, but it is the least desirable phase as it is non-reactive with water. [298, 309] There is also a x belite variant reported. [303] It is reported to show "tunnels" which enable higher reactivity than usual for belite. [303]

These are mostly accompanied by different other minerals in varying quantities from the aluminate or sulfate group like tricalcium aluminate (celite, $Ca_3Al_2O_6$, C_3A), calcium sulfate (anhydrite, $CaSO_4$, C$). These minerals dissolve in an aqueous solution and produce mainly portlandite ($Ca(OH)_2$) and amorphous calcium silicate hydrate gel (C-S-H) that solidifies subsequently. [310-312] These materials are mainly used in endodontic procedures like pulp capping, apexogenesis or root end filling. [313-315] An important difference of the CaSi based minerals to the others presented here is the lack of resorbability *in vivo*. The main use cases for these types of cements in a biomedical application are therefore aimed towards permanent augmentations. [316]

Like most reactive CaPs also these calcium silicates are usually synthesized by a high temperature solid state reaction. The simplicity of the process is the main advantage, but the high energy cost and high carbon footprint due to calcination of one of the main educts calcite, increased the attention to alternative synthesis routes. [317, 318] These include Pechini, sol-gel, solution combustion or to a lesser extent also aerosol methodologies. [319]

2.2 Cement systems

A cement is by definition a binder that sets, hardens and binds with other materials. [320] The first known human use of such a material was in ancient Rome under the name of *"opus caementitium"*. This material contained a varying combination of components: typically fly ash, volcanic dusts, tuff and rubble. [321] Nowadays the most common cement is the so-called *"Portland cement"* or *ordinary Portland cement* (OPC) it was first presented by Joseph Aspdin in 1843 [322] and contained a mixture of calcium silicates, aluminates, ferrite and gypsum. [296-298, 323] Its mainly used as a construction material and obtained from limestone and clay. [296] Following the example set first by the romans, then researched more in detail with the same purpose of building construction and civil engineering by researchers like Joseph Aspdin, nowadays many different cements with a variety of applications are being used and improved all over the world. These can be of inorganic nature like the initial examples or just take the general idea of a powder mixed with a liquid leading to a reaction that produces a paste setting into a solid product while being composed of organic monomers, polymers and/or initiators.

Non mineral cements

Suitable bone replacement cements can also be of a non-mineral fashion. Polymethyl methacrylate (PMMA) finds good use in surgery since 1943. [324] The cement sets via polymerization of a MMA monomer solution mixed with a MMA-styrene powder. [324] This reaction is an exothermic free-radical polymerization process and heats up to about 82-86°C. [325, 326] This high temperature during setting is its main drawback compared to most mineral bone cements.

Mineral cements

Hydraulic mineral cements set at significantly lower temperatures and via six distinct categories of steps involving a collection of chemical processes. [327] The categories, in usually consecutive but sometimes also in a parallel or more complex order, are:

1 *Dissolution/dissociation* in water is described by the disintegration of the cement powder surface layer. [328, 329]
2 *Diffusion* involves the transfer of the dissolved material within the paste porosity (mechanism 5, 14) or in the adsorption layer on the solids surfaces. [330, 331]
3 *Crystal* Growth is the first counterpart to the dissolution step and is characterized by a surface attachment and assembly of the dissolved material into an amorphous solid or a crystalline structure within its self-adsorption layer. [332]
4 *Nucleation* further promotes the crystal growth through precipitation of solids in a heterogenous or homogenous way on solid surfaces or in solution, respectively. [333]
5 *Complexation* is the process of different reactions occurring between ions to form ion or adsorbed molecular complexes on solid surfaces. [334, 335]
6 *Adsorption*, once a solid particle is formed, other ions or molecular units can accumulate on its interface with the surrounding liquid. [330, 332, 334]

The first four steps can control rate and the kinetics of the whole hydration reaction of a cement, and this makes it a very complex process to understand and describe in detail. [327] Many of the aforementioned CaPs can be synthesized through a precipitation pathway. Because the mechanism of dissolution and precipitation is the fundamental form of hydraulic cement hardening, they are suitable as material for a mineral cement and due to their composition, they fit for a bone replacement application. [336-338] Their precipitate can either be a conglomerate of crystals or a gel, so the hardening of these cements can be attributed to either a sol-gel transition [339] or the entanglement of the newly formed crystals [61].

2.2.1 Calcium phosphate cement (CPC) systems

To be able to turn a CaP into a calcium phosphate cement (CPC), the only requirements are a soluble CaP (preferably low Ca/P ratio and high acidity), a less soluble possible CaP at the given temperature and pH and a solvent (mostly water, phosphate buffered saline (PBS), sodium orthophosphate solutions (~0.25 M), orthophosphoric acid, citric acid (~0.5 M)[340], sodium silicate[341, 342], magnesium hydroorthophosphate[343] or revised simulated body fluid(rSBF) [344].

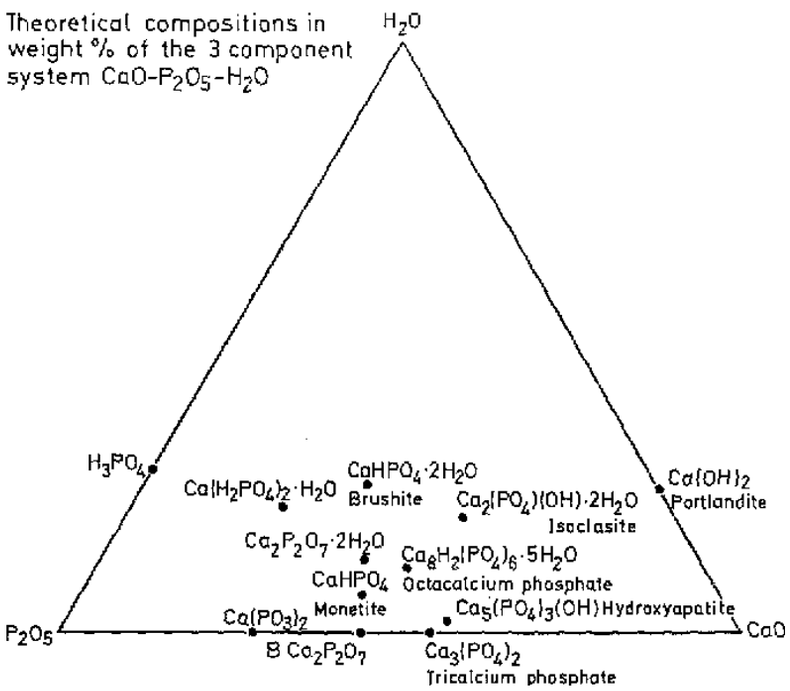

Figure 8. *Theoretical compositions in the ternary system of CaO, P_2O_5 and H_2O. Reprinted with permission from [345]. Values are presented in wt%.*

Figure 8 shows the ternary system of CaO-P_2O_5-H_2O and the twelve possible non-ion substituted CaPs, that can be formed. It is clearly visible, that even though water is not only necessary as a solvent, but also functions as a reaction partner, not a lot of water is incorporated into the products of the possible cement reactions.[338, 346, 347] The hydration product incorporating the most water during precipitation is brushite. CPCs can set generally through two types of reactions.

In literature the cement reaction has been separated into two types of reactions: acid-base reactions and hydrolysis. As with some nomenclature in literature some researchers started to use specific terms, more adapted the term and nobody would look at it critically again. Though, if looked at critically, all mineral bone cements set via a typical solution precipitation mechanism governed by the solubility of the initial mineral components in the used aqueous liquid and the following precipitation of less soluble minerals that interlock into a set mechanically stable cement. The reactions described as acid base cement reactions could be described as multi mineral component cements and the ones described as cement setting via hydrolysis can be described as single mineral component systems. But because the declaration of these cement types as acid-base and hydrolysis cements is the prevailing opinion in literature, these will be described as such in the following overview.

Acid-base reactions

In cements setting by an acid base reaction the components (e.g., one acidic and one basic) react to a neutral product. The cement system described by Brown and Chow, and consisting of a powder mixture of monetite (slightly acidic) and TTCP (basic) in an aqueous solution reacting to HAp (neutral), shows this perfectly ***Eq.(1)***[336, 348-350]:

$$2CaHPO_4 + 2Ca_4(PO_4)_20 \rightarrow \ Ca_{10}(PO_4)_6(OH)_2 \qquad \textbf{\textit{Eq.(1)}}$$

The same reaction with brushite instead of monetite yields two additional molecules of water.[351] Neither acidic nor basic products are released by these reactions, thus the pH remains around neutral. The products in ***Eq.(1)*** however are only half correct, when describing the whole setting process, as only the first precipitations yield stochiometric HA and any further growth happens in form of CDHA. [352] As a second example, the reaction between the almost neutral β-TCP and the acidic MCPM to form the less acidic DPCD presented by Lemaitre et al.[353] illustrates the results do not have to be neutral. ***Eq.(2)***

$$\beta\text{-}Ca_3(PO_4)_2 + Ca(H_2PO_4)_2{\cdot}H_2O + 7H_2O \rightarrow 4CaHPO_4{\cdot}2H_2O \qquad \textbf{\textit{Eq.(2)}}$$

This equation can serve as a template for many different reactions by swapping out either reaction partner e.g., β-TCP for α-TCP[354, 355],CDHA or HAp[356, 357] and MCPM with orthophosphoric acid[358-361]. Many of the commonly investigated and/or used self-setting CPC formulations based on the reaction mechanism demonstrated above. These include ACP + α-TCP [362], ACP + DCPD [363, 364], OCP + TTCP[365] or OCP + α-TCP[366, 367].

Hydrolysis

In contrast to the acid-base reaction-based cements the formulations utilizing a hydrolysis setting do not use a combination of two CaPs of different Ca/P ratios to result in a CaP of a third Ca/P ratio. These cements are characterized by the same Ca/P ratio for educt and product. This means, judging also by the name, an aqueous solution, possibly deviating from plain water as described earlier, is necessary to enable the reaction. A typical reaction working this way is the hydrolysis of TCP to CDHA shown in ***Eq.(3)***[191-193, 368-376]:

$$3(\alpha \text{ or } \beta)\text{-}Ca_3(PO_4)_2 + H_2O \rightarrow Ca_9(HPO_4)(PO_4)_5(OH) \qquad \textit{Eq.(3)}$$

Other common CaPs undergoing a hydrolysis reaction are ACP [377, 378], DPCD [341, 379], CDHA [342] and TTCP [343, 380-382]. Most of them result in a recrystallization to CDHA, but might be altered by an adjustment of the aqueous solution.[383] CPCs can chemically be characterized by their reaction mechanism, but for a material scientific point of view the results of the various reactions is of much higher importance. **Figure 9** shows the solubility phase diagrams for the $CaO\text{-}P_2O_5\text{-}H_2O$-system dependant on the pH. It is directly visible, there are two distinct end products for a CPC: calcium deficient/ hydroxyapatite (CDHA /HAp) or brushite/Monetite (DCPD/DCPA) mostly dependant on the pH of the solution they are precipitated from with a value either above 2.5 **(a)** or 4.2 **(b)** for apatite or below for brushite dependent on the solubility product of **(a)** Ca^{2+} or **(b)** $H_2PO_4^-/HPO_4^{2-}$. Hence CPCs are usually divided into (hydroxy)apatite- and brushite-forming systems.

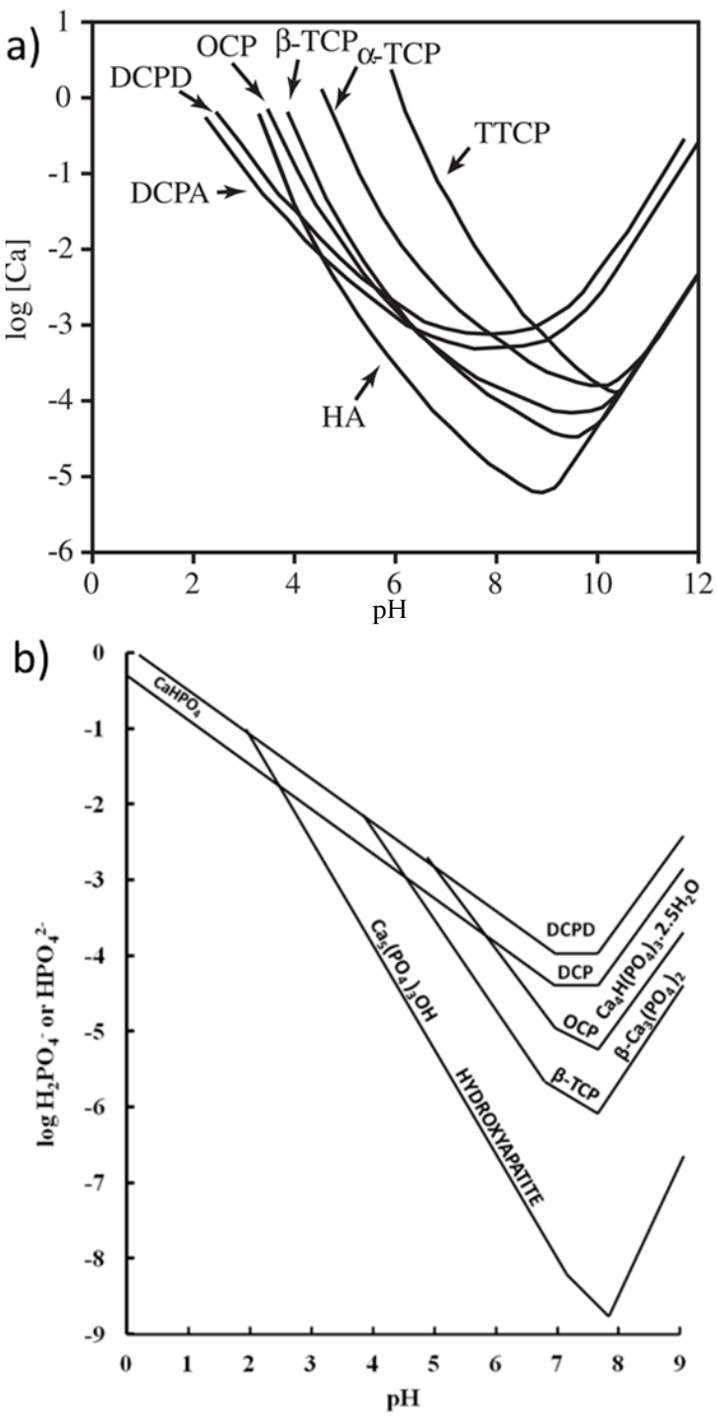

Figure 9. *Solubility phase diagrams dependent on the pH value for the ternary system, $Ca(OH)_2$–H_3PO_4–H_2O, at 25 °C, showing the solubility isotherms of $CaHPO_4$ (DCPA), $CaHPO_4{\cdot}2H_2O$ (DCPD), $Ca_8H_2(PO_4)_6{\cdot}5H_2O$ (OCP), α-$Ca_3(PO_4)_2$ (α-TCP), β-$Ca_3(PO_4)_2$ (β-TCP), $Ca_4(PO_4)_2O$ (TTCP), and $Ca_{10}(PO_4)_6{\cdot}(OH)_2$ (HA).* ***a)*** *Reprinted with permission from [384] and* ***b)*** *from [385] under the terms of the Open Archive TOULOUSE Archive Ouverte (OATAO).*

Theoretically the starting material reacts fully to the corresponding products, but in reality there is almost always residual educt. [386]

Apatite cements

The cement reactions presented in ***Eq.(1)*** and ***Eq.(3)*** result in the formation of HAp or CDHA with a Ca/P ratio between 1.5-1.67 and are therefore those of apatite-forming cements. [387] CDHA is mainly formed if the reaction takes place in an aqueous solution and crystallizes similarly to the aforementioned biological apatite (dahlite), which can be the cause of their good *in vivo* behavior, when they are set completely. [388] This might also be the case for its description of a biomimetic setting process, as the reaction also runs in a physiological environment at 37°C. [62] Due to them reacting and precipitating at practically neutral pH and being of similar composition of bone mineral, they are very stable inside the body. But they still may be slowly [389] dissolved and resorbed with the same mechanism as for natural bone mineral by a locally lowered pH induced by osteoclasts.[390]

Brushite cements

With a Ca/P ratio of 1 the chemical equation shown in ***Eq.(2)*** results in the formation of brushite (DCPD).[353, 391] By looking at **Figure 9**, it is obvious that they are not formed at physiological pH and all of them are set through an acid-base reaction. Therefore the cement is always acidic while setting [87, 360], but changes slowly to its equilibrium pH afterwards. [359] Even though brushite does not mimic the composition of natural bone it is very biocompatible. [87] Bringing the cement into physiological conditions (e.g., by implanting) brings it into a meta stable condition [392], in which it degrades by itself. This takes place faster and without the additional aid that apatite cements need. [393-395] Because of this brushite cements can cause immature bone formation by a sometimes too fast degradation rate, but there are studies solving this issue with the addition of β-TCP granules. [396, 397]

Monetite Cement

The same Ca/P ratio can be found in the mineral monetite (DCPA) and its therefore formed by so called monetite cements. The reaction is very similar to the brushite forming reaction in ***Eq.(2)*** just two less water molecules are needed. The formation of monetite against that of brushite is therefore directly governed by the availability of water during the reaction. Additionally, the ion strength is a controlling factor in the formation of monetite. Like its water rich companion brushite also monetite is very soluble *in vivo* with a solubility product of 6.63 -log(K_{sp}) and 7.02 -log(K_{sp}) at 37°C respectively. [337] So much that it even surpasses brushite in its resorption time and also its mechanical properties due to the small nanosized monetite crystals forming and interlocking. (56, 57,58)

OCP cement

The last cement that is important to note here is a cement resulting in octacalcium phosphate (OCP). OCP is often a by-product of an apatite forming cement or can be found as a precursor to HA as the final product. It can be prepared by a mixture of MCPM, calcium carbonate (Cc) and α-TCP (3:5:9 mol) combined with a sodium hydrogen phosphate buffer solution (pH 7.4). [398] There is a variety of proposed benefits and possible composite formulations discussed in literature. [399]

2.2.2 Cement properties

Setting time

Both previously presented systems have different setting times, but to be applicable as a bone replacement material they have to set within a specific time frame. They should set slow enough to be able to be applied without the risk of preliminary setting and compromising the grafts properties, while also setting fast enough to not freely flow out of the intended application site. Their setting behaviour can be described by two factors. The initial (T_i) and the final (T_f) setting time. Generally, two approaches are used to determine these times. Firstly, the Vicat needle method (ASTM C191-92) [400] and secondly the Gilmore needle method (C266-89) [401]. Both methods use a combination of a physical test and a visual examination of the sample. They use standardized weights/forces applied (DIN EN 196-3:2005(D) and EN 13279-2:2004(D)) onto the sample surface and then evaluate the time point that does not show an indentation. The last method can also be optimized by using an Imeter (MSB Messysteme, Augsburg, Germany) which automatically repeats the measurement on a fresh surface spot until the time points for T_I and T_F have been reached. As this method measures the force directly and no visual examination is needed, it is also more precise. The setting process can also be recorded continuously without destroying the sample e.g., via pulse-echo ultrasound [402, 403], isothermal scanning calorimetry [344, 370, 372, 404-408] or alternating current impedance spectroscopy [409] (see the methods section for calorimetry and I-meter measurements)

The desired values for T_I and T_F can be described as *"$3 \leq T_I \leq 8$"* and *"$T_F \leq 15$"* (values in min [61]). Additionally, the time of cohesion (T_C), the time when the paste stops to fall apart in a Ringer's solution, has to be 1 min (when mixing in a mortar 2 min) minimum. [410] In a practical clinical setting these times mean the paste should be prepared latest until T_C, applied until T_I and the wound can be closed after T_F. [61, 410].One should not that, even after T_F has been reached, only about 5-15% of the reaction has been progressed and it will usually go on for a couple of days. [371, 386]

Apatite cements usually set slow (15-20 min) [336, 348], but this has been addressed in a number of ways, either by lowering the liquid amount (lower L/P) or by the addition of additives (e.g., MCPM, H_3PO_4 or sodium phosphate salts). [339, 368, 370, 372, 374, 377, 381, 411, 412] The particle size (reduction accelerates the reaction) [413-415], the temperature and the presence of initial particles to aid nucleation (e.g., ~10% HAp powder) also influence the setting time and may be adjusted accordingly.[62, 336, 348, 416, 417]

For brushite cement one important factor to regulate the setting time is the solubility of the basic component involved in the acid-base reaction. The higher the solubility of that phase the faster the reaction runs. [56, 418] The setting times increase in the following order: HAp (few minutes) > β-TCP (0.5-1 minute) > α-TCP (few seconds).[353, 391].In contrast to apatite cements the intend with brushite cements is to delay the reaction to a suitable time. Here also different additives may be used to achieve that. [418] With citric acid or sodium citrate the paste handling may be improved. [340, 382, 419-421] Chondroitin 4-sulfate [422] or glycolic acid [423] have a comparable effect. Additionally the presence of magnesium ions can inhibit the setting mechanism [424] and reduce the setting time [56, 418].

Injectability and Rheology

The setting time is one of the regulating factors of the paste's behaviour. The chemical and physical process during setting is directly reflected in the paste viscosity. [425] Cement pastes are a suspension of small particles in a liquid. As described above these particles dissolve first and later new particles precipitate and grow. Therefore, the viscosity first decreases and later increases until the cement is set. The desired viscosity varies with the application. For a manual application with the surgeon's fingertips a high viscosity is needed to ensure good handling. If the paste is to be injected from a syringe the viscosity has to be low in comparison. [426] Literature suggests the injection option to be the preferred one at the moment. The comparatively low viscosity should be kept in the range of 100-2000 Pa·s to avoid high injection forces, while simultaneously prevent the loss of cohesion. [427]

An injection route as the chosen way of application requires several properties from the cement paste. A fitting viscosity is one part to achieve a good injectability, but cohesion after injection is also very important. [428, 429] As a means to quantify the injectability of a paste, one should specify the term. Injectability is the value used to describe the paste's ability to be pressed from a syringe through a needle (generally Ø 2mm [427, 430], but can vary [431, 432]) It is displayed as (***Eq.(4)***) the quotient of the difference between the initially loaded cement (m_i) and the residual cement (m_r) after injection divided by the amount that was initially loaded (m_i) in percent.

$$\frac{m_i - m_r}{m_i} \cdot 100 \qquad \textit{Eq.(4)}$$

This percentage is calculated after the filled syringe has been loaded with a defined maximum load (Usually 100 [410]-300N [340]).

A schematic of the experimental setup is shown in **Figure 10**.

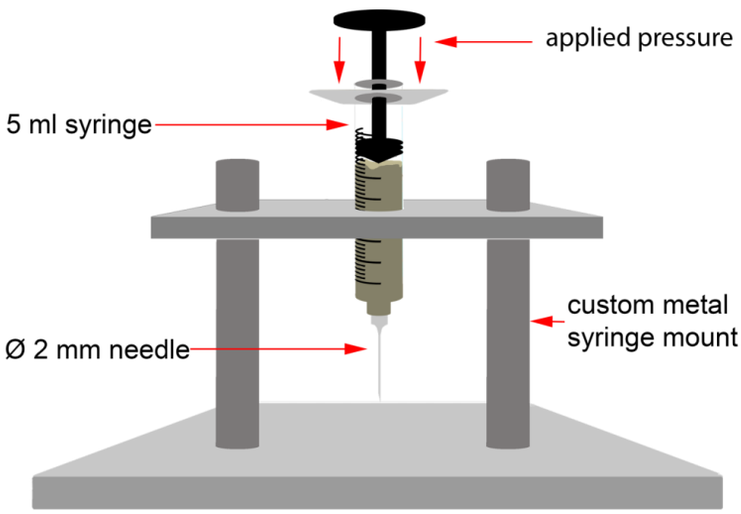

Figure 10. *Experimental setup of an injectability test.*

The process of injection can be seen as a flow of a viscous liquid through a tube. This allows the characterization of this process through rheological methods.[425, 433] Injectability and rheology of CPCs have been correlated in a wide arrays of studies already. [364, 432, 434-437]

A theoretical approach to this was done by Bohner and Baroud [427] and further described in [438]. They investigated several influencing factors on the injectability by a newly developed model combining the Hagen-Poisell equation (flow of the paste through the canulla) (***Eq.(5)***) with the derivative of Darcys Law (filtration of the liquid phase through the particle network) (***Eq.(6)***)

$$P_i = \frac{128\mu_p L_n Q_p}{\pi D_n^4} \qquad \textbf{Eq.(5)}$$

$$th^2 = \left(\frac{D_e^2}{150\mu_l}\frac{\varepsilon_m^3}{(1-\varepsilon_m)^2(1-\varepsilon)}P_c\right)t \qquad \textbf{Eq.(6)}$$

Where in ***Eq.(5)*** P_i is the injection pressure, L_n and D_n are length and diameter of the needle and Q_p and μ_p are the flow and viscosity of the paste. In ***Eq.(6)*** th is the thickness of the powder bed that acts as a filter and is described by the particle's diameter D_e, the water volume fraction of the paste and cake ε and ε_m, the time t, the pressure drop through the cake P_c and the viscosity of the liquid μ_l. They assumed that P_c and P_i are the same and the viscosity of the paste μ_p is further described by the Quemada result. (***Eq.(7)***)

$$\mu_p = \mu_l \left(1 - \frac{SVF}{SVF_{max}}\right)^{-2} \qquad \textit{Eq.(7)}$$

Where SVF_{max} (maximum solid volume fraction) was assumed to be equal to $1-\varepsilon_m$ and related to the plastic limit (PL), which is the minimum L/P to form a pasty cement. After conversion of SVF, ε and ε_m to mass ratios as in L/P and PL, the equation becomes: (***Eq.(8)***)

$$th^2 = \left(D_e^2 \frac{128}{150\mu} f(PL, L/P)) \frac{L_n}{D_n^4} Q_p\right) t \qquad \textit{Eq.(8)}$$

With ***Eq.(9)***

$$f\left(PL, \frac{L}{P}\right) = \frac{\rho_s PL^3 (1+\rho_s L/P)^3}{(1+\rho_s PL)(L/P-PL)^2} \qquad \textit{Eq.(9)}$$

This theoretical approach in ***Eq.(8)*** is not directly applicable to experimental results. The enhancing ability of an increased L/P in real experiments could be predicted by this model, but the positive effect of an increased viscosity was not predictable. [427] The reason for that was attributed to the simplifications made to handle the pressures during the process. In an experimental setup the pressure is much more complex. [439] Also the th was expected to increase with a decreased needle diameter (D_n), but the injectability tests did not reflect this expectation, probably due to a limited amount of data. [427]

This shows a lack of theoretical knowledge in the topic of injectability and rheology in combination with cement pastes. [438, 440] Experimentally the properties are monitored via rheometry. [428, 441-447] The measurement geometries of choice can be a rotational parallel plate setup with a varying shear rate (0 – 200 s^{-1}) [441, 443] or rotational cone [428]. These show that cement pastes exhibit a shear thinning behaviour. This behaviour suggests a breakup of a certain network during the injection or shearing process. The particles inside the suspension form a network of stacked (simplified) spheres and the constellation of this network is dependent on the particle size and the particle size distribution. (**Figure 11**)

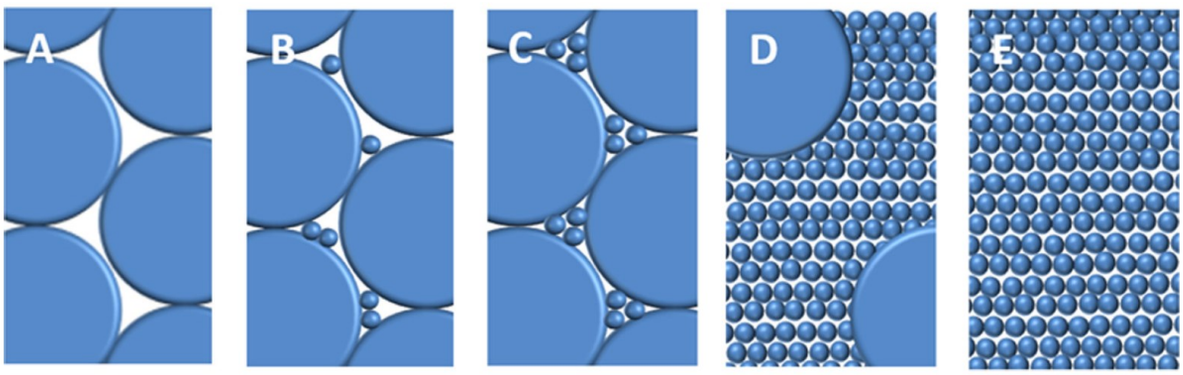

Figure 11. *Particle network dependant on the particle size and distribution shown as a schematic of mono-dispersed particles* ***(A and E)*** *and transitional bi-dispersed particles* ***(B, C and D)****. Reprinted with permission from [438].*

The addition of a small fraction of smaller particles to a powder of bigger particles can increase the solid volume fraction by replacing water inside the inter particle voids. This is one way to prevent paste separation, one of the main problems CPCs run into when they are injected. For example of the 4.5 ml of product available from Norian SRS® [48, 61] only 3 ml are injectable, probably due to this effect. [61] Many studies have addressed the issue of phase separation already, hence the knowledge is more advanced compared to the extrusion described before. [448-451] These studies could identify three mechanisms leading to phase separation:

1. *Filtration* in the syringe barrel causing the solid fracture to consolidate through the drainage of the liquids, leading to a regional change in L/P [452, 453]
2. *Suction* as the paste exits the die, expands to flow and creates dilation [449]
3. *Filtration in the needle* caused by the same effect as number 1, but further leading to a complete clogging of the needle by the formation of a solid powder mat. [451]

The mechanism of *filtration* (1) is a result of the syringe plunger pressing on the paste and trying to push it inside the die. This exerts a pressure on the paste and if this pressure is high relative to the permeability of the powder network the liquid will be pushed out of the spaces between the particles. [431, 450, 454] In pastes with a high SVF the particles have to move close past each other to be able to flow as a paste. This requires the, when not in motion, dense network to loosen by expanding the space between the individual particles. The creation of space imposes a negative pressure onto the liquid and the resulting *suction* (2) leads to an increase in the liquid content in the extrudate. [453] The same effect as in (1) can also happen when the *filtration happens in the needle* (3). The additional problem here is, that the areas of inhomogeneous L/P are big enough to completely clog the needle. These can get broken up by an increased force on the plunger, which leads to a liquid rich extrudate first and a solid rich

section afterwards often followed by a repetition of both. [451] Additionally, a good paste cohesion is a property preventing paste separation. [455]

Mechanical strength and Porosity

To function as a bone replacement material CPCs have to be on par with the mechanical properties of human bone. The lowest compressive strength (CS) of the hierarchical structure of human bone is found in the trabecular bone in the range of 4-12 MPa [456, 457] and the highest in the cortical bone measures around 130-180 MPa [457]. Compressive strengths of CPCs range from 10-100 MPa and suggest the ability to replace trabecular bone, judging only by the compressive strength.[458-460] Furthermore, this value can increase after the implantation, leading to a performance exerting values 60-70 MPa higher than normal bone. [461]. These values can be seen as mean values and might be on the lower end for brushite cements (CS 60 ~MPa)[462] or on the higher end for apatite cements (CS ~83 MPa). [463] But even though the compressive strengths fit very good for the usage as a bone replacement material, the forces that act on a bone graft are not only of compressive nature. Bones in the body experience a complex force combination of compression, bending, torsion and tension and the properties of CPCs only excel in the compression strength. [459] Their mechanical strengths comes from the entanglement of small crystals that form a network. [414] In compression these crystals are compressed even more dense until failure, while in tension the crystals interlock to withstand the force. [464] Pre-existing flaws lead the propagation of cracks formed during a brittle failure of these CPS. These flaws are much easier propagated in tension than in compression. [465] The performance of brushite and apatite cements is significantly lower in a tensile test with ~10 MPa [462] and ~16 MPa [466], respectively. However, these values do not give a usable impression of the performance under a cyclic load and due to their brittle nature CPCs are not directly comparable to human bone which are reinforced with collagen and exhibit a more flexible nature. Nevertheless, the materials are interesting for low to non-loadbearing defects and may even be improved to be used elsewhere. [467, 468] If implanted the cements properties do not stay the same over the course of time. Apatite cements have shown to be stronger to begin with [469] and this strength is increased further *in vivo*. [470] In contrast brushite cements decrease *in vivo* because the solubility is much higher compared to CDHA in a physiological environment. (**Table 1**) But implant sites of brushite cement increase their mechanical strength again after time, when new bone ingrowth occurs in the newly formed cavities of degraded brushite. [461] This ingrowth is propagated by the degradation of the cement implant forming bigger pores suitable for osteoblasts to enter. Normally hardened cements have pore dimensions that are too small for a fast bone ingrowth, which is a major drawback compared to prefabricated scaffolds. [55, 56]

CPCs usually all have a high amount (40-50%) of pores in the microporosity (8-12 µm) range. [471] The amount and size of these pores is one of the main controlling factors of the cements mechanical strength, as the porosity is inversely proportional to the mechanical strength. [472-474] This was also described in an empirical relation between the strength, S, and the porosity, P: [475](***Eq.(10)***)

$$S = S_0 e^{-bP} \qquad \textbf{Eq.(10)}$$

Where S_0 is the theoretical strength without porosity and b is an empirical constant. Experimentally, the regulating factor of this porosity is mainly the L/P: the higher the L/P, the higher the porosity. [464] [458, 476, 477] The L/P determines how much liquid (mostly water) is present in a cement paste. This ratio may only be optimized partially regarding the porosity, as it also controls the pastes rheological behaviour and workability, as illustrated above. Almost all CPC formulations are in an excess of water in respect to stoichiometry to be workable and the residual water not used in the chemical reaction is left behind and forms pores, as CPCs set at a near constant volume (density educt ≈ density product). [55, 56] Despite by the adjustment of the L/P also pressure may be applied during setting to reduce the porosity. [472, 478, 479] The control of the size and number of pores formed in a CPC is of high interest for the CPC research.

Porosity is not always disadvantageous for CPCs and there are even studies trying to control pore sizes and increase porosities to achieve certain properties in the implant. [480-501] The bioresorption of microporous cements was reported to be much higher induced by a higher surface area and a higher cellular activity due to particle degradation [55, 56, 502, 503] The usage of porogens, additives or modifications leading to a controlled and or elevated production of pores, has been investigated in a variety of studies. The main approaches are to introduce sacrificial components, that get leached out of the set cement and leave a defined pore behind [476, 481, 487, 495, 504-509] or the introduction of a foaming agent (e.g. by producing CO_2) that traps air inside the cement paste before or while its setting. [480, 506, 510-512] One goal here is to create an interconnected porous network of a pore size around 50 µm. [513-516] The pore size and distribution can be adjusted with the techniques listed above, but they seldomly lead to an interconnected system. To ensure interconnectivity the approaches have been combined with the introduction of hydrogels like sodium alginate [517], sodium hyaluronate or hyaluronic acid (HyAc) [518] and hydroxypropyl methylcellulose (HPMC) [519, 520].

The mechanical properties are among the most important characteristics of a bone cement implant *in vivo*, but their control and improvement towards a usable behaviour is difficult as these properties are dependent on almost every other aspect of the cement paste composition.

2.2.3 Cement modifications

The main properties of a bone cement and its paste, as described above, can and must be adjusted to fit the desired clinical application. Some ways to achieve that have already been shown and mostly involve changing the ratios of the cements' main components e.g., change the L/P.([431, 454] But the properties can also be changed by adjusting the components themselves (e.g., particle size and distribution[521], heat treatment) or adding new minor components, additives, to the paste. [404, 416, 522] The desired effects of these additives can vary depending on the cement paste. Brushite cements tend to react very fast, so setting retardants may be employed here [418],while apatite cements require an acceleration effect to react fast enough. [368-372, 374, 375, 377, 412] Both cements may benefit from a more viscous liquid or an overall higher paste viscosity to prevent paste separation and ensure good injectability [523], while keeping the mechanical properties in control. [517-520]

Setting speed control

For apatite cements it is common to add already formed HAp particles to the powder to act as nucleation seed and therefore promote the precipitation step of the cement reaction. [352, 416, 524-529] There are reports that this also had a secondary effect of improving the compressive strength. [352, 528] Using a cement liquid rich in PO_4^{3-} ions showed to accelerate the apatite cement reaction without having an effect on its properties after 24h [530], hence they found wide use as accelerators for CPCs. [416, 531, 532]

As already described earlier the addition of free cations (Sr^{2+}, Mg^{2}, Si^{4+}) can have a retarding effect, but they do not always enhance the hardened cements properties [533], but the delay of a brushite cement reaction can also improve the cements properties. [418, 524, 534] The presence of SO_4^{2-} ions has shown to improve the cements final strength attributed to a refined microstructure. [418] α-hydroxyl acids (citric acid, glycolic acid) have been shown to retard the setting and allow an improved mixing and handling for lower L/P, when added in form of their salts (e.g., sodium citrate). [340, 420, 421, 423, 454, 535-537] Citric acid or citrate ions form complexes with the divalent calcium ions [538], which adsorb onto the particles surface [538, 539] and therefore makes the area of the particle and the calcium ions unavailable for dissolution or precipitation once supersaturation has been reached. [540]

A retarding effect in form of an initial induction period of the cement reaction has been reported for phytate (myo-inositol hexaphosphate, IP6) [541, 542] and pyrophosphate ions (PP) by Grases, among others. [543] They showed phytate to be the best natural inhibitor for brushite precipitation ($1.21 \cdot 10^{-5}$ M prevented for at least 1h) and pyrophosphate to be the best natural

inhibitor for HAp precipitation ($2.87 \cdot 10^{-6}$ M delayed for at least 1h).[543] The nucleation of hydroxyapatite is more easily inhibited than that of brushite.[544, 545] Phytate acts similar to citric acid by complexing Ca^{2+}ions and adsorbing onto the particles surface. Here the six phosphate groups [546] chelate with the divalent metal ion. [547-549] A similar reason for the inhibitory effect through adsorption of pyrophosphate ions is reported in literature. [550-554]

Viscosity control

The latter two additives, phytate and pyrophosphate, not only influence the setting reaction, but also alter the particle-particle interactions by changing the surface properties through adsorption leading to a different paste behaviour. These can be colloidal interactions and direct frictional interactions. [438] The adsorption influences mainly the colloidal interactions., by changing the zeta (ζ) potential of the powder liquid interface. These interactions get important once the mean particle size is lower than 40 µm and increase their importance below 10 µm. [555] CPCs generally meet these criteria. Attempts to describe the forces in such a suspension can only simplify them to a sum of the attractive Van der Waals force and the repulsive electrical double layer (EDL), as it would be too complex otherwise. [556] This has been defined in the Derjaguin, Verway, Landau and Overbeek (DVLO) theory. [557, 558] (**Figure 12 a**) The charge of the particle-liquid interface leads to the formation of this double layer and to maintain charge neutrality respective ions are drawn to the surface. [559] These form the stern layer and the diffuse layer. (**Figure 12 b)** When the distance between two particles is low enough for the EDLs to overlap, they repel each other. Starting from the particles surface the surface potential gradually decreases until it reaches zero in the bulk solution. [560] As stated above, a common way to measure the extend of the surface charge and therefore the amount of particle repulsion, is to determine the zeta (ζ) potential. Due to particle repulsion the pastes with a higher magnitude zeta (ζ) potential are reported to exhibit less particle agglomeration leading to a better paste consistency and ultimately better injectability. [340] For TTCP and DCPA zeta (ζ) potential values of -18.4 ± 1.9 mV and -15.0 ± 1.8 mV have been decreased to -50.1 ± 1.0 mV and -50.6 ± 3.8 mV by the addition of trisodium citrate as opposed to the usage of pure water, respectively. Furthermore, their injectability could be increased from 59% with pure water to 94%. [340] Nevertheless this modification may have a negative effect on the paste cohesion if the zeta (ζ) potential magnitude is too high. [455]

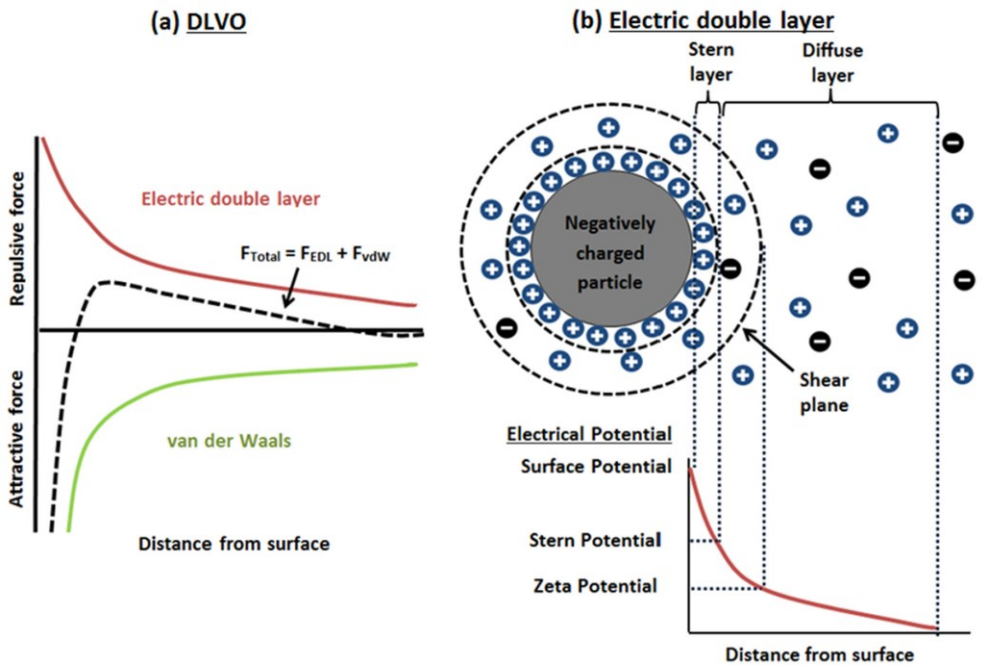

Figure 12. *Graphical description of the* ***a)*** *Derjaguin, Verway, Landau and Overbeek (DVLO) theory. [557, 558] and* ***b)*** *the electrical double layer (EDL) including the stern layer, potential, the diffuse layer and the zeta (ζ) potential. Reprinted with permission from [439]*

Methods initially used to control the setting time of CPCs, like particle size reduction or the adjustment of the L/P, may also have a beneficial effect on the paste viscosity. Additional approaches to control the porosity and cohesion of the paste through additives, as listed before, have also shown to be applicable to adjust the viscosity. [437, 561-566]

Furthermore, there are a variety of additives solely intended to affect the viscosity of cement pastes. These include polysaccharides (namely hydroxypropyl methylcellulose, HPMC and hyaluronic acid) [386, 518-520, 563, 567-571], gelatin [60, 572-578] and polyacrylic acid [579-581], which are characterized by their biocompatibility and, most importantly, their ability to significantly increase the viscosity when added even in small quantities. Solutions containing polysaccharides generally exhibit a thixotropic i.e., shear thinning, behaviour. This is beneficial as it allows an easier injection, while the shape fidelity after extrusion/injection is still ensured. [57]

2.2.4 Bone cement applications

The first medical usage of a CPC was reportedly performed in 1987 [361] and was followed by the application of TTCP – DCPA cement disks implanted in mice in 1991. [582] Further, the teeth of monkeys were treated with a CaP based cement. [583] These were only the first steps in a long list of possible applications and utilizations of CPCs in a medical setting. Their highly biocompatible, osteoconductive nature and the ease of use through their self-setting mechanism following simple chemical processes makes CPCs a valuable material to stimulate tissue regeneration. [409, 584] The flexibility of moulding the material in an individually needed shape and the possibility of a remodelling by cells during bone reconstruction [393, 585-590], while also sometimes being antimicrobial [591-595] and even able to affect osteoblast cell adhesion and gene expression [596], further solidifies their right to exist as a biomaterial for bone healing applications.

Direct applications

In a dental reconstruction setting, CPCs are used to enable teeth replacement in an animal model via HAp implants inserted into the defect and fixated with the cement. [597] Different studies investigated the usage as fillers for root canals [593, 598, 599] and pulp capping [600-602]. These CPCs were all moulded by hand during application, but also an injectable CaP cement has been used to fill gaps around dental implants in goats. [603, 604] The usage for cranio- and maxillofacial defects is benefitted by the lack of stress in these areas. Again, the shape flexibility offers great opportunities for a cosmetic use without extra cost. [605] CPCs find use as support for metal fixtures [586] and skull augmentations [606]. A pig study showed total replacement by bone ingrowth after 180 days [607] and a study in over 100 humans also showed promising results in the treatment of cranial defects [608]. The orthopaedic field of application contains a wide range of studies covering the usage of CPCs. They were used for distal radius fractures [390, 609-611], calcaneal fractures [612], hip fractures [613, 614], osteoporotic vertebral bodies [615], tibial plateau fractures [43, 611, 616-619], pedical screw fixation [620, 621], columbar burst fractures [622], cancellous bone screws [623, 624], wrist anrthodesis [625] and the fixture of titanium implants [626]. Here the CPC mostly had a reinforcing or fixing role, sometimes in combination with other implants. The surgery for the treatment of osteoporotic vertebral bodies is called vertebroplasty or kyphoplasty. The injectability is an integral property for these types of applications, as the goal is to fill the cavities in the osteoporotic or fractured bone of the spine without the need of a big surgery. This leads to a stabilization of the weakened vertebrae and is followed by a faster healing [608, 627-635] and a lower risk of mechanical failure in the future. Because the CPC implants set in ambient conditions and are biodegradable, they also fit perfectly for a drug delivery approach for a variety of drugs. [636-642]

Fabrication of 3D printed structures

Just to touch on the topic briefly. Aside from freehand moulding and injection, CPCs can be processed into a desired shape by the ways of 3D printing. [643] A big advantage is the excellent control over the macro porosity of a 3D printed scaffold. Such porous scaffolds have been fabricated previously by particle leaching, foaming or freeze drying, but this poses high limitations on the degree of control. [644, 645] The new computer guided techniques allow a direct control. [646] For a ceramic scaffold there are five relevant 3D printing techniques. [647]

The first of which is fused deposition modelling (FDM) , where a filament of ceramic particles gets heated and then extruded to be then deposited in a defined scaffold shape onto a collector. [648] In another approach called selective laser sintering (SLS), a powder bed gets sintered into defined structures by a high-power laser. [649] A similar concept is used for particle binding (PB) and inkjet printing (IP). These approaches also use a powder bed, but the scaffold is formed by a binder, that is applied in defined areas, to bind the individual powder grains together (PB) [650] or a liquid that starts a cementitious reaction with the powder is applied to then lead to a solidification by the typical cement reaction (IP) [651]. The last method is the extrusion based printing (EBP), sometimes called direct ink writing (DIW), where a viscous cement paste ("ink") gets extruded without the need of preliminary heating like in FDM and then deposited again into the desired shape. [652] Here the paste cohesion and setting time is of high interest. The last method is the most relevant for the CPCs described above, as the important properties can be adjusted to produce an extrudable paste. If the paste shows sufficient properties for an EBP print run, this method is the best to produce fast and easy prototypes of bone cement-based 3D scaffolds.[653, 654] Aside from the CPCs described above [655-668], also calcium silicates [669-674] can be used as materials to obtain a bioactive ceramic scaffold. Bioinert scaffolds may be produced from Alumina or Zirconia [675-682] precursors. Furthermore these monophasic materials may be combined into composites of two ceramics (e.g., HAp + β-TCP [683], β-TCP + bioactive glass [684]) or of ceramics combined with polymers (e.g., β-TCP + polycaprolactone [685], HAp + poly(lactic acid) [686])or hydrogels (e.g., β-TCP + collagen [687], HAp + alginate/gelatin [688]).

Chapter 3

α-TCP with phytic acid

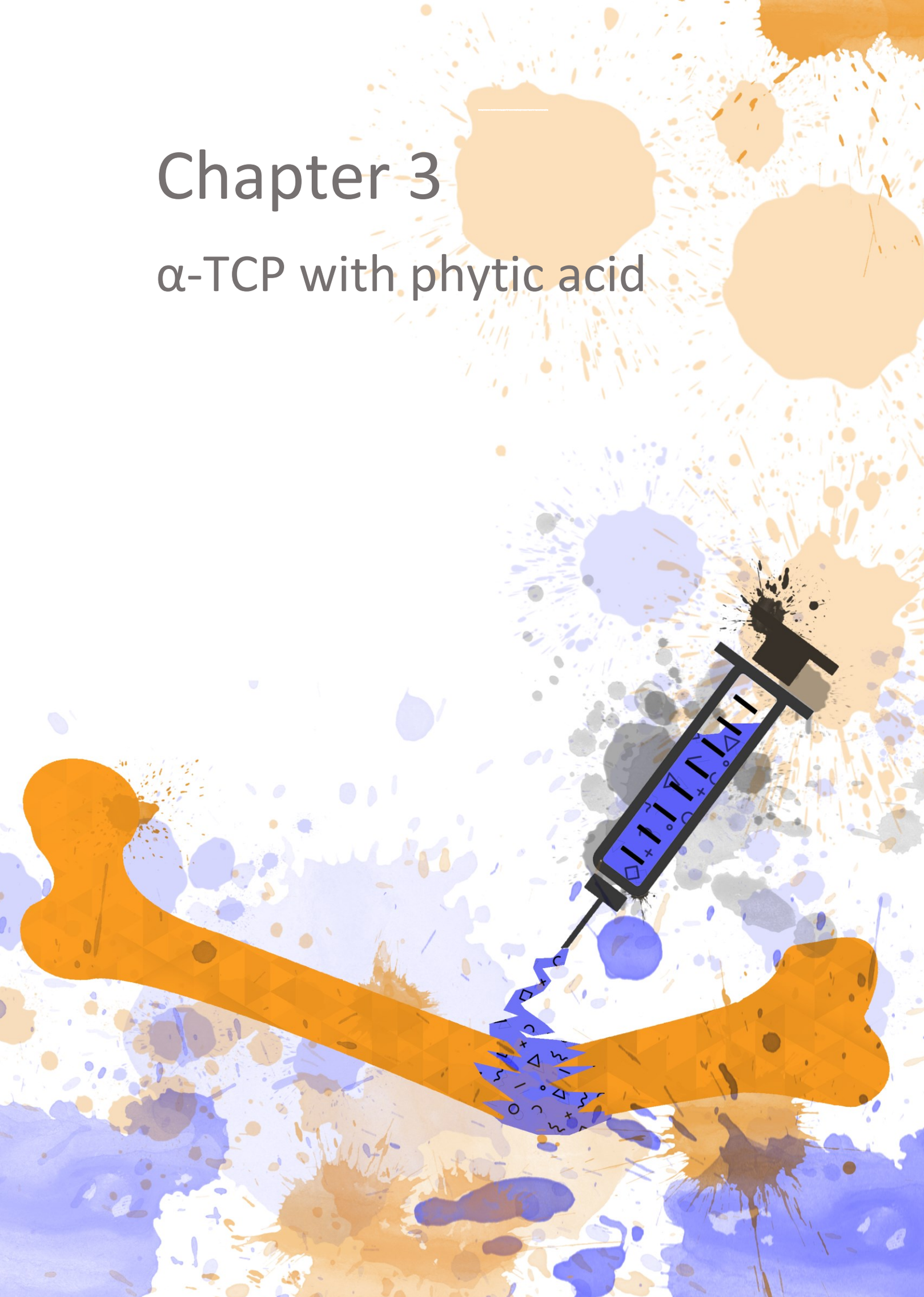

The authors contributed to the manuscript as follows:

Contributor	Contribution
Jan Weichhold	Conceived the research; conceptual planning; conducted experiments and analysed data for material characterization (particle size, zeta potential, rheology, injectability, compressive strength, porosity and scanning electron microscope)
Uwe Gbureck	Conceived the research; conceptual planning; revised and provided feedback on the manuscript
Friedlinde Goetz-Neunhoeffer	Revised and provided feedback on the manuscript
Katrin Hurle	Revised and provided feedback to the manuscript; conducted experiments and analyzed data for material characterization (XRD, calorimetry, pH)

Chapter 3

Setting Mechanism of a CDHA Forming α-TCP Cement Modified with Sodium Phytate for Improved Injectability

Chapter 3 is based on a manuscript, which is already published (June 2019; MDPI Materials, Creative Commons Attribution 4.0 International CC BY 4.0).[689]

Authors: Jan Weichhold, Uwe Gbureck, Friedlinde Goetz-Neunhoeffer and Katrin Hurle

The content of this chapter is a result of the collaboration between the University of Würzburg and the University of Erlangen-Nürnberg. The experiments have been conducted by Jan Weichhold and Katrin Hurle. They evaluated their data and discussed the work of their collaboration together.

3.1 Abstract

A calcium deficient hydroxyapatite (CDHA) forming cement with a bimodal grain size distribution, composed of α-TCP and fine grained CDHA at a weight ratio of 9:1, was modified by the addition of sodium phytate (IP6) in variable amounts ranging from 0.25 to 2 wt.%, related to the powder content. The injectability of the cement paste was drastically increased by the IP6 addition, independent of the amount of added IP6. Additionally, the cement paste viscosity during the first minutes decreased. These effects could be clearly related to a slightly more negative zeta potential. Furthermore, IP6 was shown to strongly retard the setting reaction, as can be seen both in the calorimetry and X-ray diffraction measurements. In addition, octacalcium phosphate (OCP) was identified as a further setting product. All measurements were performed at 23 °C and 37 °C to assess the effect of temperature on the setting reaction for both clinical handling by the surgeon and the final hardening in the bone defect.

3.2 Introduction

Calcium phosphate cements (CPCs) are well established in medicine for bone repair and a variety of formulations are commercially available for clinical applications. [55] Compared to calcium phosphate ceramics, they offer the advantage of being freely moldable and therefore perfectly adjustable to the bone defect. CPCs can be basically divided into apatite and brushite cements, according to their final hydration product. While brushite forms under acidic conditions at a pH < 4.2 and a physiological temperature, apatite formation occurs at neutral and alkaline pH values. [690] Apatite and brushite cements differ in their application-relevant properties. Hence, both types are of clinical interest, dependent on the properties required for specific applications. While brushite cement stands out by its high resorbability, apatite cement is advantageous with respect to its mechanical performance. [464] One approach to generate an apatite forming cement is the mixture of α–tricalcium phosphate (α–TCP) with water, which forms calcium-deficient hydroxyapatite (CDHA) according to **Eq.(11)**. [411]

$$3\ \alpha\text{-}Ca_3(PO_4)_2 + H_2O \rightarrow Ca_9(PO_4)_5(HPO_4)OH \qquad \textit{Eq.(11)}$$

For a successful clinical application of bone cements, several aspects must be considered. One important factor is the setting time, which needs to be slow enough to give the surgeon enough time for implementation, but fast enough not to delay the operation [416]. Since the hydration of crystalline α–TCP with water alone is rather slow, acceleration is necessary. One possibility is the application of Na_2HPO_4, which takes advantage of the common ion effect. [531] Furthermore, the addition of nanosized CDHA as a nucleation agent can fasten the reaction. [417]

Due to the increasing relevance of minimal-invasive applications, where the cement is directly applied to the defect by a syringe, the injectability of the cement pastes is another highly relevant aspect. [691] Different approaches were already developed to alter cement rheology and to improve injectability. [439] Although increasing the liquid to powder (L/P) ratio has a positive effect [426], it has the drawback that the mechanical properties are negatively affected due to an increase of cement porosity. [55] Second, the particle size of the cement powder can be adjusted to optimize injectability. While a certain decrease of particle size was shown to improve injectability, a prolonged milling leads to a reduction of injectability due to particle agglomeration, accompanied by a decrease in compressive strength. [374] A more efficient improvement can be achieved by adjusting a bimodal grain size distribution, for example through the addition of fine-grained filler particles. [521] Since the setting reaction occurring in cements negatively affects the injectability, the application of setting retarders can also be beneficial. [435] Another approach is the alteration of the zeta potential of cement particles by

the addition of multiple charged ions. The resulting repulsion between particles of the same charge leads to a decrease of viscosity and an improved injectability. [537] This effect was already described for citric acid and sodium citrate, respectively, in both brushite and apatite forming cements. [340, 537] Unfortunately, the application of citric acid can also have some drawbacks. For instance, previous studies indicated that the addition of citric acid was detrimental for cell attachment and the degradation of the cement *in vivo*. [692, 693] Therefore, the development of alternatives is of interest. A rather new approach is the application of phytic acid (IP6), which was already demonstrated to be cytocompatible and effective as a setting retarder in brushite cement. [541] While the effect of IP6 on cement setting, combined with a detailed study of cement paste rheology, was already analyzed in detail for a brushite cement [694], according to our knowledge no apatite cements modified with IP6 derivates were investigated so far.

Hence, the aim of the present study was the development of an injectable CDHA-forming cement based on α–TCP, which might open up new fields for application. Fine grained CDHA was added as a filler to adjust a bimodal grain size distribution. As the addition of phytic acid might result in a pH too low for CDHA formation, sodium phytate was added instead in variable amounts to investigate its effect on cement injectability and rheology. Furthermore, the influence of the additive on cement hydration at two different temperatures was investigated in detail using isothermal calorimetry and quantitative X-ray diffraction (XRD), since previous studies indicated a general acceleration of the hydration reaction with an increasing temperature through the application of isothermal calorimetry. [191, 193, 695] A detailed understanding of the hydration process is an essential prerequisite for the targeted development of bone cements for clinical applications.

3.3 Results

3.3.1 Characterization of Powder Samples

Particle Size Distribution and Specific Surface Area

The CDHA powder showed a bimodal particle size distribution, with maxima at particle sizes of 0.8 and 2.6 µm. The particle size distribution of α–TCP was unimodal with a maximum at 20 µm, while grain sizes reached down to 0.3 µm. **Figure 13** and the D_v values (**Table 3**) indicate that the CDHA powder was basically finer than the α–TCP powder.

Quantitative Phase Composition

The α–TCP starting powder was composed of 86 ± 1 wt.% crystalline α–TCP, 2.9 ± 0.1 wt.% β-TCP and 11 ± 1 wt.% amorphous TCP (ATCP). The G-factor quantification of the fine milled CDHA powder resulted in a crystalline CDHA content of 98.5 ± 0.7 wt.%, which means that practically no amorphization of CDHA had occurred during the wet milling procedure. For the model ellipsoid used to refine the anisotropic crystallinity of CDHA, values of rx = 5.73 ± 0.04 nm and rz = 16.5 ± 0.8 nm were obtained, which corresponds to a "true crystallite size" (True CS) of 13.1 ± 0.3 nm. A microstrain of 0.28 ± 0.02 was obtained.

Table 3. *D_V values obtained by laser diffraction and BET surface areas of α–TCP and CDHA; the values are the means of three independent preparations, while for the laser diffraction ten measurement runs were performed for each preparation; the errors represent the standard deviations of the three preparations.*

Parameter	α-TCP	CDHA
D_V10 [µm]	1.6 ± 0.1	0.73 ± 0.02
D_V50 [µm]	11.3 ± 0.8	2.3 ± 0.1
D_V90 [µm]	35 ± 1	10 ± 5
BET surface area [m²/g]	0.86 ± 0.06	34 ± 4

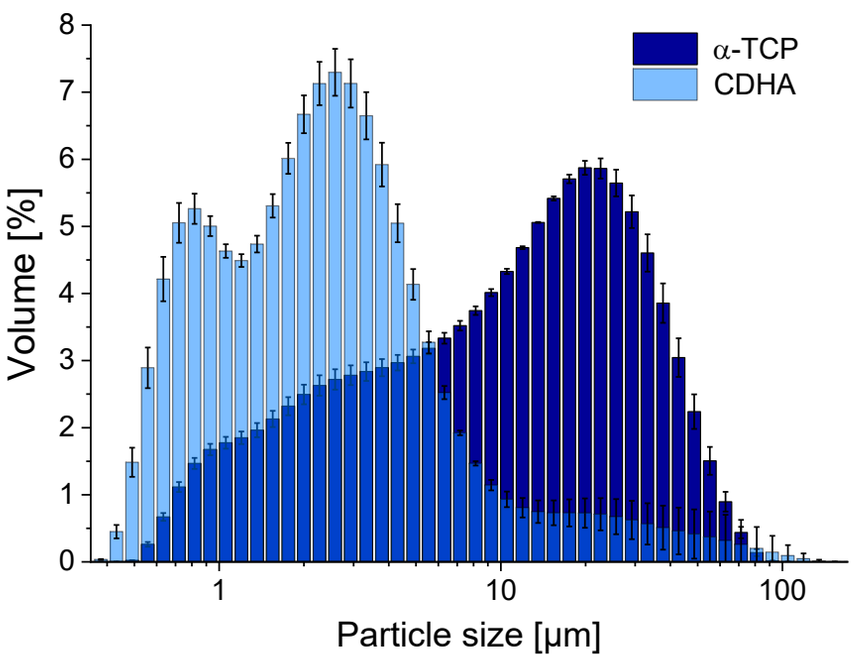

Figure 13*. Particle size distribution of α–TCP and CDHA, determined by laser diffraction using isopropyl alcohol as a lubricant; the means of three independently prepared measurements are presented; the error bars represent the standard deviation.*

Zeta Potential

The surface charge of these powders in deionized water and a sodium phytate solution is shown in **Figure 14**. It can be seen that the surface charge is much less negative in pure water or even slightly positive for the 9:1 powder mixture, compared to the sodium phytate solution. With the addition of sodium phytate in the solution, the surface charge decreased vastly by about 35 to 40 mV from –20 ± 1 mV to –55 ± 1 mV, –8 ± 1 mV to –48 ± 1 mV and 3 ± 0 mV to –40 ± 1 mV for α–TCP, CDHA and the mixture, respectively.

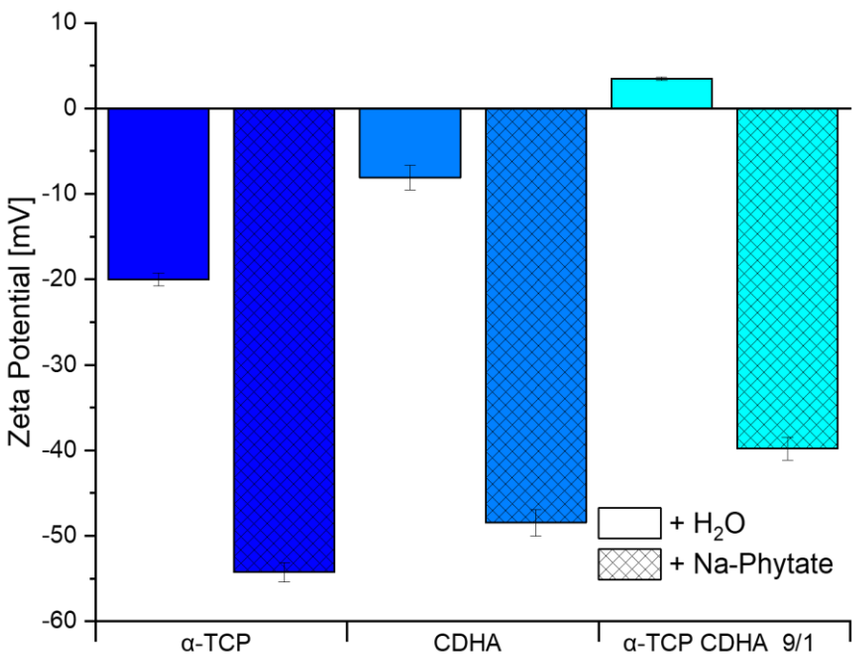

***Figure 14**. Surface charge of α-TCP, CDHA and a α-TCP/ CDHA mixture in water and a 0.002 M sodium phytate solution determined by the zeta potential measurement. Every powder was prepared independently three times, and the error bars represent the standard deviation.*

3.3.2 Cement Paste Characterization

Viscosity

As shown in **Figure 15**, the pastes show a clear shear thinning behaviour in the early stages of the reaction. The reference Phy_0.00 was not measurable, as the paste was already too thick to be prepared for the rheometer. It can be seen that the added phytate has no significant increasing liquefying effect with an increasing amount in the paste. In contrast to this, a temperature increase from 23 °C to 37 °C has a strong effect. This is shown by the fast viscosity increase after the initial shear thinning period for the samples at 37 °C, compared to the slower increase for the 23 °C samples. When the sample surface is partially hardened, the measurement system can detach from the sample, which leads initially to a decrease in the measured viscosity until it attaches again.

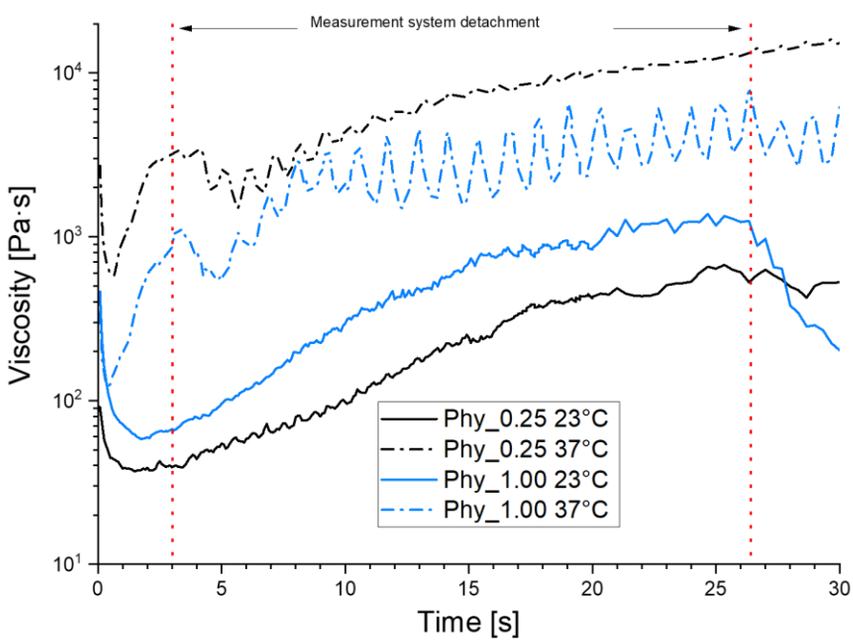

Figure 15. *The paste viscosity development of the samples Phy_0.25 (**black**) and Phy_1.00 (**blue**) at 23 °C (**line**) and 37 °C (**dotted line**). The reference Phy_0.00 was not measurable. Every sample was prepared three times independently, and one representative curve is shown.*

Injectability

The reference paste Phy_0.00, without additional modification, showed a poor injectability after all three time points (**Figure 16**). The amount injected is mostly due to filter pressing. With 30% and less it is at least three times lower than that of all of the IP6 containing mixtures. All of them are shown to be fully injectable, as the last 10% that are missing stay in the needle when the syringe plunger reaches the end of the syringe. The injectability also does not change if the pastes can set for a longer time. These results show a significant improvement in the paste injectability, even with low amounts of 0.25 wt.% additional sodium phytate.

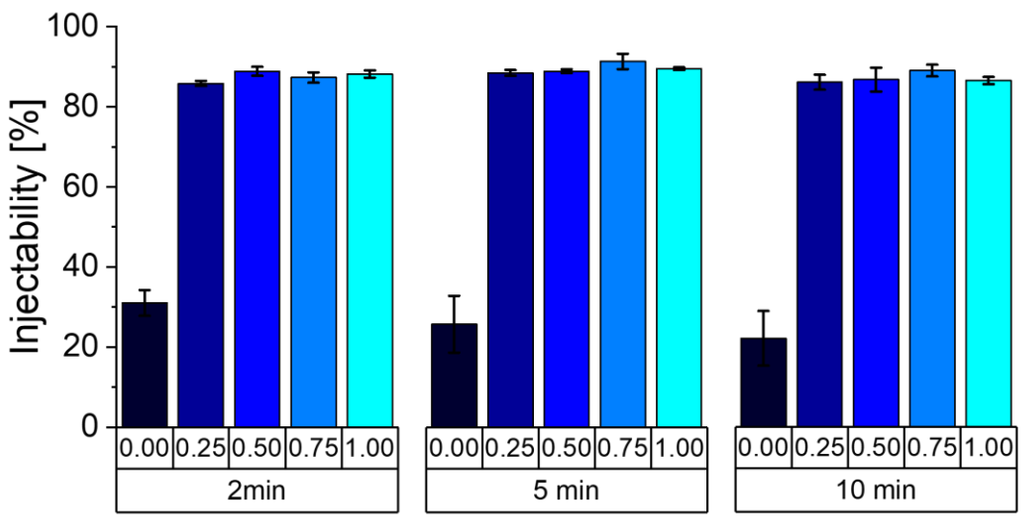

Figure 16. *Injectability of all five paste formulations (Phy_0.00 – Phy_1.00) 2, 5 and 10 min after the powder and liquid mixing. Every sample has been prepared three times, and the error bars represent the standard deviation.*

3.3.3 Hydration Reaction

Heat Flow Calorimetry

The calorimetry curves obtained at 23 °C (**Figure 17 a**) mainly exhibited three maxima: The initial heat flow already measured after a few min was followed by a sharp second maximum. Then, a third maximum occurred, which was flat and broad for all samples. While the position of the initial maximum was practically identical for all cement compositions, the maximum initial heat flow was higher for the samples containing phytate. The positions of both the second and the third maxima were shifted to later time points with an increasing phytate content. While the height of the second maximum decreased with a rising phytate content for Phy_0.00, Phy_0.25 and Phy_0.50, it increased again for Phy_0.75. The maxima of Phy_0.00 and Phy_0.25 were also sharper than those with higher phytate concentrations. The second maximum of pure α–TCP occurred later than that of the CDHA containing reference Phy_0.00, and the maximum heat flow that was reached was also far lower. For all of the samples, the measurements were well reproducible.

The total heat release measured until the completion of hydration varied in the range of 56 ± 6 J/g_{Powder} (Phy_0.75) to 70 ± 2 J/g_{Powder} (Phy_0.25) for the samples containing CDHA. No systematic correlation between the phytate content and total heat release was observed.

At 37 °C, only one heat flow maximum was visible for the samples without a phytate addition (**Figure 17 b**). Sample Phy_0.25 showed two maxima: A small shoulder followed the sharp initial maximum. The samples with a higher phytate content exhibited three maxima, including the initial one. Here, the position of the second and third maximum was increasingly postponed with an increasing phytate content. In Phy_1.00, the heat flow completely decreased to zero and even reached slightly negative values after the initial maximum. This induction period lasted about 10 h. The measurements with IP6 concentrations up to 0.5 wt.% were well reproducible, while the reproducibility was lower for higher IP6 concentrations. For example, for Phy_1.00, the position of the second maximum varied from 9.6 to 11.5 h. As for 23 °C, no systematic correlation between the total heat release and the phytate content was observed.

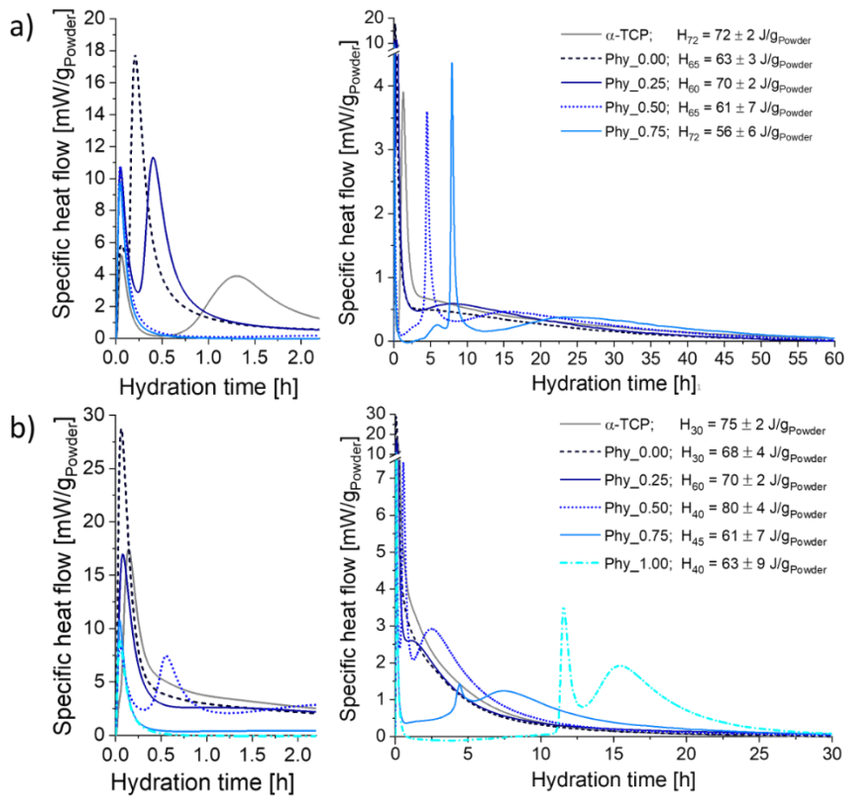

Figure 17. *The calorimetry results of the samples composed of α–TCP and CDHA (weight ratio 9:1) with different amounts of sodium phytate; a 0.2 M Na_2HPO_4 solution was used as the mixing liquid with an L/P of 0.3 ml/g_{Powder}. The measurements were performed at (**a**) T = 23 °C and (**b**) T = 37 °C; three independent measurements were run for each sample; one representative curve is shown for Phy_0.75 at T = 23 °C and for Phy_0.50, Phy_0.75 and Phy_1.00 at 37 °C, and for the other samples the mean of three independent measurements is presented.*

pH Development

While the 0.2 M Na_2HPO_4 solution was slightly basic with a pH of 9.07, the pH decreased with an increasing sodium phytate addition (**Figure 18a**), until it reached a value of 6.16 ± 0.02 for an addition of 2 wt.% sodium phytate. In Phy_0.00, a continuous decrease of the pH was observed immediately from the beginning (**Figure 18b**). After 8 h, a pH of 7.52 ± 0.03 was measured, while the initial pH (8.96 ± 0.05) was very close to that of the pure 0.2 M Na_2HPO_4 mixing liquid (9.07). In Phy_0.25, the starting pH was lower with 7.85 ± 0.01, but close to that of the mixing liquid containing the corresponding amount of sodium phytate (8.12 ± 0.04). Contrary to Phy_0.00, the pH of the cement paste in Phy_0.25 increased until 2 h after mixing, reaching a small plateau at a pH of 8.62 ± 0.05. After about 2.5 h, the pH started to decrease, similar to Phy_0.00.

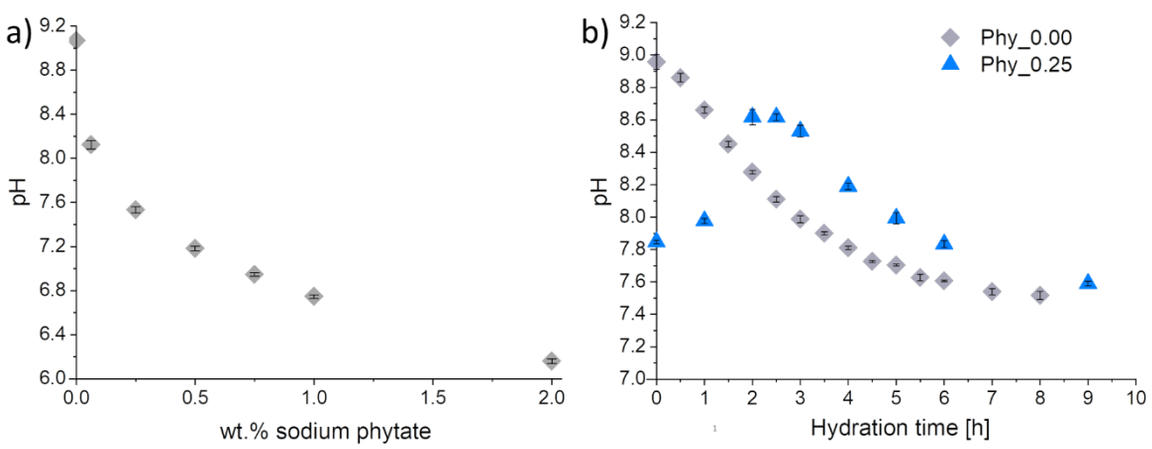

Figure 18. *The pH measurements of (**a**) 0.2 M Na_2HPO_4 aqueous solutions containing variable amounts of sodium phytate (wt.% related to the powder content of the corresponding cement pastes) and (**b**) cements composed of α–TCP and CDHA (weight ratio 9:1) with 0 and 0.25 wt.% sodium phytate; a 0.2 M Na_2HPO_4 aqueous solution was used as the mixing liquid with an L/P of 1.2 ml/g_{Powder}. The measurements were performed at T = 37 °C; three independent measurements were run for each sample, and the error bars represent the standard deviation.*

In-situ XRD

Measurements at 37 °C : The dissolution of crystalline α–TCP already started after about 0.25 h in α–TCP and Phy_0.00, while it was delayed to 0.5 h for Phy_0.25 and to 2 h for Phy_0.5. *(***Figure 19***)* An artefact of the initial increase of the α–TCP content was observed for all samples, while it was more pronounced for higher IP6 contents. This effect most likely results from the disappearance of a water film that might have been present at the beginning of the measurement, especially since the pastes with sodium phytate were rather liquid after preparation. A rapid increase of the CDHA content was observed since the beginning in α–TCP, Phy_0.00 and Phy_0.25, whereas it only started after 0.5 h in Phy_0.50. The increase became more rapid after about 2 h. A slight CDHA formation and crystalline α–TCP dissolution was measured until the end of the measurement time after 24 h for all samples that were investigated. The formation of minor amounts of OCP was detected in all samples, except α-TCP.

Measurements at 23 °C: At 23 °C, no OCP formation was detected in all of the samples investigated during the 48 h of measurement. Only the transformation of α–TCP to CDHA occurred, while the degree of hydration reached after 48 h was higher for both samples containing phytate (**Figure 20**). It further became evident that the dissolution of α–TCP was slower in these samples, compared to Phy_0.00. While the hydration reaction slowed down noticeably after about 25 h in all cases, the reaction still proceeded to a slight extent until the completion of the measurement in the phytate containing samples. In Phy_0.00, the contents of both α–TCP and CDHA reached a constant level at the end.

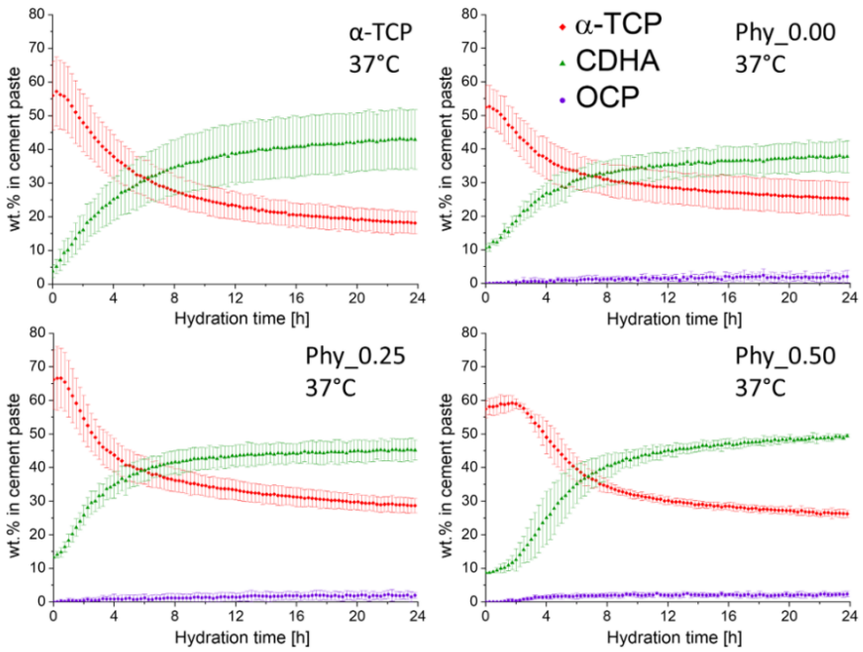

Figure 19. *The quantitative in-situ XRD results of samples composed of α–TCP and CDHA (weight ratio 9:1) with different amounts of sodium phytate; a 0.2 M Na_2HPO_4 aqueous solution was used as the mixing liquid with an L/P of 0.3 ml/g_{Powder}. The measurements were performed at T = 37 °C; three independent measurements were run for each sample, and the error bars represent the standard deviation; the data were corrected for the water loss occurring during the measurement.*

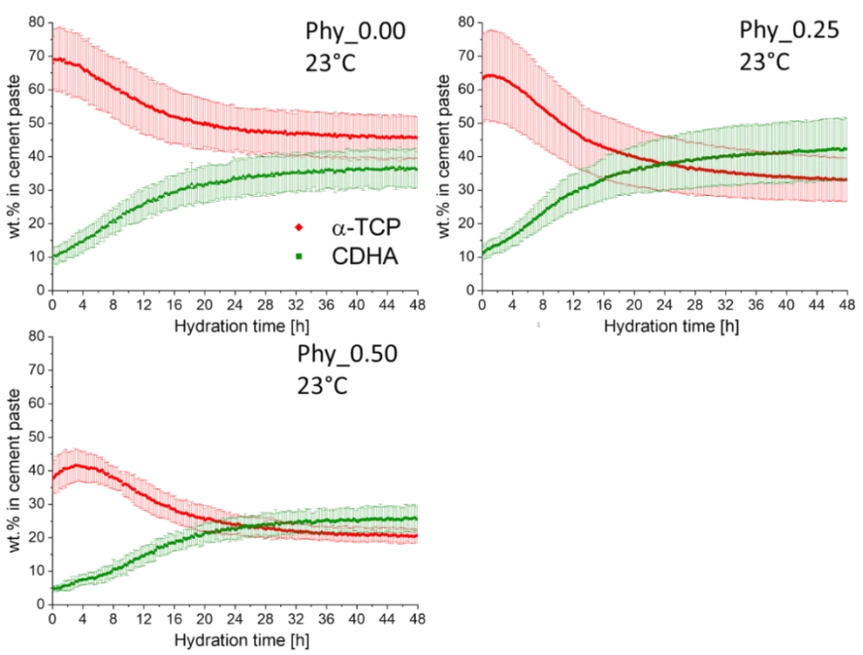

Figure 20. *The quantitative in-situ XRD results of samples composed of α–TCP and CDHA (weight ratio 9:1) with different amounts of sodium phytate; a 0.2 M Na_2HPO_4 aqueous solution was used as the mixing liquid with an L/P of 0.3 ml/g_{Powder}. The measurements were performed at T = 23 °C; three independent measurements were run for each sample, and the error bars represent the standard deviation.*

3.3.4 Characterization of Hydration Products

XRD of Hardened, Polished Samples

Samples stored at 37 °C: After 1 d of hydration, OCP was detected in small amounts in all samples except pure α–TCP (**Table 4**). The CDHA content after 1 d was identical for α–TCP, Phy_0.00 and Phy_0.50 within the error range, while it was significantly lower for Phy_1.00. Accordingly, the amount of remaining α–TCP was significantly higher for Phy_1.00. After 7 d, a further increase of CDHA quantities compared to 1 d was observed for all samples, though the difference was not significant for Phy_1.00. While no significant differences were observed between α–TCP, Phy_0.00 and Phy_0.50 for both α–TCP and CDHA, the CDHA content was still far lower for Phy_1.00, compared to the other samples. As for 1 d, OCP was detected in all samples except α–TCP, while the quantity increased in the range of Phy_0.50, Phy_0.00/Phy_2.00 and Phy_1.00.

The degree of hydration (defined as the percentage of TCP phases (ATCP + α–TCP) that have reacted) in the samples stored for 1 d, was compared to that reached in the in-situ XRD measurements after 1 d of hydration. It was evident that the hydration proceeded to a higher extent in the storage samples for Phy_0.00 and slightly for Phy_0.50, while no significant difference was observed for α–TCP.

Table 4. *The quantitative phase composition and degree of hydration of samples composed of α–TCP and CDHA (weight ratio 9:1) with different amounts of sodium phytate after 1 d and 7 d of hydration; a 0.2 M Na_2HPO_4 aqueous solution was used as the mixing liquid with an L/P of 0.3 ml/g_{Powder}; the samples were stored at 37 °C.*

	wt.% α–TCP		wt.% CDHA		wt.% OCP		Degree of hydration [%]		
Hydration time	1 d	7 d	1 d	7 d	1 d	7 d	1 d	7 d	In-situ 1 d
α–TCP	20 ± 1	9 ± 1	50 ± 2	61 ± 1	0	0	72 ± 1	87 ± 1	71 ± 1
Phy_0.00	16 ± 1	10 ± 2	47 ± 6	56 ± 4	2.5 ± 0.4	2.0 ± 0.3	72 ± 3	83 ± 3	56 ± 4
Phy_0.50	20 ± 2	6 ± 2	49 ± 2	60 ± 1	3.0 ± 1.1	0.5 ± 0.8	68 ± 3	90 ± 3	62 ± 1
Phy_1.00	33 ± 3	28 ± 9	31 ± 6	37 ± 9	1.9 ± 0.4	3.6 ± 0.4	44 ± 7	54 ± 14	-
Phy_2.00	-	17 ± 5	-	44 ± 7	-	2.2 ± 0.4	-	69 ± 10	-

A further increase of the crystallite size True CS was only observed for Phy_0.50 from 1 d to 7 d (**Table 5**). The aspect ratio rz/rx was practically identical for all samples expect α–TCP, and slightly higher than that in the CDHA added as starting powder.

Table 5. *True CS and aspect ratio rz/rx of CDHA crystallites in storage samples after 1 d and 7 d of hydration; a 0.2 M Na_2HPO_4 solution was used as the mixing liquid with an L/P of 0.3 ml/g_{Powder}; the samples were stored at 37 °C.*

	True CS [nm]		Aspect ratio rz/rx	
Hydration time	1 d	7 d	1 d	7 d
CDHA powder	13.1 ± 0.2	13.1 ± 0.2	2.9 ± 0.1	2.9 ± 0.1
α–TCP	14.1 ± 0.2	14.8 ± 0.7	5.3 ± 0.5	5.4 ± 0.4
Phy_0.00	13.8 ± 0.6	15.1 ± 0.8	3.6 ± 0.2	3.5 ± 0.4
Phy_0.50	11.4 ± 0.4	16.2 ± 0.8	3.6 ± 0.1	4.5 ± 0.4
Phy_1.00	10 ± 2	10.1 ± 0.2	3.4 ± 0.1	3.6 ± 0.1
Phy_2.00	-	9.5 ± 0.6	-	3.9 ± 0.1

Samples stored at 23 °C: For all of the samples investigated, a continuous decrease of the α-TCP content was observed up to 7 d (**Table 6**). While in the samples stored for 1 d or 2 d the α-TCP content was still significantly higher and the CDHA content was lower in Phy_1.00, compared to the other two samples, nearly no differences were observed anymore after 4 d and 7 d. No crystalline OCP was detected in all of the samples that were hydrated for 1 d and 2 d. Indeed, the main XRD reflection of OCP was clearly visible in the diffraction patterns of the samples stored for 4 d and 7 d. Accordingly, OCP could be quantified in all of these samples. The degree of hydration in the samples stored at 23 °C continuously increased up to a hydration time of 7 d (**Table 7**). While it was lower for Phy_1.00, compared to the other two samples, after 1 d and 2 d, similar values were obtained for all three samples after 4 d and 7 d.

Table 6. *The quantitative phase composition of samples composed of α–TCP and CDHA (weight ratio 9:1) with different amounts of sodium phytate after 1 d, 2 d, 4 d and 7 d of hydration; a 0.2 M Na_2HPO_4 aqueous solution was used as the mixing liquid with an L/P of 0.3 ml/g_{Powder}; the samples were stored at 23 °C.*

	wt.% α–TCP				wt.% CDHA				wt.% OCP			
Hydration time	1 d	2 d	4 d	7 d	1 d	2 d	4 d	7 d	1 d	2 d	4 d	7 d
Phy_0.00	34 ± 4	30 ± 1	23 ± 1	16 ± 1	36 ± 1	63 ± 1	64 ± 2	58 ± 4	0	0	4.1 ± 0.2	2.0 ± 0.2
Phy_0.50	39 ± 3	32 ± 2	22 ± 1	13 ± 2	36 ± 2	64 ± 5	61 ± 3	57 ± 7	0	0	3.7 ± 0.4	1.8 ± 0.6
Phy_1.00	58 ± 4	41 ± 3	21 ± 5	15 ± 3	15.0 ± 0.5	49 ± 4	56 ± 1	60 ± 2	0	0	4 ± 1	0.9 ± 0.1

Table 7. *The degree of hydration of samples composed of α–TCP and CDHA (weight ratio 9:1) with different amounts of sodium phytate after 1 d, 2 d, 4 d and 7 d of hydration; a 0.2 M Na_2HPO_4 aqueous solution was used as the mixing liquid with an L/P of 0.3 ml/g_{Powder}; the samples were stored at 23 °C.*

	Storage samples				In-situ	
Hydration time	1 d	2 d	4 d	7 d	1 d	2 d
Phy_0.00	46 ± 3	64 ± 1	72 ± 1	76 ± 1	34 ± 3	38 ± 4
Phy_0.50	43 ± 4	63 ± 1	72 ± 1	80 ± 1	44 ± 1	51 ± 1
Phy_1.00	12 ± 2	49 ± 1	71 ± 5	78 ± 4	42 ± 2	50 ± 1

A slight increase of the crystallite size True CS from 1 d up to 4 d of hydration was observed for Phy_0.00 and Phy_0.50 (**Table 8**). For Phy_1.00, a decrease of True CS was measured from 1 d to 2 d, but the differences were within the error range. After 7 d, only marginal differences in True CS could be detected between the different samples. The aspect ratio rz/rx was also comparable for all samples after 7 d. While the values obtained after 1 d differed from the others, after 2 d a constant level was reached.

Table 8. *True CS and aspect ratio rz/rx of CDHA crystallites in the storage samples after 1 d, 2 d, 4 d and 7 d of hydration; a 0.2 M Na_2HPO_4 solution was used as the mixing liquid with an L/P of 0.3 ml/g_{Powder}; the samples were stored at 37 °C.*

	True CS [nm]				Aspect ratio rz/rx			
Hydration time	1 d	2 d	4 d	7 d	1 d	2 d	4 d	7 d
Phy_0.00	10.4 ± 0.8	11.0 ± 0.4	12.0 ± 0.4	12.1 ± 0.1	4.2 ± 0.4	3.5 ± 0.2	3.4 ± 0.3	3.3 ± 0.3
Phy_0.50	9.0 ± 0.4	9.8 ± 0.3	11.0 ± 0.3	11.2 ± 0.2	4.5 ± 0.2	3.8 ± 0.1	3.9 ± 0.1	3.6 ± 0.2
Phy_1.00	9 ± 1	8.1 ± 0.3	10.7 ± 0.3	12 ± 1	2.7 ± 0.5	3.9 ± 0.1	3.9 ± 0.2	3.8 ± 0.3

Compressive Strength

Figure 21 shows the compressive strength (CS) of the prepared cement cuboids after storage at 37 °C and 100% humidity. It can be seen that the formulation Phy_0.00, without the addition of sodium phytate, initially has a lower CS of 21 MPa compared to the formulation Phy_0.25 with 25 MPa. All other formulations show a significant lower CS with 8, 4 and 0.5 MPa for the samples Phy_0.50, Phy_0.75 and Phy_1.00, respectively. After 6 more days of storage, the CS of the samples Phy_0.25 remained at about 25 MPa, and the CS of Phy_0.00 rose to the same CS. The CS for Phy_0.50, Phy_0.75 and Phy_1.00 also increased to the respective values 16, 15.5 and 9 MPa.

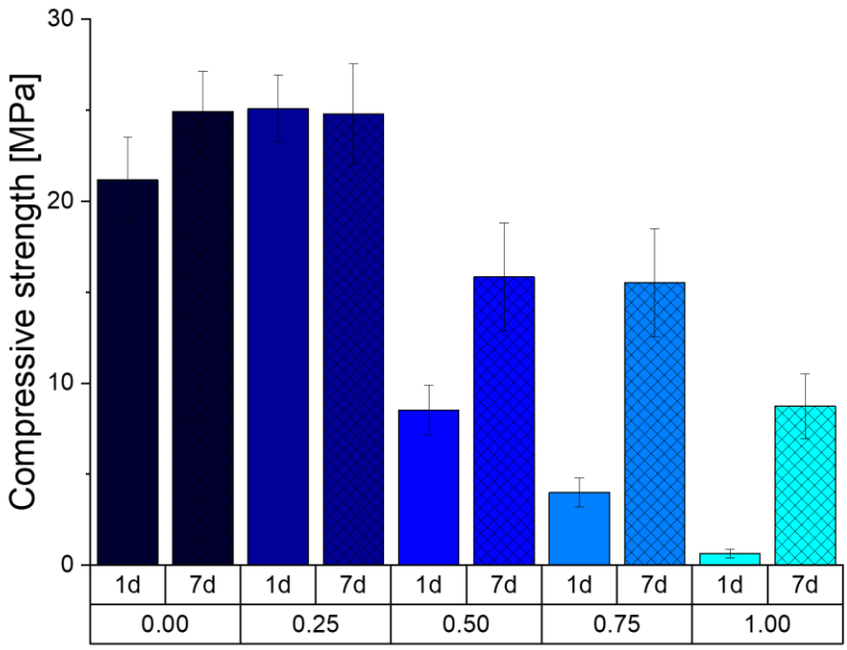

Figure 21. *The compressive strength of all five paste formulations (0.00–1.00) after 1 d and 7 d at 37 °C and 100% humidity. Every sample has been prepared independently at least 9 times, and the error bars represent the standard deviation.*

Porosity

The porosimetry data presented in **Figure 22** (left for 1 d and right for 7 d) and **Table 9** show the effects of the sodium phytate addition as well as the effect of the storage time on the development of pores of different sizes and volume. The overall total pore volume accessible by Hg porosimetry decreased during the storage of the samples Phy_0.00, Phy_0.25 and Phy_0.50 from 37% to 26%, 46% to 21% and 45% to 22%, respectively. The total porosity for the sample Phy_0.75 remains roughly the same over the 7 d of storage. The sample Phy_0.75 shows an increase in the total pore volume, and Phy_1.00 is not hardened after 1 d. The shrinkage of the pores can be best seen in the sample Phy_0.00, where the average diameter halves from 0.06 µm to 0.03 µm, but this is also present in other samples. With the addition of sodium phytate, the overall pore size after 1 d gets decreased at first from a bimodal distribution with two maxima at 0.03 µm and 0.1 µm for Phy_0.00 to a nearly monomodal distribution with a maximum at 0.1 µm and a small shoulder at 1 µm for the sample Phy_0.25. Nearly the same distribution is seen in the sample Phy_0.50, which is very similar to Phy_0.00 regarding the bimodal distribution. Phy_0.75 shows a higher number of smaller pores, which have their maximum at 0.28 µm. The total pore volume seems to be independent of the amount of added sodium phytate, as it is mostly regulated by the liquid content, which is equal throughout all of the samples.

The delayed precipitation reaction can also be observed via the SEM. In **Figure 23** the crystals for Phy_0.00 and the mixtures Phy_0.25, Phy_0.50 and Phy_1.00 are shown side by side after 1 d and 7 d of hydration. After 1 d, it can clearly be seen that the sample with the least amount of phytate shows no apparent difference to Phy_0.00. Both samples show plate-like crystals with a size of just under 3 µm. The mixture Phy_0.50 shows very small crystals, and Phy_1.00 does not show any distinguishable crystals at all. After 7 d, the crystals in Phy_0.00 and Phy_0.25 have grown larger and have become heavily entangled. Now, in Phy_0.50 and Phy_1.00 crystals with sizes of up to 1 µm can also be seen.

Table 9. *The total pore volume, porosity and average pore size of all samples stored for 1 d and 7 d at 37 °C and 100% humidity, measured by Hg-porosimetry.*

Parameter	Storage time	Phy_0.00	Phy_0.25	Phy_0.50	Phy_075	Phy_1.00
Total pore volume [cm^3/g]	1 d	0.17	0.21	0.19	0.12	-
	7 d	0.13	0.11	0.10	0.18	0.14
Total porosity [%]	1 d	37	46	45	30	-
	7 d	26	21	22	32	25
Average pore size [µm]	1 d	0.06	0.05	0.03	0.05	-
	7 d	0.03	0.04	0.05	0.04	0.05

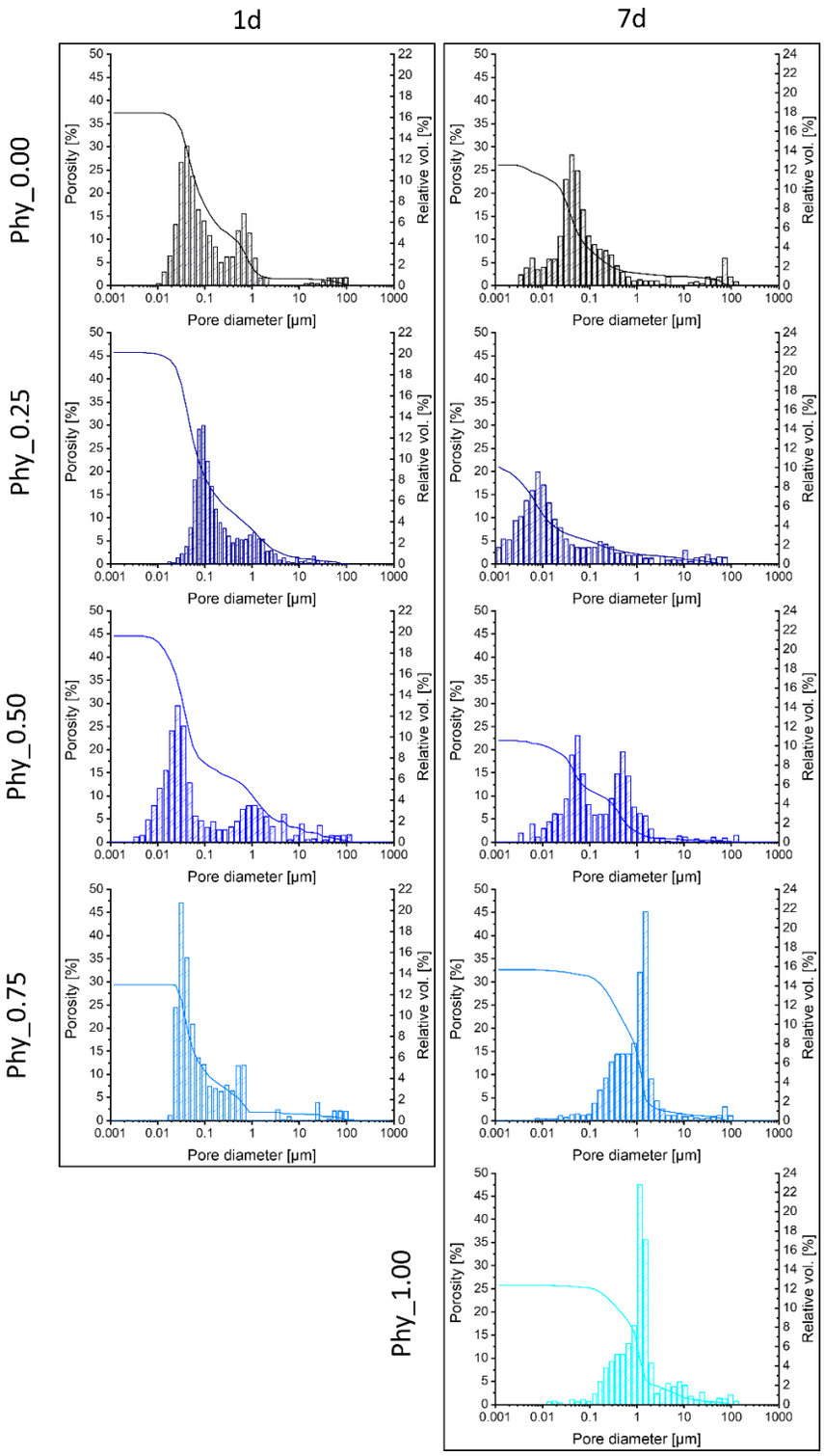

Figure 22. *The pore diameter distribution and total porosity of all mixtures after (**left**) 1 d and (**right**) 7 d of hydration at 37 °C and 100% humidity. The sample Phy_1.00 was not hardened after 1 d, so it was not possible to measure the pores.*

SEM Images

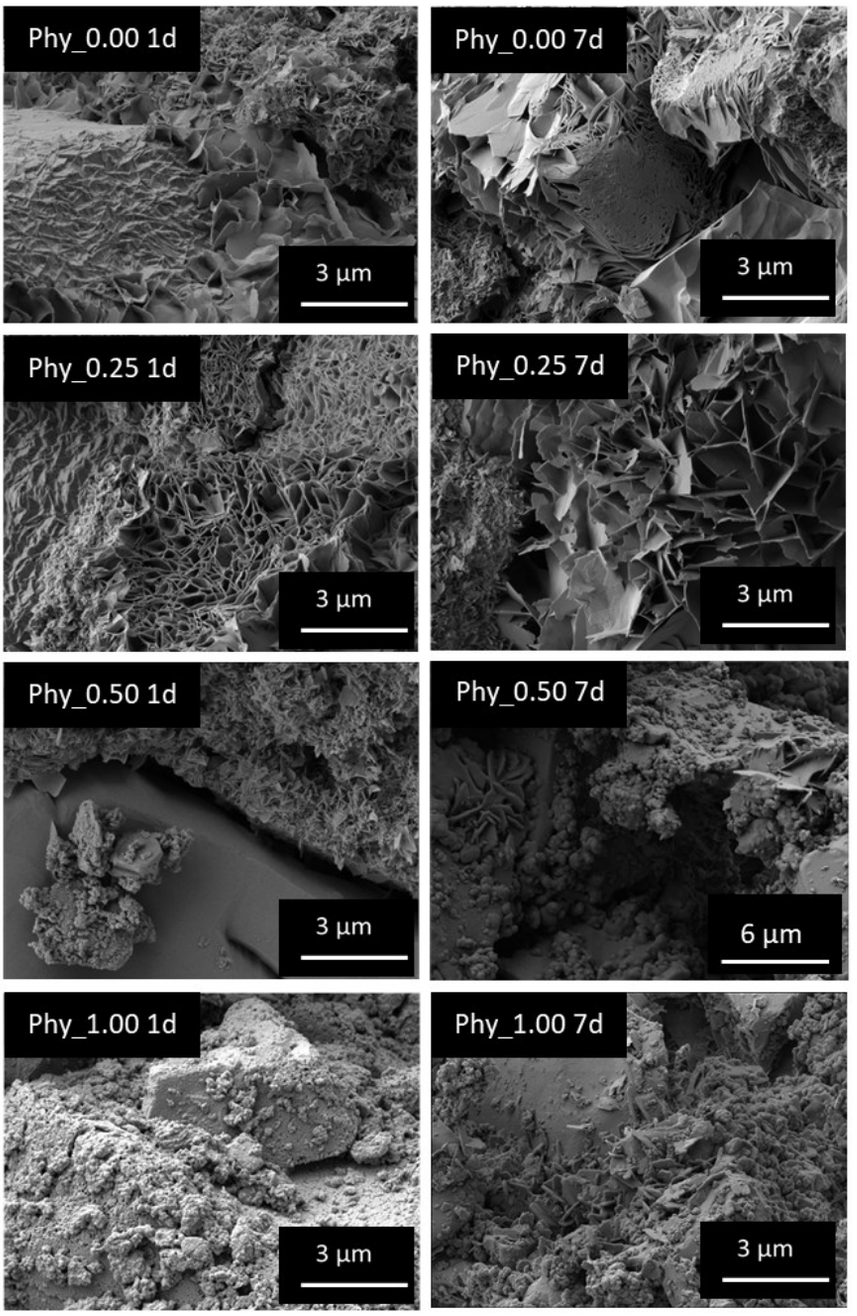

Figure 23. *CDHA crystals of the mixtures Phy_0.00, Phy_0.25, Phy_0.50 and Phy_1.00 grown for 1 d and 7 d at 37 °C and 100% humidity, visualized with the SEM. All samples have been observed on different areas, and representative images were selected for presentation.*

3.4 Discussion

Effect of CDHA Filler on the Hydration

A comparison of the hydration of Phy_0.00 (weight ratio α-TCP/CDHA = 9:1) with the pure α-TCP powder demonstrated that the CDHA had an accelerating effect on the hydration. This

was clearly visible in the calorimetry measurements performed at 23 °C and it was slightly visible at 37 °C. The fine CDHA powder most likely acts as a nucleation site during the cement hydration. [417]

Effect of Sodium Phytate on the Setting Mechanism of the Cement

The calorimetry measurements indicated that all samples, including those containing sodium phytate, showed the typical reaction mechanism established for α–TCP containing ATCP. [696] An amount of 11 ± 1 wt.% of ATCP were present in the α–TCP starting powder used in this study. The hydration of ATCP, indicated by a sharp maximum in the calorimetry measurements, is followed by a slower reaction of the crystalline α–TCP. This is supported by the in-situ XRD data, where the CDHA formation started earlier than the dissolution of crystalline α–TCP. In the not retarded mixtures α–TCP and Phy_0.00, ATCP hydration most likely proceeded so fast that this reaction cannot be separated from the initial heat flow resulting from the mixing of the cement paste. The shift of the second, small calorimetry maximum observed for the phytate-containing samples corresponds well to the retarded α–TCP dissolution measured by the in-situ XRD.

Sodium phytate was proven to have a strong retarding effect on the hydration of α–TCP, even in small concentrations below 1 wt.%. Higher concentrations (Phy_0.75 at 23 °C and Phy_1.00 at 37 °C) even resulted in a real induction period. This means that the hydration of the highly reactive ATCP was also fully impeded during an induction period of about 10 h in Phy_1.00. As expected, the reaction was generally accelerated by increasing the temperature from 23 °C to 37 °C for all cement compositions, while the general reaction kinetics remained the same.

In order to further clarify the hydration mechanism, the pH measurements were performed and correlated to the in-situ XRD measurements. The continuous decrease of the pH observed for Phy_0.00 could be clearly related to the in-situ XRD measurement performed at 37 °C, where the α–TCP dissolution and CDHA formation were observed from the beginning (**Figure 19**). The pH resulting from the dissolution of α–TCP in deionized water was determined to be around 9.2 at 37.4 °C [191] and 9.6 [354] in other studies, respectively; hence, α–TCP shows an alkaline reaction. During the formation of CDHA, the ions released from the dissolution of ATCP and α–TCP are consumed according to **Eq.(12)**. This is taking into account that the $H_2PO_4^-$ and HPO_4^{2-} species are present at the pH conditions in the cement pastes that were investigated, while the ratio of these species depends on the exact pH. [697]

$$9\ Ca^{2+} + x\ HPO_4^{2-} + (6 - x)\ H_2PO_4^{-} + (12\text{-}x)\ OH^{-} \rightarrow$$

$$Ca_9(PO_4)_5(HPO_4)OH + (11 - x)\ H_2O \quad (0 \leq x \leq 6) \qquad \textit{Eq.(12)}$$

Reaction (5) results in a decrease of the pH toward more neutral values due to the precipitation of CDHA, which involves the consumption of OH^- ions. This was observed in the current measurements and also reported from other investigations. [193, 695]

A clear difference was noticed for the phytate containing sample, where an initial increase of the pH was measured. Here, a neutralization reaction between the slightly acidic phytate and the alkaline ions resulting from the dissolution of ATCP and α–TCP might occur, with the result that the pH of the solution approaches that of the initial Na_2HPO_4 solution. Then, due to the precipitation of CDHA, the equilibrium pH is reached, as in the reference. After the completion of the reaction, the pH is close to neutral in both cases.

As the pH of the mixing liquid decreased with an increasing sodium phytate concentration, this factor might have affected the speed of the hydration reaction, since the ratio of the $H_2PO_4^-$ and HPO_4^{2-} species is affected by the pH. Actually, the pH of the mixing liquid was reported to mainly have an effect on the initial part of the hydration reaction, which occurred earlier for lower pH values. [417] Contrary to this, in the present study a decrease in the pH due to the phytate addition resulted in a retardation of the setting reaction. Therefore, it is unlikely that the pH is the relevant factor explaining the setting retardation. Another explanation might be a decrease of the availability of free Ca^{2+} ions through the formation of chelate complexes with the phytate [545], which would impede the precipitation of CDHA. Thus, the retarding effect can be compared to that of phytic acid in brushite cement. [541, 694]

The storage samples hydrated at 37 °C did not show a systematic relation between the phytate content and the amount of OCP formed in the sample. Sample Phy_2.00, which should have shown the highest OCP formation, was well within the content of the other samples. These observations suggest that the OCP formation in relation to CDHA is not significantly affected by the phytate addition and the variation of the phytate content. Interestingly, at 23 °C, OCP was only detected after 4 d and 7 d for all of the investigated samples (Phy_0.00. Phy_0.50 and Phy_1.00). Therefore, it can be concluded that the OCP formation started later than the CDHA formation at a lower temperature of 23 °C.

OCP, whose crystal structure has similarities to that of hydroxyapatite [698], is frequently reported as a transient intermediate in the formation of the more stable apatite from

solution. [699] In the present study, no decrease of the OCP content was observed in the in-situ XRD measurements during the respective measurement time. Additionally, as mentioned earlier, the formation of OCP occurred later than the CDHA formation at 23 °C, which means that OCP does not act as a typical precursor in these cases, but rather forms as a by-product during the CDHA formation. Still, it should be kept in mind here that XRD is only sensitive to crystalline phases and hence it might be possible that an amorphous precursor of OCP is already formed earlier, as it is also reported in the literature. [700]

As only a few wt.% of OCP were present in the samples that were here investigated, it is expected not to have any pronounced effect on the biological performance of the hardened cements. If any effect at all would be present, it is expected to be a positive one, as OCP is reported to have a promoting effect on bone formation. [701]

The quantitative XRD investigations of the storage samples demonstrated that at 23 °C, the phase composition obtained after 7 d was similar for all phytate concentrations that were investigated, while significant differences were obtained for the samples stored at 37 °C. Therefore, it appears that at 37 °C, the phytate reduces the overall extent of the reaction when a content of 0.5 wt.% is exceeded. Interestingly, this is not the case at 23 °C.

The crystallinity (size of coherent scattering domains) of the CDHA formed after hydration was not noticeably affected by the addition of sodium phytate. In other studies, the crystallite sizes of CDHA resulting from α–TCP hydration were remarkably affected by certain parameters, like the particle size [413] or amorphous content of the starting powder. [372, 696] Here, the authors explained this by the acceleration of the hydration by either the reduction of the particle size or an increasing amorphous content. A faster reaction leads to a higher degree of supersaturation of the solution, which favours nuclei formation and hence the precipitation of smaller crystals. [372] Apparently, this was not the case for the phytate-containing samples investigated in this study – otherwise, the phytate containing samples would have achieved higher CDHA crystallinities. Instead, at 37 °C, phytate concentrations of 1 and 2 wt.% slightly reduced the crystallite sizes, which correlates with the reduced degree of hydration observed in these samples. Hence, there are indications that phytate in higher concentrations has an impeding effect on CDHA crystallite growth.

The SEM images after 1 d and 7 d reveal a clear reduction of the CDHA crystal size for phytate concentrations exceeding 0.25 wt%. Hence, the growth of CDHA crystals is impeded by the phytate, while the crystallites detected by XRD are only affected to a minor extend. As the crystal size is in the range of a few µm, while the crystallites are only between 10 and 20 nm, it

is obvious that the crystals visible under SEM are mosaic crystals composed of several crystallites. [702]

The addition of sodium phytate resulted in a more negative zeta potential. A similar observation was made for brushite cement modified with phytic acid in a previous study. [694] This is well in accordance with the earlier studies of Takahashi et al.. [703] The phytate has six phosphate groups, which result in a strong negative surface charge, when the phytate reacts with the free calcium near the cement particle surface. This change in the overall surface charge of the powder is believed to enhance the particle dispersion and inhibit aggregate formation due to the mutual repulsion of the particles. [545] In a previous study [702], the amount of sodium phytate could be correlated with the initial paste viscosity, but the measurements here do not show this trend. This might be due to the fact that the system is already saturated with only 0.25 wt.% sodium phytate, which is also backed by the injectability tests. Here, a significant improvement in injectability can be seen with the addition of 0.25 wt.% sodium phytate, but no further improvement result from higher amounts, even at later time points of 5 and 10 min after mixing. Nevertheless, just like in the previous study, the paste stays injectable for significantly longer with sodium phytate. This can be explained by the chelate complex formation between Ca^{2+} ions and the phosphate groups of the IP6, which are likely less soluble than α–TCP. In addition, the complex formation additionally slows down the solution/precipitation cement reaction by decreasing the availability of free calcium ions. [549, 703, 704] This leads to a delayed rise in paste viscosity and also provides a good explanation for the strong retarding effect on cement hydration, as it was clearly demonstrated in this study. The most impactful factor controlling the paste viscosity seems to be the reaction temperature. With an increase from 23 °C to 37 °C, the early viscosity increase is hugely accelerated. Again, there is no noticeable difference with a higher amount of sodium phytate.

The delay in the reaction is also visible in the compressive strength measurements. Here, a sodium phytate content higher than 0.25 wt.% resulted in very low compressive strengths after 1 d and only slightly higher ones after 7 d. This is due to the fact that the reaction progresses less with more sodium phytate. The samples Phy_0.00 – Phy_0.75 show about the same initial porosity of approx. 40 %. This can be explained by the fact that the porosity is mostly regulated by the amount of liquid added to the system, and this is kept constant throughout all samples. The remarkable decrease of the total pore volume measured for samples containing up to 0.5 wt.% phytate appears surprising. As the densities of α–TCP and CDHA (2.86 g/cm^3 and 3.13 g/cm^3, respectively) are very similar, the total volume of the solid content is not expected to increase during hydration. The total pore volume might be reduced due to the shrinkage of the samples as a result of drying. Still, since the samples were stored at 100 % humidity, this effect can be excluded in this study. As a shift of the pore size distribution toward smaller diameters was observed, it is likely that the formation of CDHA crystals inside the pores led to the separation of pores into smaller ones. During this process, parts of the pore space might have been closed. These closed pores are not accessible by Hg porosity measurements, which would explain the apparent reduction of the total pore volume. Parts of the pores might also be so small that the limit of the measurement technique is reached. No direct correlation between the pore size and distribution, and the amount of added sodium phytate can be made.

3.5 Conclusions

Sodium phytate was proven to be a versatile additive for the development of an apatite cement with excellent injectability. An amount of 0.25 wt.% was already sufficient to achieve maximum injectability. The increase in injectability could be related to a decrease in the particles´ zeta potential. While a phytate amount of 1 wt.% had a drastic retarding effect on cement hydration, 0.25 wt.% of phytate only slightly affected the setting kinetics. Furthermore, this low amount of the additive had nearly no influence on the final phase composition, compressive strength, the XRD crystallinity and the crystal size of the CDHA after hardening. Therefore, a sodium phytate concentration of 0.25 wt.% can be considered as optimum for achieving a CDHA-forming cement with an optimum injectability without negatively affecting other properties at the physiological temperature of 37 °C. Higher concentrations are not recommended due to the intense retarding effect on cement setting.

Chapter 4

β-TCP with phytic acid

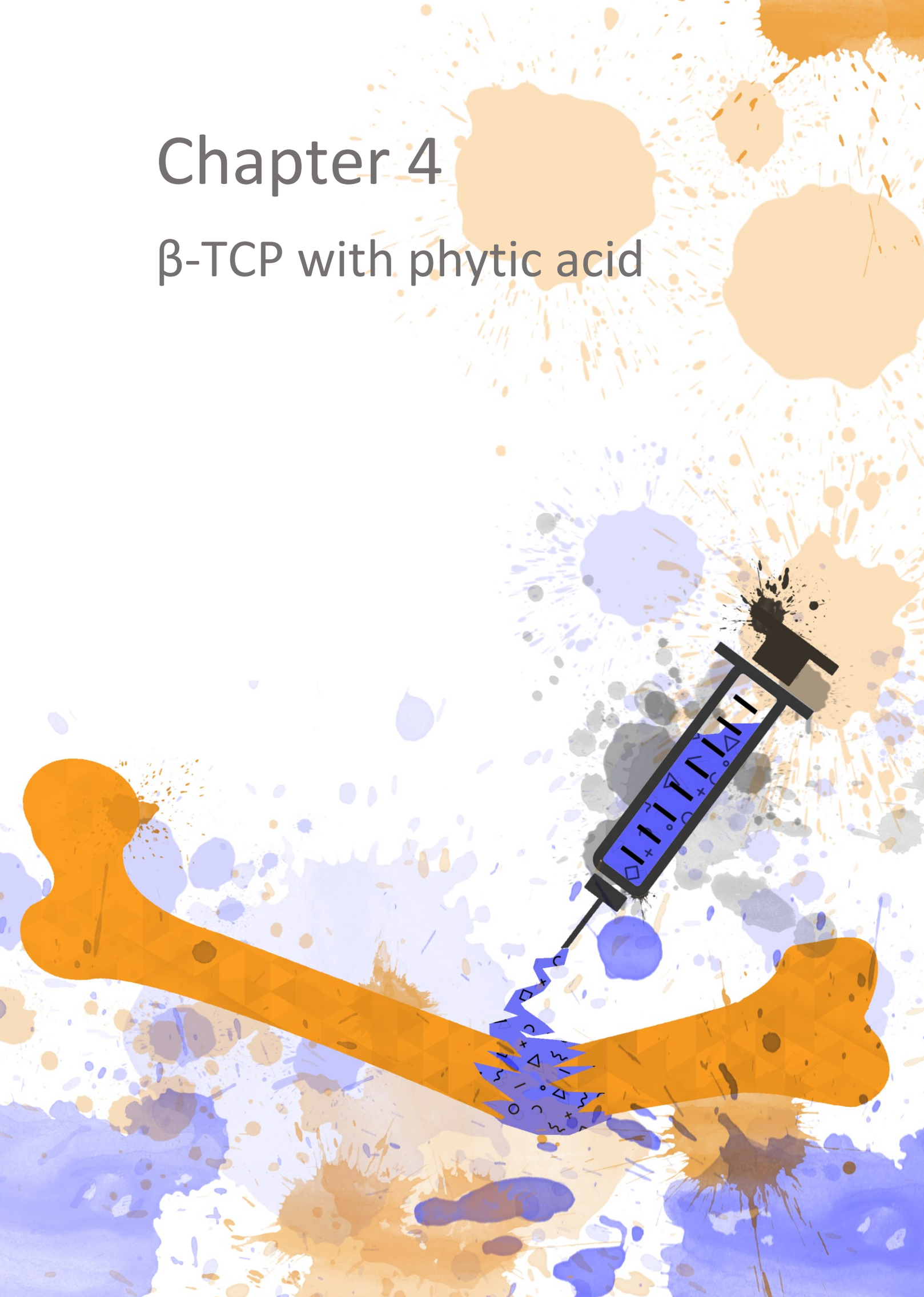

The authors contributed to the manuscript as follows:

Contributor	Contribution
Katrin Hurle	Conducted experiments and analysed data for material characterization (XRD, calorimetry, pH, NMR); revised and provided feedback to the manuscript
Jan Weichhold	Conceived the research; conceptual planning; conducted experiments and analysed data for material characterization (zeta potential, rheology, injectability, compressive strength, and scanning electron microscope)
Manuel Brueckner	Helped in the initial stages of experiments (mechanical properties)
Uwe Gbureck	Conceived the research; conceptual planning; revised and provided feedback on the manuscript
Theresa Brueckner	Helped in the initial stages of experiments (paste composition)
Friedlinde Goetz-Neunhoeffer	Revised and provided feedback on the manuscript

Chapter 4

Hydration mechanism of a calcium phosphate cement modified with phytic acid

Chapter 4 is based on a manuscript, which is already published (June 2018; Acta Biomaterialia).[694]

Authors: Katrin Hurle, Jan Weichhold, Manuel Brueckner, Uwe Gbureck, Theresa Brueckner and Friedlinde Goetz-Neunhoeffer

The content of this chapter is a result of the collaboration between the university of Würzburg and the University of Erlangen-Nürnberg. The experiments have been conducted by Jan Weichhold and Katrin Hurle with the support of Manuel Brueckner and Theresa Brueckner. They evaluated their data and discussed the work of their collaboration together.

4.1 Abstract

Calcium phosphate cements composed of β-tricalcium phosphate (β-TCP) and phosphoric acid were modified by addition of 5, 10, 12.5, 15 and 20 wt% phytic acid (IP6) related to the β-TCP

content and compared to a reference containing 0.5 M citric acid monohydrate solution as setting regulator. The hydration reaction of these cements was investigated by isothermal calorimetry and in-situ X-ray diffraction at 23 °Cand 37 °C. The cements were further characterized with respect to their injectability, rheology, zetapotential and time-resolved compressive strength development. Injectability was strongly improved by IP6 addition, while the maximum effect was already reached by the addition of 5 wt% IP6. This could be clearly related to an increase of the negative zeta potential leading to a mutual repulsion of cement particles. A further increase of the IP6 content had a detrimental effect on initial paste viscosity and shifted the gelation point to earlier time points. IP6 was further proven to act as a retarder for the cement setting reaction, whereas the effect was stronger for higher IP6concentrations. Additionally, IP6 favoured the formation of monetite instead of brushite and a better mechanical performance compared to the IP6 free reference cement.

4.2 Introduction

Brushite ($CaHPO_4 \cdot 2H_2O$) forming biocements have an improved bone regeneration capacity compared to their apatite forming counterparts [705, 706]. This stems from the higher solubility of brushite under physiological conditions, which enables not only resorption by osteoclastic cells, but also by simple chemical dissolution [707]. Brushite cement setting requires an acidic pH in the cement paste, which is usually adjusted by either using acidic calcium phosphate raw materials (e.g. monocalcium phosphate anhydrate (MCPA) or monocalcium phosphate monohydrate (MCPM)) [708] or by modifying the cement liquid with ortho- or pyrophosphoric acid [709]. Since the rate of crystal growth of brushite is high [710], setting retarders have to be applied to increase the setting time to clinically acceptable values of 5–10 min. Amongst the commonly used retarders such as citrates or pyrophosphates [360], phytic acid (Inositol-6-phosphate, IP6) has been recently described as such a setting modifier [541], whereby the influence of IP6 on the hydration mechanism and setting kinetics of brushite cements is unclear. Phytic acid has six protonated phosphate groups, which have the effect of both creating a low pH and the complexation of divalent cations such as Mg^{2+} or Ca^{2+}. The latter property was recently explored for cement formation from tricalcium phosphate and trimagnesium phosphate by a chelate setting mechanism [545, 711]. In addition, changes of zetapotential by adsorption of negatively charged phytate ions may lead to a mutual repulsion of cement particles and hence influence particle dissolution and alter rheological cement properties similar to the effect described for citric acid [537]. This study aims to investigate in detail the effect of phytic acid as setting retarder in brushite forming cements based on mixtures of ß-tricalcium phosphate (ß-TCP) and phosphoric acid. Here, an in-situ X-ray diffraction set-up, ^{1}H-NMR measurements as well as isothermal calorimetric measurements were applied to study cement setting kinetics. The results were correlated to basic cement properties like the mechanical performance and setting time. The rheological properties of the fresh cement paste were determined by measuring both injectability and paste viscosity and related to changes of the zeta-potential of cement particles after the addition of phytic acid.

4.3 Results

4.3.1 Characterization of powder samples

Phase content and surface area

The starting powder mainly consisted of β-TCP, only slight amounts of $Ca_2P_2O_7$ were detected as secondary phase. G-factor quantification resulted in a β-TCP content of 96.9 ± 0.4 wt.% and a $Ca_2P_2O_7$ content of 0.8 ± 0.1 wt.%. As the sum of crystalline phases was 97.6 ± 0.4 wt.%, no or at least only a minor content of amorphous phase was present. The BET specific surface area of the β-TCP powder was 0.53 ± 0.06 m2/g.

Zeta Potential

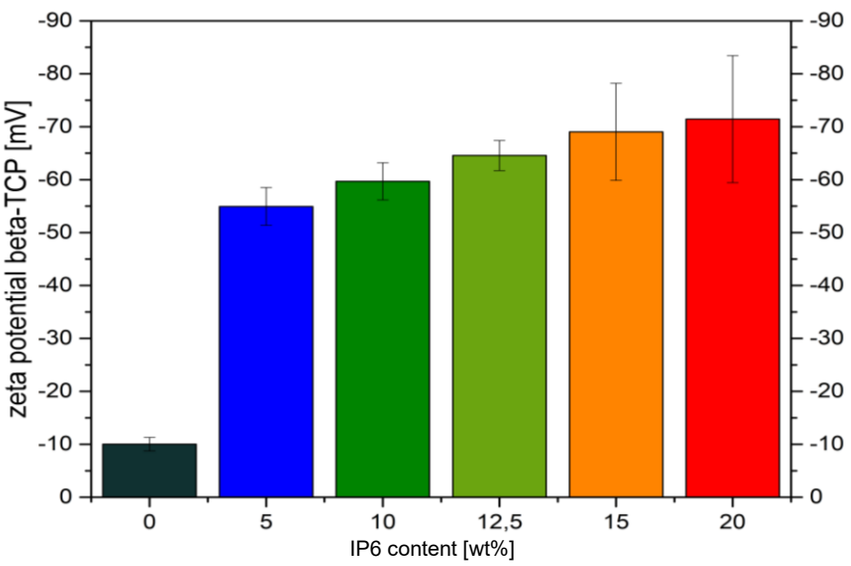

***Figure 24**. Changes in the zeta potential ζ of β-TCP depending on the amount of added phytic acid (IP6)*

Though the addition of IP6 to β-TCP seems to show a clear trend in the zeta potential change, the error increases with higher IP6 content (**Figure 24**). While the variations between samples with different IP6 concentrations are hardly significant, the difference between the reference and the samples with IP6 additions is obvious. With the addition of IP6 the zeta potential became highly negative in the range of -55.0 mV ± 3.5 mV to -71.5 mV ± 12 mV compared to the IP6-free reference with -10.0 mV ± 1.5 mV.

4.3.2 Material properties during setting

Injectability

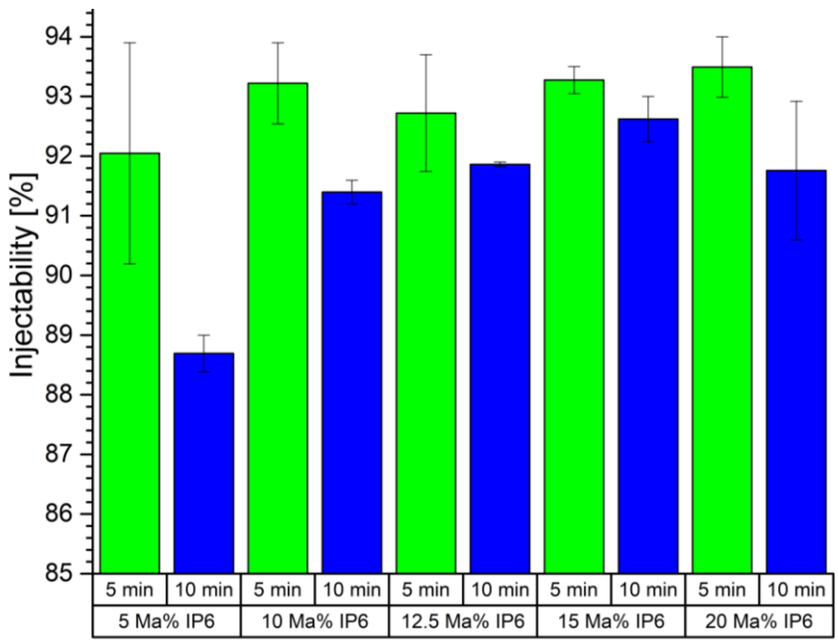

***Figure 25**. Injectability of different cement pastes as the amount injected in percent after 5 and 10 min setting time at room temperature and a L/P of 0.83 ml/g; the reference is not presented, since it was not injectable.*

Figure 25 compares the injectability of the different cement pastes at different times after mixing except the reference, as it set to fast for the measurement and was not injectable already after 2 min. Throughout all IP6 contents almost the same amount of paste could be injected after 5 min of setting. The injectability decreased after 10 min of setting for every mixture, but unlike after 5 min, a direct effect of the added amount of IP6 on the injectability was found. This accounted for IP6 concentrations up to 15 wt.%. The remaining paste was mostly in the needle and could not be pressed out, because the syringe plunger already reached the end of the syringe.

Viscosity

The results for the viscosity development during the first minutes of the hydration reaction show a clear trend with increasing IP6 content (**Figure 26a**) leading to higher cement viscosities with increasing IP6 content.

a) b)

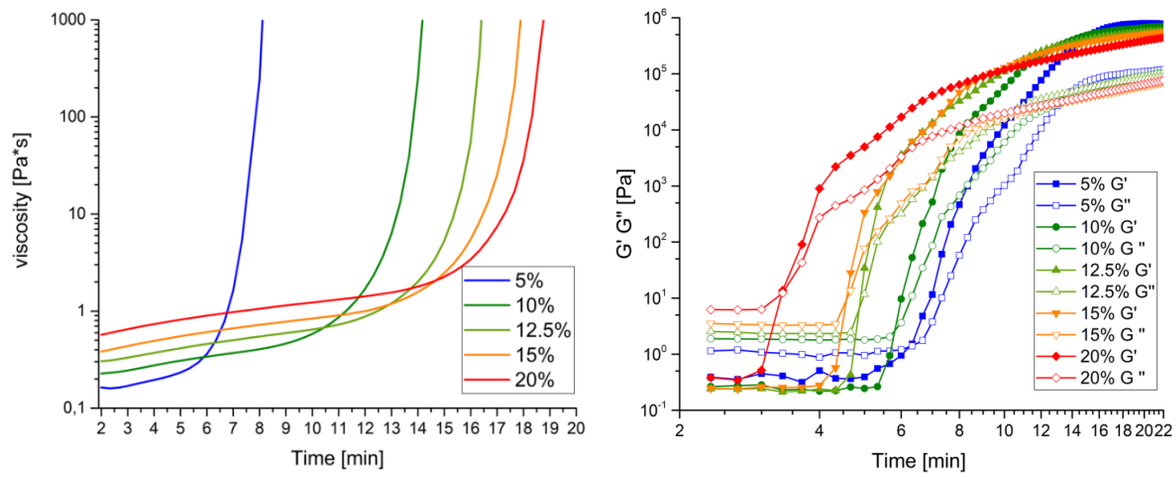

***Figure 26**. **a)** Viscosity development of the different mixtures during the first 20 minutes of the hydration reaction at 20 °C and s = 250 Pa, **b)** the mixtures' storage and loss moduli over the course of the reaction is shown 2 min after the mixing until 22 min, at 20 °C, x = 1 rad/s and c = 0.04%. The reference is not depicted as it set to fast for the measurement. Samples were measured 3 times, one representative curve is shown for each sample.*

This viscosity only slowly increases within the range fromo.1 to 1 Pa·s for a longer time period. Sample IP6_5 starts at 0.2 Pa·s but increases to >1000 Pa·s after 8 min, while sample IP6_20 starts at 0.6 Pa·s but reaches a value of above 1000 Pa·s 19 min after mixing. The oscillation experiment also showed an obvious effect of IP6 on the setting behaviour (**Figure 26b**). The addition of 5 wt.% IP6 delayed the gelation point where the graphs for the storage modulus G' and the loss modulus G" intersect and the paste became more elastic than viscous after 6.5 min. More IP6 accelerated the process, such that sample IP6_10 reaches the gelation point after about 6 min, and samples IP6_12.5, IP6_15 and IP6_20 after 5 min, 4.5 min and 3 min, respectively.

Isothermal calorimetry

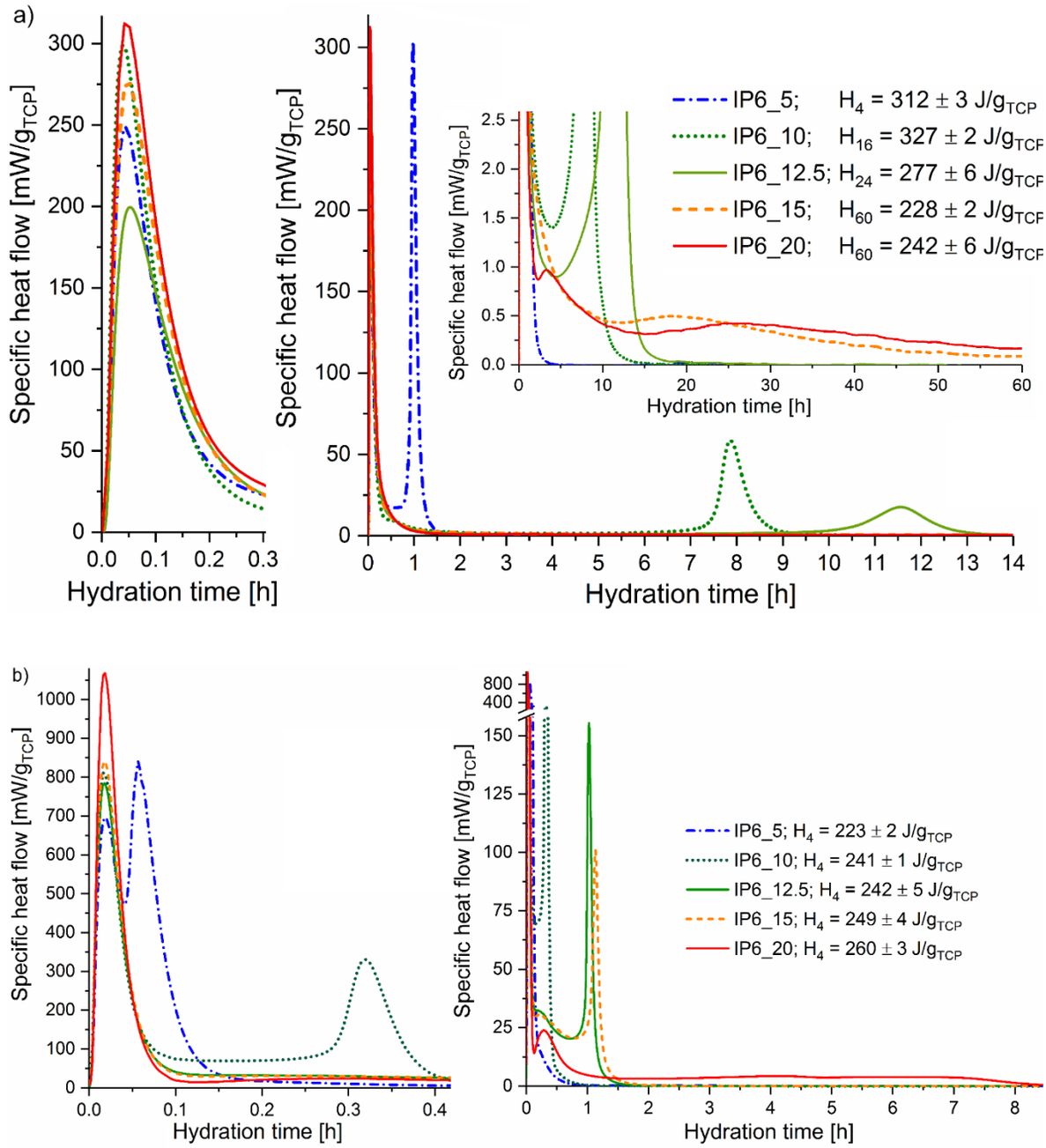

***Figure 27**. Calorimetry curves of b-TCP mixed with H_3PO_4 solution and variable concentrations of IP6 respectively 0.5 M citric acid monohydrate (reference IP6_0) at **a)** T = 23 °C; **b)** T = 37 °C; one representative curve was shown for each sample; w/c = 0.5 ml/g.*

At 23 °C, the calorimetry curves of samples IP6_5, IP6_10, IP6_12.5 and IP6_15 all showed two heat flow maxima, while for IP6_20 an additional small third maximum was visible (**Figure 27a**). The heat flow did not decrease to zero between the maxima. The first heat flow maxima, which were very sharp and high for all investigated samples, already occurred after a few minutes. No systematic correlation of the maximum height with the IP6 content of the samples was observed. The second heat flow maxima were high and sharp for the samples containing up to 12.5 wt.% IP6, while it became rather broader for IP6_15. The same accounted for the third maximum of IP6_20. Generally, the height of this maximum strongly decreased with increasing IP6 content and concurrently its position was shifted towards later time points. This change was particularly prominent for an increase from 12.5 to 15 wt.%, compared to the others. In IP6_15 and IP6_20, the reaction was not even fully completed even after a measurement time of 72 h a very slight heat flow was detected. The samples with lower IP6 contents were measured until the heat flow had decreased to zero, indicating completion of the reaction. The calorimetry curve of the reference IP6_0 was basically comparable to those of the samples modified with IP6. It showed two peaks - one rather high initial peak and a second, smaller one.

The total heat releases of the different samples varied in the range of 222 ± 11 J/gTCP (IP6_20) to 370 ± 4 J/gTCP (IP6_0). The total heat release for IP6_12.5 was below that of IP6_5 and IP6_10. For IP6_15 and IP6_20, the values were even lower. Here one should keep in mind that in these two samples the reaction could not be measured until completion. While the reproducibility of the three separately prepared measurements was were rather good well reproducible for samples IP6_5, IP6_15 and IP6_20, the position of the second maximum varied for IP6_10 from 6.9 to 8.1 h for IP6_10 and for IP6_12.5 from 9.6 to 13.5 h for IP6_12.5, which indicated lower reproducibility. For the reference, the height of the maximum varied from 46 to 146 mW/gTCP, but the maximum position was rather reproducible.

At 37 °C, the calorimetry curves of all samples exhibited two clearly separable maxima, while the height of the second maxima clearly decreased with increasing IP6 content (**Figure 27b**). For the first maxima, from the initial reaction, no clear relation of maximum height and IP6 content was observed. In all cases, the heat flow did not decrease to zero between the first and the second maximum. For sample IP6_20, the second maximum was rather flat, but in contrast to the measurements at 23 °C, the heat flow decreased to zero after about 10 h.

The total heat release until completion of the reaction slightly increased with increasing IP6 content. The reproducibility of the measurements was rather good for samples with lower IP6

contents. The measurements of samples with lower IP6 contents were well reproducible. For IP6_12.5, the position of the maximum only slightly varied from 0.9 to 1.0 h. For IP6_20, higher variations in the range of some h were observed. As the maxima were rather broad in this case, no definite position of the maximum could be given. No measurement of the reference was performed at 37 °C, since the reaction would have occurred too rapidly to obtain meaningful data.

In-situ XRD

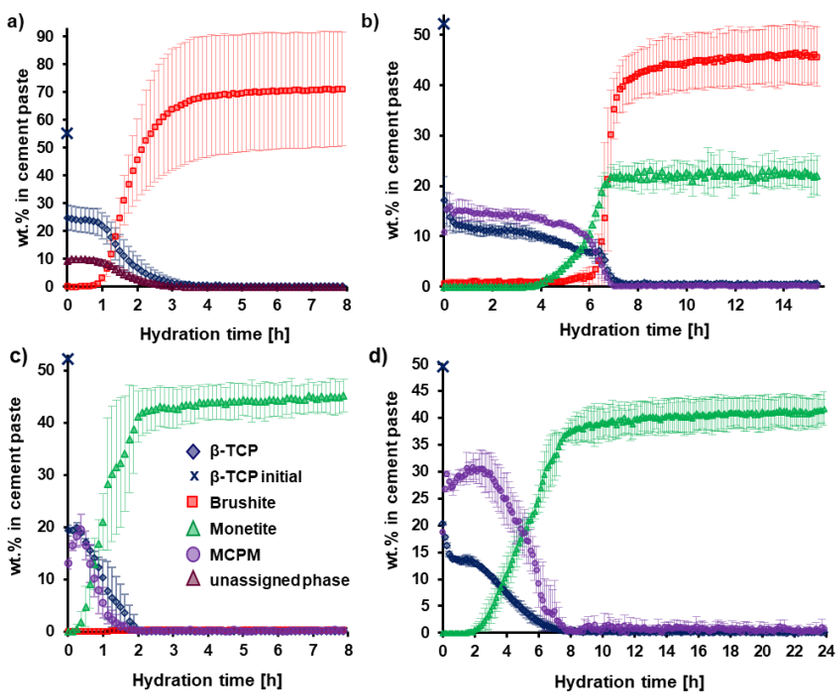

***Figure 28**. Development of quantitative phase content determined by in-situ XRD and G-factor quantification in β-TCP mixed with a solution of H_3PO_4 (molar ratio 1:1) and **a)** 0.5 M citric acid monohydrate; T = 23 °C, **b)** 10 wt% IP6 related to the β-TCP content; T = 23 °C, **c)** 10 wt% IP6 related to the β-TCP content; T = 37 °C, **d)** 20 wt% IP6 related to the β-TCP content; T = 37 °C; the means of three measurements were shown (b: two measurements); w/c = 0.5 ml/g; violet diamonds: β-TCP ; cross: β-TCP initial; red square: brushite; green triangle: Monetite violet circle: MCPM; violet triangle: unassigned phase.*

In the reference sample measured at 23 °C, rapid formation of brushite was observed, which started after about 1 h and was nearly completed after about 3 h (**Figure 28a**). The brushite exhibited a pronounced preferred orientation in the (0 1 0) direction, with March Dollase factors ranging from 0.65 to 0.89. This might explain the high variations in brushite quantities.

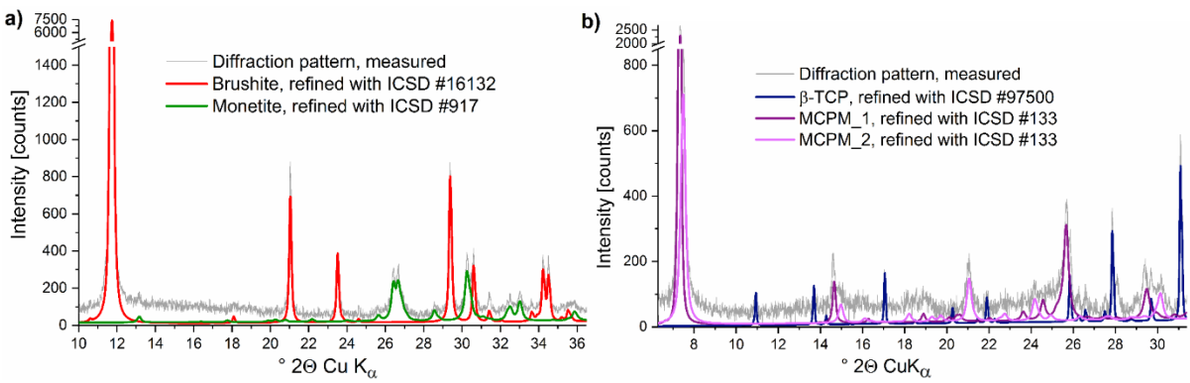

Figure 29. *Diffraction pattern of β-TCP mixed with a solution of H_3PO_4 (molar ratio 1:1) and 10 wt% IP6 related to the β-TCP content, recorded after* ***a)*** *24 h and* ***b)*** *1 h; T = 23 °C; w/c = 0.5 ml/g; the background contributions of Kapton film and water were subtracted from the measured pattern for better presentation; the diffraction patterns of the crystalline phases presented were calculated with software TOPAS 4.2 (Bruker AXS, Karlsruhe).*

From the beginning of the measurement, a crystalline phase was detected that could not be assigned in the XRD evaluation software. According to literature, it is most likely a calcium citrate [17]. Brushite formation was accompanied by a decrease of the content of β-TCP and the unassigned phase. The β-TCP content quantified in the first range (duration of measurement: 7.5 min), which was 25 ± 4 wt.%, was already far below the quantity that should have been present in the cement paste before any reaction occurred (55 wt.%).

In sample IP6_10 measured at 23 °C, both monetite and brushite were formed in significant amounts (**Figure 28 b** and **Figure 29 a**). Formation of monetite started about 2 h earlier than brushite formation, but proceeded more slowly, while brushite formation was very rapid (**Figure 28 b**). MCPM was detected as an intermediate hydration product. It was already present at the beginning of the measurement, i.e. during recording of the first measurement range. Its content remained constant for the first few h, then it decreased parallel to the content of β-TCP until both phases completely disappeared. Two different MCPM phases with differing lattice parameters were detected. This was clearly indicated by the splitting of the first diffraction peak of MCPM, which was also the most intense reflection (**Figure 29b**). Since their dissolution occurred mainly parallel, these two phases were summarized for further observations. As in the reference, the β-TCP content quantified in the first range (17 ± 5 wt.%) was far below the theoretical initial content (52 wt.%). This means that at the beginning of the hydration H_3PO_4 rapidly reacts with parts of the β-TCP to form MCPM according to equation (3):

$$\beta\text{-}Ca_3(PO_4)_2 + 4\ H_3PO_4 + 3\ H_2O \rightarrow 3\ Ca(H_2PO_4)_2{\cdot}H_2O \quad (3)$$

Following this first step, MCPM reacts with the remaining β-TCP to form monetite according to (4) and brushite according to (5):

$$Ca(H_2PO_4)_2{\cdot}H_2O + Ca_3(PO_4)_2 \rightarrow 4\ CaHPO_4 + H_2O \quad (4)$$

$$Ca(H_2PO_4)_2{\cdot}H_2O + Ca_3(PO_4)_2 + 7\ H_2O \rightarrow 4\ CaHPO_4{\cdot}2H_2O \quad (5)$$

Monetite formation was finished at approximately the same time when the dissolution of MCPM and β-TCP was completed. Formation of brushite slightly continued for a few h after the starting phases were consumed, but then its content also reached a plateau. At the end of the measurement, mixtures of brushite and monetite were present.

The time when the rapid brushite formation occurred was not reproducible, as it varied from 6 h to 10 h after beginning of the measurement. Still the general course of the reaction was comparable for all measurements. Samples with higher IP6 concentrations were not measured at 23 °C because the hydration would have proceeded too slow to obtain meaningful results in reasonable measurement times, as was indicated by the calorimetry results.

Samples IP6_10 and IP6_20 were measured at 37 °C. For both compositions, formation of monetite was observed (**Figure 28c** and **d**). Brushite was only detected in some measurements in small amounts below 1 wt.%. Similar to the measurement performed at 23 °C, MCPM was detected as an intermediate hydration product and two structures with different lattice parameters had to be included. For both IP6 concentrations, the MCPM content increased until a maximum was reached, and then decreased again. Both β-TCP and MCPM disappeared at nearly the same time. Simultaneously, the monetite content nearly reached its maximum.

The reaction was basically the same for both IP6_10 and IP6_20, with the difference that the reaction was generally slower for IP6_20. The only noticeably difference was that for IP6_20 an initial decrease of the β-TCP content was observed, which was not the case for IP6_10. At the end of the measurements, monetite was practically the only crystalline phase detected in the samples. The final crystalline monetite quantities were remarkably below the theoretical content of solid phases that should be present in the samples, which would be 72 wt.% for IP6_10 and 68 wt.% for IP6_20.The reproducibility of the measurements was good for both IP6 concentrations.

In-situ 1H-NMR

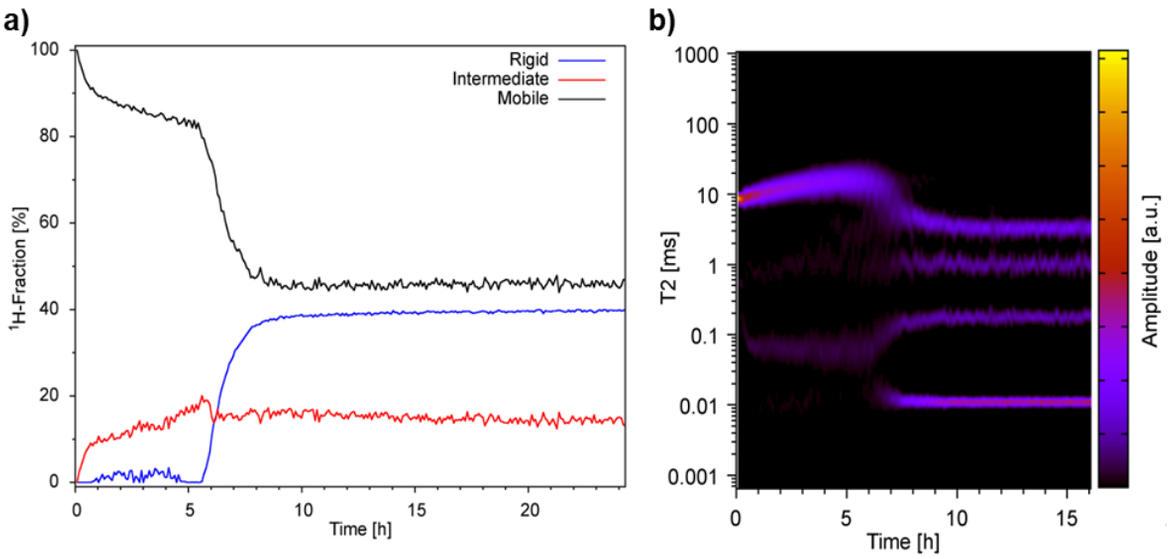

***Figure 30**. In-situ ¹H NMR results of β-TCP mixed with a solution of H_3PO_4 (molar ratio 1:1) and 10 wt% IP6 related to the β-TCP content; w/c = 0.5 ml/g; T = 23 °C; **a)** quantities of ¹H fraction; **b)** development of the relaxation times T2.*

In sample IP6_10 measured at 23 °C, formation of a hydrate phase was observed after about 6 h, which is indicated by the rapid increase of the proton fraction included in a crystalline bound hydrate phase (**Figure 30a**). This is accompanied by a decrease of the protons in the mobile fraction. In addition, ¹H-NMR evaluation suggested formation of a hydrate phase with an intermediate mobile proton fraction which formed already at the beginning. This is accompanied by a slight decrease of the mobile proton fraction. The relaxation time T2 of the mobile proton fraction, which corresponds to the mixing liquid, slightly increased during the first 6 h (**Figure 30b**). Afterwards, simultaneously to the formation of a hydrate phase, T2 decreased until it reached a rather constant plateau.

pH development during setting

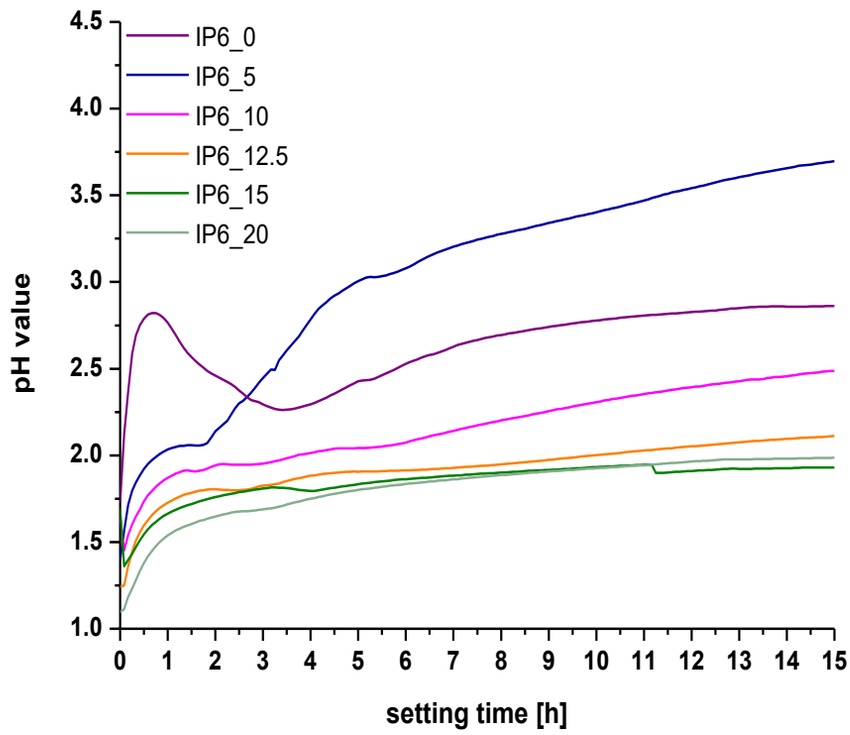

***Figure 31**. pH profile of the setting reaction of cements composed of β-TCP and 0, 5, 10, 12.5, 15 or 20 wt.% IP6 containing phosphoric acid solution at a L/P of 0.83 mL/g.*

The pH-profiles of the cement formulations as a function of the IP6 content during setting are depicted in **Figure 31**. Obviously, the strongest pH alterations took place within the first 6 h of setting, whereat the initial pH decreased with increasing IP6 concentration between 1.7 ± 0.1 (IP6_0) to 1.1 ± 0.3 (IP6_20). A steep ascent within the first hour of setting was followed by a flatter ascent, such that final values of between 3.7 ± 0.9 (IP6_5) and approximately 2 (IP6_15, IP6_20) were measured for the IP6 containing cement formulations. In contrast, the reference showed an initial increase in pH from 1.7 ± 0.1 to 2.8 ± 0.04, followed by a decrease and a new increase, so that a value of 2.9 ± 0.3 was reached after 15 h.

4.3.3 Characterization of hardened samples

XRD of samples stored at 23 °C

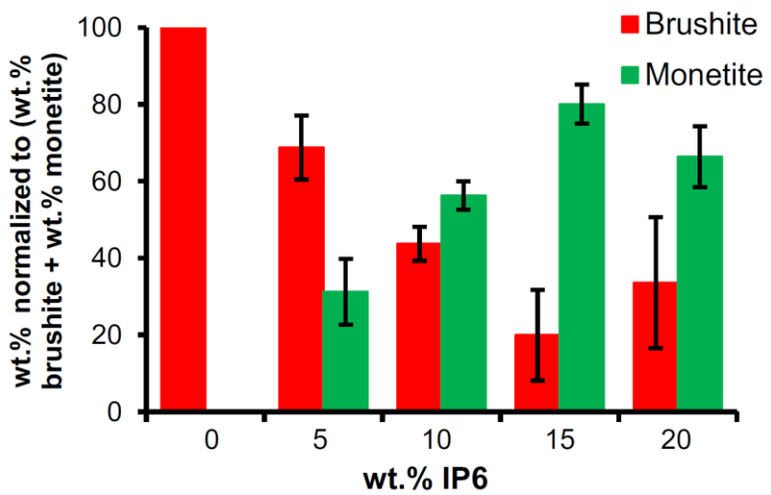

Figure 32. *Brushite and monetite content in β-TCP mixed with a solution of H_3PO_4 (molar ratio 1:1) and different wt% of IP6 related to the β-TCP content, the reference with 0 wt.% IP6 contained 0.5 M citric acid monohydrate solution; the quantities were normalized to the sum of the contents of monetite and brushite; means of three independently prepared measurements were shown; w/c = 0.5 ml/g; T = 23 °C.*

XRD measurements of the samples with different IP6 contents hardened for 72 h at 23 °C indicated that there is some relation between final phase composition and IP6 content (**Figure 32**). The data were normalized to the sum of the hydrate phases brushite and monetite to eliminate influences of variable liquid content in the different samples and possible errors in G-factor quantification affecting both phases, which might result from inhomogeneities in the sample. For IP6_5, the normalized brushite content was significantly higher, compared to the other samples. Still, there is no significant difference between IP6_10 and IP6_20, and additionally the reproducibility was not good for all samples, which is probably a result of the massive retardation. For the reference with 0.5 M citric acid monohydrate, only brushite was detected as final hydration product.

Mechanical performance

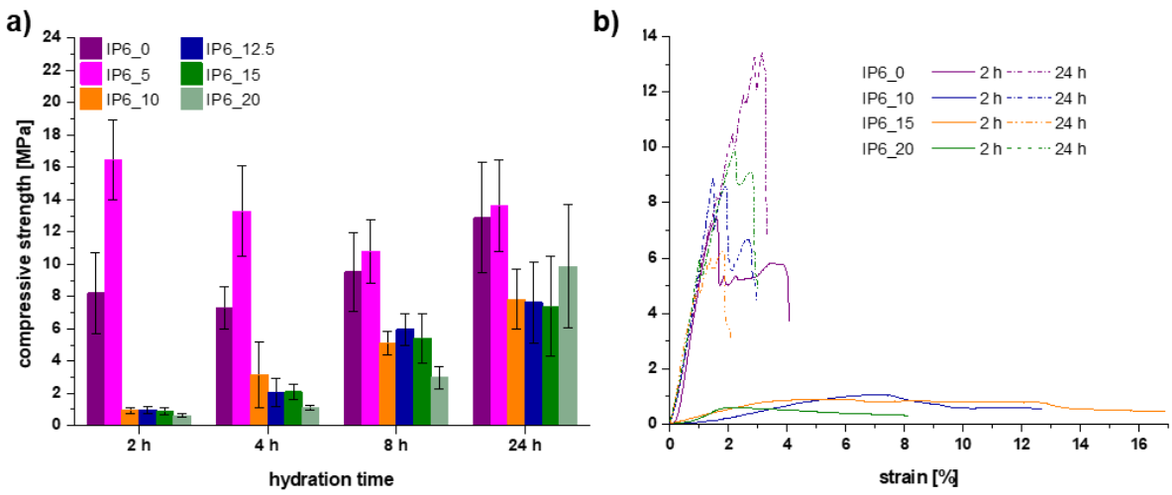

***Figure 33**. Compressive strength **a)** and corresponding selected stress-strain-curves **b)** of cuboidal cement specimens composed of β-TCP and 0, 5, 10, 12.5, 15 or 20 wt% IP6 containing phosphoric acid solution at a L/P of 0.83 mL/g after 2, 4, 8 and 24 h of setting at 37 °C and 100% humidity*

The mechanical properties of the analyzed cement specimens are revealed by **Figure 33**. Regarding the strength values after 2 h of setting, low amounts of setting modulators, as it is the case for the classic cement composition with 0.5 M citric acid (8.2 ± 2.5 MPa) or the formulation with 5 wt.% IP6 (16.5 ± 2.5 MPa), do not seem to have an impact. Actually, maximum strength values were already reached after 2 h, as only marginal changes were observed between single time points. However, using 5 wt.% IP6 instead of citric acid had a beneficial effect on the absolute strength values, as this led to their duplication after 2 h. Higher amounts of IP6 actually retarded the setting reaction in such a way, that compressive strengths of <1 MPa were observed after 2 h, which afterwards increased steadily with proceeding reaction time and gained values of approximately 7 to 10 MPa after 24 h of setting. For the first 8 h of setting, samples with the highest IP6 content exhibited the lowest compressive strength (**Figure 33a**). Selected stress-strain-diagrams of the cement specimens under compression showed that formulations with an IP6 amount of between 10 and 20 wt.% initially exhibited a more ductile fracture behavior with low strength at high strain values, while longer immersion at 100 % humidity increased their brittleness, which was characterized by higher strength at much lower strain values (**Figure 33b**).

SEM investigations of hydrated pastes

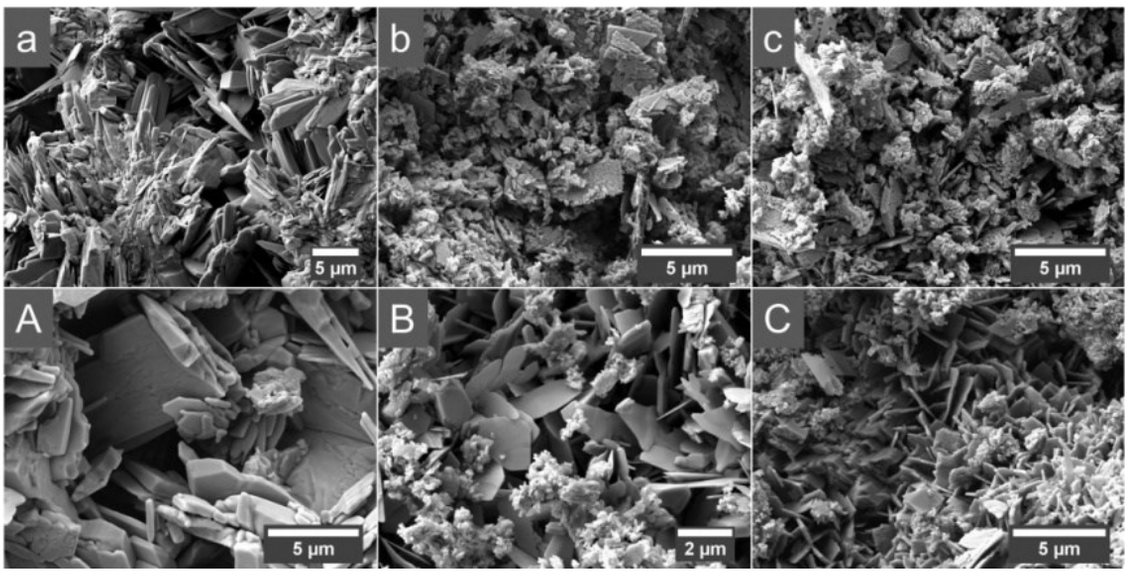

***Figure 34**. Scanning electron micrographs of fracture surfaces from cement specimens composed of β-TCP and 0 **(a, A)**, 10 **(b, B)**, or 20 wt.% **(c, C)** IP6 containing phosphoric acid solution at a L/P of 0.83 mL/g after 2 (small letter) and 24 h (capital letter) of setting at 37 °C and 100% humidity*

Crystal morphologies found in cement specimens without or with 10 or 20 wt.% IP6 are illustrated by **Figure 34**. While the reference topography mainly showed needle-like crystals with a length of approximately 5 µm as well as 10 µm long plate-like crystals after 2 h of setting, the surface of the IP6 containing cements was rather covered with platelets and smaller sized grain agglomerates. The crystal size increased in all three cases with a longer hardening time of 24 h; though the final crystal size was smaller at higher IP6 amounts. Furthermore, the quantitative *in-situ* XRD results have demonstrated that in IP6_20 only slight amounts of monetite were present after 2 h, while the sample was composed of only monetite after 24 h (**Figure 28d**)

4.4 Discussion

Hydration mechanism of the IP6 modified CPC

According to the quantitative *in-situ* results obtained at 23 °C respectively 37 °C, the starting components of the cement pastes (β-TCP and H_3PO_4) set to brushite or monetite via formation of MCPM as an intermediate hydrate phase in IP6 modified samples, which formed very rapidly. The initial increase of pH observed for all samples during the first 2 h of the reaction is a further indication that H_3PO_4 is rapidly consumed at the beginning for MCPM formation.

The general hydration mechanism at 37 °C was basically the same for IP6_10 and IP6_20, while all parts of the reaction - formation of MCPM and formation of monetite - were generally slower in IP6_20. There was only one remarkable difference concerning the dissolution of β-TCP. While in IP6_10 the β-TCP content was nearly constant during the first 30 min, in IP6_20 a rapid initial β-TCP decrease was observed until a plateau was reached. It is very likely that such an initial increase also occurred in IP6_10, but it was too rapid to be detected by XRD due to the sample preparation time of some minutes. This rapid initial decrease of β-TCP content is indeed indicated by the rapid initial formation of MCPM, which was detected already in the first XRD range for all samples.

The initial formation of MCPM is further expressed by the very high initial heat flow measured by isothermal calorimetry for all samples investigated. Due to the internal stirring procedure applied in the calorimetry measurements, the data for the initial heat flow are actually reliable and meaningful. Formation of MCPM (see reaction 1) is indeed highly exothermic with an enthalpy of hydration of -151.44 kJ/mol_{TCP}, compared to the formation of monetite and brushite from β-TCP and MCPM (-12.92 kJ/mol_{TCP} respectively -83.04 kJ/mol_{TCP}). These data were calculated according to Hess´ law [712] from the standard enthalpies of formation for the phases involved [713], which certainly explains the high initial heat flow measured for all samples.

The sharp second calorimetry maximum observed for the mixtures at 37 °C most likely results from synchronous dissolution of MCPM and β-TCP and formation of monetite. An increase of the IP6 content hence leads to a continuous retardation of monetite formation, which starts later and its maximum formation speed, indicated by the height of the calorimetry maxima, is also reduced. The difference of the sum of crystalline phases to the theoretically expected solid content after completion of hydration can be well explained by the formation of an amorphous or low crystallinity hydration product in addition to monetite. As a hkl phase similar to the

main reflections of monetite was added in the refinement procedure, it is likely that monetite with low crystallinity formed in addition to crystalline monetite.

It is further remarkable that at 23 °C in the reference, only brushite was formed, while hydration of IP6 modified cement pastes resulted in mixtures of monetite and brushite. This clearly shows that IP6 favours the formation of monetite. The reason for this might be the decrease of pH due to IP6 addition, which can promote formation of monetite instead of brushite [714]. The additional chelation of IP6 with Ca^{2+} is supposed to occur directly at the beginning of the reaction, which is indicated by the sticky consistence of the IP6 modified cement pastes shortly after mixing. Since for in-situ ^{1}H NMR measurements always a few min pass until the measurement can be started due to the sample preparation and device adjusting procedure, it is likely that the chelation reaction cannot be followed by this method.

Effect of temperature on the hydration

Hydration of the IP6 modified cement formulations was strongly accelerated by increasing the temperature from 23 °C to 37 °C. Calorimetry results combined with *in-situ* XRD investigations demonstrated that especially the formation of the final hydration product monetite was strongly accelerated by the temperature increase. The initial formation of MCPM is probably not noticeably affected by temperature, since no remarkable differences in the height of the first calorimetry maximum resulting from MCPM formation was observed between the measurements at 23 °C and 37 °C. At 37 °C the reaction was completed even for IP6_20 after 16 h, while for 23 °C the reaction in IP6_15 and IP6_20 has drastically slowed down so that completion was not achieved even after 72 h. This further confirms the promoting effect of temperature increase on cement hydration. The temperature during hydration had also a noticeably influence on the final hydration products. While hydration at 23 °C resulted in mixtures of monetite and brushite in different ratios for all IP6 modified samples, at 37 °C monetite was clearly the predominant hydration product. Hence a temperature increase clearly favours formation of monetite instead of brushite.

Thermodynamic considerations

According to the Hess´ law calculations, the enthalpy of reaction for the hydration of β-TCP and H_3PO_4 to monetite is -153.3 J/g_{TCP} respectively -47.55 kJ/mol_{TCP}. As the enthalpy of reaction is independent of the reaction path [712], the occurrence of the intermediate MCPM should not affect the overall reaction enthalpy. Hence, as in the samples measured at 37 °C monetite was detected as the only hydration product, a total heat release of -153.3 J/g_{TCP} should have been measured upon completion of the hydration. In fact, all total heat releases measured for the IP6

modified samples were considerably above that value. Therefore, it is likely that an additional heat contribution results from another reaction. This additional contribution probably results from formation of monetite with low crystallinity, which might have a different enthalpy of formation. It might further origin from the chelation of IP6. This assumption is supported by the fact that the total heat release slightly, but continuously increased with increasing IP6 content, although the final crystalline hydration product was the same for all samples.

At 23 °C, the total heat releases were higher than at 37 °C for the samples with IP6 concentrations up to 12.5 wt.%. This can be explained by the observation that at 23 °C brushite has formed in addition to monetite, since the enthalpy of reaction for the hydration of β-TCP and H_3PO_4 to brushite is more than double with -322.8 J/g_{TCP} respectively -100.14 kJ/mol_{TCP}. For higher IP6 contents, the values obtained at 23 °C were lower, which results from the fact that hydration was not completed yet in these samples and that there was a trend of increasing monetite formation compared to brushite with increasing IP6 concentration in the sample.

Correlation of strength development with the development of quantitative phase content

Samples with higher IP6 concentrations (IP6_15 and IP6_20) showed ductile performance during the first hour. This is supposed to result from a rapid initial IP6 chelation with Ca^{2+}. The transformation of this ductile to a brittle performance observed between 2 h and 24 h is then most likely a result of crystal formation (monetite) occurring during this time according to the quantitative *in-situ* XRD data. The strength development over time for the different IP6 concentrations agrees well with the phase development during setting. For the reference and IP6_5, the cements showed a high compressive strength of 8-16 MPa after 2 h setting with no further increase after 24 h. This is well in accordance with the results of in-situ XRD, where nearly completion of monetite formation was observed after 2 h for IP6_5 at 37 °C.

In contrast, higher IP6 concentrations resulted in comparatively weak cements (CS~ 1 MPa) after 2 h, which then continuously increased to final values of 8-10 MPa after 24 h. This agrees well with the formation of the setting product monetite according to the XRD results. Comparing the obtained strengths to a calcium phosphate cement consisting of 50 Mol % tetra calcium phosphate (TTCP) and 50 Mol % dicalcium phosphate anhydrous (DCPA) with a compressive strength of 30.7 MPa and 36.0 MPa after 2 h and 24 h respectively, the obtained strengths were relatively low [386]. But set in context with the common compressive strengths of brushite cements which range from around 1 MPa to 60 MPa (average 10 ± 13 MPa) for dry samples and 5 MPa to 75 MPa (average 18 ± 18 MPa) for wet samples with a respective porosity of 25 % to 70 % and 13 % to 50 %, the presented cement has a compressive strength that is well in the range of an average brushite cement [459, 715].

Compared to the reference, which was not injectable already after 2 min, with the addition of IP6 the injectability improved significantly. The paste remained well injectable even 10 minutes after mixing and only lost about 1-3 % injectability between 5 and 10 min after mixing. Increasing the amount of added IP6 to more than 5 wt.% does not seem to have an increasing effect on the injectability during the first 5 min of setting. After 10 min setting the effect of an increased amount of IP6 can be seen, as the injectability remained higher the higher the IP6 content was. A higher amount of IP6 directly increases cement viscosity during setting. This can be explained by an increase in chelate complex formation between Ca^{2+}-Ions and the phosphate groups of the IP6, which are likely less soluble than β-TCP. In addition, complex formation additionally slows down the solution/precipitation cement reaction by decreasing the availability of free calcium ions [549, 703, 704]. This leads to a delayed rise in paste viscosity and also explains well the strong retarding effect on cement hydration as clearly demonstrated in this study.

As the viscosity measurements under constant sheering destroy small crystal networks formed at early time points, the viscosity increase with time is likely underestimated by this dynamic testing regime. Here, rheological characterization by a further oscillatory test demonstrated, that the paste rheology was dominated in the first few minutes by the chelate complexes rather than the cement setting itself. At the intersection of the graphs G' and G" (gelation point) the paste switches from a viscous to an elastic behaviour. With increasing addition of IP6, this gelation point appeared earlier since more chelate complexes are formed. This is in agreement with literature, where it has been demonstrated that the chelation not only has a retarding effect on the hydration reaction, but also leads to a sticky and more elastic paste at early time-points [711].

The last parameter which very likely affects the rheological behaviour and hence injectability is the zeta potential. In this study, the value of the zeta potential increased by the factor of 4-5 by the addition of IP6, which is in accordance with the reports of Konishi, T *et al.* [544] and Takahashi, S *et al.* [545]. IP6 has six phosphate groups which result in a strong negative surface charge. This negative surface charge is believed to enhance particle dispersion and inhibit agglomeration due to mutual repulsion [545], which was confirmed in the present study for IP6 addition. Similar to the injectability, the zeta potential is not largely affected by increasing the amount of added IP6, which may be a result of an IP6 saturation of the particle surfaces.

4.5 Conclusion

In the IP6 modified CPC systems investigated in this study H_3PO_4 and β-TCP reacted to monetite or mixtures of brushite and monetite via formation of MCPM as intermediate hydration product. At 37 °C, hydration of IP6 modified samples resulted in cements composed of monetite only. This is thought to be beneficial for a clinical application since monetite has been demonstrated to have a more continuous and reliable bone remodeling ability compared to brushite due to the absence of phase changes in vivo slowing down resorption [706, 707]. As IP6 was shown to increasingly delay the reaction with increasing amount, it can be applied as a useful retarder for adjusting the hydration to the desired setting times. IP6 was further proven to be a versatile additive for achieving well injectable cement pastes, whereby the observed increase of injectability could be clearly related to a more negative zeta potential. 5 wt.% of IP6 related to the β-TCP content were already sufficient to reach maximum injectability of the cement paste. Combined with the enormous retarding effect observed for higher IP6 concentrations, it can be concluded that already small IP6 concentrations in the range of a few wt.% are sufficient to adjust a clinically favourable rheology and setting behavior.

Chapter 5

α-TCP with PP

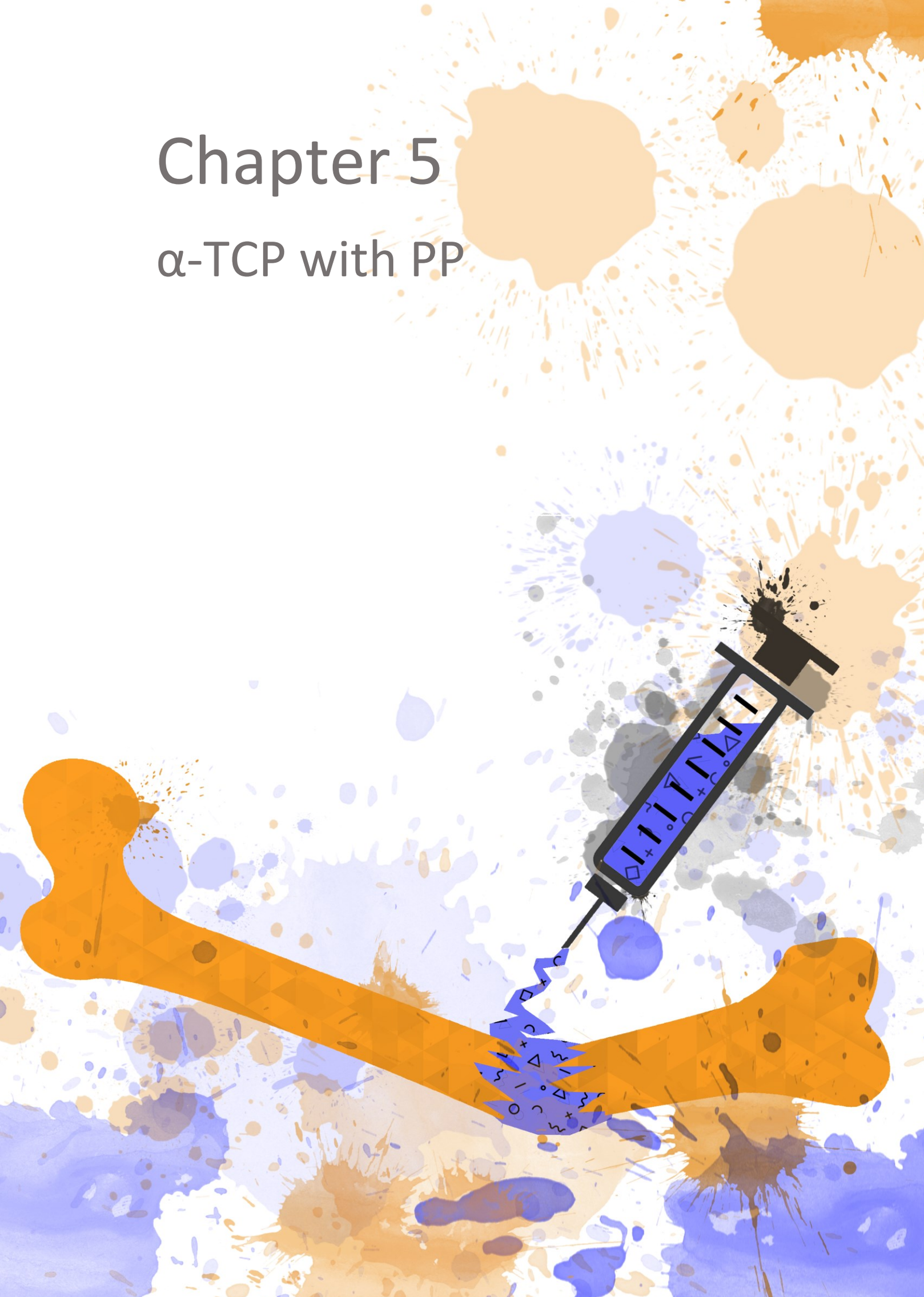

The authors contributed to the manuscript as follows:

Contributor	Contribution
Jan Weichhold	Conceived the research; conceptual planning; conducted experiments and analysed data for material characterization (particle size, pH zeta potential, rheology, injectability, XRD compressive strength, porosity and scanning electron microscope)
Friedlinde Goetz-Neunhoeffer	Revised and provided feedback on the manuscript
Katrin Hurle	Revised and provided feedback to the manuscript; conducted experiments and analysed data for material characterization (XRD, calorimetry, pore water)
Uwe Gbureck	Conceived the research; conceptual planning; revised and provided feedback on the manuscript

Chapter 5

Pyrophosphate ions inhibit calcium phosphate cement reaction and enable storage of premixed pastes with a controlled activation by orthophosphate addition

Chapter 5 is based on a manuscript, which is already published (June 2022; Ceramics International).[716]

Authors: Jan Weichhold, Friedlinde Goetz-Neunhoeffer, Katrin Hurle andUwe Gbureck

The content of this chapter is a result of the collaboration between the university of Würzburg and the University of Erlangen-Nürnberg. The experiments have been conducted by Jan Weichhold and Katrin Hurle. They evaluated their data and discussed the work of their collaboration together.

5.1 Abstract

Standard preparation of a calcium phosphate cement, which includes mixing a solid and a liquid component (reactive cement powder and mixing liquid) in an open bowl at the operating theatre, poses the risk of bacterial contamination. As interoperative bacterial contamination leads to prolonged wound discharge, superficial surgical site infection or deep periprosthetic infections, facilitating this mixing procedure is highly desirable [49]. Prefabricated cement pastes are a promising approach: The mixing liquid and a stable suspension of the cement powder are assembled and mixed in a special syringe, minimizing the risk of contamination.

In this study, a suspension of reactive α-tricalcium phosphate powder in water was stabilized by sodium pyrophosphate decahydrate (PP). Controlled activation of the hydration was accomplished by adding a concentrated Na_2HPO_4/NaH_2PO_4 (Na_2/Na) solution. Systematic assessment of the activation mechanism, including the effect of the PP concentration and the amount of Na_2/Na added, was performed by isothermal calorimetry, quantitative in-situ X-ray diffraction, rheological characterization and automated Gillmore needle measurements at 37 °C. The set cements were characterized with respect to their quantitative phase composition, compressive strength and porosity.

Prefabricated pastes with addition of at least 0.05 wt.% PP were successfully stabilized for up to 2 weeks at 25 °C, and even 4 weeks at 4 °C. Pre-storage of this pastes had no significant impact on the setting performance and the properties of the material afterwards. Increasing the PP concentration at constant Na_2/Na amount systematically retarded the setting reaction, while an elevated quantity of Na_2/Na addition at constant PP concentration resulted in an acceleration.

Based on these results, a composition stabilized with 0.05 wt.% PP and activated with 20.8 vol% Na_2/Na related to the amount of liquid in the prefabricated pastes appears ideal with respect to the desired setting performance, for the specific cement powder investigated.

5.2 Introduction

Most injectable bone replacement materials must undergo a quite fast hardening process of just a few minutes to be effectively applicable by the surgeon [427, 717, 718]. This process is generally started by mixing two or more components (mostly including powder and liquid) together to initiate a setting reaction [429, 466]. As a result, the different components have to be stored separately and then mixed onsite to prevent preliminary setting, which would prevent optimal usage. This poses several issues. First, the properties of the material must be reproducible with every use, even when prepared by different surgeons or clinical staff. But naturally, there are deviations when the pastes are prepared by different persons than just used directly from the packaging [49]. The second important part is related to the environment where the material is prepared. The different components can be sterilized and sealed off separately until they are used. But once they are opened and combined in the operating theatre, there is a high risk of contamination of the paste, as the materials are usually mixed in an open bowl [50-54].

This study aims to present a bone cement system that eliminates these factors by making the components storable in ready to use state. There have been several ideas to overcome these problems. Materials based on a common cement reaction harden through the dissolution of the cement particles in an aqueous medium and a subsequent precipitation of hydrate phases [336, 719, 720]. For example, α-tricalcium phosphate (α-TCP, α-$Ca_3(PO_4)_2$) reacts with water under formation of calcium-deficient hydroxyapatite (CDHA, $Ca_9(PO_4)_5(HPO_4)OH$) according to equation (1) [720].

$$3\ \alpha\text{-}Ca_3(PO_4)_2 + H_2O \rightarrow Ca_9(PO_4)_5(HPO_4)OH \qquad (1)$$

Replacing the aqueous solution with a non-aqueous solution such as oil [717] prevents this hydration process and enables a storable injectable paste. It hardens only when the oil is replaced by an aqueous solution during the application or afterwards e.g., when the oil gets replaced by body fluids at the application site. Other approaches still used the standard composition of cement powder and an aqueous liquid for the paste but changed the behaviour by freezing the cement pastes directly after mixing and therefore also preventing the reaction with the cement powder until the pastes are thawed and applied [358]. All these ideas require a fair amount of setup, specific non ambient storage conditions or a complete change of components of the applied paste. A different approach is to inhibit the setting reaction with additional ions in the paste. Bohner, M. *et al.* [721] already showed that Mg^{2+} ions can prevent the cement reaction until the desired time of application. Here the inhibited pastes were

activated by the addition of additional phosphate ions from different phosphate salts, or hydroxyapatite seed crystals.

This study aims to investigate a similar path, but the Mg^{2+} ions were replaced by pyrophosphate (PP) ions ($P_2O_7^{4-}$). These were added in the form of the highly soluble sodium pyrophosphate decahydrate ($Na_4P_2O_7{\cdot}10H_2O$) to obtain stable, prefabricated pastes. Pyrophosphates are known to adsorb to the particles [722-724] resulting in a retarding effect on the cement reaction of calcium phosphate-based systems. In a higher concentration, they can even stop it nearly completely. The controlled activation of the setting reaction should then be accomplished by adding orthophosphate ions (PO_4^{3-}) in the form of an aqueous solution of Na_2HPO_4/Na_2HPO_4, as the PO_4^{3-} ions are supposed to displace the PP on the cement particles′ surface [360, 543, 722, 723, 725].

To investigate the mechanisms behind the interaction of α-TCP, PP and the sodium phosphate solution, a variety of methods were used to monitor every stage the material goes through during its path from storage to application. The cement powder was synthesized and checked for phase purity via XRD. During the initial storage phase, the prefabricated paste was characterized regarding its zeta potential of the powder, the ion concentration in the liquid phase via ICP-MS and the crystalline phase composition by XRD. To monitor the setting process after orthophosphate addition, the injectability was addressed quantitatively with a manufactured setup. Furthermore, the rheological behaviour was measured during the initial setting period and the setting times were determined with an indentation test. Additionally, the phase conversion and heat development during the setting reaction were monitored by heat flow calorimetry and *in-situ* XRD. Finally, the hardened cement was again examined for its crystalline phase content after defined time points and regarding its mechanical strength and porosity to check if the PP stabilization affects the final properties achieved after hardening

5.3 Results

5.3.1 Powder characterization

Particle size distribution, specific surface area and phase composition

Determination of the quantitative phase composition according to the G-factor method resulted in contents of 87 ± 1 wt.% α-TCP, 1.6 ± 0.3 wt.% β-TCP and 12 ± 2 wt.% ATCP. Laser diffraction analysis indicated that the powder shows a monomodal grain size distribution, with a maximum at around 35 µm. The corresponding D_V values are presented in **Table 10**.

Table 10. *DV values of the α-TCP starting powder, determined by laser diffraction; the means of three independent preparations are presented (10 measurement runs per preparation), the errors represent the standard deviation.*

D_V10 [µm]	**D_V50 [µm]**	**D_V90 [µm]**
2.46 ± 0.03	21.3 ± 0.6	73 ± 4

Table 11. *pH values of solutions used for cement paste preparation; the means of three measurements are shown, the error is derived from measurements of buffers with defined pH (7 and 9).*

Solution	**pH**
PP005	7.7 ± 0.1
PP01	8.1 ± 0.1
PP02	8.7 ± 0.1
PP03	8.7 ± 0.1
PP04	8.8 ± 0.1
PP05	9.2 ± 0.1
Na_2/Na diluted	7.2 ± 0.1
Na_2/Na 30 wt.%	7.1 ± 0.1
PP005 + Na_2/Na 30 wt.%	7.2 ± 0.1
PP01 + Na_2/Na 30 wt.%	7.2 ± 0.1
PP05 + Na_2/Na 30 wt.%	7.2 ± 0.1

5.3.2 Cement paste characterization

pH of mixing liquids

The pH values of the PP solutions systematically increased with increasing PP concentration, starting from pH = 7.7 ± 0.1 for PP005 and ending at pH = 9.2 ± 0.1 for PP05 (**Table 11**). The Na_2/Na solutions, both diluted and with 30 wt.% concentration, were practically neutral (pH 7.3 ± 0), as expected for this phosphate buffer system. Accordingly, the PP solutions with Na_2/Na addition were also practically neutral, indicating that the phosphate buffer was able to compensate the slightly alkaline effect of PP. In **Figure 35** can be seen, that the addition of cement powder to the respective PP solutions raises the pH value from around neutral to a noticeably basic pH of 8.9 ± 0.2 for PP0 and 9.3 ± 0.1 for PP005. This pH is then lowered again to around neutral by the Na_2/Na solution. For Na21_PP005 the pH stays around neutral for the whole initial setting period. It only shows a slight increase of 0.3 over the course of 30 min. As opposed to that the pH value of Na21_PP0 starts increasing after 3-4 min of setting and shows a gain of 1 over the same amount of time.

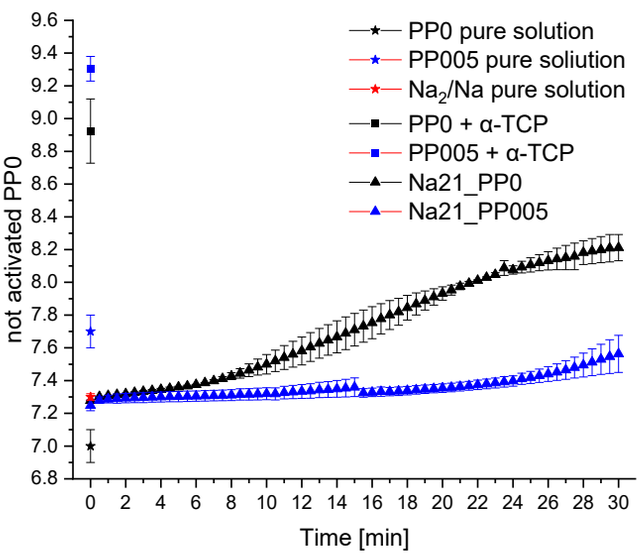

Figure 35. *pH values of the raw solutions* ***(stars)*** *mixed into the cement powder* ***(squares)*** *and the development during hardening after activation with 20.8 % Na_2/Na* ***(triangles)*** *for the samples containing no PP* ***(black)*** *and 0.05 wt% PP* ***(blue)****; n=3.*

Zeta potential

The surface charge of the cement particles significantly decreased after the addition of PP (**Figure 36**). Without PP, the particles show a charge of -22 ± 2 mV which decreases to a value of -61 to -68 ± 4 mV after PP was added. According to different publications, free molecules in the aqueous phase are adsorbed to the particle surface and alter the surface charge [726-728]. This leads to the formation of the electric double layer[729], which creates a Stern potential on the particles and the measurement of it can be done via the zeta potential [730]. The charge against the sodium orthophosphate solution was not measurable, as the electric double layer gets really thin with high salt concentrations and therefore high conductivity of the liquid (70 mS/cm) [731].This renders the zeta potential unmeasurable for that sample.

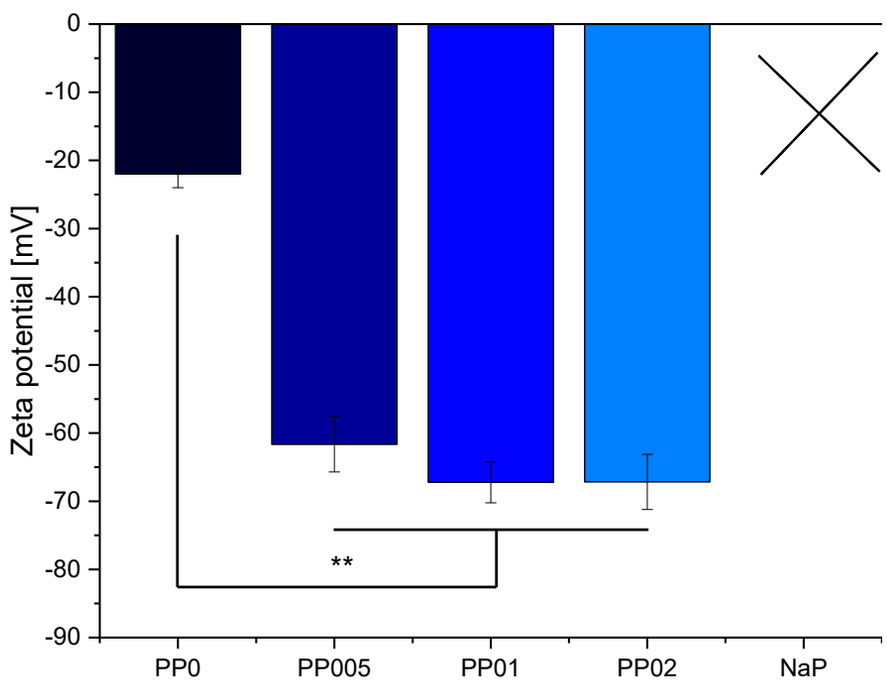

***Figure 36**. Zeta potential of alpha-TCP against water and different solutions of sodium pyrophosphate or sodium orthophosphate. A one way Anova was applied, **: p<0.001.*

The difference between the samples with PP and without is significant (one way Anova, p<0.001), but an increased amount of PP does not show a significantly increasing effect.

The XRD patterns of all four stabilized pastes after 1 to 14 d at 25 °C are shown in **Figure 37**.

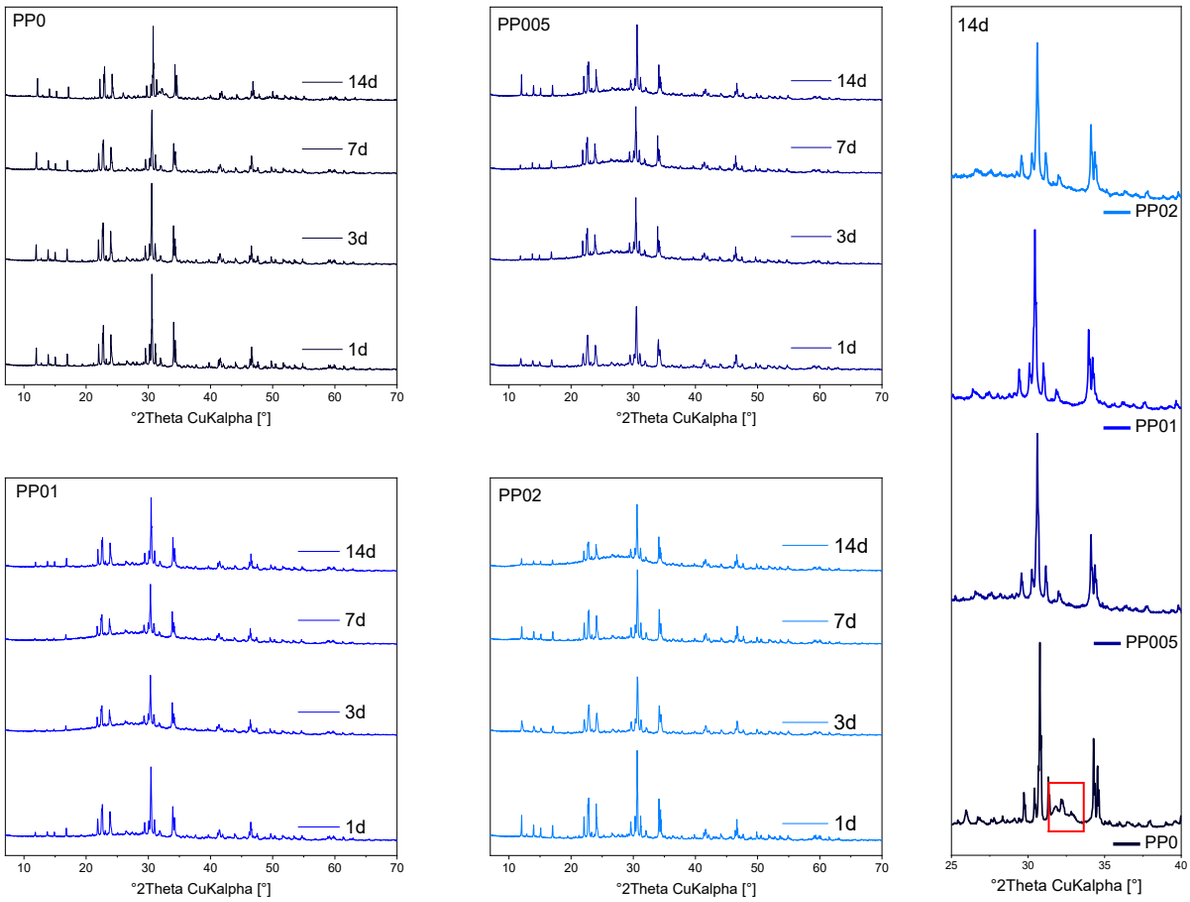

***Figure 37**. XRD analysis of the pastes PP0 to PP02 after storage at 25 °C for 1, 3, 7, and 14 d, presented as one representative curve out of three measurements and a cut out comparison of the angle range between 25° and 40° 2θ after 14 d of storage **(right side)**. The samples have been measured between 7-70° 2θ CuK$_\alpha$ with a step size of 0.022° and an integration time of 4s.*

The quantitative phase analysis via Rietveld calculations shows a consistent α-TCP fraction of 100 wt.% in the crystalline content after 1 d, 3 d and 7 d for every sample. However, as seen in **Figure 37**, the sample without PP shows a difference compared to the others after 14 d. This could be attributed to CDHA formed by the normal cement reaction of α-TCP. (Detailed view **Figure 37** right side). Accordingly, while the crystalline fraction of samples with PP was composed of 100 wt.% α-TCP even after 14 d, the crystalline fraction of PP0 contained 65 wt.% α-TCP and 35 wt.% CDHA.

In addition, samples were stored at 4 °C in a fridge to check if stabilization could be further improved by lowering the storage temperature. Here, even without PP addition, no CDHA formation was detected after storage times of 28 d or shorter.

Pore water analysis of premixed cement pastes

Both Ca and P concentrations increased with increasing storage time up to 7 d, while the values for 7 and 14 d were practically identical **Table 12**). The Ca/P ratio decreased with increasing storage time from 2.1 after 1 d to 1.6 after 7 d, approaching the ratio of α-TCP (1.5).

Table 12. *Ion concentration of Ca and P determined by pore water analysis via ICP-MS after the storage of α-TCP mixed with H_2O for 1, 3, 7 and 14 d at 4 °C; measurements were performed once, an error of ± 0.1 mmol/l can be assumed.*

Storage time at 4 °C	**Ca concentration [mmol/l]**	**P concentration [mmol/l]**	**Ca/P ratio**
1 d	1.3	0.6	2.1
3 d	2.9	1.7	1.7
7 d	5.0	3.0	1.6
14 d	4.9	3.0	1.6

The data for the different PP concentration can be found in **Table 13**. It is evident that the Ca concentration after 7 d was lower for PP005, compared to PP0, while it increased again for PP05. The Na concentrations of PP005 and PP05 were both close to the theoretically expected amounts, while the P amounts were comparatively lower.

***Table 13**. Concentration of Na, P and Ca in pore water after storage of prefabricated cement pastes for 7 d at 4 °C; measured values are means of two independently prepared measurements, the error represents deviation from the mean; the theoretical values for PP005 and PP05 are calculated from the PP concentrations of the corresponding solutions.*

	Na concentration [mmol/l]	**P concentration [mmol/l]**	**Ca concentration [mmol/l]**	**Ca/P ratio**
PP0 measured	0.082 ± 0.007	0.251 ± 0.003	1.2 ± 0.2	4.7 ± 0.7
PP005 measured	4.4 ± 0.2	1.28 ± 0.09	0.39 ± 0.04	0.31 ± 0.1
PP005 theoretical	4.48	2.24	-	-
PP05 measured	37.9 ± 0.1	14.2 ± 0.1	1.46 ± 0.01	0.103 ± 0.01
PP05 theoretical	44.8	22.4	-	-

5.3.3 Setting characterization

Paste injectability

The injectability increased with the addition of PP, but only showed a significant difference between PP0, PP005 and PP01 (one-way Anova) (**Figure 38**). The effect lead to an increase from 57 ± 11 % for the reference to a value of 89 ± 3 % and 87 ± 2 % for PP005 and PP01 respectively. Even though the error for PP02 is high at 74 ± 10 % an enhancement in the paste properties could be demonstrated.

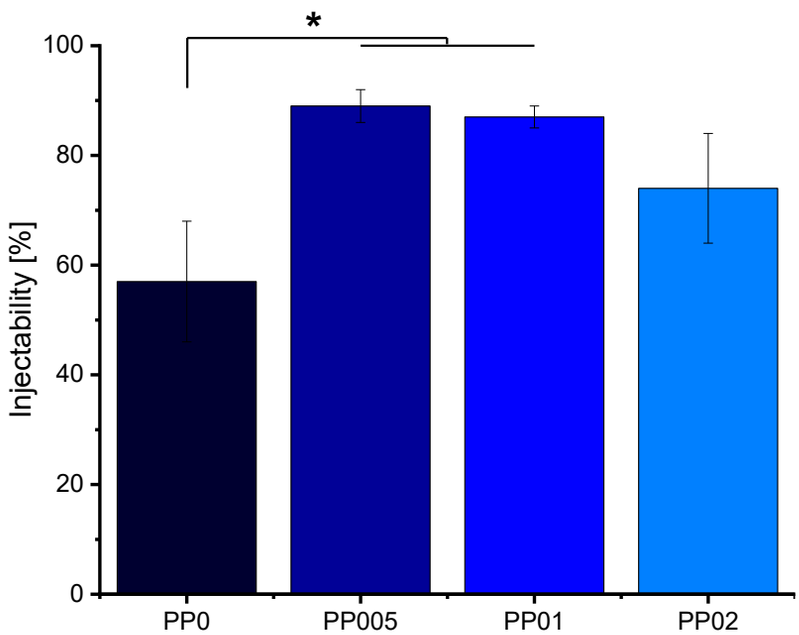

***Figure 38**. Injectability of the pastes PP0, PP005, PP01 and PP02 activated with Na21. (*: $p < 0.05$)*

Rheological behaviour

The presented pastes have been examined concerning their flow properties. The not activated stabilized, stored pastes could not be measured, because a phase separation occurred faster than the measurement could be started. From the graphs of the activated (Na21) pastes it is apparent, that the addition of PP alters the setting process in the early stages. (**Figure 39**) Na21_PP0 shows a rapid increase in both dynamic moduli (only about 4 min) which then stay stable after 5 minutes until the end of the measurement. In contrast, Na21_PP005 shows this behaviour expanded to 20 minutes. Both samples with higher PP concentrations have their dynamic moduli already significantly raised as the measurement starts. Na21_PP01 starts three powers of ten higher, but the increase to the final stable value is prolonged until 25 minutes. Na21_PP02 starts even higher and reaches its stable value very fast. All samples reach about the same values when they become stable.

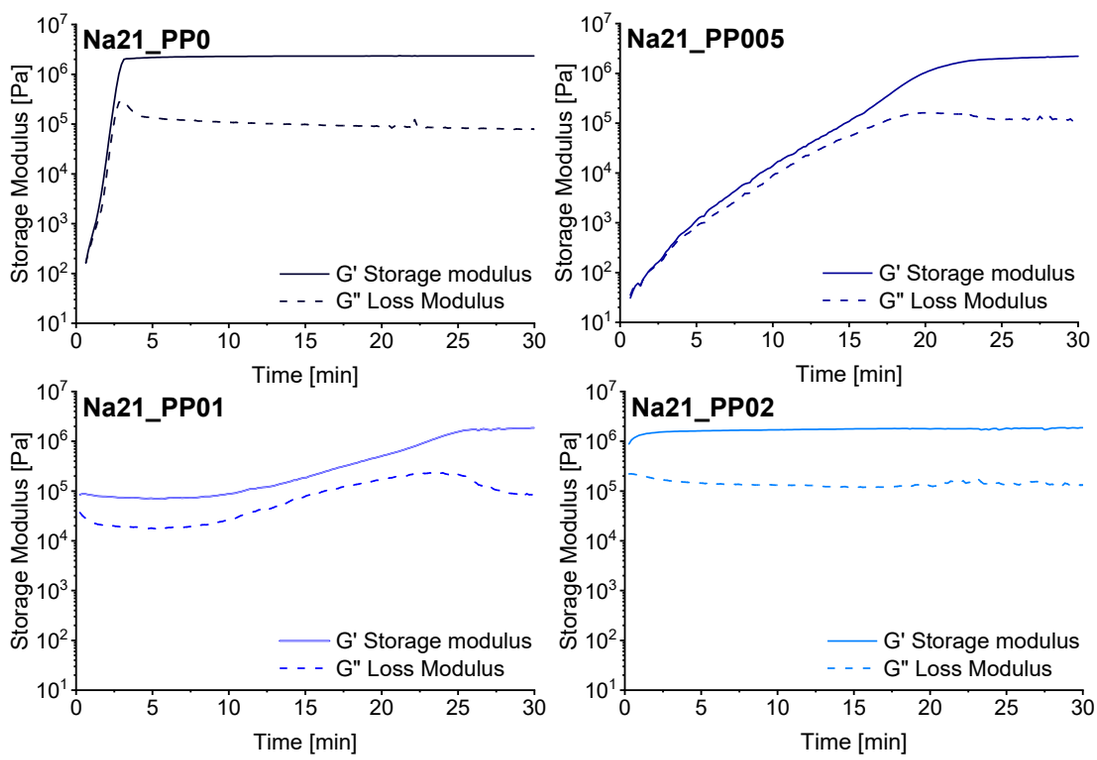

Figure 39. *Storage and loss modulus development during the first 30 minutes after the activation with Na21 for all PP concentrations. γ = 0.1%, ω = 5 rad/s, Ø = 5 cm, d = 0.6 mm. Representative curves for each sample group have been chosen; n = 3.*

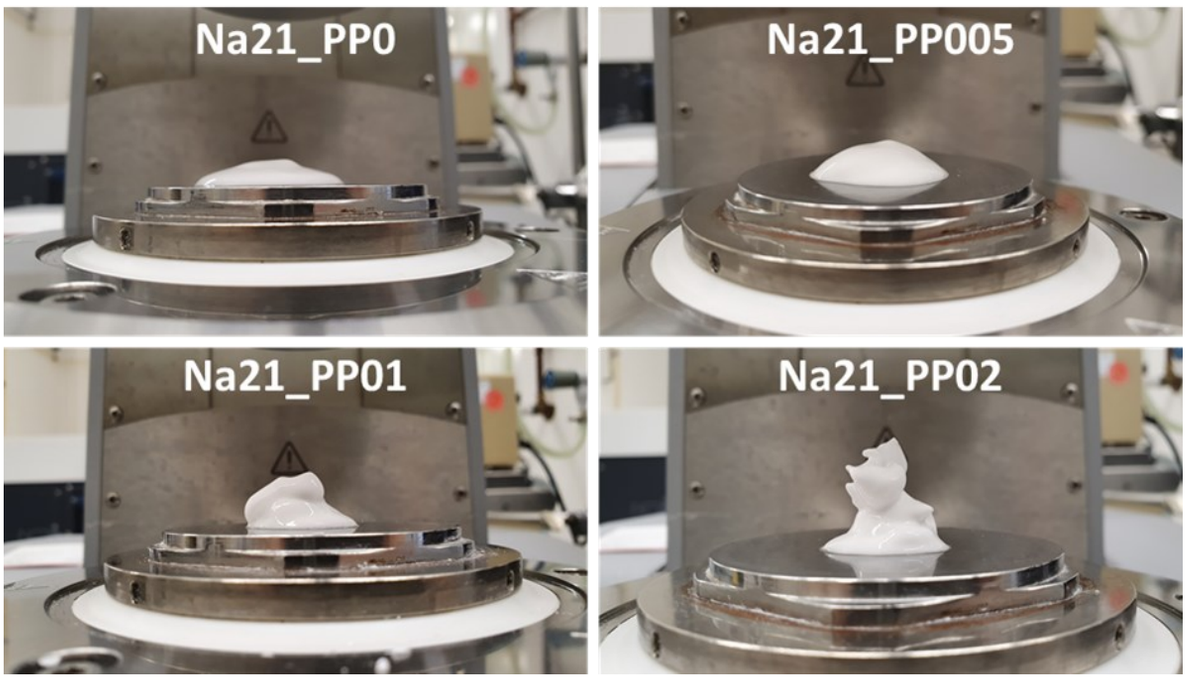

***Figure 40**. Images of the four different Na21 pastes directly after the application onto the rheometer measurement area.*

The influence of the PP on the rheological behaviour gets even more apparent looking at the images of the pastes during preparation for the measurement (**Figure 40**). Na_PP0 spreads almost evenly over the measurement area like a liquid. With PP005 to PP02 the paste was able to keep its shape after the application with the spatula and behaved more like a cream. This effect is only recognized after the addition of the Na21 solution. Imeter measurements

Isothermal calorimetry

Effect of storage time on the reactivity of pure α-TCP in water

The reaction of α-TCP mixed with deionized H_2O was significantly accelerated by storing the pastes in the fridge prior to the measurements. The duration of the induction period was reduced, and the positions of both the shoulder and the main maximum were shifted to earlier time points accordingly. Additionally, the height of the shoulder continuously increased with higher storage times.

Influence of varying the PP concentration

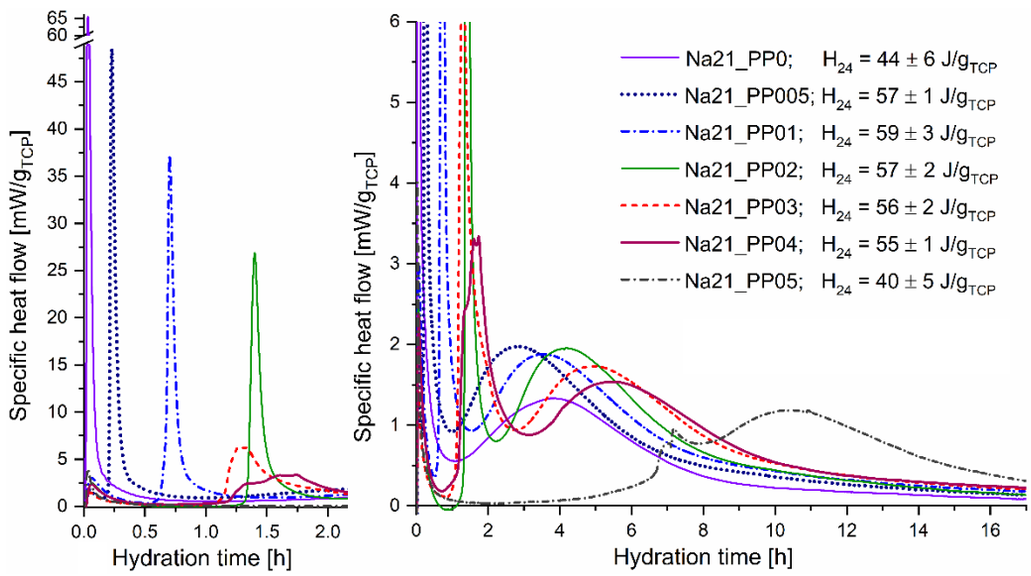

***Figure 41**. Isothermal calorimetry of samples composed of α-TCP mixed with PP solutions of variable concentrations and addition of 20.8 vol% Na_2/Na solution related to the volume of the PP solution; T = 37 °C, L/P = 0.4 ml/g in the prefabricated paste; each measurement was reproduced three times; one representative curve is presented for each sample.*

Samples with different concentration of the PP solution, but an identical amount of added Na_2/Na solution (20.8 vol%) were compared. For PP concentrations up to 0.2 wt.%, a systematic retarding effect was observed – the height of the first, sharp heat flow maximum decreased with increasing PP concentration, and accordingly the occurrence of this maximum was delayed. While in Na21_PP0 the reaction corresponding to this maximum already proceeded in the first min after beginning, it only started after about 1.25 h in Na21_PP02 (**Figure 41**). When increasing the PP concentration to 0.3 respectively 0.4 wt.%, the effect was slightly different: While the height of the maximum still decreased, the position remained nearly the same compared to Na21_PP02. Increasing the concentration to 0.5 wt.% resulted in a further strong

retardation. Accordingly, the position of the second, broader maximum varied with change in PP concentration. While for lower PP concentrations it was even accelerated, compared to Na21_PP0, it was increasingly retarded for PP concentrations of 0.2 wt.% or higher. The total heat releases of all PP containing samples except Na21_PP05 after a hydration time of 24 h were identical within the error range, while those of Na21_PP0 and Na21_PP05 were significantly lower.

When increasing the amount of added Na_2/Na solution to 41.7 vol%, the general effect was basically similar: Increasing the PP concentration from 0.05 to 0.5 wt.% resulted in a decrease of the height of the first heat flow maximum and a slight retardation. Still, the effect was less pronounced compared to the addition of 20.8 vol% Na_2/Na, probably due to the overall increased speed of the reaction. Contrarily, the second, broader maximum occurred earlier for Na42_PP05. No significant difference in the total heat release with varying PP content could be observed for all Na21 samples ($p>0.05$). A variation of ne Na content with constant PP005 shows no significant difference between Na10, Na16 and Na21, but all of them are different to Na42 ($p<0.001$). For Na42 the samples containing 0.05 wt% PP and 0.5 wt% PP show a significant difference ($p<0.001$)

Influence of varying the amount of added Na_2/Na solution

By increasing the amount of added Na_2/Na solution at a constant PP concentration of 0.05 wt.%, the occurrence of the first, sharp calorimetry maximum was accelerated and its height remarkably increased (**Figure 42**). While for Na10_PP005 a true induction period was observed, the reaction started nearly immediately for Na42_PP005. Still, the position of the second, broad maximum was postponed by increasing the Na_2/Na amount from 15.6 to 41.7 vol%. The total heat release was nearly identical for the samples with up to 20.8 vol% Na_2/Na addition, while it significantly decreased for Na42_PP005.

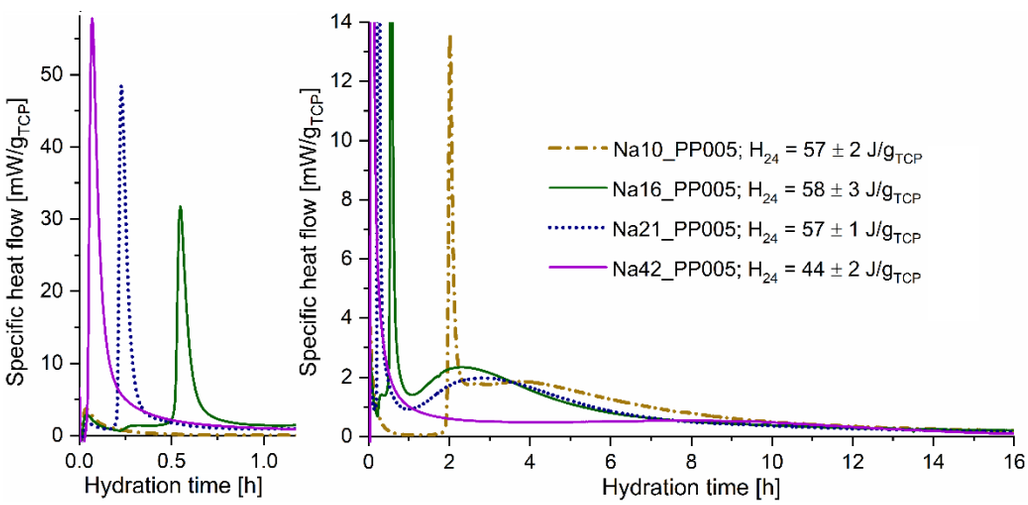

Figure 42. *Isothermal calorimetry of samples composed of α-TCP mixed with 0.05 wt.% PP solution and addition of Na2/Na solution in different vol% related to the volume of PP solution; T = 37 °C, L/P = 0.4 ml/g in the prefabricated paste; each measurement was reproduced three times; one representative curve is presented for each sample.*

In-situ XRD

Development of quantitative phase content

While in Na21_PP0 a slight dissolution of α-TCP already started from the beginning, the α-TCP content remained nearly constant in Na21_PP005 during the first 2 h (**Figure 43**). Differences were further observed with respect to the CDHA formation. While in Na21_PP0 and Na21_PP005 a few wt.% of CDHA were already detected immediately at the beginning, significant CDHA formation only started after 0.5 h in Na21_PP01. In all samples, an acceleration of CDHA formation was observed after about 2 h, which was accompanied by a more rapid dissolution of the crystalline α-TCP. At the end of measurement after 22 h, CDHA formation as well as α-TCP significantly slowed down, but still proceeded to a slight extent.In all samples investigated, formation of OCP was observed in addition to CDHA, while the content was significantly lower in Na21_PP01. Since only the main reflection of OCP located around 4.5° 2Θ was clearly visible and this reflection was rather broad due the low crystallinity of OCP, the exact OCP quantities should be considered with care.To check if prolonged storage of the prefabricated cement pastes had any influence on the hydration reaction, cement pastes of Na21_PP005 stored for 28 d in the fridge prior to activation were analysed by in-situ XRD.

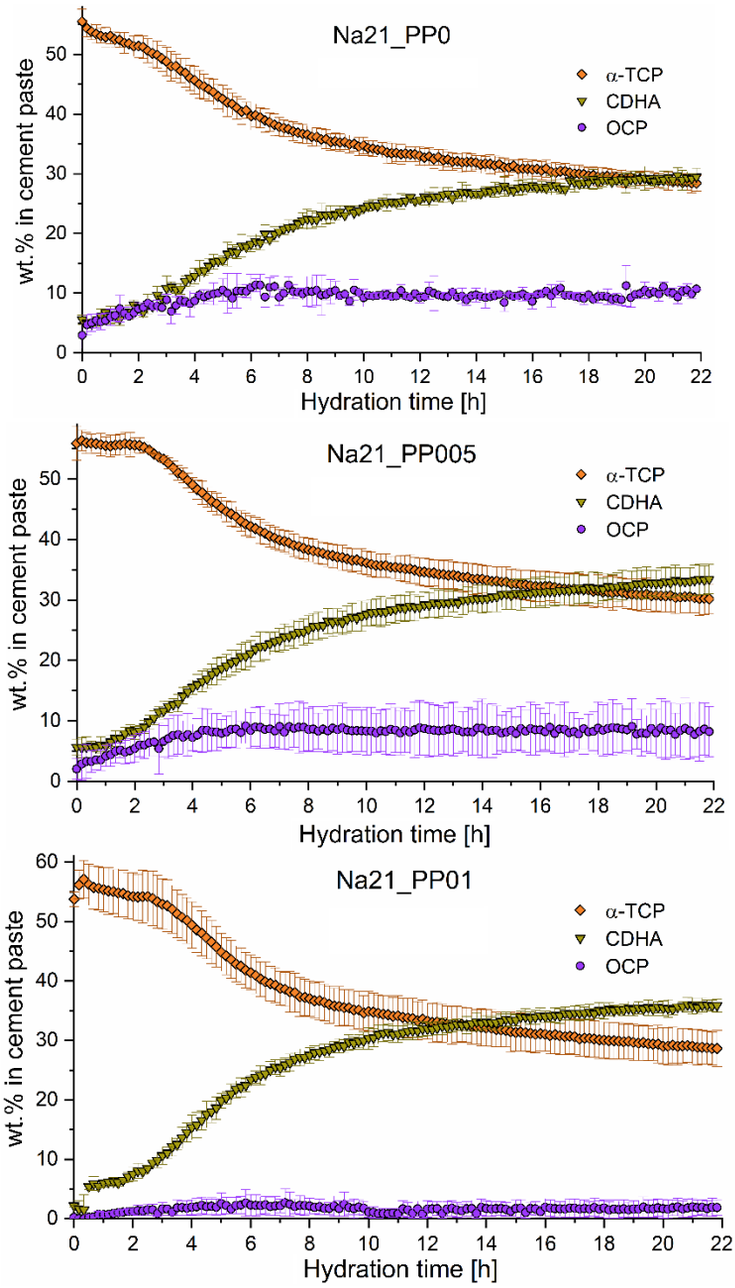

Figure 43. *In-situ XRD results of samples composed of α-TCP, PP solution in different concentrations and addition of 20.8 vol% Na2/Na solution; T = 37 °C, L/P = 0.4 ml/g in the prefabricated paste; the means of three independent measurements are presented, error bars represent the standard deviation.*

5.3.4 Characterization of hardened cement

Stored hydrated samples

By comparing the samples stored for 1 d and 7 d at 37 °C, it gets evident that the CDHA content increased, and the α-TCP content decreased for all PP concentrations (**Figure 44**). Accordingly, the degree of hydration increased from around 75 % after 1 d to around 90 % after 7 d. Though the degree of hydration after 1 d was slightly higher for the samples containing PP, no clear trend was observed. The OCP contents were a few wt.% only in all samples, no variation with time or changing PP concentration was observed.

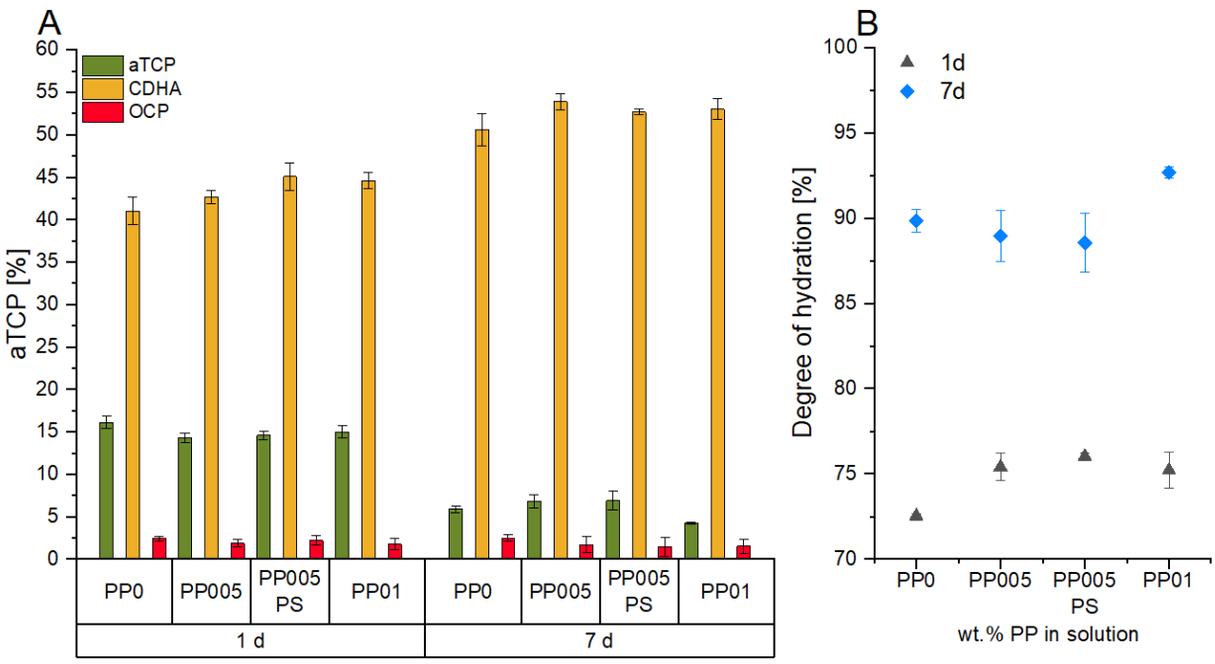

Figure 44. a) *Quantitative XRD results and* ***b)*** *degree of hydration of storage samples composed of α-TCP, PP solution in different concentrations and addition of 20.8 vol% Na_2/Na solution; T = 37 °C, L/P = 0.4 ml/g in the prefabricated paste; the means of three independent measurements are presented, error bars represent the standard deviation.*

The quantitative phase content of the storage sample Na21_PP005 with the prefabricated paste stored for 28 d at 4 °C prior to activation did not show any significant difference ($p>0.05$ after 1d and 7d) to the sample prepared from the freshly mixed paste.

Compressive strength

The difference in hydration percentage also influences the respective compressive strengths (CS). After 1 d and 7 d of hydration at 37 °C the samples show an obvious trend in their CS (**Figure 45**). The most apparent correlation is the decrease of the CS with an increased amount of the Na_2/Na activation solution across all PP concentrations. With Na16_PP0_1d being the only exception where its CS is lower than expected. The CS increases for every sample with more hydration time. After 7d hydration, the effect of the Na/Na_2 solution is still the most apparent and pronounced. Statistical examination suggests a significant difference between all Na10, Na16 and Na21 samples against their respective Na42 sample, which is always the lowest.

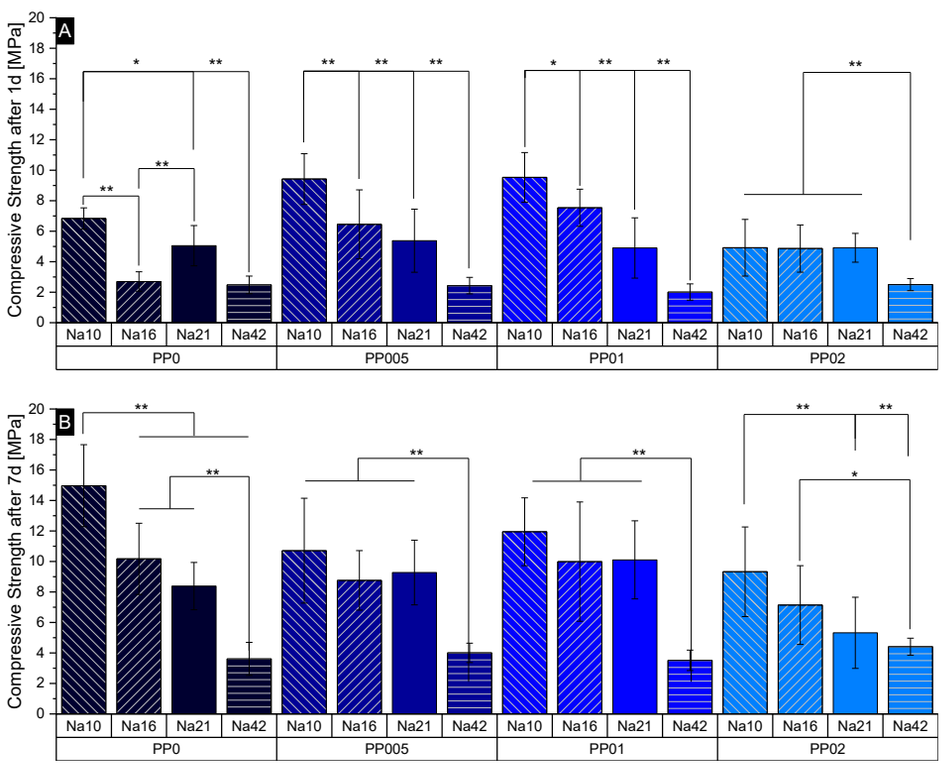

Figure 45. *Compressive strength dependent on the amount of PP (0 - 0.2 wt% in the solution) in the stabilized paste and on the amount of Na_2/Na (10 – 42 wt% relative to the liquid fraction) solution used to activate the setting process sorted by prioritising the PP amount after 1d **(A)** and 7d **(B)** of hardening in 100% humidity and 37°C (Two way Anova; * : $p < 0.03$; ** : $p < 0.001$).*

Between the different PP concentrations within one Na_2/Na group the difference is only significant for the groups Na10 and Na16. In group Na21 the sample with PP02 is significantly lower than the others. Na42 does not show an influence of the PP amount on CS. The highest CS with PP is measured with PP005 and PP01 and as they do not differ a lot with either Na16 or Na21, the sample with Na21_PP005 was chosen, because the pastes consistency and handling

was better and as shown before the increased amount of PP01 does not make a difference against PP005.

Porosity

The main pore size fraction for all different samples is in the same range with 3.7 µm, 4.2 µm, 5.8 µm and 5.5 µm for Na21_PP0, Na21_PP005, Na21_PP01 and Na21_PP02 respectively (**Figure 46**). The pore size distribution is of a monomodal shape with a long shoulder towards smaller pore diameters around 0.05 – 0.1 µm. Additionally, cumulative curves depicting the total porosities each show a plateau at either side of the shown diameter range, suggesting the complete open porosity was intruded by mercury and therefore measured and shown here.

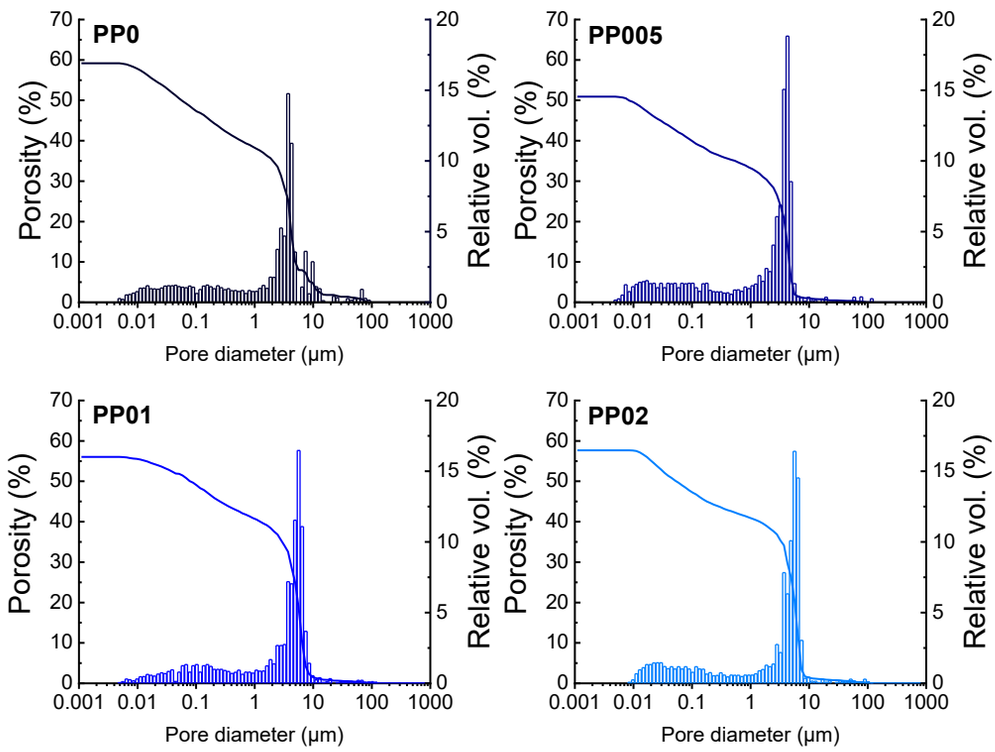

***Figure 46**. Total porosity **(left y-axis** and **line graph)** and relative pore volume **(right y-axis** and **histogram)** by pore diameter of Na21_PP0-PP02 after 1d of hardening at 100% humidity and 37°C.*

5.4 Discussion

Interaction of PP with cement particles

The tests for storage stability indicated that already a PP concentration of 0.05 wt.% (related to the water content in the prefabricated cement pastes) was enough to successfully prevent CDHA formation up until 14 d at room temperature, while CDHA was already detectable after 14 d without PP addition. It is proposed that the dissolution of α-TCP is blocked by the adsorption of the PP ions on the particle surface. The theory of adsorbed PP on the α-TCP particles is supported by the zeta potential measurements: The adsorption of the negatively charged PP ions ($P_2O_7^{4-}$) on the α-TCP particle surface should result in a more negative zeta potential, exactly as it was demonstrated in 3.2.1. Furthermore, pore water analysis of prefabricated pastes PP005 and PP05 after storage for 7 d at 4 °C demonstrated that the P concentrations measured were significantly lower than those expected from the theoretical PP content in the solutions. It can be therefore assumed that the residual PP is adsorbed on the solid phase. Additionally, the lower Ca concentrations in PP005 compared to PP0 indicate that dissolution of α-TCP is actually reduced by PP.

While there are no reports about the adsorption of PP on α-TCP so far, PP was repeatedly shown to adsorb on HAp [551, 732-734] or other calcium phosphates like brushite [552] or amorphous TCP [554]. The adsorption effect reportedly is based on active Ca sites on the surface of the mineral particles. α-TCP, just like the already investigated calcium phosphates has these Ca sites in its crystal structure [188]. For HAp, this effect is even exploited in phosphate mining: The adsorption of PP on the HAp surface hinders the adsorption of floating agents like sodium oleate, resulting in selective depression of apatite [734]. Based on these observations for other calcium phosphates, it is highly likely that adsorption also takes place on α-TCP.

The experimental results showed that the injectability of the pastes significantly increased by addition of PP. This increased injectability results mainly from a prevention of the common filter pressing effect that occurs for solid/liquid suspensions [432, 454]. Filter pressing describes the moment, when the friction between the aqueous phase and the particles is lower than the friction between the composite past and the surrounding syringe. As a result of the more negative zeta potential induced by PP adsorption, the similarly charged particles start to repel each other and are less likely to clog together like they would when filter pressing happens. This approach has already been demonstrated in previous studies for other ions like phytate, where improved injectability was also correlated to a more negative zeta potential [689, 694]. Increasing the PP concentration in the aqueous solution above 0.05 wt.% does not show a more

pronounced effect. This might indicate that the particle surfaces are already saturated with PP005. Additionally, after addition of the Na_2/Na solution, the paste setting and the interaction between the adsorbed PP ions and the newly introduced orthophosphate ions thicken the paste and therefore further act against a possible filter pressing effect increasing the injectability.

Activation by orthophosphate ions

The results of isothermal calorimetry, in-situ XRD and Imeter measurements clearly indicated that the setting reaction can be started by addition of orthophosphate in form of the Na_2/Na solution. It is therefore supposed that the orthophosphate ions can replace the PP ions, thus enabling the onset of the hydration. Starting from this theory, it appears quite logical that the beginning of hydration is retarded with increasing concentration of the PP solution, which corresponds to a higher number of PP ions. Therefore, it is plausible that it takes more time to displace a higher number of PP ions, if the number of orthophosphate ions is kept constant. In addition, PP ions are known to hinder the crystal growth of HAp [551], which might further explain the retarded hydration with increasing PP amount.

Accordingly, it is also plausible that activation can be accelerated by increased the amount of added orthophosphate at a constant amount of PP ions. Therefore, the observations made by systematically varying the parameters support the theory mentioned above.

The pH values of the stored pastes (PP0/PP005 + α-TCP) are quite basic but get buffered down to a neutral pH once the orthophosphate solution is added. During the reaction however, the pH value of Na21_PP0 constantly increases for the whole first 30 minutes. This is most likely due to the phosphate ions of the buffer getting used up in the cement reaction to build HAp, the remaining Na-ions start building NaOH with the water and therefore increasing the pH. This effect cannot be seen for Na21_PP005. Here the free PP ions most likely break up into two orthophosphate ions once the pH starts to increase, due to the effect presented above. These new orthophosphate ions prevent the enrichment of Na-ions, therefore the building of NaOH and ultimately the pH increase.

Another interesting observation is the fact that small amounts of PP (0.05 wt.%) even seem to have an accelerating effect on the setting reaction, compared to the unmodified system, as the IST for Na21_PP005 was lower than that for Na21_PP0. This might result from an improved workability of the PP modified cement paste, indicated by the qualitative observation that

Na21_PP005 was easier to prepare into sample holders than Na21_PP0, which was crumblier. This is further supported by the Imeter results: Though IST is reached earlier in Na21_PP005, Na21_PP0 starts to stiffen earlier. This might result in better reactivity.

However, increasing the PP amount to 0.1 wt.% (PP01) results in clear retardation of both the CDHA formation and onset of the hardening process, as indicated by the increased IST, compared to the reference. Here, the retarding effect of increased PP concentrations seem to outweigh the effect of improved workability.

It was further observed that the rheological behaviour of the activated cement pastes was strongly affected by the amount of PP in the pastes. A possible cause for this effect is the interaction between the highly negatively charged pyrophosphate ions ($P_2O_7^{4-}$) adsorbed to the surface of the particles and the less negatively charged orthophosphate ions (PO_4^{3-}) in the Na_2/Na solution. Even though no difference in the particles surface charge with increasing PP content was observed, the effect of increased PP concentration is obvious here. This is because even if the extra PP ions are not adsorbed on the particles surface, they are still present in the solution and can interact with the additional orthophosphate ions.

The α-TCP starting powder used for the investigations described here contained 12 ± 2 wt.% of ATCP. Previous basic studies about the hydration mechanism of partially amorphized α-TCP clearly demonstrated that in these samples the ATCP content reacts first, followed by the hydration of crystalline α-TCP [696, 735]. As the first, sharp heat flow maxima are not accompanied by a heat flow resulting from reaction of crystalline α-TCP, they must result from the reaction of ATPC, as described in [735]. The fact that this sharp maximum is also postponed by increasing the PP concentration (**Figure 41** - Calorimetry) indicates that also the hydration of the highly reactive ATCP is initially blocked by PP, which is further supported by the observation that no CDHA can be initially observed in Na21_PP01 in the in-situ XRD measurements. This is actually the prerequisite that also samples with amorphous content can be stabilized by PP addition.

Parallel to the increase of the CDHA content, an increase of the crystallite sizes True CS was observed, which indicates that the increase of CDHA content at least partly results from the growth of existing crystallites instead of the precipitation of new ones. Accordingly, the observed decrease of the aspect ratio rz/rx indicates a preferential growth in the direction of the crystallographic a axis at this stage. This growth mechanism is apparently not affected by the addition of PP.

Its known, that the liquid to powder ratio (L/P) directly influences the compressive strengths. [736, 737] While every sample has initially been prepared with the same L/P = 0.4 ml/g the addition of the different amounts of Na_2/Na solution altered this value so that the samples with a higher Na amount also have a higher L/P and therefore are expected to have a lower CS. The compressive strength of hardened cement materials is directly linked to the porosity. Here the total porosities for all samples are also very similar with 59.3% for Na21_PP0, 51.0% for Na21_PP005, 56.0% for Na21_PP01 and 57.8% for Na21_PP02. This is due to the fact, that all these samples have the same liquid amount and it's known that the amount of liquid strongly governs the porosity of the cement [458]. Therefore the amount of PP in the sample does not influence the mechanical properties of the material, but they are still controlled by the usual factors.

5.5 Conclusion

The results of the study clearly indicated that stabilization of α-TCP cement pastes by PP addition as well as the subsequent activation by orthophosphate addition are feasible and clinically acceptable setting times can be achieved by proper selection of PP and orthophosphate concentration. As the setting kinetics and the resulting phase composition of the pastes stabilized by PP addition are independent on pre-storage of the samples, the reaction is well reproducible and different pre-storage times are not expected to affect the setting performance. This is important to ensure clinical reliability of the cements. While generally stabilization of the pastes even without PP addition was possible by storage at 4 °C for 4 weeks, here the reactivity was shown to be strongly affected by variable storage times. Therefore, PP addition still has strong benefit.

The mechanical properties might be further optimized by reducing the L/P ratio of the resulting cement pastes, which might be accomplished by modifying the prefabricated cements with superplasticisers like polycarboxylate ether.

Chapter 6

Concluding Discussion and Perspectives

The authors contributed to the manuscript as follows:

Contributor	Contribution
Jan Weichhold	Conceived the research; conceptual planning; conducted experiments and analysed data for material characterization (rheology, XRD, extrudability, 3D printing, SEM, compressive strength)
Maximilian Pfeiffle	conducted experiments and analysed data for material characterization (rheology, XRD, extrudability, 3D printing, SEM, compressive strength)
Uwe Gbureck	Conceived the research; conceptual planning; revised and provided feedback to the manuscript
Valentin Steinacker	Conducted experiments and analysed data for material characterization (cell culture)

Chapter 6

Concluding Discussion and Perspectives

Parts of **Chapter 6** are based on a project of Jan Weichhold including a bachelor thesis and a not yet published paper including work from this bachelor thesis [738].

Authors: Jan Weichhold, Maximilian Pfeiffle, Uwe Gbureck,

Other parts quote a not yet finished medical doctoral thesis of Valentin Steinacker University of Würzburg

Parts of this chapter are the result of a bachelor thesis initiated and planned by Jan Weichhold. The experiments have been performed partially by Maximilan Pfeiffle under the supervision and partially by Jan Weichhold. The parts regarding the cell tests were performed by Valentin Steinacker in consultation with Jan Weichhold.

All authors gave permission for their data to be used here.

Calcium phosphate cement systems still lack some key properties to be applicable more commonly as injectable bone cement alternatives to e.g., PMMA cement. Their advantages over their organic competitors are *in vivo* degradability and lower setting temperature [325, 326]. But still the drawbacks of CPCs are huge in terms of paste properties. Therefore, this work aimed to address the possibilities to modify known cement systems to have a better controlled initial setting behaviour and simultaneously tackle the problem of filter-pressing leading to bad injectability, paste separation and inhomogeneities after injection.

Both systems presented in **Chapter 3** and **Chapter 4** have been modified to enhance their properties in respect to their injectability by the addition of sodium phytate. This introduced a retarding effect to both the apatitic and the brushitic system as the surface of their powder phase gets occupied by chelate complexes formed between the phytate and the freshly dissolved Ca^{2+}-ions. This surface layer subsequently lowered the powders zeta potential, leading to an increased repulsion force between similar charged powder particles. This repulsion plays a major role in the prevention of filter pressing as the solid parts of the paste are less likely to form a filter agglomerate through which the liquid phase gets pressed ultimately changing the paste composition inside the syringe and after extrusion / injection causing clogging of the nozzle.

The simplicity of this modification makes it easy to control and examine further towards applicability outside of the lab. Cell test have already been performed in form of a doctoral thesis of Valentin Steinacker [739], where systems were tested (α-TCP cement modified with 0.25 wt% and 0.5 wt% phytate ; β-TCP cement modified with 5 wt% and 10 wt% phytate) with osteoclastic and osteoblastic cell lines. The cell lines he used were the osteosarcoma cell line MG63 for the osteoblastic cells and RAW 264.7 for the osteoclastic cells.

The first cell line was examined concerning its cell activity through their optical density in WST-assays and their cell count in a timeframe of 9 days.In summary all α-TCP cements showed an increase in cell activity and cell count over 2, 4, 7 and 9 d. In comparison to the reference (unmodified CDHA) it can be said that the modification restricts the cell activity and count a bit, but not to a crucial extent. The β-cements also showed good results with values higher than for the brushite reference.

The RAW 264.7 cells were examined concerning their proliferation rate through TRAP activity and DNA concentration. Like the tests with the MG63 cells also the tests with RAW 264.7 cells showed a slight decrease in their compatibility for the α-TCP cements und a great increase for

the β-TCP cements. It shows that the modifications are not detrimental to cements properties as a biomaterial and can even improve these.

This data already predicts a promising future for these material systems. However, there are some points that need to be addressed further. Up until now the process of injection is mostly done by injection against no resistance in air. These injections could better be described as extrusions. A test for the paste behaviour against a resistance closer to that present, when injecting directly into a real bone defect, would be of high value for future developments of injectable bone cements. Additionally, one main drawback of CPCs is still the possible leakage outside of the defect or the desired application volume if the paste is too liquid or does not set fast enough after the injection. This effect was also not simulated in the presented studies. Further studies could focus on the development of a model defect to address both missing information simultaneously.

In **Chapter 5** an aqueous cement system was presented that had the unique property of not setting actively on its own until a specific activation solution is mixed into the main bulk paste. This property opens up the possibility to manufacture the premixed bulk paste and the activation solution precisely and store them separately until they are mixed for the application. Here, the variable of manufacturing the paste on site in an open container in the operating theatre by trained staff can be completely removed and it therefore offers a much higher control over the applied product and also prevents potential contaminations during the preparation. The effect was achieved by the addition of sodium pyrophosphate to a normal α-TCP cement. The pyrophosphate ions are known to inhibit cement setting reactions by preventing the dissolution of the cement. To activate this so-called stabilized paste, an activation solution containing high amounts of sodium orthophosphates is added. These orthophosphates dilute the pyrophosphate layer around the cement particles and take part in the cement reaction themselves leading to a normal setting behaviour of the activated paste. More so than the previous presented systems, this system should be investigated concerning paste behaviour after injection and possible leakage.

Due to the decreased interaction between the liquid phase and the powder particles, the paste shows a high degree of phase separation during storage. This is not of big concern for its application, as the paste can be remixed by shaking, vortexing or during the activation with the presented “two syringe” system when pumping back and forth the paste between both syringes. Nevertheless, the paste cohesion is a very good starting point to improve upon for this cement system. Hydroxy propyl methyl cellulose (HPMC) is a common additive to thicken a paste, but

often leads to air bubbles which in return weaken the hardened cement and can lead to inhomogeneous injection and porosity. As an alternative hyaluronic acid (HyAc) could work. This is readily available in different molecular weights allowing for good control over the viscosity. Preliminary tests of the cement system presented in **Chapter 5** modified in its viscosity by the addition of HyAc were already performed by the author of this thesis (Jan Weichhold) and Maximilian Pfeiffle during a bachelor thesis initiated and supervised by the author of this thesis and performed by Maximilian Pfeiffle. Here the secondary goal after an improvement of the paste cohesion was to achieve a printable paste for the 3D extrusion printing. This application came to mind as the normal limitation of CPCs as a 3D printing ink is the limited printing time due to the ongoing setting reaction. So, the stabilized non setting formulation would be the perfect candidate for this application.

3D printed patient specific products are making their way more and more into the regular clinical practice. There is still a long way to go, but the foundations have been laid out. Many materials can be used to produce 3D printed scaffolds for a variety of applications [740-746]. Materials for 3D bioprinting can be divided into natural and synthetic materials. Naturally derived materials like collagen, gelatin, chitosan, alginate, fibrin or hyaluronic acid (HyAc) have an inherent bioactivity [747-761]. Synthetic materials, like poly caprolactone (PCL), poly lactic acid (PLA), poly ethylene glycole (PEG) or polyether ether ketone (PEEK) on the other hand offer the better mechanical properties and can be adjusted more precisely, but in turns can have poor biocompatibility or even be toxic after degradation [762-775]. Bone cements are also getting more and more commonly used. These are synthetic materials but have already been reported to show good biocompatibility as they mimic the natural bone composition. Additionally, they have found to be usable in a powder printer set up [666, 776, 777], and as additives in extrusion based printing mixed into polymers [457, 778]. But there have also been approaches to make the traditional bone cement paste usable as an ink for extrusion-based printing while still being the main component and following the traditional setting procedure without an additional sintering step [779-782]. This poses the problem, that a printing process is usually optimized to the paste properties and limited by the setting time or behaviour .

The cement system presented in **Chapter 5** was modified with an array of HyAc in different molecular weights (Mw) from 8-15 kDa up to 2-2.5 MDa. The addition of HyAc with a Mw above 0.6-. MDa could prevent phase separation over a time frame of 21 days as shown in **Figure 47**.

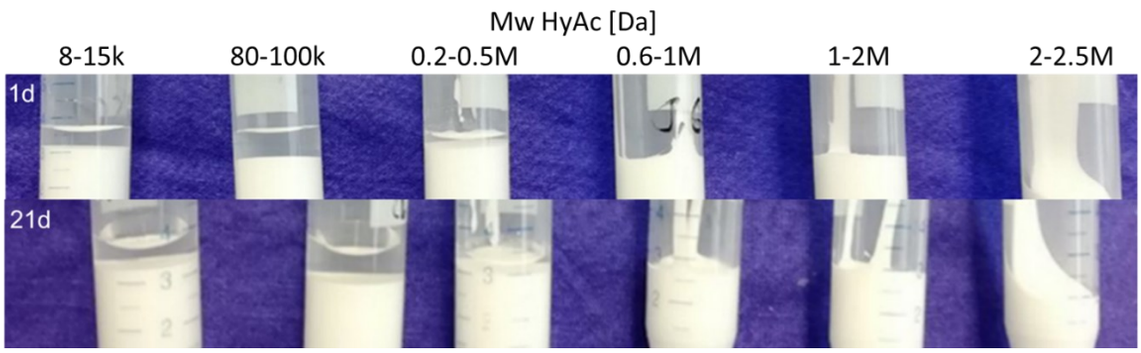

***Figure 47**. Stored pastes in 5 ml falcon tubes composed of α-TCP and hyaluronic acid solution with a range of Mw from 8-15 kDa to 2-2.5 MDa after one day of storage **(top)** and 21 days of storage **(bottom)**. (n=3, one representative has been selected) Reprinted and adjusted with permission from the bachelor thesis of Maximilian Pfeiffle [738].*

The suitability for the different pastes were assessed for a range of molecular weights and concentrations. Different pastes were used for preliminary printing test to filter the promising compositions. First the Mw was changed at a fixed 1 wt% and then the concentration was changed with the most promising Mw. The results are presented in **Table 14**. The color code shows how well the paste was extrudable (red: bad, yellow: acceptable, green: good), where the qualitative word describes how well the paste could keep its shape after extrusion. 2-2.5 MDa with 3% was the best in extrudability and 4% had the best shape fidelity afterwards.

Table 14. *Qualitative evaluation of extrudability (**color** red: bad, yellow: acceptable, green: good) and shape fidelity **(words)** of the cement pastes with 1 wt% of HyAc and a Mw range from 8-15 kDa to 2-2.5 MDa and pastes with a concentration range of 1 to 5 wt% of HyAc with a Mw of 2-2.5 MDa. Reprinted with permission from the bachelor thesis of Maximilian Pfeiffle [738].*

HyAc concentration	HyAc [Da]	8-15k	80-100k	0.2-0.5M	0.6-1M	1-2M	2-2.5M	
	0%	extrusion speed 20mm/s →					bad	extrusion speed 10mm/s →
	1%	bad	bad	bad	bad	bad	okay	
	2%						okay	
	3%						good	
	4%						Very good	
	5%						okay	

Initially the pastes were extruded and printed directly in air onto the collector and set by submerging the construct in the activation solution shown in **Chapter 5** after the printing process, but this led to fibre merging and a deformation when more layers were stacked onto each other. (**Figure 48**) To address this we decided to print directly into the solution and start the setting process once the paste leaves the nozzle. This improved the printing results. (**Figure 49**)

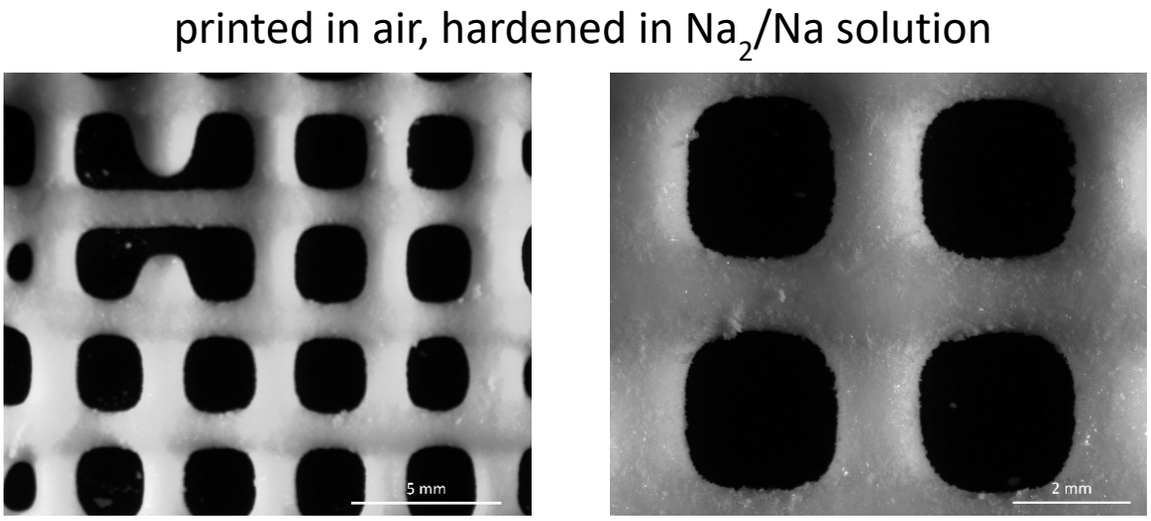

***Figure 48**. One layer scaffold of the 1 wt.% 2-2.5 MDa paste printed in air and hardened in Na_2/Na solution afterwards. Overview image **(left)** and detailed intersection **(right)**. Reprinted with permission from the bachelor thesis of Maximilian Pfeiffle [738].*

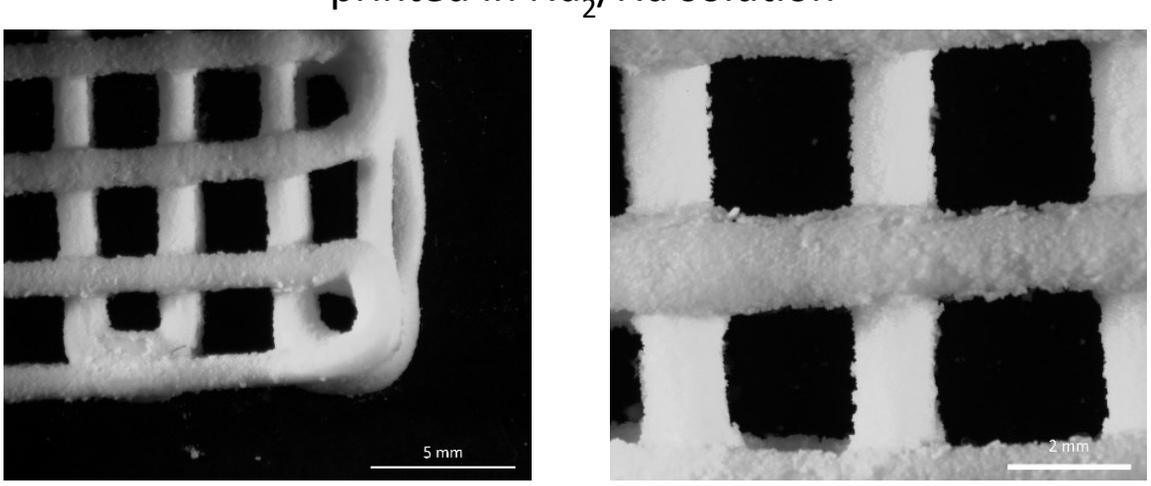

***Figure 49**. One layer scaffold of the 1wt.% 2-2.5 MDa paste printed directly in Na_2/Na solution. Overview image **(left)** and detailed intersection **(right)**. Reprinted with permission from the bachelor thesis of Maximilian Pfeiffle [738].*

Lastly the produced scaffolds were compared to normally cast samples of the same cement in respect to their compressive strengths. The dimensions of 6x6x12 mm³ were printed and cast. Comparing them qualitatively they showed similar maximum strengths, but the printed samples could even recover from the fracture. This could be seen as individual layers breaking off during the compression test. (**Figure 50**)

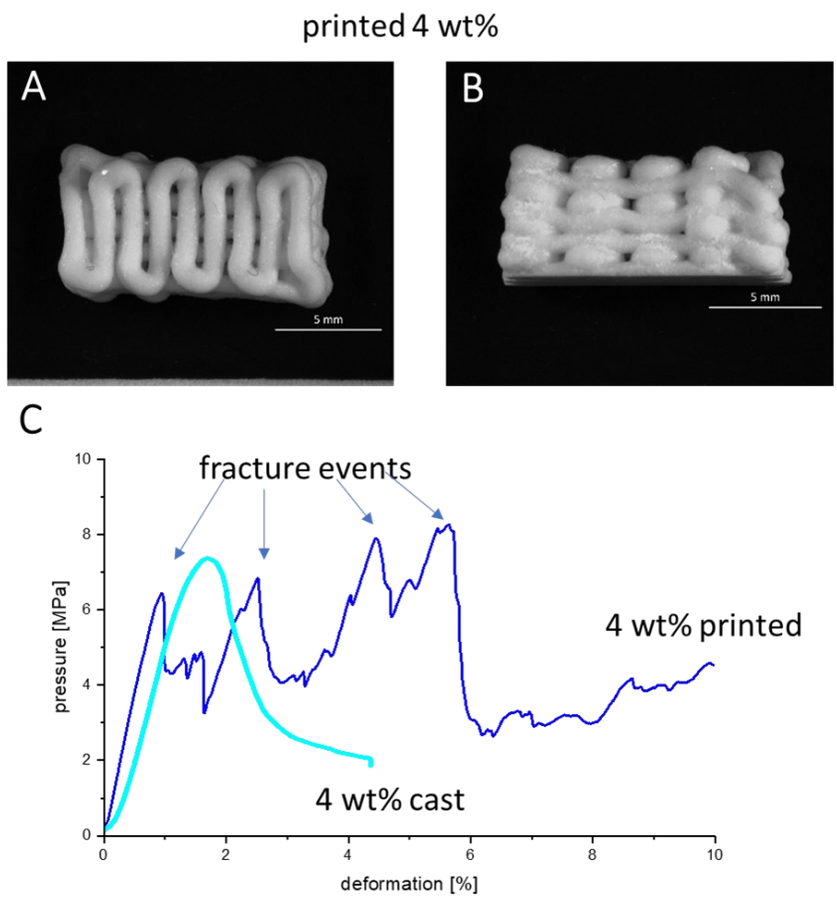

***Figure 50**. Printed sample for compressive strength tests in top view **(A)** and side view **(B)**, **(C)** representative compressive strength test curves of the cast cement sample (light blue) and the printed sample (dark blue). Reprinted and adjusted with permission from the bachelor thesis of Maximilian Pfeiffle [738].*

All in all, the project was a success and the foundation of more investigation for this system as a 3D extrusion ink. The process of printing directly inside the activation solution poses the most problems here, as the nozzle could clog if the extrusion speed was too low and the cement started to set already. Printing error could occur if parts of the cement paste would stick to one side of the nozzle and in turns affecting the angle of the deposited paste strand after extrusion. Additionally, we ran into a problem of the printer configuration in combination with this paste. The printer drives the paste forward via a plunger that gets pressed against the paste with air pressure. To have full contact and no air left in the cartridge, a semi air permeable plunger is

used and pushed into the cartridge after filling to be in full contact with the paste. This semi permeable plunger is normally sufficient as the pastes are less air permeable and get pushed forward equally. But in our case a high pressure to drive the paste was needed and could lead to local filter pressing like phase separation, where the air pushed all liquid content through the powder particles creating a channel to the nozzle ultimately preventing paste extrusion completely. This major problem could be circumvented by adding a few drops of oil onto the semi air permeable plunger after it was pushed in and in full contact with the paste, making it not permeable at all. There are more suitable paste driving systems for cement pastes on the market. The first and most interesting configuration would be a screw mechanism, that protrudes the paste via a rotating screw inside the cartridge. This system seems to be more suitable for these kinds of pastes as it is always in full contact with the paste, can be loaded easily without air bubble by rotating backwards and filling from the front and does not put locally different pressure on the paste, which may cause a filter pressing phase separation. Furthermore, the resolution needs to be addressed and refined in future experiments. Currently just under 1 mm strand thickness could be realized, but for a medical approach a finer resolution would enable a better fit to more complex defects and enable smaller radii for the corners improving form fidelity even more.

These projects that use the presented work as a foundation already show promising results and open up the potential field of further work. This thesis was the next step on the way towards more usable, better injectable bone cements.

Chapter 7

Summary

Zusammenfassung

Chapter 7.1

Summary

The human body has very good self-healing capabilities for numerous different injuries to a variety of different tissues. This includes the main human mechanical framework, the skeleton. The skeleton is limited in its healing without additional aid by medicine mostly by the defect size. When the defect reaches a size above 2.5 cm the regeneration of the defect ends up faulty. Here is where implants, defect fillers and other support approaches developed in medicine can help the body to heal the big defect still successfully.

Usually sturdy implants (auto-/allo-/xenogenic) are implanted in the defect to bridge the distance, but for auto- and allogenic implants a suitable donor site must be found and for all sources the implant needs to be shaped into the defect specific site to ensure a perfect fit, the best support and good healing. This shaping is very time consuming and prone to error, already in the planning phase. The use of a material that is moldable and sets in the desired shape shortly after applying negates these disadvantages. Cementitious materials offer exactly this property by being in a pasty stage after the powder and liquid components have been mixed and the subsequently hardening to a solid implant. These properties also enable the extrusion, and therefore may also enable the injection, of the cement via a syringe in a minimal invasive approach.

To enable a good injection of the cement modifications are necessary. This work aimed to modify commonly used calcium phosphate-based cement systems based on α-TCP (apatitic) and β-TCP (brushitic). These have been modified with sodium phytate and phytic acid, respectively. Additionally, the α-TCP system has been modified with sodium pyrophosphate, in a second study, to create a storable aqueous paste that can be activated once needed with a highly concentrated sodium orthophosphate solution.

The powder phase of the α-TCP cement system consisted of nine parts α-TCP and one part CDHA. These were prepared to have different particle sizes and therefore enable a better powder flowability through the bimodal size distribution. α-TCP had a main particle size of 20 µm and CDHA of 2.6 µm. The modification with sodium phytate led to an adsorption of phytate ions on the surface of the α-TCP particles, where they started to form complexes with the Ca^{2+} ions in the solution. This adsorption had two effects. The first was to make the calcium ions unavailable, preventing supersaturation and ultimately the precipitation of CDHA what would lead to the cement hardening. The second was the increase of the absolute value of the surface charge, zeta potential, of the powder in the cement paste. Here a decrease from +3 mV to -40 mV could be measured. A strong value for the zeta potential leads to a higher repulsion of similarly charged particles and therefore prevents powder agglomeration and clogging on the nozzle during injection. These two modifications (bimodal particles size distribution and phytic acid) lead to a significant increase in the paste injectability. The unmodified paste was injectable for 30 % only, where all modified pastes were practically fully injectable ~90 % (the residual paste remained in the nozzle, while the syringe plunger already reached the end of the syringe).

A very similar observation could be made for the β-TCP system. This system was modified with phytic acid. The zeta potential was decreased even stronger from -10 ± 1.5 mV to -71.5 ± 12 mV. The adsorption of the phytate ions and subsequent formation of chelate complexes with the newly dissolved Ca^{2+} ions also showed a retarding effect in the cements setting reaction. Where the unmodified cement was not measurable in the rheometer, as the reaction was faster than the measurement setup (~1.5 min), the modified cements showed a transition through the gel point between 3-6 min. This means the pastes stayed between 2 and 4 times longer viscous than without the modification. Like with the first cement system also here the effects of the phytate addition showed its beneficial influence in the injectability measurement. The unmodified cement was not injectable at all, due to the same issue already encountered at the rheology measurements, but all modified pastes were fully injectable for at least 5 min (lowest phytate concentration) and at least 10 min (all other concentrations) after the mixing of powder and liquid.

The main goal of the last modification with sodium pyrophosphate was to create a paste that was stable in aqueous environment without setting until the activation takes place, but it should still show good injectability as this was the desired way of application after activation. Like before also the zeta potential changed after the addition of pyrophosphate. It could be lowered from -22 ± 2mV down to -61 to -68 ± 4mV (depending on the pyrophosphate concentration). The pastes were stored in airtight containers at room temperature and checked for their phase composition over 14 days. The unmodified paste showed a beginning phase conversion to hydroxyapatite between 7 and 14 days. All other pastes were still stable and unreacted. The pastes were activated with a high concentrated (30 wt%) sodium orthophosphate solution. After the activation the pastes were checked for their injectability and showed an increase from -57 ± 11% for the unmodified paste to -89 ± 3% (practically fully injectable as described earlier) for the best modified paste (PP005).

It can be concluded that the goal of enabling full injection of conventional calcium phosphate bone cement systems was reached. Additional work produced a storage stable paste that still ensures full injectability. Subsequent work already used the storable paste and modified it with hyaluronic acid to create an ink for 3D extrusion printing. The first two cement systems have also already been investigated in cell culture for their influence on osteoblasts and osteoclasts. The next steps would have to go more into the direction of translation. Figuring out what properties still need to be checked and where the modification needs adjustment to enable a clinical use of the presented systems.

Chapter 7.2

Zusammenfassung

Der menschliche Körper verfügt über sehr gute Selbstheilungsfähigkeiten für zahlreiche verschiedene Verletzungen in unterschiedlichen Geweben. Dazu gehört auch das wichtigste mechanische Gerüst des Menschen, das Skelett. Das Skelett ist in seiner Heilung ohne zusätzliche Hilfe durch die Medizin vor allem durch die Defektgröße begrenzt. Erreicht der Defekt eine Größe von mehr als 2,5 cm, ist die Regeneration des Defekts nicht mehr gewährleistet. Hier können Implantate, Defektfüller und andere in der Medizin entwickelte Unterstützungsansätze dem Körper helfen, den großen Defekt noch erfolgreich zu heilen.

In der Regel werden stabile Implantate (auto-/allo-/xenogen) in den Defekt eingesetzt, um den Abstand zu überbrücken. Für auto- und allogene Implantate muss jedoch eine geeignete Spenderstelle gefunden werden, und für alle Quellen muss das Implantat in die defektspezifische Stelle geformt werden, um eine perfekte Passform, den besten Halt und eine gute Heilung zu gewährleisten. Diese Formgebung ist sehr zeitaufwendig und fehleranfällig, schon in der Planungsphase. Die Verwendung eines Materials, das formbar ist und kurz nach dem Auftragen in der gewünschten Form aushärtet, negiert diese Nachteile. Zementartige Materialien bieten genau diese Eigenschaft, indem sie sich nach dem Vermischen von Pulver und flüssigen Komponenten in einem pastösen Stadium befinden und anschließend zu einem festen Implantat aushärten. Diese Eigenschaften ermöglichen auch die Extrusion und damit möglicherweise auch die Injektion des Zements über eine Spritze in einem minimalinvasiven Verfahren.

Um eine gute Injektion des Zements zu ermöglichen, sind Modifikationen erforderlich. Ziel dieser Arbeit war es, die gängigen Zementsysteme auf Kalziumphosphatbasis zu modifizieren, die auf α-TCP (apatitisch) und β-TCP (brushitisch) basieren. Diese wurden mit Natriumphytat bzw. Phytinsäure modifiziert. Zusätzlich wurde das α-TCP-System in einer zweiten Studie mit Natriumpyrophosphat modifiziert, um eine lagerfähige wasserbasierte Paste zu schaffen, die bei Bedarf mit einer hochkonzentrierten Natriumorthophosphatlösung aktiviert werden kann.

Die Pulverphase des α-TCP-Zementsystems bestand aus neun Teilen α-TCP und einem Teil CDHA. Diese wurden so aufbereitet, dass sie unterschiedliche Partikelgrößen aufweisen und somit eine bessere Fließfähigkeit des Pulvers durch die bimodale Größenverteilung ermöglichen. α-TCP hatte eine Hauptpartikelgröße von 20 µm und CDHA von 2,6 µm. Die Modifizierung mit Natriumphytat führte zu einer Adsorption von Phytat-Ionen an der Oberfläche der α-TCP-Partikel, wo sie Komplexe mit den Ca^{2+}-Ionen in der Lösung zu bilden begannen. Diese Adsorption hatte zwei Auswirkungen. Die erste bestand darin, dass die Calciumionen nicht mehr verfügbar waren, wodurch die Übersättigung und letztlich die Ausfällung von CDHA verhindert wurde, was zur Erhärtung des Zements geführt hätte. Der zweite Effekt war die Erhöhung des Betrags der Oberflächenladung, des Zetapotenzials, des Pulvers in der Zementpaste. Hier konnte eine Abnahme von +3 mV auf -40 mV gemessen werden. Ein hoher Wert für das Zetapotenzial führt zu einer stärkeren Abstoßung ähnlich geladener Teilchen und verhindert somit die Agglomeration des Pulvers und das Verstopfen der Kanüle während der Injektion. Diese beiden Modifikationen (bimodale Partikelgrößenverteilung und Phytinsäure) führen zu einer deutlichen Verbesserung der Injektionsfähigkeit der Paste. Die unmodifizierte Paste war nur zu 30 % injizierbar, während alle modifizierten Pasten praktisch vollständig injizierbar waren ~90 %(die Restpaste blieb in der Kanüle, während der Spritzenkolben bereits das Ende der Spritze erreichte).

Eine sehr ähnliche Beobachtung konnte für das β-TCP-System gemacht werden. Dieses System wurde mit Phytinsäure modifiziert. Das Zetapotenzial sank noch stärker von -10 ± 1,5 mV auf -71,5 ± 12mV. Die Adsorption der Phytat-Ionen und die anschließende Bildung von Chelatkomplexen mit den neu gelösten Ca^{2+}-Ionen zeigten ebenfalls eine verzögernde Wirkung bei der Abbindereaktion des Zements. Während der unmodifizierte Zement im Rheometer nicht messbar war, da die Reaktion schneller verlief als der Messaufbau (~1,5 min), zeigten die modifizierten Zemente einen Übergang durch den Gelpunkt zwischen 3-6 min. Dies bedeutet, dass die Pasten zwischen 2 und 4 mal länger viskos blieben als ohne die Modifikation. Wie beim ersten Zementsystem zeigte sich auch hier der positive Einfluss des Phytatzusatzes bei der Messung der Injektionsfähigkeit. Der unmodifizierte Zement war überhaupt nicht injizierbar,

was auf das gleiche Problem zurückzuführen ist, das bereits bei den rheologischen Messungen aufgetreten ist, aber alle modifizierten Pasten waren mindestens 5 min (niedrigste Phytatkonzentration) und mindestens 10 min (alle anderen Konzentrationen) nach dem Mischen von Pulver und Flüssigkeit vollständig injizierbar.

Das Hauptziel der letzten Modifikation mit Natriumpyrophosphat bestand darin, eine Paste zu schaffen, die in wässriger Umgebung stabil ist und bis zur Aktivierung nicht aushärtet, die aber dennoch eine gute Injektionsfähigkeit aufweisen sollte, da dies die gewünschte Art der Anwendung nach der Aktivierung war. Wie zuvor änderte sich auch das Zetapotenzial nach der Zugabe von Pyrophosphat. Es konnte von -22 ± 2mV auf -61 bis -68 ± 4mV (abhängig von der Pyrophosphatkonzentration) gesenkt werden. Die Pasten wurden in luftdichten Behältern bei Raumtemperatur gelagert und über 14 Tage auf ihre Phasenzusammensetzung untersucht. Die unmodifizierte Paste zeigte zwischen 7 und 14 Tagen eine beginnende Phasenumwandlung in Hydroxyapatit. Alle anderen Pasten waren noch stabil und nicht umgewandelt. Die Pasten wurden mit einer hochkonzentrierten (30 Gew.-%) Natriumorthophosphatlösung aktiviert. Nach der Aktivierung wurden die Pasten auf ihre Injektionsfähigkeit geprüft und zeigten einen Anstieg von -57 ± 11 % für die unmodifizierte Paste auf -89 ± 3 % (praktisch vollständig injizierbar, wie zuvor beschrieben) für die beste modifizierte Paste (PP005).

Daraus lässt sich schließen, dass das Ziel, die vollständige Injektion herkömmlicher Kalziumphosphat-Knochenzementsysteme zu ermöglichen, erreicht wurde. Weitere Arbeiten führten zu einer lagerstabilen Paste, die dennoch eine vollständige Injektionsfähigkeit gewährleistet. In nachfolgenden Arbeiten wurde die lagerfähige Paste bereits verwendet und mit Hyaluronsäure modifiziert, um eine Tinte für den 3D-Extrusionsdruck herzustellen. Die ersten beiden Zementsysteme wurden auch bereits in Zellkulturen auf ihren Einfluss auf Osteoblasten und Osteoklasten untersucht. Die nächsten Schritte müssten mehr in Richtung Translation gehen. Es gilt herauszufinden, welche Eigenschaften noch überprüft werden müssen und wo die Modifikation angepasst werden muss, um einen klinischen Einsatz der vorgestellten Systeme zu ermöglichen.

Chapter 8

Methodology

Chapter 8

Methodology

8.1 Powder Fabrication

8.1.1 Alpha Tricalcium Phosphate (α-TCP)

The α-TCP was synthesized from 0.716 mol monetite ($CaHPO_4$) purchased from Honeywell, USA, and 0.33 mol calcite ($CaCO_3$) purchased from Merck, Germany was homogenized in a planetary ball mill PM 400 by Retsch for 1 hour. Empirical tests showed, that the theoretical stoichiometric ratio of monetite to calcite (2 mol : 1 mol) lead to secondary phases such as hydroxyapatite (HA), therefore it was adjusted to 2.15: mol : 1 mol to achieve a phase pure α-TCP. The powder mixture was sintered at 1200 °C for 5 h in a chamber oven Oyten (Vecstar, England). Afterwards the sintered powder was ground fine in the planetary ball mill again using a Zirconia milling cup and 6 zirconia milling balls with a diameter of 30 mm at 200 rpm for 2.5 hours and some drops of 2-propanol

8.1.2 Beta Tricalcium Phosphate (β-TCP)

$CaHPO_4$ (J.T. Baker, Griesheim, Germany) and $CaCO_3$ (Merck, Darmstadt, Germany) were sintered at a 2.15:1 molar ratio for 5 h at 1050 °C in a sintering furnace (Oyten Thermotechnik, Oyten, Germany). The β-tricalcium phosphate (β-TCP, β-$Ca_3(PO_4)_2$) sintering cake was crushed with a pestle and mortar and sieved through a mesh size of <355 µm. Each 125 g were dryly milled for 1 h in a planetary ball RM 400 (Retsch, Haan, Germany).

8.1.3 Calciumdeficient Hydroxyapatite (CDHA)

The apatite was synthesized by stirring α–TCP suspended in 1 l deionised water with the addition of 30 ml 2.5% Na2HPO4 solution. Due to the synthesis procedure, it can be assumed that it is a calcium-deficient hydroxyapatite ($Ca_{(10-x)}(HPO_4)_x(PO_4)_{(6-x)}(OH)_{(2-x)}$, CDHA). After 7 d, the suspension was filtered and the received powder was dried at 60 °C in an oven. Both powders were analysed for phase purity via an XRD analysis. In order to obtain a fine powder, the dried CDHA precipitate was wet milled in a planetary ball mill for 2 h in agate grinding jars. For 10 g of CDHA powder, 175 g of ZrO2:Y beads with a diameter of 1.25 mm were used as the grinding medium and 10 ml of isopropyl alcohol as lubricant. After milling, pure CDHA powder was obtained by separating the ZrO2:Y beads with a metal sieve and centrifuging the residual slurry at 3500 rpm for 90 min in a centrifuge Megafuge 1.0 (Heraeus, Hanau, Germany). Then, the supernatant isopropyl alcohol was removed with a pipette, and the samples were dried at 50 °C in a vacuum drying chamber (Binder, Tuttlingen, Germany) to remove the residual ethanol.

8.2 Particle Size Distribution and Specific Surface Area

8.2.1 α-TCP

The particle size distributions of the α–TCP and CDHA starting powders were determined by laser diffraction at a Mastersizer 3000 (Malvern Panalytical, Kassel, Germany), applying the Mie scattering model. Isopropyl alcohol was used as a dispersing agent. A data evaluation was performed using Mastersizer software V3.5 and Microcal Origin V 2017G. Three independent preparations of each sample were measured, and 10 measurement runs of each preparation were performed.

The BET (Brunauer, Emmett, Teller) surface area of α–TCP and CDHA was determined by Nitrogen adsorption using a Gemini 2360 instrument (Micromeritics, Norcross, GA, USA) in liquid N2. The samples were prepared for measurements by cleaning the surfaces at 130 °C under He flow for 3 h. Three independent measurements were performed for each powder.

8.2.2 β-TCP

The BET surface area of the samples was measured by Nitrogen adsorption using a Gemini 2360 instrument (Micromeritics, USA) in liquid N_2. Sample surfaces were cleaned at 130 °C under He flow for 3 h prior to measurement. Three independently prepared samples were measured once for each powder.

8.3 Quantitative Phase Composition

8.3.1 α-TCP

The quantitative phase composition of the powders was determined by powder X-ray diffraction (XRD) combined with Rietveld refinement and the G-factor method, an external standard method [783] . These measurements and calculations have been done by Katrin Hurle and Jan Weichhold depending on the chapter. A quartzite slice, calibrated with fully crystalline silicon powder (NIST Si Standard 640d), was used as an external standard. The details about the application of the G-factor method for the investigation of α–TCP cements can be found in [696] . XRD measurements were performed at a D8 Advance with DaVinci design (Bruker AXS, Karlsruhe, Germany) with the following measurement parameters: Range 7–70° 2θ; step size 0.0112° 2θ, integration time 0.2 s; radiation: copper Kα; generator settings: 40 kV, 40 mA; divergence slit: 0.3°; sample rotation with 30 1/min. For the Rietveld refinement, the structures ICSD# 923 (α–TCP) [784] , ICSD# 97500 (β–TCP) [785] and ICSD# 26204 (hydroxyapatite, used for the refinement of CDHA) [786] were applied together with a Chebychev polynomial of second order for the background. The refined parameters were scale factors, lattice parameters, crystallite size and microstrain. The anisotropic crystallite (coherent scattering domain) sizes of the hexagonal CDHA were modelled by a triaxial ellipsoid model [787] . Due to the constraints of the hexagonal symmetry, rx and ry were set to the same value. rx was aligned parallel to the direction of the crystallographic a-axis and rz to the direction of the crystallographic c-axis. The “true crystallite size” (True CS) was calculated as the cube root of the model ellipsoid volume. The contribution of the amorphous TCP (ATCP) present in the samples was modelled with a Peaks Phase, which means that several separate peaks were added to model the contribution of the X-ray amorphous phase.

In Chapter 5 the samples stored over 1d, 3d, 7d and 14d to check for stability were measured in a range from 7-70° 2θ, step size 0.02° 2θ, integration time 0.4s, copper K_α radiation, generator settings: 40 kV, 40 mA, a divergence slit of 0.25° and a rotation of 15 min^{-1}. For the Rietveld refinement the same structures were used as for mentioned before.

8.3.2 β-TCP

The quantitative phase composition of the β-TCP starting powder was determined by powder X-ray diffraction (XRD) and subsequent application of Rietveld refinement combined with the G-factor method, an external standard method. For XRD measurement, the powder was prepared by front loading method, 10 independent preparations of the powder were measured.

The measurements were conducted at a D8 Advance with DaVinci design (Bruker AXS, Germany). The following measurement conditions were applied: Range 6-39° 2θ; step size 0.0122° 2θ, integration time 0.15 s; radiation: copper K_α; generator settings: 40 kV, 40 mA; divergence slit: 0.3°. Qualitative evaluation of the measurements was performed with software EVA 4.1 (Bruker AXS, Karlsruhe). Rietveld refinement was accomplished with TOPAS 4.2 (Bruker AXS, Karlsruhe), the structures used for all XRD evaluations included in this study are ICSD# 97500 (β-TCP) [785], ICSD# (Ca-Pyrophosphate, $Ca_2P_2O_7$) [788], ICSD# 113 (MCPM) [789], ICSD# 917 (Monetite) [790] and ICSD# 16132 (Brushite) [253] For the powder measurements, refined parameters were the lattice parameters, scale factors, crystallite size and microstrain.

8.3.3 Quantity calculations

The G-factor method enables the determination of absolute crystalline phase contents and thus indirect quantification of amorphous content. The G-factor as a device specific calibration constant is determined from measurement of an appropriate standard according to **Eq.(13)** [783].

$$G=S_s \frac{\rho_s V_s^2 \mu_s^*}{c_s} \qquad \textit{Eq.(13)}$$

In these studies, a quartzite slice was used as standard. The quantity of crystalline quartz in the quartzite, c_s, was obtained by calibration of the quartzite with fully crystalline silicon powder (NIST Si Standard 640d) as primary standard. The mass attenuation coefficient (mac) μ^*_S of quartz was calculated from the macs of the elements involved, which were taken from the International Tables for Crystallography [791]. The quantity c_j of any crystalline phase j was then calculated according to **Eq.(14)**, where μ^*_{sample} was accordingly calculated from the macs of the elements involved [791].

$$c_j = S_j \frac{\rho_j V_j^2 \mu^*_{sample}}{G} \qquad \textit{Eq.(14)}$$

8.4 Zeta Potential

The surface charge of cement particles in the aqueous solution can be altered by different additives through the presence of ions in the liquid, a change in the pH and adsorption to the surface of the particles. This change can be measured via the Zetasizer Nano (Malvern Instruments, Malvern, Great Britain) and shows the surface charge of the suspended α-TCP particles against the surrounding liquid. Each mixture was prepared 3 times, while each preparation resulted in 3 measurements.

For **Chapter 3**, the effect of sodium phytate on the zeta potential ζ of the particles in the cement paste was investigated. For each measurement, 1 g α–TCP,CDHA or a mixture of α–TCP/CDHA in the ratio 9:1 was suspended either in a 0.002 M sodium phytate solution or as a reference in deionized water, which served as a medium for the measurement. To determine the effect of phytic acid (IP6) on the zeta potential ζ of the paste in **Chapter 4**, for each measurement, 0.1 g β-TCP and the respective amount of IP6 (5 to 20 wt.% related to the β-TCP content) or 0.1 ml of 0.5 M citric acid solution in case of the reference were added into 5 ml deionized water, which served as medium for the measurement. For the measurements in **Chapter 5**, 0.1 g α-TCP was suspended in deionized water and all three solutions of pyrophosphate (PP005, PP01 and PP02) respectively. 1 ml of these was transferred into a cuvette and placed in the measurement chamber.

8.5 Paste and Sample Composition

In **Chapter 3** all tests aside from the zeta potential measurement, the powder mixture (P) consisted of 90 wt.% α–TCP, 10 wt.% CDHA and either no sodium phytate or 0.25, 0.5, 0.75 or 1.0 wt.% sodium phytate added related to the mass of the phosphate powder for the samples Phy_0.00, Phy_0.25, Phy_0.50, Phy_0.75 and Phy_1.00, respectively. Additionally, samples with 2 wt.% sodium phytate (Phy_2.00) were prepared for XRD measurements after hardening, in order to systematically investigate the effect of phytate on OCP formation. Due to the very slow hardening of this paste, it was not included in the other investigations. The liquid phase (L) for the zeta potential measurements was a 0.05 M sodium phytate solution, but for every other measurement a 0.2 M Na2HPO4 aqueous solution was used. A liquid to powder ratio (L/P) of 0.3 ml/g was used for all experiments except the zeta potential and pH measurements.

For cement paste preparation in **Chapter 4**, five diluted phosphoric acid solutions (H_3PO_4, Merck, Darmstadt, Germany) with different concentrations of phytic acid (IP6, $C_6H_{18}O_{24}P_6$, Sigma Aldrich, Steinheim, Germany), according to **Table 15** were prepared. The single compositions were chosen to obtain a final water-to-cement ratio (w/c) of 0.5 g/ml, while the molar ratio of β-TCP to phosphoric acid was equimolar. The reference cement was mixed with a 0.5 M citric acid solution ($C_6H_8O_7{\cdot}H_2O$, Sigma Aldrich, Steinheim, Germany) instead of a solution containing IP6 as a setting modulator, because handling of non-retarded brushite cement was impossible.

The cement pastes investigated in **Chapter 5** were composed of α-TCP as starting powder, which was mixed with solutions of tetrasodium pyrophosphate decahydrate $Na_4P_2O_7{\cdot}10H_2O$ (Merck, Darmstadt, Germany) (PP) in different concentrations ranging from 0.05 to 0.5 wt.% PP. The samples were labelled PP005, PP01, …, PP05 accordingly. The liquid to powder ratio (L/P) of these prefabricated pastes was 0.4 ml/g. For activation of the setting reaction, an aqueous solution of Na_2HPO_4 (Merck, Darmstadt, Germany) NaH_2PO_4 (VWR Chemicals, Darmstadt, Germany) in a weight ratio 4:1 and an overall concentration of 30 wt.% (Na_2/Na) was additionally added. The amount of added Na_2/Na solution was normally 20.8 vol% of Na_2/Na solution (Na21) related to the amount of liquid in the prefabricated cement pastes. Accordingly, the nomenclature was Na21_PP005 etc. For the systematic investigations, the amount of added Na_2/Na solution was varied to 10.4, 15.6 and 41.7 vol% (Na10, Na16, Na42). As a consequence, the resulting L/P of the final cement pastes was increased, depending on the amount of added Na_2/Na solution. For comparison, a reference without PP addition (PP0) was investigated. For this purpose, a diluted Na_2/Na solution was fabricated. The concentration of the solution was selected in a way that cements with the same L/P and the same overall Na_2/Na concentration as the PP-stabilized and activated cement could be achieved.

***Table 15**. recipes of all IP6 solutions used in **Chapter 4**. * This solution is a 0.5 M citric acid solution and functions as a reference as a classical setting retarder.*

Label	IP6 concentration relative to β-TCP [wt%]	IP6 50% [g]	Water [ml]	Orthophosphoric acid 85% [ml]
IP6_0	0	0*	81.76	40
IP6_5	5	18.40	72.55	40
IP6_10	10	3.,87	63.35	40
IP6_12.5	12.5	46.07	58.75	40
IP6_15	15	55.22	54.15	40
IP6_20	20	73.66	44.95	40

8.6 Rheology

To compare the effect of relatively low and relatively high amounts of added sodium phytate, the development of the viscosity η of Phy_0.25 and Phy_1.00 in **Chapter 3**, was documented using an MCR 310 Rheometer (Anton Paar, Ostfildern-Scharnhausen, Germany) at room temperature and at 37 °C. For all the measurements, the measuring unit consisted of two equally sized plates with the upper plate having a circular area with a diameter of 50 mm. The lower plate was fixed, while the other plate was rotating in a defined distance of 1.0 mm above it. For the viscosity measurement, the upper plate rotated with a constant shear rate = 11/s. The measurements were reproduced 3 times for each composition. A representative measurement was chosen for comparison. The development of the viscosity η and the dynamic moduli G‘, G“ and G* of the different mixtures in **Chapter 4** described earlier were documented using a MCR 310 Rheometer (Anton Paar, Germany) at room temperature. For both measurements the measuring unit consisted of two equally sized plates with a circular area with a diameter of 50 mm. One was fixed, while the other one was rotating in a defined distance of 0.6 mm above it. To determine the viscosity development, the upper plate applied a constant shear stress τ of 250 Pa to the paste between the plates. The measurement started 2 min after mixing of the solid and liquid phases and monitored the reaction for up to 20 min or until the viscosity η reached a value of above 1000 Pa·s. For the dynamic moduli, the upper plate oscillated with a frequency of ω = 1 rad/s and the deformation was kept constant at γ= 0.04 %. The setting time of the reference without additional IP6 was too short (45 – 60 sec) to prepare it for the measurement. The gelation point as the moment where the graphs for the storage modulus G’ and the loss modulus G” intersect and the paste gets changed from viscous to elastic behaviour was determined graphically. The measurements were reproduced 3 times for each composition. To analyse the hardening process of the activated cement pastes shown in **Chapter 5**, rheology measurements were done after the activation. For these measurements, the respective pastes were measured with the Rheometer MCR 301 (Anton Paar Group AG, Graz, Austria) in a time sweep oscillation test at 25 °C with an amplitude γ = 0.1 %, an angular frequency of ω = 5 rad/s and a measurement point duration of 10 s. A plate-plate geometry with a diameter of 5 cm was used with a plate distance of 0.6 mm. The hardening process was monitored for the first 30 minutes.

8.7 Injectability

The injectability of the different pastes was measured using a custom syringe mount (**Figure 51**) and the universal testing machine Z010 (ZwickRoell GmbH & Co. KG, Ulm, Germany). A 5 ml syringe equipped with a 2 mm diameter needle was used. 2, 5 and 10 min (**Chapter 3**), 3 min (**Chapter 4**) and directly (**Chapter 5**) after mixing of the solid and liquid, the syringe filled with the cement paste (~4-6 g paste) was mounted in the Z010 universal testing machine, and pressure was applied at a crosshead speed of 30 mm/min. The measurement was finished either after the entire paste was pressed out of the syringe or the maximum force of 300 N (**Chapter 3**), 400 N (**Chapter 4**), 200 N (**Chapter 5**) was reached. Afterwards the injectability was calculated as the percentage difference between the initially loaded paste and the remaining amount at the end of the measurement (i.e., the fraction of extruded cement paste)

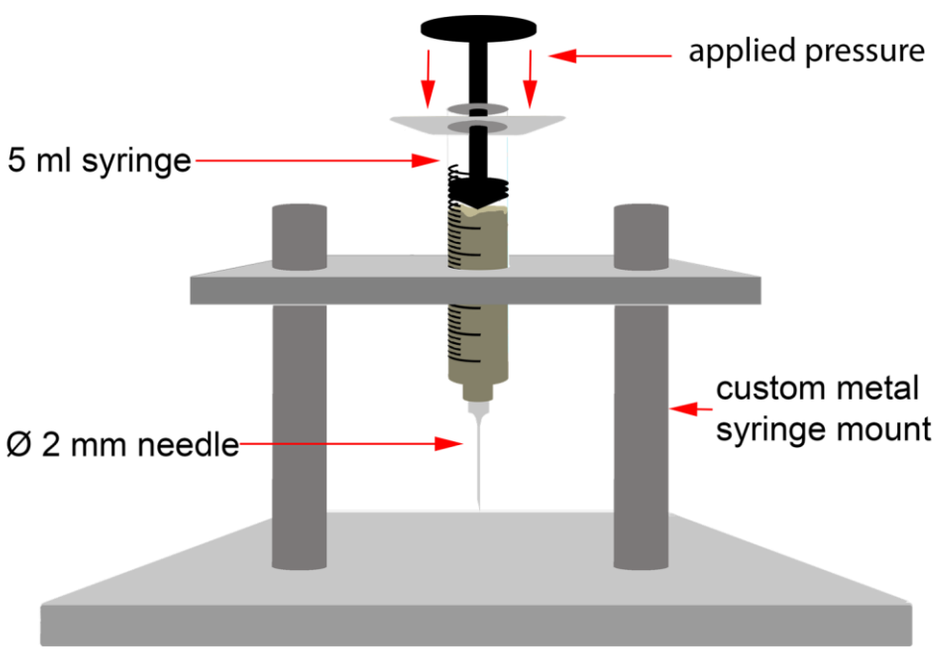

***Figure 51**. Schematic depicting the custom syringe mount used for all injectability measurements.*

8.8 Heat Flow Calorimetry

Isothermal heat flow calorimetry was conducted at a TAM Air isothermal calorimeter (TA Instruments, New Castle, DE, USA) equipped with eight twin type channels consisting of a sample and a reference chamber. It has an integrated thermostat with a temperature variance of ± 0.02 °C.

The temperature of the calorimeter was adjusted at 23 °C and 37 °C, respectively. Internal stirring using InMixEr (Injection & mixing device for internal paste preparation, FAU Erlangen, Mineralogy) was applied, while stirring was performed for 1 min (Sample IP6_0 was only stirred for 20 s) using an external motor with a constant stirring rate of 858 rpm. This method already provides reliable data for the initial part of the reaction, since disturbances by the opening of the measurement channels can be avoided. The cement mixtures containing sodium phytate were homogenized in a mixer mill Retsch MM 200 (Retsch, Haan, Germany) in a Teflon tool with four steel grinding balls for 2 x 2 min to ensure the homogeneous distribution of the phytate in the sample. The homogenized powder mixtures were then inserted into the calorimeter crucibles for the measurement. The equilibration of the samples before measurement was performed directly in the measurement channels.

Three independent measurements of each sample were performed. The evaluation of the measurements was performed by the software Microcal Origin V 2017G. The heat flow curves were corrected for the calibration constant of the InMixEr tools and the time constant [792] . In order to obtain total heat release during hydration, the calorimetry curves were integrated.

To measure the heat flow during the setting reaction in **Chapter 5** specifically**,** as a first step, the α-TCP starting powder was mixed with the respective PP-solution. These prefabricated pastes were directly filled into the calorimeter crucibles, while the Na_2/Na solution was inserted into the syringes. For investigation of the reference, the pure α-TCP starting powder was given into the crucibles and the diluted Na_2/Na solution was inserted into the syringes. This setup was allowed to equilibrate directly inside the calorimeter over night to ensure that the base line of the calorimeter reached a constant level. Then, hydration of the cement was induced by injecting the Na_2/Na solution into the prefabricated pastes respectively the α-TCP powder and stirring the cement for 1 min using an external motor with a defined, constant stirring rate of 858 rpm. Three independent measurements of each sample were conducted.

Furthermore, the hydration performance of cement pastes stored in a fridge for defined times was analysed. Here, the cement pastes were prepared by external stirring, i.e., stirring was performed manually using a metal spatula outside the calorimeter. The pastes were prepared at defined times before starting the measurement and stored in a fridge at 4 °C. Directly before starting the measurement, the cement pastes were slightly loosened by a metal spatula and directly inserted into the calorimeter, which was adjusted at a temperature of 37 °C.

8.9 In-situ XRD

Quantitative in-situ XRD measurements of α–TCP, Phy_0.00, Phy_0.25 and Phy_0.50 at 37 °C and of Phy_0.00, Phy_0.25 and Phy_0.50 at 23 °C in **Chapter 3** were performed at a D8 Advance with a DaVinci design diffractometer (Bruker AXS, Karlsruhe, Germany) by Katrin Hurle. Cements with higher phytate concentrations were not measured due to the slow setting of these pastes.

The following measurement parameters were applied: Range 3–50° 2θ; step size 0.0112° 2θ, integration time 0.2 s; radiation: copper Kα; generator settings: 40 kV, 40 mA; divergence slit: 0.3°. One range was recorded every 15 min. The desired temperature was adjusted by a Peltier element. The powder and liquid were equilibrated at 37 °C in a drying oven (Memmert, Schwabach, Germany) and in an Erlanger calorimeter at 23 °C, respectively, for at least 3 h. The cement pastes were then prepared by mixing liquid and powder for 1 min with a metal spatula, filled into a special sample holder and covered with a Kapton polyimide film (Chemplex Industries, Cat. No. 440, Palm City, FL, USA) to minimize water evaporation. Three independent measurements were performed for each sample. The overall measurement time was 24 h at 37 °C and 48 h at 23 °C. Each single range was evaluated by Rietveld refinement combined with the G-Factor method to obtain the quantitative development of the phase composition. The lattice parameters of α–TCP starting powder were fixed to the data obtained from the powder refinement. In addition to the structures used for the powder refinement, the structure ICSD #65347 [793] was applied for the refinement of octacalcium phosphate (OCP). The background contributions of water and the Kapton film were both modelled by a hkl phase [794] . For 37 °C, the data were corrected for the water loss occurring during the in-situ XRD analysis. For this purpose, the amount of residual water present at the end was determined by weighing the sample before and after drying at 60 °C in a drying oven (Memmert, Schwabach, Germany). A linear water loss during the measurement was assumed.

The development of quantitative phase content during hydration of the cement pastes in **Chapter 4** was monitored by in-situ XRD at the same diffractometer that was used for powder measurements. The following measurement conditions were applied: Range 6-39° 2θ; step size 0.0122° 2θ, integration time 0.15 s; radiation: copper K_α; generator settings: 40 kV, 40 mA; divergence slit: 0.3°. The measurement time for one range was 7.5 min. The temperature of the sample holder was adjusted to 23 °C respectively 37 °C with a Peltier element. Prior to the measurements the β-TCP powder and the mixing liquid were each equilibrated at the corresponding measurement temperature for at least 3 h in an Erlanger calorimeter (manufactured at FAU Erlangen, Mineralogy) at 23 °C or a drying oven (Memmert, Schwabach) at 37 °C.

In-situ XRD was performed for samples IP6_10 and IP6_20 at 37 °C and for IP6_0 as well as sample IP6_10 at 23 °C. For preparation of the cement pastes the samples were stirred with a metal spatula in a plastic container for 1 min. The reference was only stirred for 20 s due to its rapid hardening. The cement pastes were prepared into a special sample holder and covered with Kapton polyimide film (Chemplex Industries, Cat. No. 440) to reduce water evaporation.

Rietveld refinement and subsequent G-factor quantification were performed for each single range to obtain quantitative data from the in-situ XRD measurements. The lattice parameters of β-TCP were fixed to the values obtained in the powder refinement of the sample. Crystallite size and microstrain of the hydrate phases were refined and constrained to reasonable values. Lattice parameters of the hydrate phases were obtained from coupled refinement of the last three ranges and then fixed for in-situ evaluation. For MCPM, two different structures with different lattice parameters were included in the refinement. The background contributions of the water in the samples and the Kapton film were both modelled by a hkl phase [794]. An additional hkl phase model was added for a presumed amorphous or microcrystalline hydrate phase forming during hydration.

Quantitative in-situ XRD measurements of Na21_PP0, Na21_PP005 and Na21_PP01 with freshly prepared prefabricated pastes and additionally of Na21_PP005 with the prefabricated paste stored for 28 d at 4 °C prior to activation in **Chapter 5** were performed at a D8 Advance with DaVinci design diffractometer (Bruker AXS, Karlsruhe). The following measurement parameters were used: Range 3.5-35° 2θ; step size 0.0112° 2θ, integration time 0.19 s; radiation: copper K_α; generator settings: 40 kV, 40 mA; divergence slit: 0.3°. The measurement time for 1 range was 10 min, overall measurement time was 22 h, resulting in a number of 132 ranges recorded. The temperature of the sample holder was adjusted at 37 °C by a Peltier element.

Prior to the measurements, the components for the freshly prepared prefabricated pastes were equilibrated at 37 °C for at least 3 h in a drying oven (Binder, Tuttlingen, Germany). A few min before starting the experiment, the prefabricated pastes were prepared by mixing the α-TCP powder with the respective PP solution for 1 min with a metal spatula. Directly before starting the measurement, the Na_2/Na solution was added using a pipette, and further stirring was performed for 1 min. The cement pastes were filled into a special sample holder and covered with a Kapton polyimide film (Chemplex Industries, Cat. No. 440) to minimize water evaporation. Three independent measurements were performed for each sample.

In order to obtain the development of the quantitative phase composition during cement setting, each single range was evaluated by Rietveld refinement combined with the G-Factor method. The lattice parameters of α-TCP were taken from the Rietveld refinement of the powder sample and fixed. In addition to the α-TCP structure used for powder refinement, the structures ICSD# 26204 [786] (hydroxyapatite, used for refinement of CDHA) and ICSD #65347 [793] (octacalcium phosphate) were applied. As the CDHA formed during hydration showed anisotropic crystallinity, i.e. an anisotropic size of the coherent scattering domains (CSDs), a special model was applied for the refinement. [787] The CSDs were refined using a model ellipsoid, where rx and ry were set to the same value due to the constraints of the hexagonal symmetry. rx was aligned parallel to the direction of the crystallographic a-axis and rz to the direction of the crystallographic c-axis. The “true crystallite size” (True CS) was calculated as the cube root of the model ellipsoid volume. The background contributions of water and the Kapton film were each modelled by a hkl phase. [795]

8.10 Storage stability of cement pastes

The stability during storage is a key advantage of the presented cement pastes. To prove that this property was achieved, in **Chapter 5** the cement pastes were prepared by Katrin Hurle by mixing the α-TCP powder with either deionized H_2O or aqueous PP solutions in different concentrations. 5 g of all cement pastes were filled into 10 ml falcon tubes, sealed airtight with parafilm (Bemis Company, Neenah, USA) and stored at 25 °C in a climate-controlled room to monitor the stability under normal room temperature.

Additionally, samples with H_2O or PP solutions were stored in a fridge at 4 °C to investigate the storage stability at low temperatures. These pastes were prepared into plastic containers (inner diameter 23 mm; inner height 3 mm) which were closed with a lid and sealed with parafilm to avoid water evaporation. After defined storage times up to 28 d, the phase composition was analysed by XRD at a D8 Advance with DaVinci design diffractometer (Bruker AXS, Karlsruhe) with the following measurement parameters: Range 3-70° 2θ; step size 0.0112° 2θ, integration time 0.2 s; radiation: copper K_α; generator settings: 40 kV, 40 mA; divergence slit: 0.3°.

8.11 Pore water analysis during storage

To investigate if dissolution of α-TCP occurred during storage of the prefabricated cement pastes mixed with H_2O at 4 °C, the ion concentrations in the pore water were analysed after 1, 3, 7 and 14 d. This measurement was performed by Katrin Hurle. Furthermore, samples PP0, PP005 and P05 were analysed after 7 d to check if the PP had any effect on α-TCP dissolution and if it was adsorbed on the α-TCP particle surface. The pore water was extracted by centrifugation at 4,000 rpm for 8 min in a centrifuge Megafuge 1.0 (Heraeus Instruments, Hanau, Germany). The supernatant liquid was filled into a syringe and injected through a 0.2 µm sieve to remove residual particles. The extracted solutions were stabilized by addition of a 33 % SupraPur HNO_3 solution in a vol% ratio of pore water: HNO_3 = 2 : 1. Concentrations of Na, Ca and P were measured using an iCAP Qc ICP-MS (Thermo Scientific, Waltham, MA, USA), the operating conditions can be found in **Table 16**.

Table 16. *Operating conditions for ICP-MS measurements.*

Model	iCAP Qc ICP-MS
Company	Thermo Scientific
Autosampler	ESI SC-2DXS
Plasma Power	1550 W
Cool gas flow	14 l/min
Auxiliary gas flow	0.65 l/min
Nebulizer gas flow	1.03 l/min
CCT (KED mode) flow	5 l/min
CCT gas	8 % H_2 in He
Sampler/Skimmer	material: Nickel
SprayChamber Temperature	2.7 °C
Dwell time	10 ms
Number of replicates	3
RSD (3 replicates) typical	< 1 %
Number of Sweeps	70
Sample flow	0.4 ml/min
LOD typical	< 0.1 ppb

8.12 pH Development

The pH measurements in **Chapter 3** were performed by Katrin Hurle with an InoLab Level 1 pH meter, equipped with a SenTix 61 pH electrode (Xylem Analytics Germany Sales GmbH & Co. KG, WTW, Weilheim, Germany). The electrode was filled with 3 M KCl electrolyte. The pH of the 0.2 M Na2HPO4 mixing liquid was recorded, as well as the pHs of the mixing liquids containing the same amount of sodium phytate as the cement pastes used for the other investigations. For this purpose, the corresponding amount of sodium phytate was dissolved into the 0.2 M Na2HPO4 aqueous solution. Furthermore, the pH of Phy_0.00 and Phy_0.25 was recorded over time to investigate the effect of the sodium phytate addition on the pH development during hydration. The P/L of the cement pastes was increased to 1.2 ml/g to ensure that the cements remained paste-like during the process of hydration and that the pH electrode could be removed afterwards. Hence, the actual content of sodium phytate in the solution decreased to 1/4 and would correspond to an amount of 0.0625 wt.%. The pastes were filled into centrifuge tubes after mixing for 1 min with a metal spatula. The tubes were then stored in a water bath adjusted at 37 °C for hydration. After certain time intervals, the cement pastes were loosened with a metal spatula, and the pH electrode was inserted for measurement. For both compositions, three independently prepared measurements were performed to check reproducibility. The measurements were performed over 9 h to cover the main part of the reaction. The pH profiles (n=3) of the setting reactions in **Chapter 4** during the first 15 h after setting initiation were recorded by Jan Weichhold every 5 s with an InoLab pH meter and Mettler-Toledo pH electrode (Weilheim, Germany). The pH values of the liquids in **Chapter 5** with different PP concentration and the Na_2/Na solutions (30 wt.% and diluted) were recorded by Katrin Hurle using a SevenCompact S220-Uni (Mettler-Toledo, Gießen, Germany), measurements were performed in triplicate. In addition, mixtures of PP005, PP01 and PP05 with the 30 wt.% Na_2/Na solution in the same vol% ratio as in the activated cement pastes were analysed. To monitor the pH development during setting Na21_PP0 and Na21_PP005 were prepared, and their pH value was recorded via a InoLab Level 2 P pH meter (WTW, Weilheim, Germany) every 30 s for a total of 30 min. This was also carried out thrice.

8.13 1H NMR

In-situ ^{1}H-NMR measurements of sample IP6_10 were performed at a Bruker minispec mq20 operating at 19.95 MHz, equipped with a temperature-controlled probe head. These measurements were performed by Katrin Hurle at the Geozentrum Nordbayern. The temperature was adjusted at 23 °C. For the measurement, the cement paste was prepared by stirring for 1 min with a metal spatula. Then the paste was pipetted into the glass tube used for

NMR measurements. The measurement was reproduced three times. A combined solid echo - CPMG sequence was applied for determination of relaxation times T_2. Evaluation of the data was performed with the MinErSys framework based on the Contin software [796].

8.14 3D Printing

The scaffolds shown in the outlook in **Chapter 6** have been prepared using a 3D extrustion printer (3D Discovery, RegenHU, Switzerland). This printer operates with pressurized air and a G-code controlled printhead. The cement pastes were filled into cartridges, the plunger was inserted and sealed off with a drop of oil when the plunger was in position. A cannula with 0.84 mm outlet was mounted to the cartridge and it was placed into the printhead. For a smooth printing the applied pressure was always adjusted with the fresh prepared paste, but it was always in a range around 0.15 bar to 3 bar, depending on the paste composition. Scaffolds of 24 x 24 mm with 4 layers, 12 x 12 mm scaffolds with 4 layers and 6x12 mm scaffolds with 8 layers were printed.

8.15 XRD of Hardened Samples

In order to investigate the quantitative phase composition after different time points in **Chapter 3**, the mixed cement pastes were prepared into special plastic containers (inner diameter 23 mm; inner height 3 mm) that could be tightly closed with a lid. The closed containers were further sealed with Parafilm. By these means, water loss during the storage of the samples was avoided. In addition to the pastes Phy_0.00 – Phy_1.00, a sample with 2 wt.% sodium phytate (Phy_2.00) was also measured here to further investigate the OCP formation. The samples were allowed to harden in a drying oven (Memmert, Schwabach, Germany) at 37 °C for 1 d or 7 d, respectively, or in an Erlanger calorimeter at 23 °C for 1 d, 2 d, 4 d or 7 d. After hardening, the lid was removed and the sample surface was polished with grit 180 grinding paper. The quantitative phase content of the cements of **Chapter 5** 1 d and 7 d after activation was determined by fabricating storage samples. For this purpose, the activated cement pastes (same samples and mixing procedure as for in-situ XRD) were prepared into plastic containers analogous to the samples used for storage stability testing. The samples were allowed to harden in an incubator Heratherm (Thermo Fisher Scientific, Schwerte, Germany) at 37 °C. After the defined storage times, the lid was removed, and the sample surface was polished using a 120-grit sandpaper.

The samples for both **Chapters 3** and **5** were then prepared into special sample holders and covered with Kapton polyimide film (Chemplex Industries, Cat. No. 440, Palm City, FL, USA) for XRD measurements; an angle range of 3° to 70° (2θ) was measured, and the other parameters were the same as for in-situ XRD measurements. Three independently prepared samples were analyzed for each temperature, time and sample composition. The quantitative phase composition was then determined by Rietveld refinement and G-factor quantification, applying the same procedure as for in-situ XRD.

8.16 Controlled setting

To prevent the reaction of the cement pastes in **Chapter 5** with the activation Na_2/Na solution during storage, both mixtures were stored in separate syringes. (**Figure 52**) The mixing was carried out by attaching both Luer lock ends of the respective syringes with a connector piece together and pumping the solutions back and forth from one syringe into the other. This was done 10 times to ensure a homogenous distribution of Na_2/Na in the cement paste. Afterwards the paste was completely pushed into the bigger syringe and the rest was unscrewed. This procedure was used for the samples used for the injectability tests, the rheology tests, mechanical tests, and the porosity measurements. For all the other measurements, where the stabilized paste was mixed with the Na_2/Na solution, both parts were mixed directly in a container and then further used as described in the respective sections.

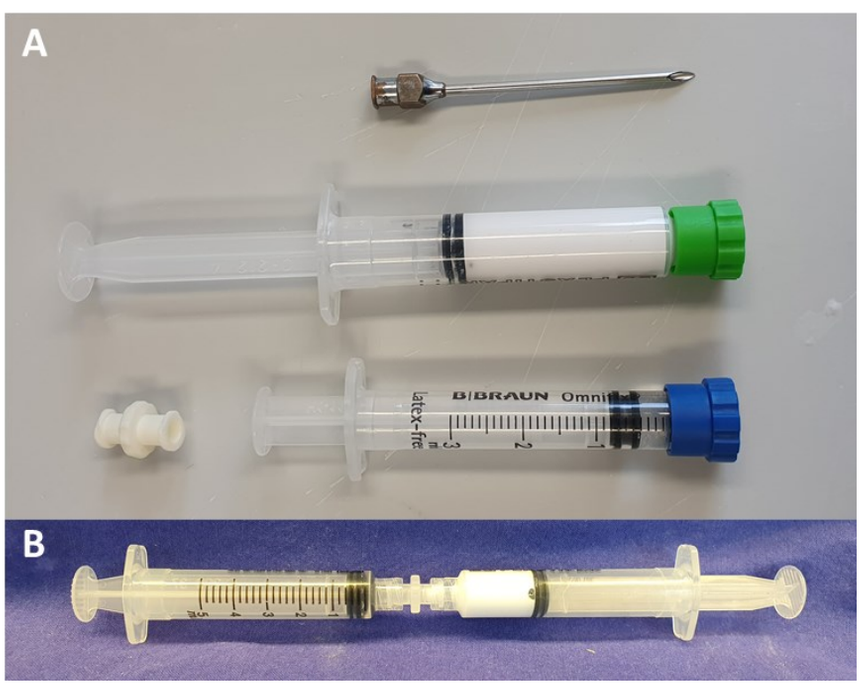

***Figure 52**.(A) Utensils used to store, mix and inject the cement paste: metal cannula (Ø: 2 mm), syringe with cap filled with the stabilized paste (5 ml, top, green cap), syringe with cap filled with the Na_2/Na solution (3 ml, bottom, blue cap) and the Luer lock connector. **(B)** shows the configuration of the two syringes for the mixing process.*

8.17 Imeter

Hardening of the cement pastes Na21_PP0, Na21_PP005 and Na21_PP01 was analysed with an IMETER (IMETER / MSB Breitwieser MessSysteme, Augsburg, Germany) using the „Auto-Gillmore-Needle" approach. Katrin Hurle performed the measurement with the IMETER. The method Nr. 20 was applied, providing the H_{i20} data as a measure for the hardness of the cement [797]. For this method, a cylindrical indenter with defined weight was applied. During the measurement, the cement sample was lifted against this indenter, resulting in load relief. The extent of load relief is dependent on the hardness of the cement. The initial and final setting times of the brushite cements were automatically determined according to the definition for biocements. The criterion for the initial setting time was H_{i20} = 3.94 MPa/mm and H_{i20} = 63.0 MPa/mm for the final setting time.

Prior to the measurements, the components for the freshly prepared prefabricated pastes were equilibrated at 37 °C for at least 3 h in a drying oven (Binder, Tuttlingen, Germany). A few min before starting the experiment, the prefabricated pastes were prepared by mixing the α-TCP powder with the respective PP solution for 1 min with a metal spatula. Directly before starting the measurement, the Na_2/Na solution was added using a pipette, and further stirring was performed for 1 min.

Immediately after mixing, the cement pastes were prepared into a circular sample holder, which was automatically moved after each measurement to ensure that an intact spot is available for the following measurement. As the setting was rather rapid in the initial part, lower pause times between two measurements in the range of 60 to 125 s were chosen. In the later part of the experiment, the pause time was increased up to 20 min. The temperature in the sample chamber was adjusted at 37 °C.

8.18 Compressive Strength

The respective pastes were filled into silicon moulds with the dimensions of 6x6x12 mm^3 for each mixture. The samples were stored at 37 °C and 100 % humidity. They have been prepared and stored as listed below. The measurement was performed at the universal testing machine Z010 (Zwick Roell GmbH & Co. KG, Ulm, Germany) with a crosshead speed of 1 mm/min and a load cell of 2.5 kN until a major failure was produced. The compressive strength was then calculated according to **Eq.(15)** where F_{max} is the force at failure and A is the area of the sample in contact with the machine:

$$\sigma = \frac{F_{max}}{A} \qquad \textit{Eq.(15)}$$

The samples of **Chapter 3** for the compressive strength (CS) tests were prepared as follows: each sample batch consisted of 14.4 g α–TCP, 1.6 g CDHA and the respective amount of Na–phytate ranging from 0 to 1 wt.% related to the total amount of cement powder. Every powder was mixed with 4.8 ml of an 0.2 M $NaHPO_4$ aqueous solution (L/P = 0.3 ml/g) and was stirred for 1 min. Then, the paste was transferred into 24 moulds. After 1 d, 12 samples per mixture were removed from the storage and demoulded to be ready for the measurement. The second batch of 12 samples was handled the same, but after 7 d of storage.

For mechanical tests in **Chapter 4**, the β-TCP dry powder and corresponding liquid phases were mixed homogeneously in a liquid-to-powder ratio (L/P) of 0.83 mL/g for 30 s on a glass slab. The cement pastes were transferred into 12 molds and hardened for 2, 4, 8 and 24 h, while demolding took place 1 h after cement paste preparation.

In **Chapter 5** after 1 d, 12 samples per mixture were removed from the storage and demoulded to be ready for the measurement. The second batch of 12 samples was handled the same, but after 7 d of storage.

8.19 Porosity

Identical samples to those used for the compressive strength tests, after 1 and 7 d of reaction time were used to measure the influence of the addition of PP and the Na_2/Na activation solution on the porosity. For every measurement, a sample piece was put into a dilatometer and measured in the mercury porosimeters Pascal 140 and 440 (Thermo, Italy). At the Pascal 140, the dilatometer got evacuated to 0.01 kPa and filled with mercury. During the measurement at the Pascal 140, the pressure was increased linearly from 0.01 to 400 kPa. After that, the sample was transferred into the Pascal 440, where the pressure was increased from 0.1 to 400 MPa.

The size of the pores corresponding to each pressure was calculated by the Washburn **Eq.(16)**[798]

$$r=\frac{2\gamma^{*}\cos\theta}{P} \qquad \textit{Eq.(16)}$$

Where r is the calculated pore radius, γ the surface tension of mercury (480 dyne/cm), θ the contact angle of mercury (140°) and P the pressure in kPa. With 1 kPa = 104 dyne/cm² the equation can be simplified to **Eq.(17)**

$$r=\frac{735403}{P} \qquad \textit{Eq.(17)}$$

Together with the volume change registered at the specific pressure, the relative pore volume can be calculated.

8.20 SEM Imaging and Light Microscopy

The pieces left from the compressive strength tests and were used for SEM. These were coated with a 4 nm platinum layer in an ACE600 (Leica, Wetzlar, Germany) sputter coating unit and then put into a Crossbeam 340 (Zeiss, Oberkochen, Germany) SEM for the measurement. Secondary electron pictures were taken in a high vacuum, with an acceleration voltage of 2 kV **(Chapter 3)** and 5.0 kV **(Chapter 4)**.

8.21 Statistics

In **Chapter 3** for all of the quantitative XRD data, pH values, calorimetry data, BET and injectability measurements, the errors were determined as the standard deviations of three independently performed measurements. For the laser diffraction, three independent preparations with 10 measurement runs for each were analysed, and the 30 resulting data sets were averaged. Three independent preparations for the zeta potential measurement resulted in nine values that were used to determine the mean and the standard deviation. Not all prepared samples were suitable to use for the mechanical tests, but there was a minimum of nine independently prepared samples per mixture.

The errors of the data achieved in **Chapter 4** by BET, X-ray diffraction, isothermal calorimetry, pH and injectability measurements were each determined by calculating the standard deviation of the results of three independent measurements. Mechanical tests were performed 6-8 times for each sample and standard deviations were calculated. For zeta potential measurements, the standard deviation of 9 measurements (3 measurements for each of 3 independent preparations) were determined.

In **Chapter 5** Quantitative XRD (powder and storage samples, in-situ XRD), laser diffraction, storage stability, injectability, isothermal calorimetry, Imeter, compressive strength and porosity measurements were all reproduced in triplicate, the results were presented as mean ± standard deviation. A one-way Anova was performed for the zeta potential, the injectability, the calorimetry, true crystallinity, and the phase content of the stored hydrated samples. Two-way Anova for the compressive strength.

Appendix

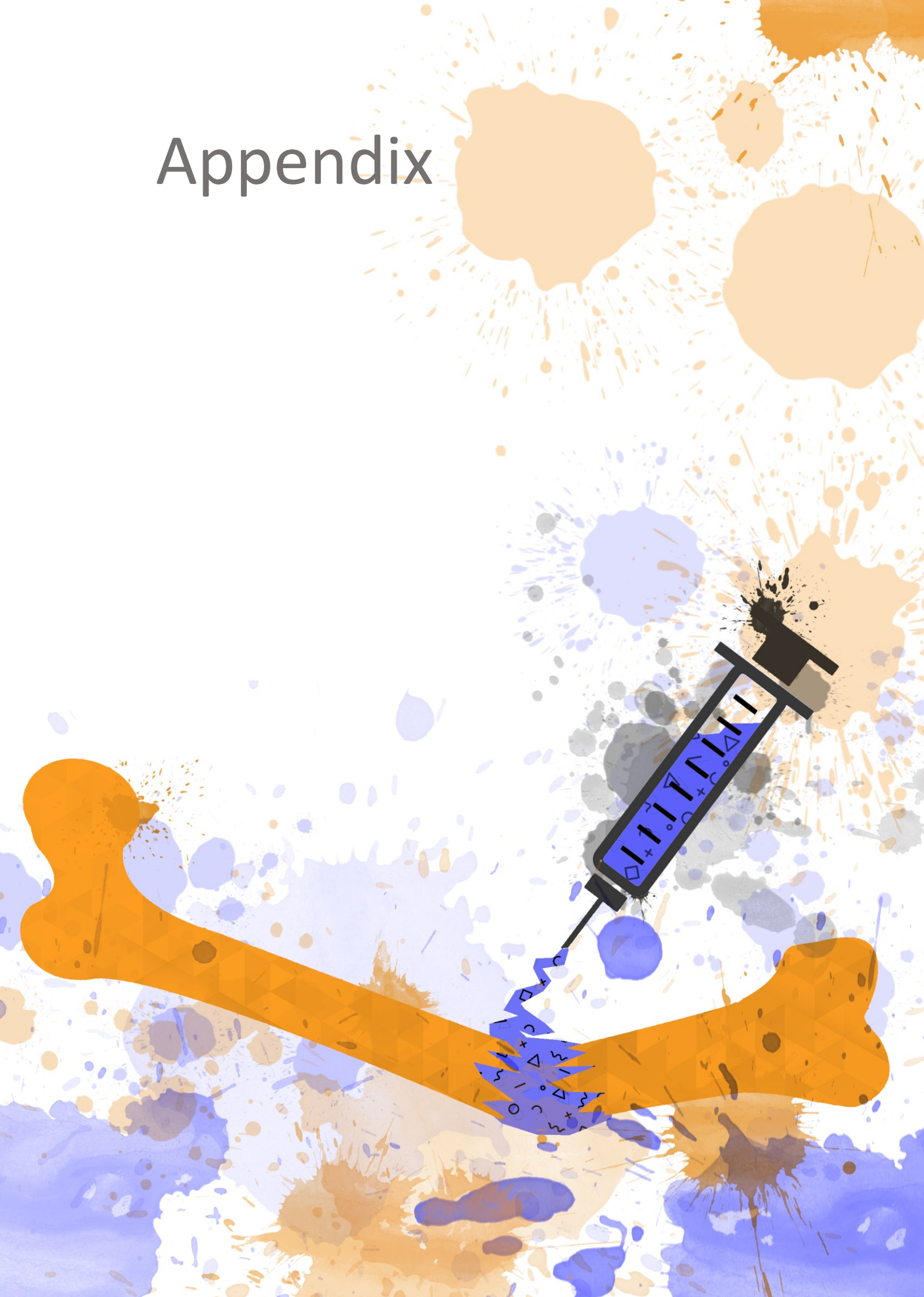

9.1 Circulum Vitae

9.2 Publications and Conference Contributions

Relevant to this thesis

Hurle, Katrin, et al. "Hydration mechanism of a calcium phosphate cement modified with phytic acid." *Acta Biomaterialia* 80 (2018): 378-389.[694]

Weichhold, Jan, et al. "Setting mechanism of a CDHA forming α-TCP cement modified with sodium phytate for improved injectability." *Materials* 12.13 (2019): 2098.[689]

Weichhold, Jan, et al. "Pyrophosphate ions inhibit calcium phosphate cement reaction and enable storage of premixed pastes with a controlled activation by orthophosphate addition." *Ceramics International* 48.11 (2022): 15390-15404.[716]

Collaborations or supporting role:

Böhm, Christoph, et al. "The Multiweek Thermal Stability of Medical-Grade Poly (ε-caprolactone) During Melt Electrowriting." *Small* 18.3 (2022): 2104193.[799]

Seifert, Annika, et al. "Phase Conversion of Ice-Templated α-Tricalcium Phosphate Scaffolds into Low-Temperature Calcium Phosphates with Anisotropic Open Porosity." *Advanced Engineering Materials* 23.5 (2021): 2001417.[800]

Kaiser, Friederike, et al. "Accelerated bone regeneration through rational design of magnesium phosphate cements." *Acta Biomaterialia* (2022).[801]

Blum, Carina, et al. "Controlling Topography and Crystallinity of Melt Electrowritten Poly (ε-Caprolactone) Fibers." *3D Printing and Additive Manufacturing* 8.5 (2021): 315-321.[802]

Kade, Juliane C., et al. "Melt electrowriting of poly (vinylidene fluoride-co-trifluoroethylene)." *Polymer International* 70.12 (2021): 1725-1732.[803]

Holzmeister, Ib, et al. "Hydraulic reactivity and cement formation of baghdadite." *Journal of the American Ceramic Society* 104.7 (2021): 3554-3561.[804]

Conferences with active participation

Year	Type	Conference
2018	**Poster**	**25. DGBM Annual Meeting, Braunschweig** Hydration mechanism of a β-tricalcium phosphate (β-TCP) modified with phytic acid (IP6)
2019	**Talk**	**94.DKG Annual Meeting Symposium Ceramics, Leoben** Hydration mechanism of a ß-tricalcium phosphate cement (ß-TCP) modified with phytic acid
2019	**Talk**	**30.ESB + 26. DGBM Annual Meeting, Dresden** Setting mechanism of a modified apatitic bone cement for better injectability
2019	**Poster**	**31. Bioceramics Annual Meeting, New Orleans** Injectable apatite forming α tricalcium phosphate (α-TCP) cement modified by sodium phytate addition 2nd Poster price

9.3 Affidavit

I hereby confirm that my thesis entitled:

>> **Injectable calcium phosphate-based bone replacement cements** <<

is the result of my own work. I did not receive any help or support from commercial consultants. All sources and / or materials applied are listed and specified in the thesis.

Furthermore, I confirm that this thesis has not yet been submitted as part of another examination process neither in identical nor in similar form.

_____ _____

Place, Date Signature

9.4 Eidesstattliche Erklärung

Hiermit erkläre ich an Eides statt, die Dissertation:

>> **Injizierbare calciumphosphat-basierte Knochenersatzzemente** <<

eigenständig, d.h. insbesondere selbständig und ohne Hilfe eines kommerziellen Promotionsberaters, angefertigt und keine anderen als die von mir angegebenen Quellen und Hilfsmittel verwendet zu haben.

Ich erkläre außerdem, dass die Dissertation weder in gleicher noch in ähnlicher Form bereits in einem anderen Prüfungsverfahren vorgelegen hat.

_____ _____

Ort, Datum Unterschrift

9.6 Contribution to Figures and Tables

Statement of individual author contributions to figures/tables of manuscripts included in the dissertation

KH : Katrin Hurle ; JW : Jan Weichhold ; MP : Maximilian Pfeiffle ; MB : Manuel Brückner ; TB : Theresa Brückner

The order of contributors, from left to right, reflects their qualitative impact on the respective figure or table in descending order separated by manuscript (1 : **Table 17** ; 2 : **Table 18** ; 3 :**Table 19** ; 4 : **Table 20**). Numbering is referring to the respective number in this thesis.

Table 17. *Qualitative contributions for Manuscript 1 used in* ***Chapter 3****.*

Manuscript 1: Weichhold, J., Gbureck, U., Goetz-Neunhoeffer, F., & Hurle, K. (2019). Setting mechanism of a CDHA forming α-TCP cement modified with sodium phytate for improved injectability. *Materials*, *12*(13), 2098 [689].

Figure	**Author Initials,** Responsibility decreasing from left to right	
13	JW	KH
14	JW	KH
15	JW	KH
16	JW	KH
17	KH	JW
18	KH	JW
19	KH	JW
20	KH	JW
21	JW	KH
22	JW	KH
23	JW	KH
Table	**Author Initials,** Responsibility decreasing from left to right	
3	JW	KH
4	KH	JW
5	KH	JW
6	KH	JW
7	KH	JW
8	KH	JW
9	JW	KH

Explanations (if applicable):

All data was discussed in cooperation from the beginning of evaluation through to the creation of the respective figures/tables.

***Table 18**. Qualitative contributions for Manuscript 2 used in **Chapter 4**.*

Manuscript 2 : Hurle, K., Weichhold, J., Brueckner, M., Gbureck, U., Brueckner, T., & Goetz-Neunhoeffer, F. (2018). Hydration mechanism of a calcium phosphate cement modified with phytic acid. *Acta Biomaterialia, 80*, 378-389 [694].

Figure	**Author Initials,** Responsibility decreasing from left to right		
24	JW	KH	
25	JW	KH	
26	JW	KH	
27	KH	JW	
28	KH	JW	
29	KH	JW	
30	KH	JW	
31	KH	JW	
32	TB	JW	MB
33	TB	JW	MB
34	TB	JW	MB

Explanations (if applicable):

The experiments have been conducted by Jan Weichhold (JW) and Katrin Hurle (KH) with the support of Manuel Brueckner (MB) and Theresa Brueckner (TB). TB and MB startet the work as part of a project work initiated and supervised by TB and done by MB. JW and KH then added onto that and conducted additional experiments.

***Table 19**. Qualitative contributions for Manuscript 3 used in **Chapter 5**.*

Manuscript 3 : Weichhold, J., Goetz-Neunhoeffer, F., Hurle, K., & Gbureck, U. (2022). Pyrophosphate ions inhibit calcium phosphate cement reaction and enable storage of premixed pastes with a controlled activation by orthophosphate addition. *Ceramics International*, *48*(11), 15390-15404 [716].

Figure	**Author Initials,** Responsibility decreasing from left to right	
35	JW	KH
36	JW	KH
37	JW	KH
38	JW	KH
39	JW	KH
40	JW	
41	KH	JW
42	KH	JW
43	KH	JW
44	KH	JW
45	JW	KH
46	JW	KH
Table	**Author Initials,** Responsibility decreasing from left to right	
10	KH	JW
11	JW	KH
12	KH	JW
13	KH	JW

Explanations (if applicable):

All data was discussed in cooperation from the beginning of evaluation through to the creation of the respective figures/tables.

***Table 20**. Qualitative contributions for Manuscript 4 used in **Chapter 6**.*

Manuscript 4 : Bachelor thesis Maxmilan Pfeiffel [738].		
Figure	**Author Initials,** Responsibility decreasing from left to right	
47	JW	MP
48	JW	MP
49	JW	MP
50	JW	MP
Table	**Author Initials,** Responsibility decreasing from left to right	
14	JW	MP

Explanations (if applicable):

The figures and tables used in Chapter 6 are based on parts of the results of a bachelor thesis done by MP. This thesis was initiated and planned by JW, who also helped with the experiments. Figures and tables were partially adjusted and expanded with additional information from the bachelor thesis by JW to fit into **Chapter 6**.

I also confirm my primary supervisor's acceptance.

_____

Doctoral Researcher's Name Date Place Signature

Statement of individual author contributions and of legal second publication rights to manuscripts included in the dissertation

KH : Katrin Hurle ; JW : Jan Weichhold ; MP : Maximilian Pfeiffle ; MB : Manuel Brückner ; TB : Theresa Brückner ; FGN : Friedlinde Goetz-Neunhoeffer

The order of contributors, from left to right, reflects their qualitative impact on the respective figure or table in descending order separated by manuscript (1 : **Table 21**; 2 : **Table 22Table 18** ; 3 : **Table 23** ; 4 :**Table 24**).

Table 21**. Qualitative contributions for Manuscript 1 used in **Chapter 3

Manuscript 1 : Weichhold, J., Gbureck, U., Goetz-Neunhoeffer, F., & Hurle, K. (2019). Setting mechanism of a CDHA forming α-TCP cement modified with sodium phytate for improved injectability. *Materials*, *12*(13), 2098 [689].

Participated in	**Author Initials,** Responsibility decreasing from left to right		
Study Design	JW	UG	KH
Methods Development	JW	KH	UG
Data Collection	JW / KH		
Data Analysis and Interpretation	JW / KH	UG	
Manuscript Writing	JW / KH	UG	FGN
Writing of Introduction	JW / KH	UG	
Writing of Materials & Methods	JW / KH		
Writing of Discussion	JW / KH	UG	FGN
Writing of First Draft	JW / KH		

Explanations (if applicable):

All data was discussed in cooperation from the beginning of evaluation through to the creation of the respective figures/tables.

Table 22**. Qualitative contributions for Manuscript 1 used in **Chapter 4

Manuscript 2 : Hurle, K., Weichhold, J., Brueckner, M., Gbureck, U., Brueckner, T., & Goetz-Neunhoeffer, F. (2018). Hydration mechanism of a calcium phosphate cement modified with phytic acid. *Acta Biomaterialia*, *80*, 378-389 [694].

Participated in	**Author Initials,** Responsibility decreasing from left to right			
Study Design	KH	UG	JW	
Methods Development	JW	KH	UG	
Data Collection	JW /KH	TB	MB	
Data Analysis and Interpretation	KH / JW	UG	TB	MB
Manuscript Writing	JW /KH	UG	FGN	
Writing of Introduction	KH / JW	UG		
Writing of Materials & Methods	JW / KH			
Writing of Discussion	KH / JW	UG	FGN	
Writing of First Draft	KH / JW			

Explanations (if applicable):

The experiments have been conducted by Jan Weichhold (JW) and Katrin Hurle (KH) with the support of Manuel Brueckner (MB) and Theresa Brueckner (TB). TB and MB startet the work as part of a project work initiated and supervised by TB and done by MB. JW and KH then added onto that and conducted additional experiments.

Table 23**. Qualitative contributions for Manuscript 1 used in **Chapter 5

Manuscript 3 : Weichhold, J., Goetz-Neunhoeffer, F., Hurle, K., & Gbureck, U. (2022). Pyrophosphate ions inhibit calcium phosphate cement reaction and enable storage of premixed pastes with a controlled activation by orthophosphate addition. *Ceramics International*, *48*(11), 15390-15404 [716].

Participated in	**Author Initials,** Responsibility decreasing from left to right		
Study Design	JW	UG	KH
Methods Development	JW	KH	UG
Data Collection	JW / KH		
Data Analysis and Interpretation	JW / KH	UG	
Manuscript Writing	JW / KH	UG	FGN
Writing of Introduction	JW / KH	UG	
Writing of Materials & Methods	JW / KH		
Writing of Discussion	JW / KH	UG	FGN
Writing of First Draft	JW / KH		

Explanations (if applicable):

All data was discussed in cooperation from the beginning of evaluation through to the creation of the respective figures/tables.

Table 24**. Qualitative contributions for Manuscript 1 used in **Chapter 6

Manuscript 4 : Bachelor thesis Maximilian Pfeiffel [738]

Participated in	**Author Initials,** Responsibility decreasing from left to right	
Study Design	JW	
Methods Development	JW	
Data Collection	MP	JW
Data Analysis and Interpretation	JW/MP	
Manuscript Writing	JW	MP
Writing of Introduction	MP	JW
Writing of Materials & Methods	MP	JW
Writing of Discussion	JW	MP
Writing of First Draft	MP	JW

Explanations (if applicable):

The Bachelor thesis by MP was initiated and planned by JW, who also helped with the experiments. Results and texts were translated, partially adjusted, and expanded with additional information from the bachelor thesis by Jan Weichhold to fit into **Chapter 6**.

If applicable, the doctoral researcher confirms that she/he has obtained permission from both the publishers (copyright) and the co-authors for legal second publication.

The doctoral researcher and the primary supervisor confirm the correctness of the above mentioned assessment.

Doctoral Researcher's Name	Date	Place	Signature

Primary Supervisor's Name	Date	Place	Signature

9.7 Acknowledgement | Danksagung

Nach 226 Seiten im gesamten Dokument, 207 im nummerierten Teil und, bis zum Anfang dieses Satzes, 50 387 Wörtern bestehend aus 310 066 Zeichen (inklusive Leerzeichen) kommt jetzt einer der schwersten Teile dieser Arbeit. Die persönlichen Beziehungen, Freundschaften und Kooperationen, die ich die vergangenen fünf Jahre knüpfen durfte, die gemeinsamen Erlebnisse – gute wie schlechte -, die wir gemeinsam gemeistert haben, und alles andere, woraus ich Motivation geschöpft habe auf ein paar DIN A4 Seiten zusammenzufassen scheint schier unmöglich. Ich bin aber sicher, dass jeder, dem mein Dank gebührt, das weiß und sich im schlimmsten Fall auch ungenannt wertgeschätzt fühlt.

Zuallererst möchte ich mich bei meinem Doktorvater Uwe bedanken. Als ich meine Arbeit am FMZ begann hatte ich keine Vorstellung, wie ich mir einen guten Doktorvater vorstellen kann und wen ich mir als Unterstützung in dieser neuen spannenden, aber auch herausfordernden, Aufgabe wünschen würde. Jetzt, nachdem ich alles hinter mir habe, hat sich das geändert. Die Kombination aus nahbarem Chef, mit dem man auf ehrlicher Augenhöhe reden kann, gepaart mit der Leidenschaft fürs Kochen, und Umsetzen spannender schneller Ideen macht dich aus. Das hat mir immer ein sicheres Gefühl gegeben, in dir einen idealen Ansprechpartner für meine Anliegen zu finden. Sei es beruflich oder auch privat. Du bringst die Leute zusammen, lässt sie miteinander reden und erlaubst ihnen dabei, sie selbst zu bleiben. Danke Uwe, für die schöne Zeit!

Uwes Arbeit, die ich mit meinem Teil unterstützen durfte, wäre nicht möglich ohne das Vertrauen und die Unterstützung von unserem >>Chef-Chef<< Prof. Dr. Jürgen Groll. Vielen Dank für die Führung des FMZ und ihr Vertrauen in die Doktoranden. Sie haben es mir nicht nur ermöglicht als Wissenschaftler zu wachsen, sondern mich auch persönlich weiterzuentwickeln. Für diese außergewöhnliche Erfahrungen danke ich ihnen.

Neben der Institutsleitung und dem Doktorvater habe ich auch durch die weitern Mitglieder meines Prüfungskomitees eine exzellente Führung erfahren. Dr. Katrin Hurle, du hast mich schon seit dem Bachelorabschluss begleitet und ich konnte seitdem von dir lernen. Unser, zuerst von deiner Seite betreuendes, Verhältnis hat sich mit dem Beginn meiner Doktorarbeit in ein Kooperatives gewandelt. Die Zusammenarbeit und der Austausch mit dir war immer erfrischend einfach und zielführend. Du hast für mich maßgeblich dazu beigetragen, dass die vergangenen Jahre so gut in meinem Gedächtnis bleiben. Katrin, dafür danke ich dir!

Prof. Dr. Torsten Blunk, sie haben mein Prüfungskomitee perfekt abgerundet. Neben ihrer fachlichen Expertise, die mir immer einen anderen Blickwinkel aufgezeigt mich gleichzeitig in meiner Arbeit bestätigt hat, haben sie mit ihrer ruhigen, aber sehr interessierten Art immer einen spannenden Gesprächspartner dargestellt. Vielen Dank für ihre Führung.

Dieses ganze Unterfangen hätte ich wahrscheinlich nie angefangen ohne die außergewöhnliche Unterstützung meiner Eltern. Schon immer steht ihr hinter mir, unterstützt mich bei allen Ideen und Vorhaben, die ich mir ausgemalt habe. Nie habe ich gespürt, dass ich einem bestimmten Bild gerecht werden musste. Nie stand ich durch eure Unterstützung in einer Schuld. Im Gegenteil! Selbst nachdem ich mein Studienfach gewechselt habe, habe ich unentwegt euer Verständnis gespürt nach dem Motto: >> Er wird schon wissen was er tut, und wir tun unser Möglichstes, um ihn dabei zu unterstützen<<. In jungen Jahren nimmt man so etwas vielleicht als gegeben hin: >>Sind ja meine Eltern<<. Aber je mehr ich von der Welt erfahre, je mehr ich von Freunden und Bekannten höre, desto mehr ist mit klar geworden, dass das alles andere als selbstverständlich ist. Ich möchte mich deshalb von ganzem Herzen bei euch bedanken, dass ich so gut behütet aufwachsen durfte und es mich zu dem Menschen gemacht hat, der ich heute bin. Was ich von euch bekommen habe, versuche ich so gut es geht weiterzugeben! Für dieses große Geschenk kann ich euch nicht genug danken. Danke Mama und Papa!

Neben meinen Eltern möchte ich auch ihren Eltern, meinen Großeltern, danken. Auch wenn ich nicht alle meiner Großeltern lange erleben durfte, sind es doch ihre Werte, die sie über meine Eltern an mich weitergegeben haben. Ihr, eure Vergangenheit, eure Taten und eure Errungenschaften erfüllen mich immer wieder mit Stolz und Bewunderung. Danke!

Neben der direkt verwandten Familie war es vor Allem die Wahlfamilie, die mir immer geholfen hat. Allen voran meine Partnerin Ilona mit Familie Rosemarie, Rudi und Christian. Wir haben uns in Würzburg kennengelernt und haben uns seither in allen Situationen gegenseitig unterstützt. Bei dir kann ich immer auf ehrliche, knallharte Kritik zählen, aber auch auf entspannte, witzige Ablenkung, wenn es mal nötig ist abzuschalten. Ohne dich wären die letzten Jahre ganz anders abgelaufen und ich kann mit Bestimmtheit sagen, dass sie nicht so schön gewesen wären wie sie es schließlich waren. Wir ergänzen uns wunderbar. Vielen Dank, dass es dich gibt, und vielen Dank, dass du mit mir zusammen durchs Leben gehst.

Der Ort, an dem man meistens seinen Emotionen aufgrund eines missglückten Experiments, einer doofen Aufgabe oder auch vielleicht einfach persönlicher Probleme als erstes Luft macht, ist das Büro. Das würde das Büro erstmal zu einem sehr negativ konnotierten Ort machen. Aber bei mir, bei uns am FMZ war das ganz anders! Es war immer ein Ort des freudigen Austauschs, der gegenseitigen Hilfe und der offenen Ohren. Mein Büro hat sich über die Jahre öfter in Standort und Zusammensetzung geändert. Dabei gab es aber eine Konstante. Die warst du Ib. Ich danke dir dafür, wie du mich aufgenommen hast, wie wir zusammen alles, was uns die Doktorarbeit in den Weg geworfen hat, gemeistert haben, wie wir privat in unseren Hobbys voneinander gelernt haben und auch Neue zusammengefunden haben. Wir haben uns oft blind bzw. ehr stumm verstanden, danke dir dafür. Auch dir Friederike, möchte ich für die Zeit im Büro, aber auch außerhalb, danken. Du bist als perfekte Ergänzung in unser Team gekommen und ich habe von dir erheblich mehr gelernt als es dir vielleicht klar ist. Deine offene und ehrlich Art und die Gewissenhaftigkeit haben dich zu einer Person gemacht, auf die ich immer zählen kann. Ich bin sehr dankbar, dass wir uns einen Teil des Weges geteilt haben. Danke Ib, Danke Friederike!

Ein weiterer Dank gilt neben Uwe, Ib und Friederike, Allen anderen >>Zementies<<, sei es andere Doktoranden bzw. Postdocs der Zementgruppe, Bacheloranden / Masteranden, die ich begleiten dufte wie Max, Zahnis / Medis, allen voran Sandra, Silvia, Valentin und Tobi.

Ich habe jetzt ganz viel über einzelne Personen gesprochen und meine Zeit am FMZ mit ihnen umrissen, aber ein wichtiger Teil davon fehlt noch. Wer ist denn das FMZ? Ich kann mit gutem Gewissen behaupten, dass für mich und viele andere die Powerfrau aus dem 3ten Stock Isabell, die beiden genialen Tüftler aus der Werkstatt Harald und Toni, das Organisations- und Abschweifungstalent Jörg und nicht zuletzt die beiden Verwaltungsgenies Tanja und Birgit die wichtigsten Personen am FMZ sind. Ihr seid das Fundament, auf dem alles sicher steht! Dafür danke ich euch.

Unter den Personen, die sicher auf diesem Fundament stehen, waren anfangs nur Unbekannte. Aus diesen Unbekannten wurden recht schnell Kollegen und einige davon wurden schlussendlich auch zu Freunden. Allen diesen Leuten möchte ich für die Zeit zusammen danken, den Freunden aber noch einmal namentlich für die tollen Erlebnisse, Erfahrungen und auch hoffentlich noch langanhaltenden Beziehungen. Annika mit Janosch, Jessi mit Benni, Vicky mit Marius, Jun, Christoph, Michael, Alessandro, Csaba, Manuel, Philipp mit Verena, Alice, Matze, Kiki, Tomasz, Berat, Ali und Biranche. Ihr alle habt mich begleitet und werdet das hoffentlich noch weiter als Freunde tun. Danke!

Wer mich kennt weiß natürlich, dass ich nicht erst am FMZ Freunde gefunden habe. Ich wäre nicht der Mensch, der ich heute bin, den ihr kennengelernt habt, ohne meine Familie, aber auch nicht ohne meine Freunde. Die Grabbelgruppe wurde einfach von unseren Müttern gegründet, aber im Endeffekt war es das beste was uns passieren konnte. Luki, Chris und Steffen, euch danke ich, weil ihr die Freunde seid, die sich wie Brüder anfühlen. Später haben sich dann noch Josh und Lars bzw. Lipsi, Lea, Lisl und Sabine in diesen Kreis eingefunden. Ich treffe immer wieder auf Menschen, die erstaunt sind wie lange wir befreundet sind und werde dadurch jedes Mal aufs Neue erinnert was für ein wunderbares Geschenk ihr seid. Lieb euch!

Last but not least komme ich zu meinem wilden Haufen an Jungs, die sich irgendwann in der 8ten Klasse geschworen haben, zusammen zu bleiben. Das tun sie bis heute. Ihr seid so wertvoll. Auch wenn wir uns über die Jahre immer weniger sehen, ist es mir immer wieder ein inneres Weizeneinschenken mit euch! Die sogenannten Hartzer sind etwas was jeder in seinem Leben bräuchte, aber die wenigsten sind so privilegiert wie wir. Danke, dass es euch gibt Jungs!

Außerdem danke ich allen anderen Personen, die mich in den letzten Jahren auf einem Teil meines oder ihres Weges begleitet haben.

References

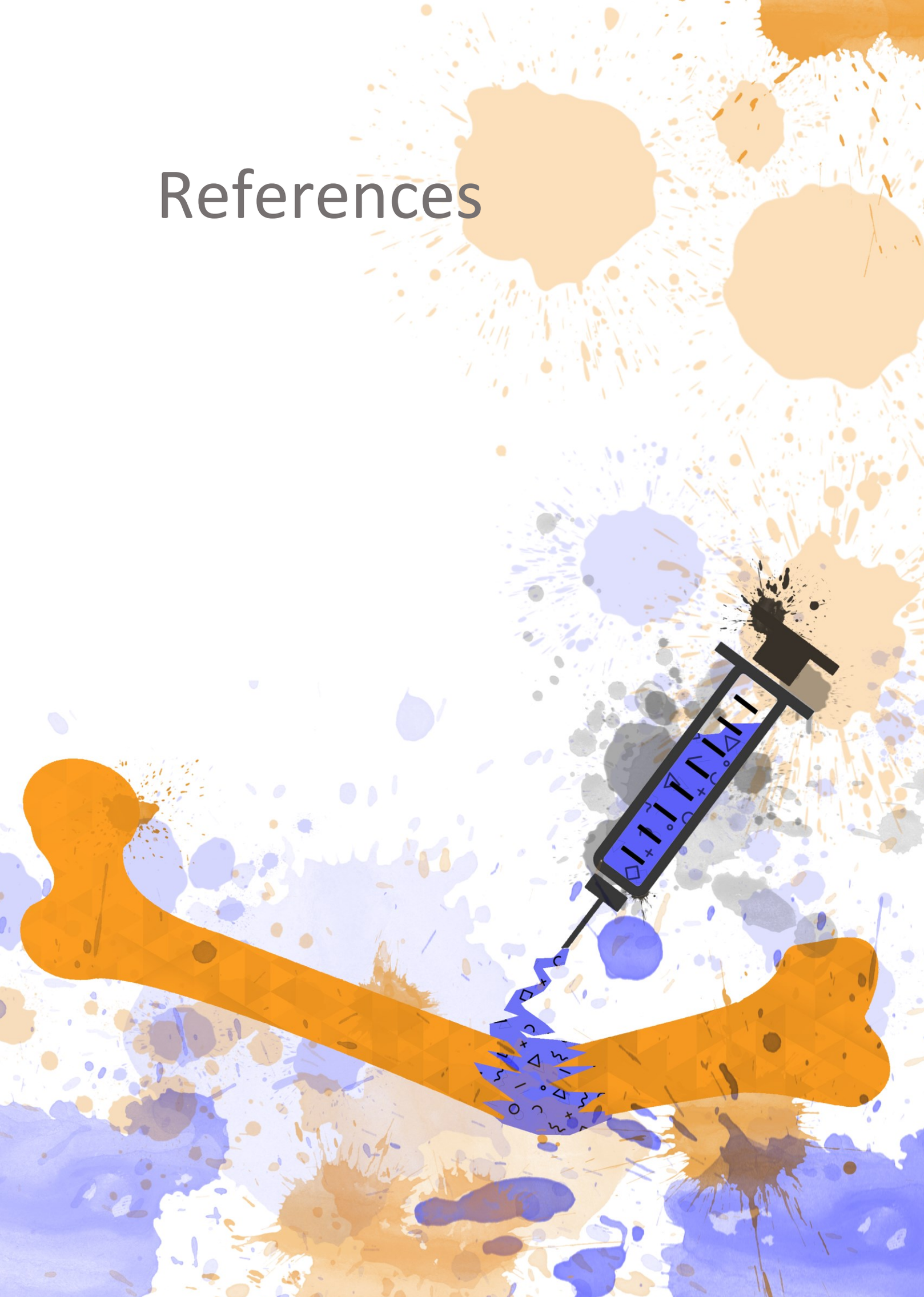

References

[1]D. De Catanzaro, Evolutionary limits to self-preservation, Ethology and Sociobiology 12(1) (1991) 13-28.

[2]E. Khantzian, J.E. Mack, Self-preservation and the care of the self: Ego instincts reconsidered, The Psychoanalytic Study of the Child 38(1) (1983) 209-232.

[3]K.D. Birnbaum, A.S. Alvarado, Slicing across kingdoms: regeneration in plants and animals, Cell 132(4) (2008) 697-710.

[4]B.J. Blaiszik, S.L. Kramer, S.C. Olugebefola, J.S. Moore, N.R. Sottos, S.R. White, Self-healing polymers and composites, Annual review of Materials Research 40(1) (2010) 179-211.

[5]C.E. Diesendruck, N.R. Sottos, J.S. Moore, S.R. White, Biomimetic self-healing, Angew. Chem. Int. Ed. 54(36) (2015) 10428-10447.

[6]P. Rohatgi, M. Nosonovskiĭ, Biomimetics in Materials Science: Self-healing, Self-lubricating, and Self-cleaning Materials (Springer Series in Materials Science), Springer2012.

[7]A. Sancar, Structure and function of DNA photolyase and cryptochrome blue-light photoreceptors, Chem. Rev. 103(6) (2003) 2203-2238.

[8]R. Weinkamer, J.W. Dunlop, Y. Bréchet, P. Fratzl, All but diamonds–biological materials are not forever, Acta Mater. 61(3) (2013) 880-889.

[9]A. Castiglioni, A history of medicine, Routledge2019.

[10]R.H. Shryock, The development of modern medicine: an interpretation of the social and scientific factors involved, University of Pennsylvania Press2017.

[11]M.A. Hossain, Significance of the structure of human skeleton, American Journal of Medical Science and Medicine 6(1) (2018) 1-4.

[12]D.G. Steele, C.A. Bramblett, The anatomy and biology of the human skeleton, Texas A&M University Press1988.

[13]E.H. Schemitsch, Size matters: defining critical in bone defect size!, J. Orthop. Trauma 31 (2017) S20-S22.

[14]A. Vajgel, N. Mardas, B.C. Farias, A. Petrie, R. Cimões, N. Donos, A systematic review on the critical size defect model, Clin. Oral Implants Res. 25(8) (2014) 879-893.

[15]J.O. Hollinger, J.C. Kleinschmidt, The critical size defect as an experimental model to test bone repair materials, J. Craniofac. Surg. 1(1) (1990) 60-68.

[16]R.R. Betz, Limitations of autograft and allograft: new synthetic solutions, Orthopedics 25(5) (2002) S561-S570.

[17]P. Hernigou, Bone transplantation and tissue engineering. Part II: bone graft and osteogenesis in the seventeenth, eighteenth and nineteenth centuries (Duhamel, Haller, Ollier and MacEwen), Int. Orthop. 39(1) (2015) 193-204.

[18]P.-J. Meeder, C. Eggers, 1. The history of autogenous bone grafting, Injury 25 (1994) SA2-SA4.

[19]A.H. Schmidt, Autologous bone graft: Is it still the gold standard?, Injury 52 (2021) S18-S22.

[20]N. Shibuya, D.C. Jupiter, Bone graft substitute: allograft and xenograft, Clin. Podiatr. Med. Surg. 32(1) (2015) 21-34.

[21]R. Amid, A. Kheiri, L. Kheiri, M. Kadkhodazadeh, M. Ekhlasmandkermani, Structural and chemical features of xenograft bone substitutes: A systematic review of in vitro studies, Biotechnology and Applied Biochemistry 68(6) (2021) 1432-1452.

[22]P. Hernigou, Bone transplantation and tissue engineering, part I. Mythology, miracles and fantasy: from Chimera to the Miracle of the Black Leg of Saints Cosmas and Damian and the cock of John Hunter, Int. Orthop. 38(12) (2014) 2631-2638.

[23]J. Older, Introduction: history and research on bone transplantation, Bone Implant grafting (1992).

[24]E.D. Arrington, W.J. Smith, H.G. Chambers, A.L. Bucknell, N.A. Davino, Complications of iliac crest bone graft harvesting, Clinical Orthopaedics and Related Research® 329 (1996) 300-309.

[25]J.C. Banwart, M.A. Asher, R.S. Hassanein, Iliac crest bone graft harvest donor site morbidity. A statistical evaluation, Spine 20(9) (1995) 1055-1060.

[26]J. Seiler 3rd, J. Johnson, Iliac crest autogenous bone grafting: donor site complications, J. South. Orthop. Assoc. 9(2) (2000) 91-97.

[27]Y. Fillingham, J. Jacobs, Bone grafts and their substitutes, The bone & joint journal 98(1_Supple_A) (2016) 6-9.

[28]M. Broom, J. Banta, T. Renshaw, Spinal fusion augmented by luque-rod segmental instrumentation for neuromuscular scoliosis, The Journal of Bone and Joint Surgery. American Volume 71(1) (1989) 32-44.

[29]P. Henman, D. Finlayson, Ordering allograft by weight: suggestions for the efficient use of frozen bone-graft for impaction grafting, The Journal of Arthroplasty 15(3) (2000) 368-371.

[30]R.W. Hu, H. Bohlman, Fracture at the iliac bone graft harvest site after fusion of the spine, Clinical Orthopaedics and Related Research® (309) (1994) 208-213.

[31]J. Kartus, T. Movin, J. Karlsson, Donor-site morbidity and anterior knee problems after anterior cruciate ligament reconstruction using autografts, Arthroscopy: The Journal of Arthroscopic & Related Surgery 17(9) (2001) 971-980.

[32]R.F. LaPrade, J.C. Botker, Donor-site morbidity after osteochondral autograft transfer procedures, Arthroscopy: The Journal of Arthroscopic & Related Surgery 20(7) (2004) e69-e73.
[33]X.F. Ling, X. Peng, What is the price to pay for a free fibula flap? A systematic review of donor-site morbidity following free fibula flap surgery, Plast. Reconstr. Surg. 129(3) (2012) 657-674.
[34]G. Kumar, B. Narayan, Morbidity at bone graft donor sites, Classic Papers in Orthopaedics, Springer2014, pp. 503-505.
[35]T. Blattert, G. Delling, A. Weckbach, Evaluation of an injectable calcium phosphate cement as an autograft substitute for transpedicular lumbar interbody fusion: a controlled, prospective study in the sheep model, Eur. Spine J. 12(2) (2003) 216-223.
[36]S.C.S.X.B. Cavalcanti, C.L. Pereira, R. Mazzonetto, M. de Moraes, R.W.F. Moreira, Histological and histomorphometric analyses of calcium phosphate cement in rabbit calvaria, Journal of Cranio-Maxillofacial Surgery 36(6) (2008) 354-359.
[37]F. Correia, D.H. Pozza, S. Gouveia, A.C. Felino, R. Faria-Almeida, Advantages of porcine xenograft over autograft in sinus lift: A randomised clinical trial, Materials 14(12) (2021) 3439.
[38]M. Kamal, F. Gremse, S. Rosenhain, A.K. Bartella, F. Hölzle, P. Kessler, B. Lethaus, Comparison of bone grafts from various donor sites in human bone specimens, J. Craniofac. Surg. 29(6) (2018) 1661-1665.
[39]S.N. Khan, F.P. Cammisa Jr, H.S. Sandhu, A.D. Diwan, F.P. Girardi, J.M. Lane, The biology of bone grafting, JAAOS-Journal of the American Academy of Orthopaedic Surgeons 13(1) (2005) 77-86.
[40]M.M. Stevens, Biomaterials for bone tissue engineering, Mater. Today 11(5) (2008) 18-25.
[41]M. Hamadouche, L. Sedel, Ceramics in orthopaedics, The Journal of Bone and Joint Surgery. British volume 82(8) (2000) 1095-1099.
[42]P. Ruhe, O. Boerman, F. Russel, A. Mikos, P. Spauwen, J. Jansen, In vivo release of rhBMP-2 loaded porous calcium phosphate cement pretreated with albumin, J. Mater. Sci. Mater. Med. 17(10) (2006) 919-927.
[43]C. Combes, R. Bareille, C. Rey, Calcium carbonate–calcium phosphate mixed cement compositions for bone reconstruction, Journal of Biomedical Materials Research Part A: An Official Journal of The Society for Biomaterials, The Japanese Society for Biomaterials, and The Australian Society for Biomaterials and the Korean Society for Biomaterials 79(2) (2006) 318-328.
[44]C. Cassidy, J.B. Jupiter, M. Cohen, M. Delli-Santi, C. Fennell, C. Leinberry, J. Husband, A. Ladd, W.R. Seitz, B. Constanz, Norian SRS cement compared with conventional fixation in distal radial fractures: a randomized study, JBJS 85(11) (2003) 2127-2137.
[45]P. Lobenhoffer, T. Gerich, F. Witte, H. Tscherne, Use of an injectable calcium phosphate bone cement in the treatment of tibial plateau fractures: a prospective study of twenty-six cases with twenty-month mean follow-up, J. Orthop. Trauma 16(3) (2002) 143-149.
[46]J. Sanchez-Sotelo, L. Munuera, R. Madero, Treatment of fractures of the distal radius with a remodellable bone cement: a prospective, randomised study using Norian SRS, The Journal of Bone and Joint Surgery. British volume 82(6) (2000) 856-863.
[47]R. Schmidt, B. Cakir, T. Mattes, M. Wegener, W. Puhl, M. Richter, Cement leakage during vertebroplasty: an underestimated problem?, Eur. Spine J. 14(5) (2005) 466-473.
[48]M. Bohner, DESIGN OF CERAMIC-BASED CEMENTS AND PUTTIES FOR BONE GRAFT SUBSTITUTION, Eur. Cells Mater. 20 (2010) 1-12.
[49]B.A.S. Knobben, J. Van Horn, H. Van der Mei, H. Busscher, Evaluation of measures to decrease intra-operative bacterial contamination in orthopaedic implant surgery, J. Hosp. Infect. 62(2) (2006) 174-180.
[50]O.M. Lidwell, Clean air at operation and subsequent sepsis in the joint, Clinical Orthopaedics and Related Research® (211) (1986) 91-102.
[51]F. Howorth, Prevention of airborne infection during surgery, The Lancet 325(8425) (1985) 386-388.
[52]W. Whyte, R. Hodgson, J. Tinkler, The importance of airborne bacterial contamination of wounds, J. Hosp. Infect. 3(2) (1982) 123-135.
[53]G. Ha'eri, A. Wiley, Total hip replacement in a laminar flow environment with special reference to deep infections, Clinical Orthopaedics and Related Research® (148) (1980) 163-168.
[54]J. Duguid, Air infection with dust liberated from clothing, Selected Materials on Environmental Aspects of Staphylococcal Disease (646) (1959) 59.
[55]M. Bohner, Calcium orthophosphates in medicine: from ceramics to calcium phosphate cements, Injury 31 (2000) D37-D47.
[56]M. Bohner, Physical and chemical aspects of calcium phosphates used in spinal surgery, Eur. Spine J. 10(2) (2001) S114-S121.
[57]S.V. Dorozhkin, Self-setting calcium orthophosphate formulations, Journal of Functional Biomaterials 4(4) (2013) 209-311.

[58]Z. Gu, J. Fu, H. Lin, Y. He, Development of 3D bioprinting: From printing methods to biomedical applications, Asian Journal of Pharmaceutical Sciences 15(5) (2020) 529-557.
[59]L. Zhang, G. Yang, B.N. Johnson, X. Jia, Three-dimensional (3D) printed scaffold and material selection for bone repair, Acta Biomater. 84 (2019) 16-33.
[60]A. Bigi, B. Bracci, S. Panzavolta, Effect of added gelatin on the properties of calcium phosphate cement, Biomaterials 25(14) (2004) 2893-2899.
[61]F. Driessens, J. Planell, M. Boltong, I. Khairoun, M. Ginebra, Osteotransductive bone cements, Proceedings of the Institution of Mechanical Engineers, Part H: Journal of Engineering in Medicine 212(6) (1998) 427-435.
[62]M.-P. Ginebra, T. Traykova, J.A. Planell, Calcium phosphate cements as bone drug delivery systems: a review, Journal of Controlled Release 113(2) (2006) 102-110.
[63]M.-P. Ginebra, T. Traykova, J.A. Planell, Calcium phosphate cements: competitive drug carriers for the musculoskeletal system?, Biomaterials 27(10) (2006) 2171-2177.
[64]C.G. Simon Jr, W.F. Guthrie, F.W. Wang, Cell seeding into calcium phosphate cement, Journal of Biomedical Materials Research Part A 68(4) (2004) 628-639.
[65]H.H. Xu, M.D. Weir, C.G. Simon, Injectable and strong nano-apatite scaffolds for cell/growth factor delivery and bone regeneration, Dent. Mater. 24(9) (2008) 1212-1222.
[66]T. Yoshikawa, Y. Suwa, H. Ohgushi, S. Tamai, K. Ichijima, Self-setting hydroxyapatite cement as a carrier for bone-forming cells, Bio-Medical Materials and Engineering 6(5) (1996) 345-351.
[67]L.E. Carey, H.H. Xu, C.G. Simon Jr, S. Takagi, L.C. Chow, Premixed rapid-setting calcium phosphate composites for bone repair, Biomaterials 26(24) (2005) 5002-5014.
[68]L.C. Chow, S. Takagi, Dual-phase cement precursor systems for bone repair, Google Patents, 2016.
[69]J. LeMaitre, C. Pittet, D. Brendlen, Pasty or liquid multiple constituent compositions for injectable calcium phosphate cements, Google Patents, 2008.
[70]I. Rajzer, O. Castano, E. Engel, J. Planell, Injectable and fast resorbable calcium phosphate cement for body-setting bone grafts, J. Mater. Sci. Mater. Med. 21(7) (2010) 2049-2056.
[71]Y. Shimada, L.C. Chow, S. Takagi, J. Tagami, Properties of injectable apatite-forming premixed cements, J. Res. Natl. Inst. Stand. Technol. 115(4) (2010) 233.
[72]A. Sugawara, K. Fujikawa, S. Hirayama, S. Takagi, L.C. Chow, In vivo characteristics of premixed calcium phosphate cements when implanted in subcutaneous tissues and periodontal bone defects, J. Res. Natl. Inst. Stand. Technol. 115(4) (2010) 277.
[73]S. Takagi, L.C. Chow, S. Hirayama, A. Sugawara, Premixed calcium–phosphate cement pastes, Journal of Biomedical Materials Research Part B: Applied Biomaterials: An Official Journal of the Society for Biomaterials, the Japanese Society for Biomaterials, and the Australian Society for Biomaterials and the Korean Society for Biomaterials 67(2) (2003) 689-696.
[74]H.H. Xu, L.E. Carey, C.G. Simon Jr, S. Takagi, L.C. Chow, Premixed calcium phosphate cements: synthesis, physical properties, and cell cytotoxicity, Dent. Mater. 23(4) (2007) 433-441.
[75]L. Vidal, C. Kampleitner, M.Á. Brennan, A. Hoornaert, P. Layrolle, Reconstruction of large skeletal defects: current clinical therapeutic strategies and future directions using 3D printing, Frontiers in Bioengineering and Biotechnology 8 (2020) 61.
[76]T. Lohman, Z. Wang, S.B. Going, Human body composition, Human Kinetics2005.
[77]R.M. Malina, 2 Quantification of Fat, Muscle and Bone in Man, Clinical Orthopaedics and Related Research® 65 (1969) 9-38.
[78]M. Trotter, R.R. Peterson, Weight of the skeleton during postnatal development, Am. J. Phys. Anthropol. 33(3) (1970) 313-323.
[79]S.V. Dorozhkin, Calcium orthophosphates (CaPO4): occurrence and properties, Morphologie 101(334) (2017) 125-142.
[80]S.V. Dorozhkin, Bioceramics of calcium orthophosphates, Biomaterials 31(7) (2010) 1465-1485.
[81]S.V. Dorozhkin, Calcium orthophosphates, Journal of Materials Science 42(4) (2007) 1061-1095.
[82]J.C. Elliott, Calcium phosphate biominerals, Reviews in Mineralogy and Geochemistry 48(1) (2002) 427-453.
[83]S.V. Dorozhkin, M. Epple, Biological and medical significance of calcium phosphates, Angew. Chem. Int. Ed. 41(17) (2002) 3130-3146.
[84]K. De Groot, Bioceramics consisting of calcium phosphate salts, Biomaterials 1(1) (1980) 47-50.
[85]D. Lide, Handbook of Chemistry and Physics, 86th edn. CRC, Taylor & Francis, 2005.
[86]R.Z. LeGeros, Calcium phosphates in oral biology and medicine, Monographs in oral sciences 15 (1991) 109-111.
[87]J. Elliott, Structure and Chemistry of the Apatites and Other Calcium Orthophosphates.
[88]Z. Amjad, Calcium phosphates in biological and industrial systems, (1998).

[89]Y. Pan, M.E. Fleet, Compositions of the apatite-group minerals: substitution mechanisms and controlling factors, Reviews in Mineralogy and Geochemistry 48(1) (2002) 13-49.
[90]N. Trueman, Substitutions for phosphate ions in apatite, Nature 210(5039) (1966) 937-938.
[91]L. Mitchell, G. Faust, S. Hendricks, D. Reynolds, The mineralogy and genesis of hydroxylapatite, American Mineralogist: Journal of Earth and Planetary Materials 28(6) (1943) 356-371.
[92]P. Becker, Phosphates and phosphoric acid; raw materials, technology, and economics of the wet process Pierre Becker, 1989.
[93]J.F. Rakovan, J.D. Pasteris, A technological gem: materials, medical, and environmental mineralogy of apatite, Elements 11(3) (2015) 195-200.
[94]P.J. Cook, J.H. Shergold, Phosphate deposits of the world: Volume 1: Proterozoic and Cambrian phosphorites, Cambridge University Press2005.
[95]J.A. Dumoulin, J.F. Slack, M.T. Whalen, A.G. Harris, Depositional setting and geochemistry of phosphorites and metalliferous black shales in the carboniferous-permian lisburne group, northern Alaska, US Geological Survey, 2011.
[96]H.N. Schulz, H.D. Schulz, Large sulfur bacteria and the formation of phosphorite, Science 307(5708) (2005) 416-418.
[97]G.H. McClellan, Mineralogy of carbonate fluorapatites, J. Geol. Soc. London 137(6) (1980) 675-681.
[98]J. McArthur, Francolite geochemistry—compositional controls during formation, diagenesis, metamorphism and weathering, Geochim. Cosmochim. Acta 49(1) (1985) 23-35.
[99]Y.N. Zanin, The classification of calcium phosphates of phosphorites, Lithology and Mineral Resources 39(3) (2004) 281.
[100]A. Lapin, A. Lyagushkin, The Kovdor apatite-francolite deposit as a prospective source of phosphate ore, Geology of Ore Deposits 56(1) (2014) 61-80.
[101]A.F. Rogers, Collophane, a much neglected mineral, Am. J. Sci. 5(16) (1922) 269-276.
[102]Q.B. Cao, S.M. Weng, C.X. Li, S.J. Bai, D. Liu, Investigation on beneficiation strategy for collophane, Advanced Materials Research, Trans Tech Publ, 2013, pp. 3404-3407.
[103]A.R. Chakhmouradian, L. Medici, Clinohydroxylapatite: a new apatite-group mineral from northwestern Ontario (Canada), and new data on the extent of Na-S substitution in natural apatites, Eur. J. Mineral. 18(1) (2006) 105-112.
[104]H.E. Mason, F.M. McCubbin, A. Smirnov, B.L. Phillips, Solid-state NMR and IR spectroscopic investigation of the role of structural water and F in carbonate-rich fluorapatite, Am. Mineral. 94(4) (2009) 507-516.
[105]C. Klein, Brushite from the island of Mona (between Haiti and Puerto Rico), Sitzber K Preuss Aka (1901) 720-725.
[106]A. Kaflak-Hachulska, A. Slosarczyk, W. Kolodziejski, Kinetics of NMR cross-polarization from protons to phosphorus-31 in natural brushite, Solid State Nucl. Magn. Reson. 15(4) (2000) 237-238.
[107]G. Hilgenstock, Eine neue Verbindung von P2O5 und CaO, Stahl Eisen 3 (1883) 498.
[108]B. Grguric, ANTHONY, JW, BIDEAUX, RA, BLADH, KW & NICHOLS, MC 1997. Handbook of Mineralogy. Volume III. Halides, Hydroxides, Oxides. xi+ 628 pp. Tucson: Mineral Data Publishing. Price US $106.00 (inc. surface postage); hard covers. ISBN 0 9622097 2 4, Geol. Mag. 136(6) (1999) 697-711.
[109]C. Frondel, Whitlockite: a new calcium phosphate, Ca3 (PO4) 2, American Mineralogist: Journal of Earth and Planetary Materials 26(3) (1941) 145-152.
[110]C. Frondel, Mineralogy of the calcium phosphates in insular phosphate rock, American Mineralogist: Journal of Earth and Planetary Materials 28(4) (1943) 215-232.
[111]R. Gopal, C. Calvo, Structural relationship of whitlockite and βCa3 (PO4) 2, Nature Physical Science 237(71) (1972) 30-32.
[112]S.J. Omelon, M.D. Grynpas, Relationships between polyphosphate chemistry, biochemistry and apatite biomineralization, Chem. Rev. 108(11) (2008) 4694-4715.
[113]C. Rey, C. Combes, C. Drouet, H. Sfihi, Chemical diversity of apatites, Advances in Science and Technology, Trans Tech Publ, 2006, pp. 27-36.
[114]H.A. Lowenstam, S. Weiner, On biomineralization, Oxford University Press on Demand1989.
[115]W. O'neill, The fallacy of the calcium-phosphorus product, Kidney Int. 72(7) (2007) 792-796.
[116]R. LeGeros, Formation and transformation of calcium phosphates: relevance to vascular calcification, Z. Kardiol. 90(3) (2001) 116-124.
[117]B. Wopenka, J.D. Pasteris, A mineralogical perspective on the apatite in bone, Materials Science and Engineering: C 25(2) (2005) 131-143.
[118]J.D. Pasteris, B. Wopenka, E. Valsami-Jones, Bone and tooth mineralization: why apatite?, Elements 4(2) (2008) 97-104.

[119]Y. Sun, E.N. Hanley Jr, Calcium-containing crystals and osteoarthritis, Curr. Opin. Orthop. 18(5) (2007) 472-478.
[120]G. Bocchi, G. Valdre, Physical, chemical, and mineralogical characterization of carbonate-hydroxyapatite concretions of the human pineal gland, J. Inorg. Biochem. 49(3) (1993) 209-220.
[121]R. Young, Biological apatite vs hydroxyapatite at the atomic level, Clinical Orthopaedics and Related Research® (113) (1975) 249-262.
[122]S. Danilchenko, The Approach for Determination of Concentration and Location of Major Impurities (Mg, Na, K) in Biological Apatite of Mineralized Tissues, Journal of Nano-& Electronic Physics 5(3) (2013).
[123]T. Nakano, K. Kaibara, Y. Tabata, N. Nagata, S. Enomoto, E. Marukawa, Y. Umakoshi, Unique alignment and texture of biological apatite crystallites in typical calcified tissues analyzed by microbeam X-ray diffractometer system, Bone 31(4) (2002) 479-487.
[124]M.D. Grynpas, S. Omelon, Transient precursor strategy or very small biological apatite crystals?, Elsevier, 2007, pp. 162-164.
[125]D. Bazin, A. Dessombz, C. Nguyen, H.K. Ea, F. Lioté, J. Rehr, C. Chappard, S. Rouzière, D. Thiaudière, S. Reguer, The status of strontium in biological apatites: an XANES/EXAFS investigation, Journal of Synchrotron Radiation 21(1) (2014) 136-142.
[126]H. Lowenstam, S. Weiner, Transformation of amorphous calcium phosphate to crystalline dahllite in the radular teeth of chitons, Science 227(4682) (1985) 51-53.
[127]E. Fernandez, J. Planell, S. Best, W. Bonfield, Synthesis of dahllite through a cement setting reaction, J. Mater. Sci. Mater. Med. 9(12) (1998) 789-792.
[128]H. Skinner, Biominerals, Mineralogical Magazine 69(5) (2005) 621-641.
[129]G. Daculsi, J.-M. Bouler, R. LeGeros, Adaptive crystal formation in normal and pathological calcifications in synthetic calcium phosphate and related biomaterials, Int. Rev. Cytol. 172 (1997) 129-191.
[130]J. Floege, J. Kim, E. Ireland, C. Chazot, T. Drueke, A. de Francisco, F. Kronenberg, D. Marcelli, J. Passlick-Deetjen, G. Schernthaner, Serum iPTH, calcium and phosphate, and the risk of mortality in a European haemodialysis population, Nephrology Dialysis Transplantation 26(6) (2011) 1948-1955.
[131]M. Suller, V. Anthony, S. Mathur, R. Feneley, J. Greenman, D. Stickler, Factors modulating the pH at which calcium and magnesium phosphates precipitate from human urine, Urol. Res. 33(4) (2005) 254-260.
[132]C.A. Prompt, P.M. Quinto, C.R. Kleeman, High concentrations of sweat calcium, magnesium and phosphate in chronic renal failure, Nephron 20(1) (1978) 4-9.
[133]C. Holt, Inorganic constituents of milk III. The colloidal calcium phosphate of cow's milk, J. Dairy Res. 49(1) (1982) 29-38.
[134]S. Lenton, T. Nylander, S. Teixeira, C. Holt, A review of the biology of calcium phosphate sequestration with special reference to milk, Dairy science & technology 95(1) (2015) 3-14.
[135]N. Loveridge, Bone: more than a stick, J. Anim. Sci. 77(suppl_2) (1999) 190-196.
[136]L.C. Palmer, C.J. Newcomb, S.R. Kaltz, E.D. Spoerke, S.I. Stupp, Biomimetic systems for hydroxyapatite mineralization inspired by bone and enamel, Chem. Rev. 108(11) (2008) 4754-4783.
[137]J. Nightingale, D. Lewis, Pole figures of the orientation of apatite in bones, Nature 232(5309) (1971) 334-335.
[138]J.D. Currey, The structure and mechanics of bone, Journal of Materials Science 47(1) (2012) 41-54.
[139]J.-Y. Rho, L. Kuhn-Spearing, P. Zioupos, Mechanical properties and the hierarchical structure of bone, Med. Eng. Phys. 20(2) (1998) 92-102.
[140]M. Tzaphlidou, Bone architecture: collagen structure and calcium/phosphorus maps, J. Biol. Phys. 34(1) (2008) 39-49.
[141]J. Elorza, H. Astibia, X. Murelaga, X. Pereda-Suberbiola, Francolite as a diagenetic mineral in dinosaur and other Upper Cretaceous reptile bones (Laño, Iberian Peninsula): microstructural, petrological and geochemical features, Cretaceous Res. 20(2) (1999) 169-187.
[142]R.A. Eagle, E.A. Schauble, A.K. Tripati, T. Tütken, R.C. Hulbert, J.M. Eiler, Body temperatures of modern and extinct vertebrates from 13C-18O bond abundances in bioapatite, Proceedings of the National Academy of Sciences 107(23) (2010) 10377-10382.
[143]V. Haynes, Radiocarbon: analysis of inorganic carbon of fossil bone and enamel, Science 161(3842) (1968) 687-688.
[144]J.M. Rensberger, M. Watabe, Fine structure of bone in dinosaurs, birds and mammals, Nature 406(6796) (2000) 619-622.
[145]Y. Kolodny, B. Luz, M. Sander, W. Clemens, Dinosaur bones: fossils or pseudomorphs? The pitfalls of physiology reconstruction from apatitic fossils, Palaeogeogr., Palaeoclimatol., Palaeoecol. 126(1-2) (1996) 161-171.
[146]C.N. Trueman, N. Tuross, Trace elements in recent and fossil bone apatite, Reviews in Mineralogy and Geochemistry 48(1) (2002) 489-521.

[147]J. Hubert, P. Panish, D. Chure, K. Prostak, Chemistry, microstructure, petrology, and diagenetic model of Jurassic dinosaur bones, Dinosaur National Monument, Utah, Journal of Sedimentary Research 66(3) (1996) 531-547.
[148]H. Brooke, XVI. On percylite, a mineral not hitherto described, The London, Edinburgh, and Dublin Philosophical Magazine and Journal of Science 36(241) (1850) 131-134.
[149]C. Palache, C. Frondel, H. Berman, The System of Mineralogy of James Dwight Dana and Edward Salisbury Dana, John Wiley and Sons, Incorporated1963.
[150]E. Sandell, M. Hey, D. McConnell, The composition of francolite, Mineralogical magazine and journal of the Mineralogical Society 25(166) (1939) 395-401.
[151]C.H. Turner, D.B. Burr, Basic biomechanical measurements of bone: a tutorial, Bone 14(4) (1993) 595-608.
[152]J.D. Currey, Tensile yield in compact bone is determined by strain, post-yield behaviour by mineral content, J. Biomech. 37(4) (2004) 549-556.
[153]J.D. Currey, K. Brear, P. Zioupos, Notch sensitivity of mammalian mineralized tissues in impact, Proc. R. Soc. Lond. B. Biol. Sci. 271(1538) (2004) 517-522.
[154]H.-B. Pan, B. Darvell, Calcium phosphate solubility: the need for re-evaluation, Cryst. Growth Des. 9(2) (2009) 639-645.
[155]S.V. Dorozhkin, Calcium orthophosphates: occurrence, properties, biomineralization, pathological calcification and biomimetic applications, Biomatter 1(2) (2011) 121-164.
[156]C.-K. Loong, C. Rey, L. Kuhn, C. Combes, Y. Wu, S.-H. Chen, M. Glimcher, Evidence of hydroxyl-ion deficiency in bone apatites: an inelastic neutron-scattering study, Bone 26(6) (2000) 599-602.
[157]S.J. Seo, S.B. Song, J.H. Chae, J.Y. Kim, J.H. Ahn, T.W. Kim, H.C. Hwang, J. Kim, K.W. Lee, N.H. Kang, Hydroxyl groups in demineralized bone matrix, Key Eng. Mater., Trans Tech Publ, 2007, pp. 381-384.
[158]C. Rey, J. Miquel, L. Facchini, A. Legrand, M. Glimcher, Hydroxyl groups in bone mineral, Bone 16(5) (1995) 583-586.
[159]U. Plate, T. Tkotz, H. Wiesmann, U. Stratmann, U. Joos, H. Höhling, Early mineralization of matrix vesicles in the epiphyseal growth plate, J. Microsc. 183(1) (1996) 102-107.
[160]U. Stratmann, K. Schaarschmidt, H. Wiesmann, U. Plate, H. Höhling, Mineralization during matrix-vesicle-mediated mantle dentine formation in molars of albino rats: a microanalytical and ultrastructural study, Cell and Tissue Research 284(2) (1996) 223-230.
[161]H.A. Lowenstam, Minerals formed by organisms, Science 211(4487) (1981) 1126-1131.
[162]H. Lowenstam, S. Weiner, Mineralization by organisms and the evolution of biomineralization, Biomineralization and Biological Metal Accumulation, Springer1983, pp. 191-203.
[163]S. Weiner, H.D. Wagner, The material bone: structure-mechanical function relations, Annu. Rev. Mater. Sci. 28(1) (1998) 271-298.
[164]S. Weiner, W. Traub, H.D. Wagner, Lamellar bone: structure–function relations, J. Struct. Biol. 126(3) (1999) 241-255.
[165]A.L. Boskey, Mineralization of bones and teeth, Elements 3(6) (2007) 385-391.
[166]M.J. Glimcher, Bone: nature of the calcium phosphate crystals and cellular, structural, and physical chemical mechanisms in their formation, Reviews in Mineralogy and Geochemistry 64(1) (2006) 223-282.
[167]C. Delloye, O. Cornu, V. Druez, O. Barbier, Bone allografts: what they can offer and what they cannot, The Journal of Bone and Joint Surgery. British volume 89(5) (2007) 574-580.
[168]M. Araújo, E. Linder, J. Lindhe, Effect of a xenograft on early bone formation in extraction sockets: an experimental study in dog, Clin. Oral Implants Res. 20(1) (2009) 1-6.
[169]R.B. Heimann, Plasma-Sprayed Hydroxylapatite Coatings as Biocompatible Intermediaries Between Inorganic Implant Surfaces and Living Tissue, J. Therm. Spray Technol. 27(8) (2018) 1212-1237.
[170]S. Serena, L. Carbajal, M.A. Sainz, A. Caballero, Thermodynamic Assessment of the System CaO–P2O5: Application of the Ionic Two-Sublattice Model to Glass-Forming Melts, J. Am. Ceram. Soc. 94(9) (2011) 3094-3103.
[171]S.V. Dorozhkin, Calcium orthophosphates: applications in nature, biology, and medicine, CRC Press2012.
[172]L. Wang, G.H. Nancollas, Calcium orthophosphates: crystallization and dissolution, Chem. Rev. 108(11) (2008) 4628-4669.
[173]M. Mathew, S. Takagi, Crystal structures of calcium orthophosphates, (2001).
[174]B.-Q. Lu, T. Willhammar, B.-B. Sun, N. Hedin, J.D. Gale, D. Gebauer, Introducing the crystalline phase of dicalcium phosphate monohydrate, Nature Communications 11(1) (2020) 1-8.
[175]M. Bredig, H. Franch, H. Füldner, Beiträge zur Kenntnis der Kalk-Phosphorsäure-Verbindungen, Zeitschrift für Elektrochemie und angewandte physikalische Chemie 38(3) (1932) 158-164.
[176]G. Trömel, Beiträge zur kenntnis des systems Kalziumoxyd-phosphorpentoxyd, Verlag Stahleisen1932.

[177]J. Welch, W. Gutt, 874. High-temperature studies of the system calcium oxide–phosphorus pentoxide, Journal of the Chemical Society (Resumed) (1961) 4442-4444.
[178]P. Hudon, I.-H. Jung, Critical evaluation and thermodynamic optimization of the CaO-P2O5 system, Metallurgical and Materials Transactions B 46(1) (2015) 494-522.
[179]A. Roine, Outokumpu HSC Chemistry for Windows. Chemical Reaction and Equilibrium Software with Extensive Thermochemical Database, Pori: Outokumpu Research OY 448 (2002).
[180]I. Barin, Thermodynamical Data of Pure Substances, PartI&II, VCH Verlags Gesellschaft, Weinheim, 1993.
[181]W.F. Bale, J.F. Bonner, H.C. Hodge, H. Adler, A. Wreath, R. Bell, Optical and X-ray diffraction studies of certain calcium phosphates, Industrial & Engineering Chemistry Analytical Edition 17(8) (1945) 491-495.
[182]X. Yin, M.J. Stott, Biological calcium phosphates and Posner's cluster, The Journal of Chemical Physics 118(8) (2003) 3717-3723.
[183]R. Nurse, J. Welch, W. Gutt, 220. High-temperature phase equilibria in the system dicalcium silicate–tricalcium phosphate, Journal of the Chemical Society (Resumed) (1959) 1077-1083.
[184]M. Sayer, A. Stratilatov, J. Reid, L. Calderin, M. Stott, X. Yin, M. MacKenzie, T. Smith, J. Hendry, S. Langstaff, Structure and composition of silicon-stabilized tricalcium phosphate, Biomaterials 24(3) (2003) 369-382.
[185]J. Reid, A. Pietak, M. Sayer, D. Dunfield, T. Smith, Phase formation and evolution in the silicon substituted tricalcium phosphate/apatite system, Biomaterials 26(16) (2005) 2887-2897.
[186]J.W. Reid, L. Tuck, M. Sayer, K. Fargo, J.A. Hendry, Synthesis and characterization of single-phase silicon-substituted α-tricalcium phosphate, Biomaterials 27(15) (2006) 2916-2925.
[187]K. Momma, F. Izumi, VESTA 3 for three-dimensional visualization of crystal, volumetric and morphology data, J. Appl. Crystallogr. 44(6) (2011) 1272-1276.
[188]M. Mathew, L. Schroeder, B. Dickens, W. Brown, The crystal structure of α-Ca3 (PO4) 2, Acta Crystallographica Section B: Structural Crystallography and Crystal Chemistry 33(5) (1977) 1325-1333.
[189]X. Yin, M. Stott, A. Rubio, α-and β-tricalcium phosphate: A density functional study, Physical Review B 68(20) (2003) 205205.
[190]L. Liang, P. Rulis, W. Ching, Mechanical properties, electronic structure and bonding of α-and β-tricalcium phosphates with surface characterization, Acta Biomater. 6(9) (2010) 3763-3771.
[191]K.S. TenHuisen, P.W. Brown, Formation of calcium-deficient hydroxyapatite from α-tricalcium phosphate, Biomaterials 19(23) (1998) 2209-2217.
[192]C. Durucan, P. Brown, α-Tricalcium phosphate hydrolysis to hydroxyapatite at and near physiological temperature, J. Mater. Sci. Mater. Med. 11(6) (2000) 365-371.
[193]C. Durucan, P.W. Brown, Kinetic model for α–tricalcium phosphate hydrolysis, J. Am. Ceram. Soc. 85(8) (2002) 2013-2018.
[194]C. Camiré, U. Gbureck, W. Hirsiger, M. Bohner, Correlating crystallinity and reactivity in an α-tricalcium phosphate, Biomaterials 26(16) (2005) 2787-2794.
[195]S. Budavari, M. O'Neil, A. Smith, P. Heckelman, J. Kinneary, The Merk Index. An Encyclopedia of Chemicals, Drugs and Biologicals 13 Ed), Merck and Co, Inc., whitehouse station, NJ 1097 (2001) 1946.
[196]H.H. Stein, C. Kadzere, S. Kim, P. Miller, Influence of dietary phosphorus concentration on the digestibility of phosphorus in monocalcium phosphate by growing pigs, J. Anim. Sci. 86(8) (2008) 1861-1867.
[197]M. Kamitakahara, C. Ohtsuki, T. Miyazaki, Behavior of ceramic biomaterials derived from tricalcium phosphate in physiological condition, J. Biomater. Appl. 23(3) (2008) 197-212.
[198]R.G. Carrodeguas, S. De Aza, α-Tricalcium phosphate: Synthesis, properties and biomedical applications, Acta Biomater. 7(10) (2011) 3536-3546.
[199]B. Dickens, L. Schroeder, W. Brown, Crystallographic studies of the role of Mg as a stabilizing impurity in β-Ca3 (PO4) 2. The crystal structure of pure β-Ca3 (PO4) 2, J. Solid State Chem. 10(3) (1974) 232-248.
[200]J. Tao, W. Jiang, H. Zhai, H. Pan, X. Xu, R. Tang, Structural components and anisotropic dissolution behaviors in one hexagonal single crystal of β-tricalcium phosphate, Cryst. Growth Des. 8(7) (2008) 2227-2234.
[201]J. Tao, H. Pan, H. Zhai, J. Wang, L. Li, J. Wu, W. Jiang, X. Xu, R. Tang, Controls of tricalcium phosphate single-crystal formation from its amorphous precursor by interfacial energy, Cryst. Growth Des. 9(7) (2009) 3154-3160.
[202]X. Li, A. Ito, Y. Sogo, X. Wang, R. LeGeros, Solubility of Mg-containing β-tricalcium phosphate at 25 C, Acta Biomater. 5(1) (2009) 508-517.
[203]T. Kodaka, K. Debari, S. Higashi, Magnesium-containing crystals in human dental calculus, Microscopy 37(2) (1988) 73-80.
[204]J.D. Reid, M.E. Andersen, Medial calcification (whitlockite) in the aorta, Atherosclerosis 101(2) (1993) 213-224.
[205]C.A. Scotchford, S.Y. Ali, Magnesium whitlockite deposition in articular cartilage: a study of 80 specimens from 70 patients, Ann. Rheum. Dis. 54(5) (1995) 339-344.

[206]C.H. P'ng, R. Boadle, M. Horton, M. Bilous, F. Bonar, Magnesium whitlockite of the aorta, Pathology 40(5) (2008) 539-540.
[207]X. Hou, K. Mao, D. Chen, Bone formation performance of beta-tricalcium phosphate sintered bone, J Clin Rehabil Tiss Eng Res 12 (2008) 9627-9630.
[208]H.-H. Horch, R. Sader, C. Pautke, A. Neff, H. Deppe, A. Kolk, Synthetic, pure-phase beta-tricalcium phosphate ceramic granules (Cerasorb®) for bone regeneration in the reconstructive surgery of the jaws, Int. J. Oral Maxillofac. Surg. 35(8) (2006) 708-713.
[209]A. Ogose, N. Kondo, H. Umezu, T. Hotta, H. Kawashima, K. Tokunaga, T. Ito, N. Kudo, M. Hoshino, W. Gu, Histological assessment in grafts of highly purified beta-tricalcium phosphate (OSferion®) in human bones, Biomaterials 27(8) (2006) 1542-1549.
[210]Y. Liu, G. Pei, S. Jiang, G. Ren, New porous beta-tricalcium phosphate as a scaffold for bone tissue engineering, Chinese Journal of Tissue Engineering Research (2008) 4563-4567.
[211]N.E. Epstein, Beta tricalcium phosphate: observation of use in 100 posterolateral lumbar instrumented fusions, The Spine Journal 9(8) (2009) 630-638.
[212]B. Liu, D.x. Lun, Current application of β-tricalcium phosphate composites in orthopaedics, Orthop. Surg. 4(3) (2012) 139-144.
[213]C. Güngörmüş, A. Kılıç, M.T. Akay, D. Kolankaya, The effects of maternal exposure to food additive E341 (tricalcium phosphate) on foetal development of rats, Environmental Toxicology and Pharmacology 29(2) (2010) 111-116.
[214]H.C.W. Skinner, Studies in the basic mineralizing system, CaO-P2O5-H2O, Calcif. Tissue Res. 14(1) (1974) 3-14.
[215]M.I. Kay, R. Young, A. Posner, Crystal structure of hydroxyapatite, Nature 204(4963) (1964) 1050-1052.
[216]M. Mathew, S. Takagi, Structures of biological minerals in dental research, J. Res. Natl. Inst. Stand. Technol. 106(6) (2001) 1035.
[217]T.J. White, Z. Dong, Structural derivation and crystal chemistry of apatites, Acta Crystallogr. Sect. B: Struct. Sci. 59(1) (2003) 1-16.
[218]J. Elliott, Handbook of Structure and Chemistry of the Apatite and Other Calcium Orthophosphates. Vol. 18, Elsevier Science: BV, 1994.
[219]J. Elliott, Recent studies of apatites and other calcium orthophospates, Calcium Phosphate Materials, Fundamentals. Monpellier: Sauramps Medical (1998) 25.
[220]N. Rangavittal, A. Landa-Cánovas, J. González-Calbet, M. Vallet-Regi, Structural study and stability of hydroxyapatite and β-tricalcium phosphate: Two important bioceramics, J. Biomed. Mater. Res. 51(4) (2000) 660-668.
[221]J.Y. Kim, R.R. Fenton, B.A. Hunter, B.J. Kennedy, Powder diffraction studies of synthetic calcium and lead apatites, Aust. J. Chem. 53(8) (2000) 679-686.
[222]H. El Briak-BenAbdeslam, M. Ginebra, M. Vert, P. Boudeville, Wet or dry mechanochemical synthesis of calcium phosphates? Influence of the water content on DCPD–CaO reaction kinetics, Acta Biomater. 4(2) (2008) 378-386.
[223]M. Markovic, B.O. Fowler, M.S. Tung, Preparation and comprehensive characterization of a calcium hydroxyapatite reference material, J. Res. Natl. Inst. Stand. Technol. 109(6) (2004) 553.
[224]W. Suchanek, M. Yoshimura, Processing and properties of hydroxyapatite-based biomaterials for use as hard tissue replacement implants, J. Mater. Res. 13(1) (1998) 94-117.
[225]L. Sun, C.C. Berndt, K.A. Gross, A. Kucuk, Material fundamentals and clinical performance of plasma-sprayed hydroxyapatite coatings: A review, Journal of Biomedical Materials Research: An Official Journal of The Society for Biomaterials, The Japanese Society for Biomaterials, and The Australian Society for Biomaterials and the Korean Society for Biomaterials 58(5) (2001) 570-592.
[226]J.L. Ong, D.C. Chan, Hydroxyapatite and their use as coatings in dental implants: a review, Critical Reviews™ in Biomedical Engineering 28(5&6) (2000).
[227]Y. Yuan, P. Huang, Q. Peng, C. Zhang, J. Weng, Osteogenesis of porous bioceramics scaffolds consisted of hydroxyapatite spherules after implanted in different non-osseous sites, Mater. Sci. Forum, Trans Tech Publ, 2009, pp. 1335-1338.
[228]N.O. Engin, A.C. Tas, Manufacture of macroporous calcium hydroxyapatite bioceramics, J. Eur. Ceram. Soc. 19(13-14) (1999) 2569-2572.
[229]C. Mangano, A. Piattelli, V. Perrotti, G. Iezzi, Dense hydroxyapatite inserted into postextraction sockets: a histologic and histomorphometric 20-year case report, J. Periodontol. 79(5) (2008) 929-933.
[230]S.V. Dorozhkin, A detailed history of calcium orthophosphates from 1770s till 1950, Materials Science and Engineering: C 33(6) (2013) 3085-3110.

[231]S.V. Dorozhkin, Calcium orthophosphates and human beings: A historical perspective from the 1770s until 1940, Biomatter 2(2) (2012) 53-70.
[232]R.M. Wilson, J.C. Elliott, S.E. Dowker, L.M. Rodriguez-Lorenzo, Rietveld refinements and spectroscopic studies of the structure of Ca-deficient apatite, Biomaterials 26(11) (2005) 1317-1327.
[233]D. Zahn, O. Hochrein, On the composition and atomic arrangement of calcium-deficient hydroxyapatite: An ab-initio analysis, J. Solid State Chem. 181(8) (2008) 1712-1716.
[234]A. Sinha, S. Nayar, A. Agrawal, D. Bhattacharyya, P. Ramachandrarao, Synthesis of nanosized and microporous precipitated hydroxyapatite in synthetic polymers and biopolymers, J. Am. Ceram. Soc. 86(2) (2003) 357-359.
[235]I. Mayer, O. Jacobsohn, T. Niazov, J. Werckmann, M. Iliescu, M. Richard-Plouet, O. Burghaus, D. Reinen, Manganese in precipitated hydroxyapatites, Eur. J. Inorg. Chem. 2003(7) (2003) 1445-1451.
[236]S.V. Dorozhkin, Biphasic, triphasic and multiphasic calcium orthophosphates, Acta Biomater. 8(3) (2012) 963-977.
[237]B. Bourgeois, O. Laboux, L. Obadia, O. Gauthier, E. Betti, E. Aguado, G. Daculsi, J.M. Bouler, Calcium-deficient apatite: A first in vivo study concerning bone ingrowth, Journal of Biomedical Materials Research Part A: An Official Journal of The Society for Biomaterials, The Japanese Society for Biomaterials, and The Australian Society for Biomaterials and the Korean Society for Biomaterials 65(3) (2003) 402-408.
[238]H.B. Jones, XV. Contributions to the chemistry of the urine. On the variations in the alkaline and earthy phosphates in the healthy state, and on the alkalescence of the urine from fixed alkalies, Philos. Trans. R. Soc. London (135) (1845) 335-349.
[239]S.V. Dorozhkin, Amorphous calcium orthophosphates: nature, chemistry and biomedical applications, Int. J. Mater. Chem 2(1) (2012) 19-46.
[240]N. Blumenthal, A. Posner, J. Holmes, Effect of preparation conditions on the properties and transformation of amorphous calcium phosphate, Mater. Res. Bull. 7(11) (1972) 1181-1189.
[241]S.V. Dorozhkin, Calcium orthophosphates in dentistry, J. Mater. Sci. Mater. Med. 24(6) (2013) 1335-1363.
[242]D. Tadic, M. Epple, Amorphous calcium phosphates as bone substitution materials, Eur J Trauma 28 (2002) 136-137.
[243]J. Percy, CXVIII. Notice of a new hydrated phosphate of lime, Memoirs and Proceedings of the Chemical Society, Royal Society of Chemistry, 1843, pp. 222-223.
[244]R.Z. LeGeros, Preparation of octacalcium phosphate (OCP): a direct fast method, Calcif. Tissue Int. 37(2) (1985) 194-197.
[245]A. Nakahira, S. Aoki, K. Sakamoto, S. Yamaguchi, Synthesis and evaluation of various layered octacalcium phosphates by wet-chemical processing, J. Mater. Sci. Mater. Med. 12(9) (2001) 793-800.
[246]M. Arellano-Jiménez, R. García-García, J. Reyes-Gasga, Synthesis and hydrolysis of octacalcium phosphate and its characterization by electron microscopy and X-ray diffraction, Journal of Physics and Chemistry of Solids 70(2) (2009) 390-395.
[247]O. Suzuki, Octacalcium phosphate: osteoconductivity and crystal chemistry, Acta Biomater. 6(9) (2010) 3379-3387.
[248]D. Shurtakova, B. Yavkin, M. Gafurov, G. Mamin, S. Orlinskii, L. Kuznetsova, S. Bakhteev, I. Ignatyev, I. Smirnov, A. Fedotov, Study of radiation-induced stable radicals in synthetic octacalcium phosphate by pulsed EPR, Magnetic Resonance in Solids. Electronic Journal 21(1) (2019) 5-5.
[249]W.E. Brown, J.P. Smith, J.R. Lehr, A.W. Frazier, Octacalcium phosphate and hydroxyapatite: crystallographic and chemical relations between octacalcium phosphate and hydroxyapatite, Nature 196(4859) (1962) 1050-1055.
[250]W. Nicholson, A General System of Chemical Knowledge: And Its Application to the Phenomena of Nature and Art. In Eleven Vols, Cadell and Davies1804.
[251]G.E. Moore, ART. V.--On Brushite, a new mineral occurring in Phosphatic Guano, American Journal of Science and Arts (1820-1879) 39(115) (1865) 43.
[252]R. Hamai, T. Toshima, M. Tafu, T. Masutani, T. Chohji, Effect of anions on morphology control of brushite particles, Key Eng. Mater., Trans Tech Publ, 2013, pp. 55-60.
[253]N. Curry, D. Jones, Crystal structure of brushite, calcium hydrogen orthophosphate dihydrate: a neutron-diffraction investigation, Journal of the Chemical Society A: Inorganic, Physical, Theoretical (1971) 3725-3729.
[254]J. Sutter, H. McDowell, W.E. Brown, Solubility study of calcium hydrogen phosphate. Ion-pair formation, Inorganic Chemistry 10(8) (1971) 1638-1643.
[255]H.E. Roscoe, C. Schorlemmer, A treatise on chemistry, Macmillan1923.

[256]C.U. Shepard, C. SHEPARD Jr, ART. XLVII.--On two New Minerals, Monetite and Monite, with a notice of Pyroclasite, American Journal of Science (1880-1910) 23(137) (1882) 400.
[257]G. Sivakumar, E. Girija, S. Narayana Kalkura, C. Subramanian, Crystallization and characterization of calcium phosphates: brushite and monetite, Crystal Research and Technology: Journal of Experimental and Industrial Crystallography 33(2) (1998) 197-205.
[258]A.C. Tas, Monetite (CaHPO4) synthesis in ethanol at room temperature, J. Am. Ceram. Soc. 92(12) (2009) 2907-2912.
[259]G. Chen, G. Luo, L. Yang, J. Xu, Y. Sun, J. Wang, Synthesis and size control of CaHPO4 particles in a two-liquid phase micro-mixing process, J. Cryst. Growth 279(3-4) (2005) 501-507.
[260]F. Tamimi, J. Torres, D. Bassett, J. Barralet, E.L. Cabarcos, Resorption of monetite granules in alveolar bone defects in human patients, Biomaterials 31(10) (2010) 2762-2769.
[261]R.B. Wang, W.J. Weng, X.L. Deng, K. Cheng, X.G. Liu, P.Y. Du, G. Shen, G.R. Han, Dissolution behavior of submicron biphasic tricalcium phosphate powders, Key Eng. Mater., Trans Tech Publ, 2006, pp. 223-226.
[262]Y.B. Li, D.X. Li, W.J. Weng, In vitro dissolution behavior of biphasic tricalcium phosphate composite powders composed of α-tricalcium phosphate and β-tricalcium phosphate, Key Eng. Mater., Trans Tech Publ, 2008, pp. 1206-1208.
[263]Y. Li, W. Weng, K.C. Tam, Novel highly biodegradable biphasic tricalcium phosphates composed of α-tricalcium phosphate and β-tricalcium phosphate, Acta Biomater. 3(2) (2007) 251-254.
[264]R. Ellinger, Histological assessment of periodontal osseous defects following implantation of hydroxyapatite and biphasic calcium phosphate ceramics: a case report, Int. J. Periodont. Restor. Dent. 6 (1986) 23-33.
[265]L.L. Pan, Y.B. Li, W.J. Weng, K. Cheng, C.L. Song, P.Y. Du, G.L. Zhao, G. Shen, J.X. Wang, G.R. Han, Preparation of submicron biphasic α-TCP/HA powders, Key Eng. Mater., Trans Tech Publ, 2006, pp. 219-222.
[266]K. Cheng, Slip casting derived α-TCP/HA biphasic ceramics, Key Eng. Mater., Trans Tech Publ, 2007, pp. 51-54.
[267]Y. Li, F. Kong, W. Weng, Preparation and characterization of novel biphasic calcium phosphate powders (α-TCP/HA) derived from carbonated amorphous calcium phosphates, Journal of Biomedical Materials Research Part B: Applied Biomaterials: An Official Journal of The Society for Biomaterials, The Japanese Society for Biomaterials, and The Australian Society for Biomaterials and the Korean Society for Biomaterials 89(2) (2009) 508-517.
[268]P.W. Brown, J. Gulick, J. Dumm, The System MgO─ P2O5─ H2O at 25° C, J. Am. Ceram. Soc. 76(6) (1993) 1558-1562.
[269]C. Chau, F. Qiao, Z. Li, Potentiometric study of the formation of magnesium potassium phosphate hexahydrate, J. Mater. Civ. Eng. 24(5) (2012) 586-591.
[270]S. Mousa, Study on synthesis of magnesium phosphate materials, Phosphorus Research Bulletin 24 (2010) 16-21.
[271]B. Sales, B. Chakoumakos, L. Boatner, J. Ramey, Structural properties of the amorphous phases produced by heating crystalline MgHPO4· 3H2O, Journal of Non-crystalline Solids 159(1-2) (1993) 121-139.
[272]B. Abdelrazig, J. Sharp, Phase changes on heating ammonium magnesium phosphate hydrates, Thermochim. Acta 129(2) (1988) 197-215.
[273]C. Chau, F. Qiao, Z. Li, Microstructure of magnesium potassium phosphate cement, Construction and Building Materials 25(6) (2011) 2911-2917.
[274]M. Mathew, P. Kingsbury, S. Takagi, W. Brown, A new struvite-type compound, magnesium sodium phosphate heptahydrate, Acta Crystallographica Section B: Structural Crystallography and Crystal Chemistry 38(1) (1982) 40-44.
[275]S. Vinokurov, Y.M. Kulyako, O. Slyunchev, S. Rovnyi, A. Wagh, M. Maloney, B. Myasoedov, Magnesium potassium phosphate matrices for immobilization of high-level liquid wastes, Radiochemistry 51(1) (2009) 65-72.
[276]D.A. Hall, R. Stevens, B.E. Jazairi, Effect of water content on the structure and mechanical properties of magnesia-phosphate cement mortar, J. Am. Ceram. Soc. 81(6) (1998) 1550-1556.
[277]A.W. Frazier, J.R. Lehr, J.P. Smith, The magnesium phosphates hannayite, schertelite and bobierrite, American Mineralogist: Journal of Earth and Planetary Materials 48(5-6) (1963) 635-641.
[278]Z. Amjad, P. Koutsoukos, G. Nancollas, The crystallization of hydroxyapatite and fluorapatite in the presence of magnesium ions, Journal of Colloid and Interface Science 101(1) (1984) 250-256.
[279]A. Boskey, A. Posner, Magnesium stabilization of amorphous calcium phosphate: a kinetic study, Mater. Res. Bull. 9(7) (1974) 907-916.
[280]E. Eanes, S. Rattner, The effect of magnesium on apatite formation in seeded supersaturated solutions at pH 7.4, J. Dent. Res. 60(9) (1981) 1719-1723.

[281]M. Salimi, J. Heughebaert, G. Nancollas, Crystal growth of calcium phosphates in the presence of magnesium ions, Langmuir 1(1) (1985) 119-122.
[282]M. Tung, B. Tomazic, W. Brown, The effects of magnesium and fluoride on the hydrolysis of octacalcium phosphate, Arch. Oral Biol. 37(7) (1992) 585-591.
[283]H. Zhou, S. Bhaduri, Novel microwave synthesis of amorphous calcium phosphate nanospheres, Journal of Biomedical Materials Research Part B: Applied Biomaterials 100(4) (2012) 1142-1150.
[284]H. Zhou, T.J. Luchini, S.B. Bhaduri, Microwave assisted synthesis of amorphous magnesium phosphate nanospheres, J. Mater. Sci. Mater. Med. 23(12) (2012) 2831-2837.
[285]I. Cacciotti, A. Bianco, High thermally stable Mg-substituted tricalcium phosphate via precipitation, Ceram. Int. 37(1) (2011) 127-137.
[286]H.-S. Ryu, K.S. Hong, J.-K. Lee, D.J. Kim, Variations of structure and composition in magnesium incorporated hydroxyapatite/β-tricalcium phosphate, J. Mater. Res. 21(2) (2006) 428-436.
[287]R. Enderle, F. Götz-Neunhoeffer, M. Göbbels, F. Müller, P. Greil, Influence of magnesium doping on the phase transformation temperature of β-TCP ceramics examined by Rietveld refinement, Biomaterials 26(17) (2005) 3379-3384.
[288]X. Zhang, F. Jiang, T. Groth, K.S. Vecchio, Preparation, characterization and mechanical performance of dense β-TCP ceramics with/without magnesium substitution, J. Mater. Sci. Mater. Med. 19(9) (2008) 3063-3070.
[289]W. Xue, K. Dahlquist, A. Banerjee, A. Bandyopadhyay, S. Bose, Synthesis and characterization of tricalcium phosphate with Zn and Mg based dopants, J. Mater. Sci. Mater. Med. 19(7) (2008) 2669-2677.
[290]M. Nabiyouni, T. Brückner, H. Zhou, U. Gbureck, S.B. Bhaduri, Magnesium-based bioceramics in orthopedic applications, Acta Biomater. 66 (2018) 23-43.
[291]A. Bigi, G. Falini, E. Foresti, M. Gazzano, A. Ripmonti, N. Roveri, Rietveld structure refinements of calcium hydroxylapatite containing magnesium, Acta Crystallogr. Sect. B: Struct. Sci. 52(1) (1996) 87-92.
[292]A. Yasukawa, S. Ouchi, K. Kandori, T. Ishikawa, Preparation and characterization of magnesium–calcium hydroxyapatites, J. Mater. Chem. 6(8) (1996) 1401-1405.
[293]E. Boanini, M. Gazzano, A. Bigi, Ionic substitutions in calcium phosphates synthesized at low temperature, Acta Biomater. 6(6) (2010) 1882-1894.
[294]E. Landi, G. Logroscino, L. Proietti, A. Tampieri, M. Sandri, S. Sprio, Biomimetic Mg-substituted hydroxyapatite: from synthesis to in vivo behaviour, J. Mater. Sci. Mater. Med. 19(1) (2008) 239-247.
[295]D. Lee, P.N. Kumta, Chemical synthesis and stabilization of magnesium substituted brushite, Materials Science and Engineering: C 30(7) (2010) 934-943.
[296]N. Betancur-Granados, J.I. Tobón, O.J. Restrepo-Baena, Alternative production processes of calcium silicate phases of portland cement: a review, Civ. Eng. Res. J 5 (2018) 555665.
[297]A. Gaki, R. Chrysafi, G. Kakali, Chemical synthesis of hydraulic calcium aluminate compounds using the Pechini technique, J. Eur. Ceram. Soc. 27(2-3) (2007) 1781-1784.
[298]A. Wesselsky, O.M. Jensen, Synthesis of pure Portland cement phases, Cem. Concr. Res. 39(11) (2009) 973-980.
[299]L. Nicoleau, A. Nonat, D. Perrey, The di-and tricalcium silicate dissolutions, Cem. Concr. Res. 47 (2013) 14-30.
[300]Y.P. Arias Jaramillo, Incidencia de la temperatura ambiente en la formación de compuestos cementantes mediante la activación alcalina de cenizas de carbón, Escuela de Ingeniería de Materiales (2013).
[301]X. Li, X. Shen, M. Tang, X. Li, Stability of tricalcium silicate and other primary phases in portland cement clinker, Ind. Eng. Chem. Res. 53(5) (2014) 1954-1964.
[302]H.F. Taylor, Cement chemistry, Thomas Telford London1997.
[303]H.-M. Ludwig, W. Zhang, Research review of cement clinker chemistry, Cem. Concr. Res. 78 (2015) 24-37.
[304]A. Bazzoni, S. Ma, Q. Wang, X. Shen, M. Cantoni, K.L. Scrivener, The effect of magnesium and zinc ions on the hydration kinetics of C3S, J. Am. Ceram. Soc. 97(11) (2014) 3684-3693.
[305]M.-N. De Noirfontaine, F. Dunstetter, M. Courtial, G. Gasecki, M. Signes-Frehel, Polymorphism of tricalcium silicate, the major compound of Portland cement clinker: 2. Modelling alite for Rietveld analysis, an industrial challenge, Cem. Concr. Res. 36(1) (2006) 54-64.
[306]F. Dunstetter, M.-N. De Noirfontaine, M. Courtial, Polymorphism of tricalcium silicate, the major compound of Portland cement clinker: 1. Structural data: review and unified analysis, Cem. Concr. Res. 36(1) (2006) 39-53.
[307]K. Urabe, T. Shirakami, M. Iwashima, Superstructure in a triclinic phase of tricalcium silicate, J. Am. Ceram. Soc. 83(5) (2000) 1253-1258.
[308]N.B. Singh, S. Rai, N. Singh, Highly Reactive β-Dicalcium Silicate, J. Am. Ceram. Soc. 85(9) (2002) 2171-2176.

[309]N. Yamnova, N. Zubkova, N. Eremin, A. Zadov, V. Gazeev, Crystal structure of larnite β-Ca2SiO4 and specific features of polymorphic transitions in dicalcium orthosilicate, Crystallography Reports 56(2) (2011) 210-220.
[310]J. Camilleri, Hydration mechanisms of mineral trioxide aggregate, Int. Endod. J. 40(6) (2007) 462-470.
[311]J. Camilleri, The chemical composition of mineral trioxide aggregate, Journal of Conservative Dentistry: JCD 11(4) (2008) 141.
[312]A.E. Dawood, P. Parashos, R.H. Wong, E.C. Reynolds, D.J. Manton, Calcium silicate-based cements: composition, properties, and clinical applications, J. Investig. Clin. Dent. 8(2) (2017) e12195.
[313]J. Ma, Y. Shen, S. Stojicic, M. Haapasalo, Biocompatibility of two novel root repair materials, J. Endod. 37(6) (2011) 793-798.
[314]N. Sarkar, R. Caicedo, P. Ritwik, R. Moiseyeva, I. Kawashima, Physicochemical basis of the biologic properties of mineral trioxide aggregate, J. Endod. 31(2) (2005) 97-100.
[315]X. Wang, J. Chang, S. Hu, A study on the sealing ability and antibacterial activity of Ca3SiO5/CaCl2 composite cement for dental applications, Dent. Mater. 31(4) (2012) 617-622.
[316]C. Prati, M.G. Gandolfi, Calcium silicate bioactive cements: Biological perspectives and clinical applications, Dent. Mater. 31(4) (2015) 351-370.
[317]J.C. Restrepo, A. Chavarriaga, O.J. Restrepo, J.I. Tobón, Synthesis of hydraulically active calcium silicates produced by combustion methods, MRS Online Proceedings Library (OPL) 1768 (2015).
[318]D. Stephan, P. Wilhelm, Synthesis of Pure Cementitious Phases by Sol-Gel Process as Precursor, Z. Anorg. Allg. Chem. 630(10) (2004) 1477-1483.
[319]G. Constantinides, Nanoscience and nanoengineering of cement-based materials, Nanotechnology in Eco-Efficient Construction, Elsevier2013, pp. 9-37a.
[320]Wikipedia, Cement. https://en.wikipedia.org/wiki/Cement. (Accessed 8.2 2022).
[321]Wikipedia, Opus caementitium. https://en.wikipedia.org/wiki/Roman_concrete. (Accessed 8.2. 2022).
[322]Wikipedia, Joseph Aspdin. https://en.wikipedia.org/wiki/Joseph_Aspdin. (Accessed 8.2. 2022).
[323]Wikipedia, Portland cement. https://en.wikipedia.org/wiki/Roman_concrete. (Accessed 8.2. 2022).
[324]M. Arora, E.K. Chan, S. Gupta, A.D. Diwan, Polymethylmethacrylate bone cements and additives: A review of the literature, World journal of orthopedics 4(2) (2013) 67.
[325]G. Biehl, J. Harms, U. Hanser, Experimentelle Untersuchungen über die Wärmeentwicklung im Knochen bei der Polymerisation von Knochenzement, Archiv für orthopädische und Unfall-Chirurgie, mit besonderer Berücksichtigung der Frakturenlehre und der orthopädisch-chirurgischen Technik 78(1) (1974) 62-69.
[326]H. Fukushima, Y. Hashimoto, S. Yoshiya, M. Kurosaka, M. Matsuda, S. Kawamura, T. Iwatsubo, Conduction analysis of cement interface temperature in total knee arthroplasty, Kobe J. Med. Sci. 48(1/2) (2002) 63-72.
[327]J.W. Bullard, H.M. Jennings, R.A. Livingston, A. Nonat, G.W. Scherer, J.S. Schweitzer, K.L. Scrivener, J.J. Thomas, Mechanisms of cement hydration, Cem. Concr. Res. 41(12) (2011) 1208-1223.
[328]P.M. Dove, N. Han, Kinetics of mineral dissolution and growth as reciprocal microscopic surface processes across chemical driving force, AIP Conf. Proc., American Institute of Physics, 2007, pp. 215-234.
[329]P.M. Dove, N. Han, J.J. De Yoreo, Mechanisms of classical crystal growth theory explain quartz and silicate dissolution behavior, Proceedings of the National Academy of Sciences 102(43) (2005) 15357-15362.
[330]A.W. Adamson, A.P. Gast, Physical chemistry of surfaces, Interscience publishers New York1967.
[331]G.A. Somorjai, Y. Li, Introduction to surface chemistry and catalysis, John Wiley & Sons2010.
[332]W.-K. Burton, N. Cabrera, F. Frank, The growth of crystals and the equilibrium structure of their surfaces, Philosophical Transactions of the Royal Society of London. Series A, Mathematical and Physical Sciences 243(866) (1951) 299-358.
[333]D. Kashchiev, G. Van Rosmalen, Nucleation in solutions revisited, Crystal Research and Technology: Journal of Experimental and Industrial Crystallography 38(7-8) (2003) 555-574.
[334]F.M. Morel, Principles of aquatic chemistry, John Wiley and Sons, New York NY. 1983. 446 (1983).
[335]W. Stumm, J.J. Morgan, J.I. Drever, Aquatic chemistry, J. Environ. Qual. 25(5) (1996) 1162.
[336]W.E. Brown, A new calcium phosphate, water-setting cement, Cements research progress (1987) 351-379.
[337]F. Gil, M. Ginebra, F. Driessens, J. Planell, S. Best, Calcium phosphate bone cements for clinical applications. Part I: solution chemistry, J. Mater. Sci. Mater. Med. 10(3) (1999) 169-176.
[338]D.D. Weiss, M.A. Sachs, C.R. Woodard, Calcium phosphate bone cements: a comprehensive review, Journal of Long-term Effects of Medical Implants 13(1) (2003).
[339]F. Driessens, E. De Maeyer, E. Fernández, M. Boltong, G. Berger, R. Verbeeck, M. Ginebra, J. Planell, Amorphous calcium phosphate cements and their transformation into calcium deficient hydroxyapatite, Bioceramics 9 (1996) 231-234.

[340]U. Gbureck, J.E. Barralet, K. Spatz, L.M. Grover, R. Thull, Ionic modification of calcium phosphate cement viscosity. Part I: hypodermic injection and strength improvement of apatite cement, Biomaterials 25(11) (2004) 2187-2195.

[341]A. Generosi, J.V. Rau, V.S. Komlev, V.R. Albertini, A.Y. Fedotov, S.M. Barinov, Anomalous hardening behavior of a calcium phosphate bone cement, The Journal of Physical Chemistry B 114(2) (2010) 973-979.

[342]J.V. Rau, A. Generosi, V.S. Komlev, M. Fosca, S.M. Barinov, V.R. Albertini, Real-time monitoring of the mechanism of poorly crystalline apatite cement conversion in the presence of chitosan, simulated body fluid and human blood, Dalton Transactions 39(47) (2010) 11412-11423.

[343]V.V. Smirnov, J.V. Rau, A. Generosi, V.R. Albertini, D. Ferro, S.M. Barinov, Elucidation of real-time hardening mechanisms of two novel high-strength calcium phosphate bone cements, Journal of Biomedical Materials Research Part B: Applied Biomaterials: An Official Journal of The Society for Biomaterials, The Japanese Society for Biomaterials, and The Australian Society for Biomaterials and the Korean Society for Biomaterials 93(1) (2010) 74-83.

[344]M. Tagaya, H. Goto, M. Iinuma, N. Wakamatsu, Y. Tamura, Y. Doi, Development of self-setting Te-Cp/α-TCP cement for pulpotomy, Dent. Mater. 24(4) (2005) 555-561.

[345]H.C.W.S.P. D., Studies in the basic mineralizing system, CaO-P2O5-H2O, Calcif. Tissue Res. 14 (2005) 3-14.

[346]B.L. Eppley, Reconstruction of Bone Using Calcium Phosphate Bone Cements: A Critical Review, J. Craniofac. Surg. 12(1) (2001) 102.

[347]J. Lacout, E. Mejdoubi, M. Hamad, Crystallization mechanisms of calcium phosphate cement for biological uses, J. Mater. Sci. Mater. Med. 7(6) (1996) 371-374.

[348]W. Brown, Dental restorative cement pastes, United States Patent# 4518430 (1985).

[349]S. Gruniger, Evaluation of the biocompatibility of a new calcium phosphate setting cement (abstract no. 270), J. Dent. Res. 63 (1984) 200.

[350]W. Brown, A new calcium phosphate settimg cement, J. Dent. Res. 62 (1983) 672.

[351]K. TenHuisen, P. Brown, The formation of hydroxyapatite-ionomer cements at 38 C, J. Dent. Res. 73(3) (1994) 598-606.

[352]P.W. Brown, M. Fulmer, Kinetics of hydroxyapatite formation at low temperature, J. Am. Ceram. Soc. 74(5) (1991) 934-940.

[353]J. Lemaitre, A. Mirtchi, A. Mortier, Calcium phosphate cements for medical use: state of the art and perspectives of development, Silic. Indus. 52(9-10) (1987) 141-146.

[354]E. Fernandez, F. Gil, M. Ginebra, F. Driessens, J. Planell, S. Best, Production and characterization of new calcium phosphate bone cements in the CaHPO4-alpha-Ca3 (PO4) 2 system: pH, workability and setting times, J. Mater. Sci. Mater. Med. 10(4) (1999) 223-230.

[355]E. Fernandez, F. Gil, S. Best, M. Ginebra, F. Driessens, J. Planell, The cement setting reaction in the CaHPO4-α-Ca3 (PO4) 2 system: An X-ray diffraction study, Journal of Biomedical Materials Research: An Official Journal of The Society for Biomaterials, The Japanese Society for Biomaterials, and the Australian Society for Biomaterials 42(3) (1998) 403-406.

[356]K. Lilley, U. Gbureck, A. Wright, D. Farrar, J. Barralet, Cement from nanocrystalline hydroxyapatite: effect of calcium phosphate ratio, J. Mater. Sci. Mater. Med. 16(12) (2005) 1185-1190.

[357]J. Barralet, K. Lilley, L. Grover, D. Farrar, C. Ansell, U. Gbureck, Cements from nanocrystalline hydroxyapatite, J. Mater. Sci. Mater. Med. 15(4) (2004) 407-411.

[358]L.M. Grover, M.P. Hofmann, U. Gbureck, B. Kumarasami, J.E. Barralet, Frozen delivery of brushite calcium phosphate cements, Acta Biomater. 4(6) (2008) 1916-1923.

[359]M. Bohner, P. Van Landuyt, H. Merkle, J. Lemaitre, Composition effects on the pH of a hydraulic calcium phosphate cement, J. Mater. Sci. Mater. Med. 8(11) (1997) 675-681.

[360]M. Bohner, J. Lemaitre, T.A. Ring, Effects of sulfate, pyrophosphate, and citrate ions on the physicochemical properties of cements made of β-tricalcium phosphate-phosphoric acid-water mixtures, J. Am. Ceram. Soc. 79(6) (1996) 1427-1434.

[361]A.A. Mirtchi, J. Lemaitre, N. Terao, Calcium phosphate cements: study of the β-tricalcium phosphate—monocalcium phosphate system, Biomaterials 10(7) (1989) 475-480.

[362]X. Wang, J. Ye, Y. Wang, X. Wu, B. Bai, Control of crystallinity of hydrated products in a calcium phosphate bone cement, Journal of Biomedical Materials Research Part A 81(4) (2007) 781-790.

[363]A. Tofighi, K. Schaffer, R. Palazzolo, Calcium phosphate cement (CPC): a critical development path, Key Eng. Mater., Trans Tech Publ, 2008, pp. 303-306.

[364]X. Wang, J. Ye, H. Wang, Effects of additives on the rheological properties and injectability of a calcium phosphate bone substitute material, Journal of Biomedical Materials Research Part B: Applied Biomaterials: An Official Journal of The Society for Biomaterials, The Japanese Society for Biomaterials, and The Australian Society for Biomaterials and the Korean Society for Biomaterials 78(2) (2006) 259-264.

[365]E.A. De Maeyer, R.M. Verbeeck, C.W. Vercruysse, Conversion of octacalcium phosphate in calcium phosphate cements, J. Biomed. Mater. Res. 52(1) (2000) 95-106.
[366]Y. Nakano, Preparation and Characterization of Porous Octacalcium Phosphate Setting Inproved by α-Tricalcium Phosphate Additive, Dent. Mater. J. 19 (2000) 65-76.
[367]Y. Nakano, M. Ohgaki, S. Nakamura, Y. Takagi, K. Yamashita, In vitro and in vivo characterization and mechanical properties of α-TCP/OCP settings, Bioceramics: Volume 12, World Scientific1999, pp. 315-318.
[368]H.L.R. Alves, L.A. dos Santos, C.P. Bergmann, Injectability evaluation of tricalcium phosphate bone cement, J. Mater. Sci. Mater. Med. 19(5) (2008) 2241-2246.
[369]M. Bohner, A.K. Malsy, C.L. Camiré, U. Gbureck, Combining particle size distribution and isothermal calorimetry data to determine the reaction kinetics of α-tricalcium phosphate–water mixtures, Acta Biomater. 2(3) (2006) 343-348.
[370]T.J. Brunner, R.N. Grass, M. Bohner, W.J. Stark, Effect of particle size, crystal phase and crystallinity on the reactivity of tricalcium phosphate cements for bone reconstruction, J. Mater. Chem. 17(38) (2007) 4072-4078.
[371]E. Fernandez, M. Ginebra, M. Boltong, F. Driessens, J. Planell, J. Ginebra, E. De Maeyer, R. Verbeeck, Kinetic study of the setting reaction of a calcium phosphate bone cement, Journal of Biomedical Materials Research: An Official Journal of The Society for Biomaterials and The Japanese Society for Biomaterials 32(3) (1996) 367-374.
[372]U. Gbureck, J.E. Barralet, L. Radu, H.G. Klinger, R. Thull, Amorphous α-tricalcium phosphate: preparation and aqueous setting reaction, J. Am. Ceram. Soc. 87(6) (2004) 1126-1132.
[373]M.P. Ginebra, E. Fernández, F.C. Driessens, J.A. Planell, Modeling of the Hydrolysis of α-Tricalcium Phosphate, J. Am. Ceram. Soc. 82(10) (1999) 2808-2812.
[374]V. Jack, F. Buchanan, N. Dunne, Particle attrition of α-tricalcium phosphate: effect on mechanical, handling, and injectability properties of calcium phosphate cements, Proceedings of the Institution of Mechanical Engineers, Part H: Journal of Engineering in Medicine 222(1) (2008) 19-28.
[375]H. MONMA, T. KANAZAW, The Hydration of-Tricalcium Phosphate, 窯業協会誌 84(4) (1976) 209-213.
[376]S. Oh, G.-S. Lee, J.-H. Park, H.-W. Kim, Osteoclastic cell behaviors affected by the α-tricalcium phosphate based bone cements, J. Mater. Sci. Mater. Med. 21(11) (2010) 3019-3027.
[377]D. Knaack, M. Goad, M. Aiolova, C. Rey, A. Tofighi, P. Chakravarthy, D.D. Lee, Resorbable calcium phosphate bone substitute, J. Biomed. Mater. Res. 43(4) (1998) 399-409.
[378]A. Tofighi, P. Chakravarthy, D. Lee, S. Mounic, C. Rey, Setting reactions involved in injectable cements based on amorphous calcium phosphate, Key Eng. Mater. 192 (2001).
[379]M. Fulmer, P. Brown, Hydrolysis of dicalcium phosphate dihydrate to hydroxyapatite, J. Mater. Sci. Mater. Med. 9(4) (1998) 197-202.
[380]L.C. Chow, M. Markovic, S.A. Frukhtbeyn, S. Takagi, Hydrolysis of tetracalcium phosphate under a near-constant-composition condition—effects of pH and particle size, Biomaterials 26(4) (2005) 393-401.
[381]U. Gbureck, J. Barralet, M. Hofmann, R. Thulĺ, Nanocrystalline tetracalcium phosphate cement, J. Dent. Res. 83(5) (2004) 425-428.
[382]U. Gbureck, J.E. Barralet, M. Hofmann, R. Thull, Mechanical activation of tetracalcium phosphate, J. Am. Ceram. Soc. 87(2) (2004) 311-313.
[383]A.C. Tas, Porous, Biphasic CaCO3-Calcium Phosphate Biomedical Cement Scaffolds from Calcite (CaCO3) Powder, International Journal of Applied Ceramic Technology 4(2) (2007) 152-163.
[384]M. Akiyama, S. Kawasaki, Novel grout material comprised of calcium phosphate compounds: in vitro evaluation of crystal precipitation and strength reinforcement, Engineering Geology 125 (2012) 119-128.
[385]I.J. Macha, U. Boonyang, S. Cazalbou, B. Ben-Nissan, C. Charvillat, F.N. Oktar, D. Grossin, Comparative study of Coral Conversion, Part 2: Microstructural evolution of calcium phosphate, Journal of The Australian Ceramic Society 51(2) (2015) pp. 149-159.
[386]Y. Fukase, E. Eanes, S. Takagp, L. Chow, W. Brown, Setting reactions and compressive strengths of calcium phosphate cements, J. Dent. Res. 69(12) (1990) 1852-1856.
[387]M. Bohner, U. Gbureck, J. Barralet, Technological issues for the development of more efficient calcium phosphate bone cements: a critical assessment, Biomaterials 26(33) (2005) 6423-6429.
[388]Y. Miyamoto, K. Ishikawa, M. Takechi, T. Toh, T. Yuasa, M. Nagayama, K. Suzuki, Histological and compositional evaluations of three types of calcium phosphate cements when implanted in subcutaneous tissue immediately after mixing, Journal of Biomedical Materials Research: An Official Journal of The Society for Biomaterials, The Japanese Society for Biomaterials, and The Australian Society for Biomaterials 48(1) (1999) 36-42.

[389]R. Poser, S. Young, M. Holde, S. Gunasekaran, B. Constantz, The correlation of radiographic, MRI and histologic evaluations over two years of a carbonated apatite cement in a rabbit model, J. Orthop. Trauma 13(4) (1999) 301.

[390]B.R. Constantz, I.C. Ison, M.T. Fulmer, R.D. Poser, S.T. Smith, M. VanWagoner, J. Ross, S.A. Goldstein, J.B. Jupiter, D.I. Rosenthal, Skeletal repair by in situ formation of the mineral phase of bone, Science 267(5205) (1995) 1796-1799.

[391]P.K. Bajpai, C.M. Fuchs, D.E. McCullum, Development of tricalcium phosphate ceramic cements, ASTM International1987.

[392]G. Vereecke, J. Lemaître, Calculation of the solubility diagrams in the system Ca (OH) 2-H3PO4-KOH-HNO3-CO2-H2O, J. Cryst. Growth 104(4) (1990) 820-832.

[393]D. Apelt, F. Theiss, A. El-Warrak, K. Zlinszky, R. Bettschart-Wolfisberger, M. Bohner, S. Matter, J.A. Auer, B. von Rechenberg, In vivo behavior of three different injectable hydraulic calcium phosphate cements, Biomaterials 25(7-8) (2004) 1439-1451.

[394]C.P. Klein, K. De Groot, A. Drissen, H. Van der Lubbe, Interaction of biodegradable β-whitlockite ceramics with bone tissue: An in vivo study, Biomaterials 6(3) (1985) 189-192.

[395]C. Liu, W. Shen, J. Chen, Solution property of calcium phosphate cement hardening body, Materials Chemistry and Physics 58(1) (1999) 78-82.

[396]K. Ohura, M. Bohner, P. Hardouin, J. Lemaître, G. Pasquier, B. Flautre, Resorption of, and bone formation from, new β-tricalcium phosphate-monocalcium phosphate cements: An in vivo study, Journal of Biomedical Materials Research: An Official Journal of The Society for Biomaterials and The Japanese Society for Biomaterials 30(2) (1996) 193-200.

[397]B. Flautre, C. Maynou, J. Lemaitre, P. Van Landuyt, P. Hardouin, Bone colonization of β–TCP granules incorporated in brushite cements, Journal of Biomedical Materials Research: An Official Journal of The Society for Biomaterials, The Japanese Society for Biomaterials, and The Australian Society for Biomaterials and the Korean Society for Biomaterials 63(4) (2002) 413-417.

[398]M. Sena, Y. Yamashita, Y. Nakano, M. Ohgaki, S. Nakamura, K. Yamashita, Y. Takagi, Octacalcium phosphate–based cement as a pulp-capping agent in rats, Oral Surgery, Oral Medicine, Oral Pathology, Oral Radiology, and Endodontology 97(6) (2004) 749-755.

[399]O. Suzuki, Octacalcium phosphate (OCP)-based bone substitute materials, Jpn. Dent. Sci. Rev. 49(2) (2013) 58-71.

[400]ASTM, Standard test method for time of setting of hydraulic cement
paste by Vicat needle. ASTM C191-92., Annual book of ASTM standards: Cement, Lime, Gypsum.
, American Society for Testing and Materials, Philadelphia, USA, 1993, p. 2.

[401]ASTM, Standard test method for time of setting of hydraulic cement
paste by Gillmore needles. ASTM C266-89., Annual book of ASTM standards: Cement, Lime, Gypsum., American Society for Testing and Materials, Philadelphia, USA, 1993, p. 2.

[402]J. Carlson, M. Nilsson, E. Fernández, J. Planell, An ultrasonic pulse-echo technique for monitoring the setting of CaSO4-based bone cement, Biomaterials 24(1) (2003) 71-77.

[403]M. Nilsson, J. Carlson, E. Fernandez, J. Planell, Monitoring the setting of calcium-based bone cements using pulse-echo ultrasound, J. Mater. Sci. Mater. Med. 13(12) (2002) 1135-1141.

[404]T.J. Brunner, M. Bohner, C. Dora, C. Gerber, W.J. Stark, Comparison of amorphous TCP nanoparticles to micron-sized α-TCP as starting materials for calcium phosphate cements, Journal of Biomedical Materials Research Part B: Applied Biomaterials: An Official Journal of The Society for Biomaterials, The Japanese Society for Biomaterials, and The Australian Society for Biomaterials and the Korean Society for Biomaterials 83(2) (2007) 400-407.

[405]M. Hofmann, S. Nazhat, U. Gbureck, J. Barralet, Real-time monitoring of the setting reaction of brushite-forming cement using isothermal differential scanning calorimetry, Journal of Biomedical Materials Research Part B: Applied Biomaterials: An Official Journal of The Society for Biomaterials, The Japanese Society for Biomaterials, and The Australian Society for Biomaterials and the Korean Society for Biomaterials 79(2) (2006) 360-364.

[406]M. Hofmann, A. Young, S.N. Nazhat, U. Gbureck, J. Barralet, Setting kinetics observation of a brushite cement by FTIR and DSC, Key Eng. Mater., Trans Tech Publ, 2006, pp. 837-840.

[407]K.S. Leung, W.S. Siu, S.F. Li, L. Qin, W.H. Cheung, K.F. Tam, P.P.Y. Lui, An in vitro optimized injectable calcium phosphate cement for augmenting screw fixation in osteopenic goats, Journal of Biomedical Materials Research Part B: Applied Biomaterials: An Official Journal of The Society for Biomaterials, The Japanese Society for Biomaterials, and The Australian Society for Biomaterials and the Korean Society for Biomaterials 78(1) (2006) 153-160.

[408]R. Martin, P. Brown, The effects of magnesium on hydroxyapatite formation in vitro from CaHPO4 and Ca4 (PO4) 2O at 37.4 C, Calcif. Tissue Int. 60(6) (1997) 538-546.
[409]C. Liu, Y. Huang, H. Zheng, Study of the hydration process of calcium phosphate cement by AC impedance spectroscopy, J. Am. Ceram. Soc. 82(4) (1999) 1052-1057.
[410]I. Khairoun, M. Boltong, F. Driessens, J. Planell, Limited compliance of some apatitic calcium phosphate bone cements with clinical requirements, J. Mater. Sci. Mater. Med. 9(11) (1998) 667-671.
[411]H. Monma, T. KANAZAWA, Millennial special leading papers on ceramics in the 20th century: the best of jcersj the hydration of α-tricalcium phosphate, J. Ceram. Soc. Jpn. 108(1260) (2000) S75-S80.
[412]M. Takechi, Y. Miyamoto, K. Ishikawa, T. Toh, T. Yuasa, M. Nagayama, K. Suzuki, Initial histological evaluation of anti-washout type fast-setting calcium phosphate cement following subcutaneous implantation, Biomaterials 19(22) (1998) 2057-2063.
[413]M. Ginebra, F. Driessens, J. Planell, Effect of the particle size on the micro and nanostructural features of a calcium phosphate cement: a kinetic analysis, Biomaterials 25(17) (2004) 3453-3462.
[414]C. Liu, H. Shao, F. Chen, H. Zheng, Effects of the granularity of raw materials on the hydration and hardening process of calcium phosphate cement, Biomaterials 24(23) (2003) 4103-4113.
[415]M. Otsuka, Y. Matsuda, Y. Suwa, J.L. Fox, W.I. Higuchi, Effect of particle size of metastable calcium phosphates on mechanical strength of a novel self-setting bioactive calcium phosphate cement, J. Biomed. Mater. Res. 29(1) (1995) 25-32.
[416]M. Bohner, Reactivity of calcium phosphate cements, J. Mater. Chem. 17(38) (2007) 3980-3986.
[417]M. Bohner, T.J. Brunner, W.J. Stark, Controlling the reactivity of calcium phosphate cements, J. Mater. Chem. 18(46) (2008) 5669-5675.
[418]M. Bohner, H. Merkle, P.V. Landuyt, G. Trophardy, J. Lemaitre, Effect of several additives and their admixtures on the physico-chemical properties of a calcium phosphate cement, J. Mater. Sci. Mater. Med. 11(2) (2000) 111-116.
[419]L. Grover, J. Knowles, G. Fleming, J. Barralet, In vitro ageing of brushite calcium phosphate cement, Biomaterials 24(23) (2003) 4133-4141.
[420]X. Qi, J. Ye, Y. Wang, Improved injectability and in vitro degradation of a calcium phosphate cement containing poly (lactide-co-glycolide) microspheres, Acta Biomater. 4(6) (2008) 1837-1845.
[421]S. Sarda, E. Fernández, M. Nilsson, M. Balcells, J. Planell, Kinetic study of citric acid influence on calcium phosphate bone cements as water-reducing agent, Journal of Biomedical Materials Research: An Official Journal of The Society for Biomaterials, The Japanese Society for Biomaterials, and The Australian Society for Biomaterials and the Korean Society for Biomaterials 61(4) (2002) 653-659.
[422]F. Tamimi-Mariño, J. Mastio, C. Rueda, L. Blanco, E. López-Cabarcos, Increase of the final setting time of brushite cements by using chondroitin 4-sulfate and silica gel, J. Mater. Sci. Mater. Med. 18(6) (2007) 1195-1201.
[423]F.T. Mariño, J. Torres, M. Hamdan, C.R. Rodríguez, E.L. Cabarcos, Advantages of using glycolic acid as a retardant in a brushite forming cement, Journal of Biomedical Materials Research Part B: Applied Biomaterials: An Official Journal of The Society for Biomaterials, The Japanese Society for Biomaterials, and The Australian Society for Biomaterials and the Korean Society for Biomaterials 83(2) (2007) 571-579.
[424]J. Xie, C. Riley, K. Chittur, Effect of albumin on brushite transformation to hydroxyapatite, Journal of Biomedical Materials Research: An Official Journal of The Society for Biomaterials, The Japanese Society for Biomaterials, and The Australian Society for Biomaterials and the Korean Society for Biomaterials 57(3) (2001) 357-365.
[425]S. Alenezi, S. Jerban, S. Elkoun, Importance of the PMMA viscoelastic rheology on the reduction of the leakage risk during osteoporotic bone augmentation: A numerical leakage model through a porous media, J. Mech. Behav. Biomed. Mater. 65 (2017) 29-41.
[426]I. Khairoun, M. Boltong, F.M. Driessens, J. Planell, Some factors controlling the injectability of calcium phosphate bone cements, J. Mater. Sci. Mater. Med. 9(8) (1998) 425-428.
[427]G. Baroud, M. Bohner, P. Heini, T. Steffen, Injection biomechanics of bone cements used in vertebroplasty, Bio-Medical Materials and Engineering 14(4) (2004) 487-504.
[428]C. Liu, H. Shao, F. Chen, H. Zheng, Rheological properties of concentrated aqueous injectable calcium phosphate cement slurry, Biomaterials 27(29) (2006) 5003-5013.
[429]S. Sarda, E. Fernández, J. Llorens, S. Martinez, M. Nilsson, J. Planell, Rheological properties of an apatitic bone cement during initial setting, J. Mater. Sci. Mater. Med. 12(10) (2001) 905-909.
[430]I. Khairoun, M. Boltong, F. Driessens, J. Planell, Some factors controlling the injectability of calcium phosphate bone cements, J. Mater. Sci. Mater. Med. 9(8) (1998) 425-428.
[431]E.F. Burguera, H.H. Xu, L. Sun, Injectable calcium phosphate cement: Effects of powder-to-liquid ratio and needle size, Journal of Biomedical Materials Research Part B: Applied Biomaterials: An Official Journal

of The Society for Biomaterials, The Japanese Society for Biomaterials, and The Australian Society for Biomaterials and the Korean Society for Biomaterials 84(2) (2008) 493-502.
[432]M. Habib, G. Baroud, F. Gitzhofer, M. Bohner, Mechanisms underlying the limited injectability of hydraulic calcium phosphate paste, Acta Biomater. 4(5) (2008) 1465-1471.
[433]M. Maas, U. Hess, K. Rezwan, The contribution of rheology for designing hydroxyapatite biomaterials, Current opinion in colloid & interface science 19(6) (2014) 585-593.
[434]S. Gouveia, S. Olhero, A. Kaushal, J. Ferreira, Injectability of calcium phosphate pastes: effects of particle size and state of aggregation of β-tricalcium phosphate powders, Acta Biomater. 21 (2015) 204-216.
[435]E. Montufar, Y. Maazouz, M. Ginebra, Relevance of the setting reaction to the injectability of tricalcium phosphate pastes, Acta Biomater. 9(4) (2013) 6188-6198.
[436]X. Qi, J. Ye, Mechanical and rheological properties and injectability of calcium phosphate cement containing poly (lactic-co-glycolic acid) microspheres, Materials Science and Engineering: C 29(6) (2009) 1901-1906.
[437]X. Wang, L. Chen, H. Xiang, J. Ye, Influence of anti-washout agents on the rheological properties and injectability of a calcium phosphate cement, Journal of Biomedical Materials Research Part B: Applied Biomaterials: An Official Journal of The Society for Biomaterials, The Japanese Society for Biomaterials, and The Australian Society for Biomaterials and the Korean Society for Biomaterials 81(2) (2007) 410-418.
[438]R. O'Neill, H. McCarthy, E. Montufar, M.-P. Ginebra, D. Wilson, A. Lennon, N. Dunne, Critical review: Injectability of calcium phosphate pastes and cements, Acta Immaterial 50 (2017) 1-19.
[439]R. O'Neill, H. McCarthy, E. Montufar, M.-P. Ginebra, D.I. Wilson, A. Lennon, N. Dunne, Critical review: Injectability of calcium phosphate pastes and cements, Acta Biomater. 50 (2017) 1-19.
[440]P. Coussot, C. Ancey, Rheophysical classification of concentrated suspensions and granular pastes, Physical Review E 59(4) (1999) 4445.
[441]G. Baroud, E. Cayer, M. Bohner, Rheological characterization of concentrated aqueous β-tricalcium phosphate suspensions: The effect of liquid-to-powder ratio, milling time, and additives, Acta Biomater. 1(3) (2005) 357-363.
[442]J.E. Bujake Jr, Rheology of concentrated dicalcium phosphate suspensions, J. Pharm. Sci. 54(11) (1965) 1599-1604.
[443]J. Friberg, E. Fernández, S. Sarda, M. Nilsson, M. Ginebra, J. Planell, S. Martinez, An experimental approach to the study of the rheology behaviour of synthetic bone calcium phosphate cements, Key Eng. Mater. 192 (2001).
[444]J. Knowles, S. Callcut, G. Georgiou, Characterisation of the rheological properties and zeta potential of a range of hydroxyapatite powders, Biomaterials 21(13) (2000) 1387-1392.
[445]D.-M. Liu, Preparation and characterisation of porous hydroxyapatite bioceramic via a slip-casting route, Ceram. Int. 24(6) (1998) 441-446.
[446]R.R. Rao, T.S. Kannan, Dispersion and slip casting of hydroxyapatite, J. Am. Ceram. Soc. 84(8) (2001) 1710-1716.
[447]J. Tian, Y. Zhang, X. Guo, L. Dong, Preparation and characterization of hydroxyapatite suspensions for solid freeform fabrication, Ceram. Int. 28(3) (2002) 299-302.
[448]H. Khelifi, A. Perrot, T. Lecompte, D. Rangeard, G. Ausias, Prediction of extrusion load and liquid phase filtration during ram extrusion of high solid volume fraction pastes, Powder Technol. 249 (2013) 258-268.
[449]M. Patel, S. Blackburn, D.I. Wilson, Modelling of paste flows subject to liquid phase migration, International Journal for Numerical Methods in Engineering 72(10) (2007) 1157-1180.
[450]S. Rough, D. Wilson, J. Bridgwater, A model describing liquid phase migration within an extruding microcrystalline cellulose paste, Chem. Eng. Res. Des. 80(7) (2002) 701-714.
[451]P. Yaras, D. Kalyon, U. Yilmazer, Flow instabilities in capillary flow of concentrated suspensions, Rheol. Acta 33(1) (1994) 48-59.
[452]M. Zhang, S. Rough, R. Ward, C. Seiler, D. Wilson, A comparison of ram extrusion by single-holed and multi-holed dies for extrusion–spheronisation of microcrystalline-based pastes, Int. J. Pharm. 416(1) (2011) 210-222.
[453]M.J. Patel, Theoretical aspects of paste formulation for extrusion, University of Cambridge, 2008.
[454]M. Bohner, G. Baroud, Injectability of calcium phosphate pastes, Biomaterials 26(13) (2005) 1553-1563.
[455]M. Bohner, N. Doebelin, G. Baroud, Theoretical and experimental approach to test the cohesion of calcium phosphate pastes, Eur Cell Mater 12(1473-2262) (2006) 26-35.
[456]M. Ginebra, O.B. DEZ, M. Boltong, F. Driessens, J. PLANELL, Dimensional and thermal behaviour of calcium phosphate cements during setting compared to PMMA bone cements, J. Mater. Sci. Lett. 14 (1995) 4-5.
[457]A.J.W. Johnson, B.A. Herschler, A review of the mechanical behavior of CaP and CaP/polymer composites for applications in bone replacement and repair, Acta Biomater. 7(1) (2011) 16-30.

[458]K. Ishikawa, K. Asaoka, Estimation of ideal mechanical strength and critical porosity of calcium phosphate cement, J. Biomed. Mater. Res. 29(12) (1995) 1537-1543.
[459]E. Charrière, S. Terrazzoni, C. Pittet, P. Mordasini, M. Dutoit, J. Lemaıtre, P. Zysset, Mechanical characterization of brushite and hydroxyapatite cements, Biomaterials 22(21) (2001) 2937-2945.
[460]J.P. Morgan, R.H. Dauskardt, Notch strength insensitivity of self-setting hydroxyapatite bone cements, J. Mater. Sci. Mater. Med. 14(7) (2003) 647-653.
[461]M. Ikenaga, P. Hardouin, J. Lemaître, H. Andrianjatovo, B. Flautre, Biomechanical characterization of a biodegradable calcium phosphate hydraulic cement: a comparison with porous biphasic calcium phosphate ceramics, Journal of Biomedical Materials Research: An Official Journal of The Society for Biomaterials, The Japanese Society for Biomaterials, and the Australian Society for Biomaterials 40(1) (1998) 139-144.
[462]H. Andrianjatovo, F. Jose, J. Lemaitre, Effect of β-TCP granularity on setting time and strength of calcium phosphate hydraulic cements, J. Mater. Sci. Mater. Med. 7(1) (1996) 34-39.
[463]F. Driessens, Chemistry and applied aspects of calcium orthophosphate bone cements, Proceedings of Concepts and Clinical Applications of Ionic Cements, 15th European Conference on Biomaterials, Bordeaux, France, 1999.
[464]J. Zhang, W. Liu, V. Schnitzler, F. Tancret, J.-M. Bouler, Calcium phosphate cements for bone substitution: chemistry, handling and mechanical properties, Acta Biomater. 10(3) (2014) 1035-1049.
[465]D.R. Jones, M.F. Ashby, Engineering materials 1: An introduction to properties, applications and design, Butterworth-Heinemann2018.
[466]M. Ginebra, E. Fernandez, F. Driessens, M. Boltong, J. Muntasell, J. Font, J. Planell, The effects of temperature on the behaviour of an apatitic calcium phosphate cement, J. Mater. Sci. Mater. Med. 6(12) (1995) 857-860.
[467]L.C. CHOW, Next generation calcium phosphate-based biomaterials, Dent. Mater. 28(1) (2009) 1-10.
[468]R. Krüger, J. Groll, Fiber reinforced calcium phosphate cements–on the way to degradable load bearing bone substitutes?, Biomaterials 33(25) (2012) 5887-5900.
[469]S.V. Dorozhkin, Calcium orthophosphate cements for biomedical application, Journal of Materials Science 43(9) (2008) 3028-3057.
[470]Y. Miyamoto, K. Ishikawa, H. Fukao, M. Sawada, M. Nagayama, M. Kon, K. Asaoka, In vivo setting behaviour of fast-setting calcium phosphate cement, Biomaterials 16(11) (1995) 855-860.
[471]P.D. Costantino, C.D. Friedman, K. Jones, L.C. Chow, G.A. Sisson, Experimental hydroxyapatite cement cranioplasty, Plast. Reconstr. Surg. 90(2) (1992) 174-85; discussion 186.
[472]J. Barralet, T. Gaunt, A. Wright, I.R. Gibson, J. Knowles, Effect of porosity reduction by compaction on compressive strength and microstructure of calcium phosphate cement, Journal of Biomedical Materials Research: An Official Journal of The Society for Biomaterials, The Japanese Society for Biomaterials, and The Australian Society for Biomaterials and the Korean Society for Biomaterials 63(1) (2002) 1-9.
[473]B. Feng, M. Guolin, Y. Yuan, L. Changshen, W. Zhen, L. Jian, Role of macropore size in the mechanical properties and in vitro degradation of porous calcium phosphate cements, Mater. Lett. 64(18) (2010) 2028-2031.
[474]T. Takahashi, M. Yamamoto, K. Ioku, S. Goto, Relationship between compressive strength and pore structure of hardened cement pastes, Advances in Cement Research 9(33) (1997) 25-30.
[475]Y. Zhang, H.H. Xu, S. Takagi, L.C. Chow, In-situ hardening hydroxyapatite-based scaffold for bone repair, J. Mater. Sci. Mater. Med. 17(5) (2006) 437-445.
[476]J. Zhang, F. Tancret, J.-M. Bouler, Fabrication and mechanical properties of calcium phosphate cements (CPC) for bone substitution, Materials Science and Engineering: C 31(4) (2011) 740-747.
[477]R. Martin, P. Brown, Mechanical properties of hydroxyapatite formed at physiological temperature, J. Mater. Sci. Mater. Med. 6(3) (1995) 138-143.
[478]L.C. Chow, E.D. Eanes, Octacalcium phosphate, Karger Medical and Scientific Publishers2001.
[479]L.C. Chow, S. Hirayama, S. Takagi, E. Parry, Diametral tensile strength and compressive strength of a calcium phosphate cement: effect of applied pressure, Journal of Biomedical Materials Research: An Official Journal of The Society for Biomaterials, The Japanese Society for Biomaterials, and The Australian Society for Biomaterials and the Korean Society for Biomaterials 53(5) (2000) 511-517.
[480]A. Almirall, G. Larrecq, J. Delgado, S. Martınez, J. Planell, M. Ginebra, Fabrication of low temperature macroporous hydroxyapatite scaffolds by foaming and hydrolysis of an α-TCP paste, Biomaterials 25(17) (2004) 3671-3680.
[481]J. Barralet, L. Grover, T. Gaunt, A. Wright, I.R. Gibson, Preparation of macroporous calcium phosphate cement tissue engineering scaffold, Biomaterials 23(15) (2002) 3063-3072.

[482]G. Cama, F. Barberis, R. Botter, P. Cirillo, M. Capurro, R. Quarto, S. Scaglione, E. Finocchio, V. Mussi, U. Valbusa, Preparation and properties of macroporous brushite bone cements, Acta Biomater. 5(6) (2009) 2161-2168.

[483]S.G. Fullana, H.l.n. Ternet, M. Freche, J.-L. Lacout, F. Rodriguez, Controlled release properties and final macroporosity of a pectin microspheres–calcium phosphate composite bone cement, Acta Biomater. 6(6) (2010) 2294-2300.

[484]W. Habraken, L. De Jonge, J. Wolke, L. Yubao, A. Mikos, J. Jansen, Introduction of gelatin microspheres into an injectable calcium phosphate cement, Journal of Biomedical Materials Research Part A: An Official Journal of The Society for Biomaterials, The Japanese Society for Biomaterials, and The Australian Society for Biomaterials and the Korean Society for Biomaterials 87(3) (2008) 643-655.

[485]W. Habraken, J. Wolke, A. Mikos, J. Jansen, PLGA microsphere/calcium phosphate cement composites for tissue engineering: in vitro release and degradation characteristics, J. Biomater. Sci. Polym. Ed. 19(9) (2008) 1171-1188.

[486]W.J. Habraken, Z. Zhang, J.G. Wolke, D.W. Grijpma, A.G. Mikos, J. Feijen, J.A. Jansen, Introduction of enzymatically degradable poly (trimethylene carbonate) microspheres into an injectable calcium phosphate cement, Biomaterials 29(16) (2008) 2464-2476.

[487]M. Li, X. Liu, X. Liu, B. Ge, K. Chen, Creation of macroporous calcium phosphate cements as bone substitutes by using genipin-crosslinked gelatin microspheres, J. Mater. Sci. Mater. Med. 20(4) (2009) 925-934.

[488]D.P. Link, J. Van den Dolder, W.J. Jurgens, J.G. Wolke, J.A. Jansen, Mechanical evaluation of implanted calcium phosphate cement incorporated with PLGA microparticles, Biomaterials 27(28) (2006) 4941-4947.

[489]D.P. Link, J. van den Dolder, J.J. van den Beucken, V.M. Cuijpers, J.G. Wolke, A.G. Mikos, J.A. Jansen, Evaluation of the biocompatibility of calcium phosphate cement/PLGA microparticle composites, Journal of Biomedical Materials Research Part A: An Official Journal of The Society for Biomaterials, The Japanese Society for Biomaterials, and The Australian Society for Biomaterials and the Korean Society for Biomaterials 87(3) (2008) 760-769.

[490]M. Markovic, S. Takagi, L.C. Chow, Formation of macropores in calcium phosphate cements through the use of mannitol crystals, (2001).

[491]P.Q. Ruhé, E.L. Hedberg, N.T. Padron, P.H. Spauwen, J.A. Jansen, A.G. Mikos, Biocompatibility and degradation of poly (dl-lactic-co-glycolic acid)/calcium phosphate cement composites, Journal of Biomedical Materials Research Part A: An Official Journal of The Society for Biomaterials, The Japanese Society for Biomaterials, and The Australian Society for Biomaterials and the Korean Society for Biomaterials 74(4) (2005) 533-544.

[492]R. Shimogoryo, T. Eguro, E. Kimura, M. Maruta, S. Matsuya, K. Ishikawa, Effects of added mannitol on the setting reaction and mechanical strength of apatite cement, Dent. Mater. 28(5) (2009) 627-633.

[493]C.G. Simon Jr, C.A. Khatri, S.A. Wight, F.W. Wang, Preliminary report on the biocompatibility of a moldable, resorbable, composite bone graft consisting of calcium phosphate cement and poly (lactide-co-glycolide) microspheres, Journal of Orthopaedic Research 20(3) (2002) 473-482.

[494]S. Tajima, Y. Kishi, M. Oda, M. Maruta, S. Matsuya, K. Ishikawa, Fabrication of biporous low-crystalline apatite based on mannitol dissolution from apatite cement, Dent. Mater. 25(3) (2006) 616-620.

[495]S. Takagi, L.C. Chow, Formation of macropores in calcium phosphate cement implants, J. Mater. Sci. Mater. Med. 12(2) (2001) 135-139.

[496]P.F. Tang, G. Li, J.F. Wang, Q.J. Zheng, Y. Wang, Development, characterization, and validation of porous carbonated hydroxyapatite bone cement, Journal of Biomedical Materials Research Part B: Applied Biomaterials: An Official Journal of The Society for Biomaterials, The Japanese Society for Biomaterials, and The Australian Society for Biomaterials and the Korean Society for Biomaterials 90(2) (2009) 886-893.

[497]A.C. Tas, Preparation of porous apatite granules from calcium phosphate cement, J. Mater. Sci. Mater. Med. 19(5) (2008) 2231-2239.

[498]A.C. Tas, Preparation of self-setting cement-based micro-and macroporous granules of carbonated apatitic calcium phosphate, Advances in Bioceramics and Biocomposites II, Ceramic Engineering and Science Proceedings 312 (2009) 49.

[499]D. Vazquez, S. Takagi, S. Frukhtbeyn, L.C. Chow, Effects of addition of mannitol crystals on the porosity and dissolution rates of a calcium phosphate cement, J. Res. Natl. Inst. Stand. Technol. 115(4) (2010) 225.

[500]X. Wang, J. Ye, X. Li, H. Dong, Production of in-situ macropores in an injectable calcium phosphate cement by introduction of cetyltrimethyl ammonium bromide, J. Mater. Sci. Mater. Med. 19(10) (2008) 3221-3225.

[501]H.H. Xu, M.D. Weir, E.F. Burguera, A.M. Fraser, Injectable and macroporous calcium phosphate cement scaffold, Biomaterials 27(24) (2006) 4279-4287.

[502]R. Del Real, E. Ooms, J. Wolke, M. Vallet-Regi, J. Jansen, In vivo bone response to porous calcium phosphate cement, Journal of Biomedical Materials Research Part A: An Official Journal of The Society for

Biomaterials, The Japanese Society for Biomaterials, and The Australian Society for Biomaterials and the Korean Society for Biomaterials 65(1) (2003) 30-36.

[503]S.d. Valle, N. Miño, F. Muñoz, A. González, J.A. Planell, M.-P. Ginebra, In vivo evaluation of an injectable macroporous calcium phosphate cement, J. Mater. Sci. Mater. Med. 18(2) (2007) 353-361.

[504]H. Guo, J. Su, J. Wei, H. Kong, C. Liu, Biocompatibility and osteogenicity of degradable Ca-deficient hydroxyapatite scaffolds from calcium phosphate cement for bone tissue engineering, Acta Biomater. 5(1) (2009) 268-278.

[505]W. Habraken, H. Liao, Z. Zhang, J. Wolke, D. Grijpma, A. Mikos, J. Feijen, J. Jansen, In vivo degradation of calcium phosphate cement incorporated into biodegradable microspheres, Acta Biomater. 6(6) (2010) 2200-2211.

[506]R.J. Klijn, J.J. van den Beucken, R.P. Félix Lanao, G. Veldhuis, S.C. Leeuwenburgh, J.G. Wolke, G.J. Meijer, J.A. Jansen, Three different strategies to obtain porous calcium phosphate cements: comparison of performance in a rat skull bone augmentation model, Tissue Engineering Part A 18(11-12) (2012) 1171-1182.

[507]R.F. Lanao, S. Leeuwenburgh, J. Wolke, J. Jansen, In vitro degradation rate of apatitic calcium phosphate cement with incorporated PLGA microspheres, Acta Biomater. 7(9) (2011) 3459-3468.

[508]D.P. Link, J. van den Dolder, J.J. van den Beucken, W. Habraken, A. Soede, O.C. Boerman, A.G. Mikos, J.A. Jansen, Evaluation of an orthotopically implanted calcium phosphate cement containing gelatin microparticles, Journal of Biomedical Materials Research Part A: An Official Journal of The Society for Biomaterials, The Japanese Society for Biomaterials, and The Australian Society for Biomaterials and the Korean Society for Biomaterials 90(2) (2009) 372-379.

[509]H.H. Xu, J.B. Quinn, S. Takagi, L.C. Chow, F.C. Eichmiller, Strong and macroporous calcium phosphate cement: Effects of porosity and fiber reinforcement on mechanical properties, Journal of Biomedical Materials Research: An Official Journal of The Society for Biomaterials, The Japanese Society for Biomaterials, and The Australian Society for Biomaterials and the Korean Society for Biomaterials 57(3) (2001) 457-466.

[510]W. Chen, H. Zhou, M. Tang, M.D. Weir, C. Bao, H.H. Xu, Gas-foaming calcium phosphate cement scaffold encapsulating human umbilical cord stem cells, Tissue Engineering Part A 18(7-8) (2012) 816-827.

[511]R. Del Real, J. Wolke, M. Vallet-Regı, J. Jansen, A new method to produce macropores in calcium phosphate cements, Biomaterials 23(17) (2002) 3673-3680.

[512]S. Hesaraki, F. Moztarzadeh, D. Sharifi, Formation of interconnected macropores in apatitic calcium phosphate bone cement with the use of an effervescent additive, Journal of Biomedical Materials Research Part A: An Official Journal of The Society for Biomaterials, The Japanese Society for Biomaterials, and The Australian Society for Biomaterials and the Korean Society for Biomaterials 83(1) (2007) 80-87.

[513]M. Bohner, F. Baumgart, Theoretical model to determine the effects of geometrical factors on the resorption of calcium phosphate bone substitutes, Biomaterials 25(17) (2004) 3569-3582.

[514]V. Karageorgiou, D. Kaplan, Porosity of 3D biomaterial scaffolds and osteogenesis, Biomaterials 26(27) (2005) 5474-5491.

[515]J. Lu, B. Flautre, K. Anselme, P. Hardouin, A. Gallur, M. Descamps, B. Thierry, Role of interconnections in porous bioceramics on bone recolonization in vitro and in vivo, J. Mater. Sci. Mater. Med. 10(2) (1999) 111-120.

[516]M.-C. von Doernberg, B. von Rechenberg, M. Bohner, S. Grünenfelder, G.H. van Lenthe, R. Müller, B. Gasser, R. Mathys, G. Baroud, J. Auer, In vivo behavior of calcium phosphate scaffolds with four different pore sizes, Biomaterials 27(30) (2006) 5186-5198.

[517]C. Klein, H. van der Lubbe, K. De Groot, A plastic composite of alginate with calcium phosphate granulate as implant material: an in vivo study, Biomaterials 8(4) (1987) 308-310.

[518]M. Chazono, T. Tanaka, H. Komaki, K. Fujii, Bone formation and bioresorption after implantation of injectable β-tricalcium phosphate granules–hyaluronate complex in rabbit bone defects, Journal of Biomedical Materials Research Part A: An Official Journal of The Society for Biomaterials, The Japanese Society for Biomaterials, and The Australian Society for Biomaterials and the Korean Society for Biomaterials 70(4) (2004) 542-549.

[519]A. Dupraz, J. Delecrin, A. Moreau, P. Pilet, N. Passuti, Long-term bone response to particulate injectable ceramic, Journal of Biomedical Materials Research: An Official Journal of The Society for Biomaterials, The Japanese Society for Biomaterials, and the Australian Society for Biomaterials 42(3) (1998) 368-375.

[520]G. Grimandi, P. Weiss, F. Millot, G. Daculsi, In vitro evaluation of a new injectable calcium phosphate material, Journal of Biomedical Materials Research: An Official Journal of The Society for Biomaterials, The Japanese Society for Biomaterials, and the Australian Society for Biomaterials 39(4) (1998) 660-666.

[521]U. Gbureck, K. Spatz, R. Thull, J. Barralet, Rheological enhancement of mechanically activated α-tricalcium phosphate cements, Journal of Biomedical Materials Research Part B: Applied Biomaterials: An Official Journal of The Society for Biomaterials, The Japanese Society for Biomaterials, and The Australian Society for Biomaterials and the Korean Society for Biomaterials 73(1) (2005) 1-6.
[522]M. Bohner, R. Luginbühl, C. Reber, N. Doebelin, G. Baroud, E. Conforto, A physical approach to modify the hydraulic reactivity of α-tricalcium phosphate powder, Acta Biomater. 5(9) (2009) 3524-3535.
[523]K.L. Low, S.H. Tan, S.H.S. Zein, J.A. Roether, V. Mourino, A.R. Boccaccini, Calcium phosphate-based composites as injectable bone substitute materials, Journal of Biomedical Materials Research Part B: Applied Biomaterials 94(1) (2010) 273-286.
[524]C. Durucan, P. Brown, Reactivity of α-tricalcium phosphate, Journal of Materials Science 37(5) (2002) 963-969.
[525]C. Liu, W. Shen, Effect of crystal seeding on the hydration of calcium phosphate cement, J. Mater. Sci. Mater. Med. 8(12) (1997) 803-807.
[526]Q. Yang, T. Troczynski, D.-M. Liu, Influence of apatite seeds on the synthesis of calcium phosphate cement, Biomaterials 23(13) (2002) 2751-2760.
[527]O. Bermudez, M. Boltong, F. Driessens, J. Planell, Compressive strength and diametral tensile strength of some calcium-orthophosphate cements: a pilot study, J. Mater. Sci. Mater. Med. 4(4) (1993) 389-393.
[528]O. Bermudez, M. Boltong, F. Driessens, J. Planell, Development of some calcium phosphate cements from combinations of α-TCP, MCPM and CaO, J. Mater. Sci. Mater. Med. 5(3) (1994) 160-163.
[529]C. Liu, W. Shen, Y. Gu, L. Hu, Mechanism of the hardening process for a hydroxyapatite cement, Journal of Biomedical Materials Research: An Official Journal of The Society for Biomaterials and The Japanese Society for Biomaterials 35(1) (1997) 75-80.
[530]K. Ishikawa, S. Takagi, L.C. Chow, Y. Ishikawa, Properties and mechanisms of fast-setting calcium phosphate cements, J. Mater. Sci. Mater. Med. 6(9) (1995) 528-533.
[531]E. Fernández, M. Boltong, M. Ginebra, O. Bermúdez, F. Driessens, J. Planell, Common ion effect on some calcium phosphate cements, Clin. Mater. 16(2) (1994) 99-103.
[532]I. Khairoun, M. Boltong, F. Driessens, J. Planell, Effect of calcium carbonate on clinical compliance of apatitic calcium phosphate bone cement, J. Biomed. Mater. Res. 38(4) (1997) 356-360.
[533]K. Lilley, U. Gbureck, J. Knowles, D. Farrar, J. Barralet, Cement from magnesium substituted hydroxyapatite, J. Mater. Sci. Mater. Med. 16(5) (2005) 455-460.
[534]E. Fernandez, F. Gil, S. Best, M. Ginebra, F. Driessens, J. Planell, Improvement of the mechanical properties of new calcium phosphate bone cements in the CaHPO4-α-Ca3 (PO4) 2 system: Compressive strength and microstructural development, Journal of Biomedical Materials Research: An Official Journal of The Society for Biomaterials, The Japanese Society for Biomaterials, and the Australian Society for Biomaterials 41(4) (1998) 560-567.
[535]R.W. Bucholz, Nonallograft osteoconductive bone graft substitutes, Clinical Orthopaedics and Related Research® 395 (2002) 44-52.
[536]J.E. Barralet, M. Hofmann, L.M. Grover, U. Gbureck, High-strength apatitic cement by modification with α-hydroxy acid salts, Adv. Mater. 15(24) (2003) 2091-2094.
[537]J. Barralet, L. Grover, U. Gbureck, Ionic modification of calcium phosphate cement viscosity. Part II: hypodermic injection and strength improvement of brushite cement, Biomaterials 25(11) (2004) 2197-2203.
[538]H.M. Myers, Structure-activity relationships (SAR) of hydroxyapatite-binding molecules, Calcif. Tissue Int. 40(6) (1987) 344-348.
[539]L. Brecević, H. Füredi-Milhofer, Precipitation of calcium phosphates from electrolyte solutions. V. The influence of citrate ions, Calcif. Tissue Int. 28(2) (1979) 131-136.
[540]K. Tenhuisen, P. Brown, The effects of citric and acetic acids on the formation of calcium-deficient hydroxyapatite at 38 C, J. Mater. Sci. Mater. Med. 5(5) (1994) 291-298.
[541]S. Meininger, C. Blum, M. Schamel, J.E. Barralet, A. Ignatius, U. Gbureck, Phytic acid as alternative setting retarder enhanced biological performance of dicalcium phosphate cement in vitro, Sci. Rep. 7(1) (2017) 558.
[542]L. Medvecky, R. Stulajterova, M. Giretova, T. Sopcak, Z. Molcanova, K. Koval, Enzymatically hardened calcium phosphate biocement with phytic acid addition, J. Mater. Sci. Mater. Med. 31 (2020) 54.
[543]F. Grases, M. Ramis, A. Costa-Bauza, Effects of phytate and pyrophosphate on brushite and hydroxyapatite crystallization, Urol. Res. 28(2) (2000) 136-140.
[544]T. Konishi, Z. Zhuang, M. Mizumoto, M. Honda, M. Aizawa, Fabrication of chelate-setting cement from hydroxyapatite powder prepared by simultaneously grinding and surface-modifying with sodium inositol hexaphosphate and their material properties, J. Ceram. Soc. Jpn. 120(1401) (2012) 159-165.

[545]S. Takahashi, T. Konishi, K. Nishiyama, M. Mizumoto, M. Honda, Y. Horiguchi, K. Oribe, M. Aizawa, Fabrication of novel bioresorbable β-tricalcium phosphate cement on the basis of chelate-setting mechanism of inositol phosphate and its evaluation, J. Ceram. Soc. Jpn. 119(1385) (2011) 35-42.
[546]L. Johnson, M. Tate, Structure of" phytic acids", Can. J. Chem. 47(1) (1969) 63-73.
[547]P. Vohra, G. Gray, F. Kratzer, Phytic acid-metal complexes, Proceedings of the Society for Experimental Biology and Medicine 120(2) (1965) 447-449.
[548]C. Martin, W. Evans, Phytic acid-metal ion interactions. II. The effect of pH on Ca (II) binding, J. Inorg. Biochem. 27(1) (1986) 17-30.
[549]B. Luttrell, The biological relevance of the binding of calcium ions by inositol phosphates, J. Biol. Chem. 268(3) (1993) 1521-1524.
[550]H. Fleisch, R. Russell, S. Bisaz, J. Termine, A. Posner, Influence of pyrophosphate on the transformation of amorphous to crystalline calcium phosphate, Calcif. Tissue Res. 2(1) (1968) 49-59.
[551]D. Fernández, J. Ortega-Castro, J. Frau, Theoretical study of the HAP crystal growth inhibition potency of pyrophosphate, etidronate, citrate and phytate. Deciphered the adsorbed conformation of phytate on the HAP (001) surface, Appl. Surf. Sci. 408 (2017) 110-116.
[552]T. Vasudevan, P. Somasundaran, C. Howie-Meyers, D. Elliott, K. Ananthapadmanabhan, Interaction of pyrophosphate with calcium phosphates, Langmuir 10(1) (1994) 320-325.
[553]J. Kroesbergen, W. Gelsema, C. De Ligny, 99mTc bone scanning agents—I. Influence of experimental conditions on the formation and gel chromatography of 99mTc (Sn) pyrophosphate complexes, Int. J. Nucl. Med. Biol. 12(2) (1985) 83-88.
[554]J. Kroesbergen, A. van Steijn, W. Gelsema, C. De Ligny, 99mTc bone scanning agents--II. Adsorption of 99mTc (Sn) pyrophosphate complexes on the mineral phase of bone, Int. J. Nucl. Med. Biol. 12(6) (1986) 411-417.
[555]R. Holdich, Colloids and agglomeration, Fundamentals of Particle Technology, Midland Information Technology and Publishing (2002).
[556]S.B. Johnson, G.V. Franks, P.J. Scales, D.V. Boger, T.W. Healy, Surface chemistry–rheology relationships in concentrated mineral suspensions, Int. J. Miner. Process. 58(1-4) (2000) 267-304.
[557]B. Derjaguin, L. Landau, Theory of the stability of strongly charged lyophobic sols and of the adhesion of strongly charged particles in solutions of electrolytes, Prog. Surf. Sci. 43(1-4) (1993) 30-59.
[558]E.J.W. Verwey, Theory of the stability of lyophobic colloids, The Journal of Physical Chemistry 51(3) (1947) 631-636.
[559]S. Verma, D. Burgess, Solid nanosuspensions: the emerging technology and pharmaceutical applications as nanomedicine, Pharmaceutical Suspensions, Springer2010, pp. 285-318.
[560]A. Concha, Particle aggregation by coagulation and flocculation, Solid-Liquid Separation in the Mining Industry, Springer2014, pp. 143-172.
[561]K. Ishikawa, Y. Miyamoto, M. Takechi, T. Toh, M. Kon, M. Nagayama, K. Asaoka, Non-decay type fast-setting calcium phosphate cement: Hydroxyapatite putty containing an increased amount of sodium alginate, Journal of Biomedical Materials Research: An Official Journal of The Society for Biomaterials and The Japanese Society for Biomaterials 36(3) (1997) 393-399.
[562]M. Alkhraisat, C. Rueda, F. Marino, J. Torres, L. Jerez, U. Gbureck, E. Cabarcos, The effect of hyaluronic acid on brushite cement cohesion, Acta Biomater. 5(8) (2009) 3150-3156.
[563]A. Cherng, S. Takagi, L. Chow, Effects of hydroxypropyl methylcellulose and other gelling agents on the handling properties of calcium phosphate cement, Journal of Biomedical Materials Research: An Official Journal of The Society for Biomaterials and The Japanese Society for Biomaterials 35(3) (1997) 273-277.
[564]W. Liu, J. Zhang, P. Weiss, F. Tancret, J.-M. Bouler, The influence of different cellulose ethers on both the handling and mechanical properties of calcium phosphate cements for bone substitution, Acta Biomater. 9(3) (2013) 5740-5750.
[565]H. Liu, H. Li, W. Cheng, Y. Yang, M. Zhu, C. Zhou, Novel injectable calcium phosphate/chitosan composites for bone substitute materials, Acta Biomater. 2(5) (2006) 557-565.
[566]S. Takagi, L.C. Chow, S. Hirayama, F.C. Eichmiller, Properties of elastomeric calcium phosphate cement–chitosan composites, Dent. Mater. 19(8) (2003) 797-804.
[567]J.A. Burdick, G.D. Prestwich, Hyaluronic acid hydrogels for biomedical applications, Adv. Mater. 23(12) (2011) H41-H56.
[568]E.F. Burguera, H.H. Xu, M.D. Weir, Injectable and rapid-setting calcium phosphate bone cement with dicalcium phosphate dihydrate, Journal of Biomedical Materials Research Part B: Applied Biomaterials: An Official Journal of The Society for Biomaterials, The Japanese Society for Biomaterials, and The Australian Society for Biomaterials and the Korean Society for Biomaterials 77(1) (2006) 126-134.

[569]H. Andrianjatovo, J. Lemaitre, Effects of polysaccharides on the cement properties in the monocalcium phosphate/β-tricalcium phosphate system, Innovation et technologie en biologie et médecine 16 (1995) 140-147.

[570]A. Yokoyama, H. Matsuno, S. Yamamoto, T. Kawasaki, T. Kohgo, M. Uo, F. Watari, M. Nakasu, Tissue response to a newly developed calcium phosphate cement containing succinic acid and carboxymethyl-chitin, Journal of Biomedical Materials Research Part A: An Official Journal of The Society for Biomaterials, The Japanese Society for Biomaterials, and The Australian Society for Biomaterials and the Korean Society for Biomaterials 64(3) (2003) 491-501.

[571]M.A. Jyoti, Y.K. Min, B.-T. Lee, H.-Y. Song, In vitro bioactivity and biocompatibility of calcium phosphate cements using Hydroxy-propyl-methyl-Cellulose (HPMC), Appl. Surf. Sci. 257(5) (2010) 1533-1539.

[572]A. Bigi, S. Panzavolta, K. Rubini, Setting mechanism of a biomimetic bone cement, Chem. Mater. 16(19) (2004) 3740-3745.

[573]A. Bigi, S. Panzavolta, L. Sturba, P. Torricelli, M. Fini, R. Giardino, Normal and osteopenic bone-derived osteoblast response to a biomimetic gelatin–calcium phosphate bone cement, Journal of Biomedical Materials Research Part A: An Official Journal of The Society for Biomaterials, The Japanese Society for Biomaterials, and The Australian Society for Biomaterials and the Korean Society for Biomaterials 78(4) (2006) 739-745.

[574]A. Bigi, P. Torricelli, M. Fini, B. Bracci, S. Panzavolta, L. Sturba, R. Giardino, A biomimetic gelatin-calcium phosphate bone cement, The International Journal of Artificial Organs 27(8) (2004) 664-673.

[575]Y. Fujishiro, K. Takahashi, T. Sato, Preparation and compressive strength of α-tricalcium phosphate/gelatin gel composite cement, Journal of Biomedical Materials Research: An Official Journal of The Society for Biomaterials, The Japanese Society for Biomaterials, and The Australian Society for Biomaterials and the Korean Society for Biomaterials 54(4) (2001) 525-530.

[576]S. Panzavolta, P. Torricelli, L. Sturba, B. Bracci, R. Giardino, A. Bigi, Setting properties and in vitro bioactivity of strontium-enriched gelatin–calcium phosphate bone cements, Journal of Biomedical Materials Research Part A: An Official Journal of The Society for Biomaterials, The Japanese Society for Biomaterials, and The Australian Society for Biomaterials and the Korean Society for Biomaterials 84(4) (2008) 965-972.

[577]M.-Y. Shie, D.C.-H. Chen, C.-Y. Wang, T.-Y. Chiang, S.-J. Ding, Immersion behavior of gelatin-containing calcium phosphate cement, Acta Biomater. 4(3) (2008) 646-655.

[578]L.-X. Xu, X.-T. Shi, Y.-P. Wang, Z.-L. Shi, Performance of calcium phosphate bone cement using chitosan and gelatin as well as citric acid as hardening liquid, 中國組織工程研究與臨床康復 12(32) (2008) 6381-6384.

[579]W.-C. Chen, C.-P. Ju, J.-C. Wang, C.-C. Hung, J.-H.C. Lin, Brittle and ductile adjustable cement derived from calcium phosphate cement/polyacrylic acid composites, Dent. Mater. 24(12) (2008) 1616-1622.

[580]A. Majekodunmi, S. Deb, Poly (acrylic acid) modified calcium phosphate cements: the effect of the composition of the cement powder and of the molecular weight and concentration of the polymeric acid, J. Mater. Sci. Mater. Med. 18(9) (2007) 1883-1888.

[581]A. Majekodunmi, S. Deb, J. Nicholson, Effect of molecular weight and concentration of poly (acrylic acid) on the formation of a polymeric calcium phosphate cement, J. Mater. Sci. Mater. Med. 14(9) (2003) 747-752.

[582]P.D. Costantino, C.D. Friedman, K. Jones, L.C. Chow, H.J. Pelzer, G.A. Sisson, Hydroxyapatite cement: I. Basic chemistry and histologic properties, Archives of Otolaryngology–Head & Neck Surgery 117(4) (1991) 379-384.

[583]Y. Hong, J. Wang, C. Hong, W. Brown, L. Chow, The periapical tissue reactions to a calcium phosphate cement in the teeth of monkeys, J. Biomed. Mater. Res. 25(4) (1991) 485-498.

[584]J.P. Schmitz, J.O. Hollinger, S.B. Milam, Reconstruction of bone using calcium phosphate bone cements: a critical review, Journal of Oral and Maxillofacial Surgery 57(9) (1999) 1122-1126.

[585]K. Kurashina, H. Kurita, M. Hirano, A. Kotani, C. Klein, K. De Groot, In vivo study of calcium phosphate cements: implantation of an α-tricalcium phosphate/dicalcium phosphate dibasic/tetracalcium phosphate monoxide cement paste, Biomaterials 18(7) (1997) 539-543.

[586]C.D. Friedman, P.D. Costantino, S. Takagi, L.C. Chow, BoneSource™ hydroxyapatite cement: a novel biomaterial for craniofacial skeletal tissue engineering and reconstruction, J. Biomed. Mater. Res. 43(4) (1998) 428-432.

[587]E. Ooms, J. Wolke, M. Van de Heuvel, B. Jeschke, J. Jansen, Histological evaluation of the bone response to calcium phosphate cement implanted in cortical bone, Biomaterials 24(6) (2003) 989-1000.

[588]J. Jansen, J. De Ruijter, H. Schaeken, J. Van der Waerden, J. Planell, F. Driessens, Evaluation of tricalciumphosphate/hydroxyapatite cement for tooth replacement: an experimental animal study, J. Mater. Sci. Mater. Med. 6(11) (1995) 653-657.

[589]S. Larsson, T.W. Bauer, Use of injectable calcium phosphate cement for fracture fixation: a review, Clinical Orthopaedics and Related Research® 395 (2002) 23-32.
[590]R. Oshtory, D.P. Lindsey, N.J. Giori, F.M. Mirza, Bioabsorbable tricalcium phosphate bone cement strengthens fixation of suture anchors, Clinical Orthopaedics and Related Research® 468(12) (2010) 3406-3412.
[591]H. El Briak, D. Durand, P. Boudeville, Study of a hydraulic DCPA/CaO-based cement for dental applications, J. Mater. Sci. Mater. Med. 19(2) (2008) 737-744.
[592]Z. Huan, J. Chang, Novel tricalcium silicate/monocalcium phosphate monohydrate composite bone cement, Journal of Biomedical Materials Research Part B: Applied Biomaterials: An Official Journal of The Society for Biomaterials, The Japanese Society for Biomaterials, and The Australian Society for Biomaterials and the Korean Society for Biomaterials 82(2) (2007) 352-359.
[593]P. Michaïlesco, M. Kouassi, H. El Briak, A. Armynot, P. Boudeville, Antimicrobial activity and tightness of a DCPD–CaO-based hydraulic calcium phosphate cement for root canal filling, Journal of Biomedical Materials Research Part B: Applied Biomaterials: An Official Journal of The Society for Biomaterials, The Japanese Society for Biomaterials, and The Australian Society for Biomaterials and the Korean Society for Biomaterials 74(2) (2005) 760-767.
[594]S. Serraj, P. Michaïlesco, J. Margerit, B. Bernard, P. Boudeville, Study of a hydraulic calcium phosphate cement for dental applications, J. Mater. Sci. Mater. Med. 13(1) (2002) 125-131.
[595]U. Gbureck, O. Knappe, N. Hofmann, J.E. Barralet, Antimicrobial properties of nanocrystalline tetracalcium phosphate cements, Journal of Biomedical Materials Research Part B: Applied Biomaterials: An Official Journal of The Society for Biomaterials, The Japanese Society for Biomaterials, and The Australian Society for Biomaterials and the Korean Society for Biomaterials 83(1) (2007) 132-137.
[596]S. Sethuraman, L.S. Nair, S. El-Amin, M.T.N. Nguyen, Y.E. Greish, J.D. Bender, P.W. Brown, H.R. Allcock, C.T. Laurencin, Novel low temperature setting nanocrystalline calcium phosphate cements for bone repair: Osteoblast cellular response and gene expression studies, Journal of Biomedical Materials Research Part A: An Official Journal of The Society for Biomaterials, The Japanese Society for Biomaterials, and The Australian Society for Biomaterials and the Korean Society for Biomaterials 82(4) (2007) 884-891.
[597]A. Sugawara, K. Fujikawa, K. Kusama, M. Nishiyama, S. Murai, S. Takagi, L.C. Chow, Histopathologic reaction of a calcium phosphate cement for alveolar ridge augmentation, Journal of Biomedical Materials Research: An Official Journal of The Society for Biomaterials, The Japanese Society for Biomaterials, and The Australian Society for Biomaterials and the Korean Society for Biomaterials 61(1) (2002) 47-52.
[598]A. Sugawara, L.C. Chow, S. Takagi, H. Chohayeb, In vitro evaluation of the sealing ability of a calcium phosphate cement when used as a root canal sealer-filler, J. Endod. 16(4) (1990) 162-165.
[599]J. Noetzel, K. Özer, B.-H. Reisshauer, A. Anil, R. Rössler, K. Neumann, A.M. Kielbassa, Tissue responses to an experimental calcium phosphate cement and mineral trioxide aggregate as materials for furcation perforation repair: a histological study in dogs, Clin. Oral Investig. 10(1) (2006) 77-83.
[600]W. Zhang, X.F. Walboomers, J.A. Jansen, The formation of tertiary dentin after pulp capping with a calcium phosphate cement, loaded with PLGA microparticles containing TGF-β1, Journal of Biomedical Materials Research Part A: An Official Journal of The Society for Biomaterials, The Japanese Society for Biomaterials, and The Australian Society for Biomaterials and the Korean Society for Biomaterials 85(2) (2008) 439-444.
[601]S.-K. Lee, S.-K. Lee, S.-I. Lee, J.-H. Park, J.-H. Jang, H.-W. Kim, E.-C. Kim, Effect of calcium phosphate cements on growth and odontoblastic differentiation in human dental pulp cells, J. Endod. 36(9) (2010) 1537-1542.
[602]H. Chaung, C. Hong, C. Chiang, S. Lin, Y. Kuo, W. Lan, C. Hsieh, Comparison of calcium phosphate cement mixture and pure calcium hydroxide as direct pulp-capping agents, Journal of the Formosan Medical Association 95(7) (1996) 545-550.
[603]L. Comuzzi, E. Ooms, J.A. Jansen, Injectable calcium phosphate cement as a filler for bone defects around oral implants: an experimental study in goats, Clin. Oral Implants Res. 13(3) (2002) 304-311.
[604]V. Arısan, A. Anıl, J. Wolke, K. Özer, The effect of injectable calcium phosphate cement on bone anchorage of titanium implants: an experimental feasibility study in dogs, Int. J. Oral Maxillofac. Surg. 39(5) (2010) 463-468.
[605]A.J. Ambard, L. Mueninghoff, Calcium phosphate cement: review of mechanical and biological properties, Journal of Prosthodontics 15(5) (2006) 321-328.
[606]M.L. Shindo, P.D. Costantino, C.D. Friedman, L.C. Chow, Facial skeletal augmentation using hydroxyapatite cement, Archives of Otolaryngology–Head & Neck Surgery 119(2) (1993) 185-190.
[607]J.E. Losee, J. Karmacharya, F.H. Gannon, A.E. Slemp, G. Ong, O. Hunenko, A.D. Gorden, S.P. Bartlett, R.E. Kirschner, Reconstruction of the immature craniofacial skeleton with a carbonated calcium phosphate bone cement: Interaction with bioresorbable mesh, J. Craniofac. Surg. 14(1) (2003) 117-124.

[608]M. Vlad, L. Del Valle, I. Poeata, M. Barracó, J. López, R. Torres, E. Fernández, Injectable iron-modified apatitic bone cement intended for kyphoplasty: cytocompatibility study, J. Mater. Sci. Mater. Med. 19(12) (2008) 3575-3583.

[609]P. Liverneaux, Osteoporotic distal radius curettage–filling with an injectable calcium phosphate cement. A cadaveric study, Eur. J. Orthop. Surg. Traumatol. 15(1) (2005) 1-6.

[610]P. Liverneaux, P. Vernet, C. Robert, P. Diacono, Cement pinning of osteoporotic distal radius fractures with an injectable calcium phosphate bone substitute: report of 6 cases, Eur. J. Orthop. Surg. Traumatol. 16(1) (2006) 10-16.

[611]C. Ryf, S. Goldhahn, M. Radziejowski, M. Blauth, B. Hanson, A new injectable brushite cement: first results in distal radius and proximal tibia fractures, Eur. J. Trauma Emerg. Surg. 35(4) (2009) 389-396.

[612]D.B. Thordarson, T.P. Hedman, D.N. Yetkinler, E. Eskander, T. Lawrence, R.D. Poser, Superior compressive strength of a calcaneal fracture construct augmented with remodelable cancellous bone cement, JBJS 81(2) (1999) 239-246.

[613]S.B. Goodman, T.W. Bauer, D. Carter, P.P. Casteleyn, S.A. Goldstein, R.F. Kyle, S. Larsson, C. Stankewich, M.F. Swiontkowski, A.F. Tencer, Norian SRS cement augmentation in hip fracture treatment. Laboratory and initial clinical results, Clinical Orthopaedics and Related Research® (348) (1998) 42-50.

[614]C. Stankewich, M.F. Swiontkowski, A.F. Tencer, D.N. Yetkinler, R.D. Poser, Augmentation of femoral neck fracture fixation with an injectable calcium-phosphate bone mineral cement, Journal of Orthopaedic Research 14(5) (1996) 786-793.

[615]B. Bai, L.M. Jazrawi, F.J. Kummer, J.M. Spivak, The use of an injectable, biodegradable calcium phosphate bone substitute for the prophylactic augmentation of osteoporotic vertebrae and the management of vertebral compression fractures, Spine 24(15) (1999) 1521.

[616]W. Horstmann, C. Verheyen, R. Leemans, An injectable calcium phosphate cement as a bone-graft substitute in the treatment of displaced lateral tibial plateau fractures, Injury 34(2) (2003) 141-144.

[617]J. Keating, C. Hajducka, J. Harper, Minimal internal fixation and calcium-phosphate cement in the treatment of fractures of the tibial plateau: a pilot study, The Journal of Bone and Joint Surgery. British volume 85(1) (2003) 68-73.

[618]D. Simpson, J. Keating, Outcome of tibial plateau fractures managed with calcium phosphate cement, Injury 35(9) (2004) 913-918.

[619]R.D. Welch, H. Zhang, D.G. Bronson, Experimental tibial plateau fractures augmented with calcium phosphate cement or autologous bone graft, JBJS 85(2) (2003) 222-231.

[620]W. Cho, C. Wu, S. Erkan, M.M. Kang, A.A. Mehbod, E.E. Transfeldt, The effect on the pullout strength by the timing of pedicle screw insertion after calcium phosphate cement injection, Clinical Spine Surgery 24(2) (2011) 116-120.

[621]D.C. Moore, R.S. Maitra, L.A. Farjo, G.P. Graziano, S.A. Goldstein, Restoration of pedicle screw fixation with an in situ setting calcium phosphate cement, Spine 22(15) (1997) 1696-1705.

[622]L.E. Mermelstein, R.F. McLain, S.A. Yerby, Reinforcement of thoracolumbar burst fractures with calcium phosphate cement: a biomechanical study, Spine 23(6) (1998) 664-670.

[623]L. Mermelstein, L. Chow, C. Friedman, J. Crisco Iii, The reinforcement of cancellous bone screws with calcium phosphate cement, J. Orthop. Trauma 10(1) (1996) 15-20.

[624]V.A. Stadelmann, E. Bretton, A. Terrier, P. Procter, D.P. Pioletti, Calcium phosphate cement augmentation of cancellous bone screws can compensate for the absence of cortical fixation, J. Biomech. 43(15) (2010) 2869-2874.

[625]P. Liverneaux, R. Khallouk, Calcium phosphate cement in wrist arthrodesis: three cases, J. Orthop. Sci. 11(3) (2006) 289-293.

[626]E. Ooms, J. Wolke, J. Van der Waerden, J. Jansen, Use of injectable calcium-phosphate cement for the fixation of titanium implants: An experimental study in goats, Journal of Biomedical Materials Research Part B: Applied Biomaterials: An Official Journal of The Society for Biomaterials, The Japanese Society for Biomaterials, and The Australian Society for Biomaterials and the Korean Society for Biomaterials 66(1) (2003) 447-456.

[627]G. Lewis, Injectable bone cements for use in vertebroplasty and kyphoplasty: State-of-the-art review, Journal of Biomedical Materials Research Part B: Applied Biomaterials: An Official Journal of The Society for Biomaterials, The Japanese Society for Biomaterials, and The Australian Society for Biomaterials and the Korean Society for Biomaterials 76(2) (2006) 456-468.

[628]S.M. Belkoff, J.M. Mathis, L.E. Jasper, H. Deramond, An ex vivo biomechanical evaluation of a hydroxyapatite cement for use with vertebroplasty, Spine 26(14) (2001) 1542-1546.

[629]P.F. Heini, U. Berlemann, M. Kaufmann, K. Lippuner, C. Fankhauser, P. van Landuyt, Augmentation of mechanical properties in osteoporotic vertebral bones–a biomechanical investigation of vertebroplasty efficacy with different bone cements, Eur. Spine J. 10(2) (2001) 164-171.

[630]T. Hisatome, Y. Yasunaga, Y. Ikuta, Y. Fujimoto, Effects on articular cartilage of subchondral replacement with polymethylmethacrylate and calcium phosphate cement, Journal of Biomedical Materials Research: An Official Journal of The Society for Biomaterials, The Japanese Society for Biomaterials, and The Australian Society for Biomaterials and the Korean Society for Biomaterials 59(3) (2002) 490-498.

[631]A.J. Khanna, S. Lee, M. Villarraga, J. Gimbel, D. Steffey, J. Schwardt, Biomechanical evaluation of kyphoplasty with calcium phosphate cement in a 2-functional spinal unit vertebral compression fracture model, The Spine Journal 8(5) (2008) 770-777.

[632]M. Libicher, J. Hillmeier, U. Liegibel, U. Sommer, W. Pyerin, M. Vetter, H.-P. Meinzer, I. Grafe, P. Meeder, G. Nöldge, Osseous integration of calcium phosphate in osteoporotic vertebral fractures after kyphoplasty: initial results from a clinical and experimental pilot study, Osteoporosis International 17(8) (2006) 1208-1215.

[633]T.-H. Lim, G.T. Brebach, S.M. Renner, W.-J. Kim, J.G. Kim, R.E. Lee, G.B. Andersson, H.S. An, Biomechanical evaluation of an injectable calcium phosphate cement for vertebroplasty, Spine 27(12) (2002) 1297-1302.

[634]S. Tomita, A. Kin, M. Yazu, M. Abe, Biomechanical evaluation of kyphoplasty and vertebroplasty with calcium phosphate cement in a simulated osteoporotic compression fracture, J. Orthop. Sci. 8(2) (2003) 192-197.

[635]X. Zhu, Z. Zhang, H. Mao, D. Geng, G. Wang, M. Gan, H. Yang, Biomechanics of calcium phosphate cement in vertebroplasty, J. Clin. Rehabil. Tissue Eng. Res 12 (2008) 8071-8074.

[636]M. Bohner, J. Lemaître, P. Van Landuyt, P.-Y. Zambelli, H.P. Merkle, B. Gander, Gentamicin-loaded hydraulic calcium phosphate bone cement as antibiotic delivery system, J. Pharm. Sci. 86(5) (1997) 565-572.

[637]Z. Fei, Y. Hu, D. Wu, H. Wu, R. Lu, J. Bai, H. Song, Preparation and property of a novel bone graft composite consisting of rhBMP-2 loaded PLGA microspheres and calcium phosphate cement, J. Mater. Sci. Mater. Med. 19(3) (2008) 1109-1116.

[638]A. Kamegai, N. Shimamura, K. Naitou, K. Nagahara, N. Kanematsu, M. Mori, Bone formation under the influence of bone morphogenetic protein/self-setting apatite cement composite as a delivery system, Bio-Medical Materials and Engineering 4(4) (1994) 291-307.

[639]D. Le Nihouannen, S.A. Hacking, U. Gbureck, S.V. Komarova, J.E. Barralet, The use of RANKL-coated brushite cement to stimulate bone remodelling, Biomaterials 29(22) (2008) 3253-3259.

[640]D. Li, H. Fan, X. Zhu, Y. Tan, W. Xiao, J. Lu, Y. Xiao, J. Chen, X. Zhang, Controllable release of salmon-calcitonin in injectable calcium phosphate cement modified by chitosan oligosaccharide and collagen polypeptide, J. Mater. Sci. Mater. Med. 18(11) (2007) 2225-2231.

[641]S. Panzavolta, P. Torricelli, B. Bracci, M. Fini, A. Bigi, Alendronate and Pamidronate calcium phosphate bone cements: setting properties and in vitro response of osteoblast and osteoclast cells, J. Inorg. Biochem. 103(1) (2009) 101-106.

[642]D. Yu, J. Wong, Y. Matsuda, J.L. Fox, W.I. Higuchi, M. Otsuka, Self-setting hydroxyapatite cement: A novel skeletal drug-delivery system for antibiotics, J. Pharm. Sci. 81(6) (1992) 529-531.

[643]X. Du, S. Fu, Y. Zhu, 3D printing of ceramic-based scaffolds for bone tissue engineering: an overview, Journal of Materials Chemistry B 6(27) (2018) 4397-4412.

[644]S. Shaunak, B. S Dhinsa, W. S Khan, The role of 3D modelling and printing in orthopaedic tissue engineering: a review of the current literature, Curr. Stem Cell Res. Ther. 12(3) (2017) 225-232.

[645]M. Zhu, J. Zhang, S. Zhao, Y. Zhu, Three-dimensional printing of cerium-incorporated mesoporous calcium-silicate scaffolds for bone repair, J. Endod. 51(2) (2016) 836-844.

[646]P. Tack, J. Victor, P. Gemmel, L. Annemans, 3D-printing techniques in a medical setting: a systematic literature review, Biomed. Eng. Online 15(1) (2016) 1-21.

[647]M. Guvendiren, J. Molde, R. Soares, J. Kohn, Designing biomaterials for 3D printing. ACS Biomater Sci Eng 2: 1679–1693, 2016.

[648]I. Zein, D.W. Hutmacher, K.C. Tan, S.H. Teoh, Fused deposition modeling of novel scaffold architectures for tissue engineering applications, Biomaterials 23(4) (2002) 1169-1185.

[649]J.M. Williams, A. Adewunmi, R.M. Schek, C.L. Flanagan, P.H. Krebsbach, S.E. Feinberg, S.J. Hollister, S. Das, Bone tissue engineering using polycaprolactone scaffolds fabricated via selective laser sintering, Biomaterials 26(23) (2005) 4817-4827.

[650]K. Shahzad, J. Deckers, S. Boury, B. Neirinck, J.-P. Kruth, J. Vleugels, Preparation and indirect selective laser sintering of alumina/PA microspheres, Ceram. Int. 38(2) (2012) 1241-1247.

[651]B. Derby, Inkjet printing of functional and structural materials: fluid property requirements, feature stability, and resolution, Annual Review of Materials Research 40 (2010) 395-414.

[652]G.-H. Wu, S.-h. Hsu, polymeric-based 3D printing for tissue engineering, Journal of Medical and Biological Engineering 35(3) (2015) 285-292.
[653]J. Zhang, S. Zhao, Y. Zhu, Y. Huang, M. Zhu, C. Tao, C. Zhang, Three-dimensional printing of strontium-containing mesoporous bioactive glass scaffolds for bone regeneration, Acta Biomater. 10(5) (2014) 2269-2281.
[654]M. Zhu, T. Huang, X. Du, Y. ZHU, Progress of the 3D printing technology for biomaterials, Journal of University of Shanghai for Science and Technology 39(5) (2017) 473-489.
[655]T. Almela, I.M. Brook, K. Khoshroo, M. Rasoulianboroujeni, F. Fahimipour, M. Tahriri, E. Dashtimoghadam, A. El-Awa, L. Tayebi, K. Moharamzadeh, Simulation of cortico-cancellous bone structure by 3D printing of bilayer calcium phosphate-based scaffolds, Bioprinting 6 (2017) 1-7.
[656]A. Butscher, M. Bohner, N. Doebelin, L. Galea, O. Loeffel, R. Müller, Moisture based three-dimensional printing of calcium phosphate structures for scaffold engineering, Acta Biomater. 9(2) (2013) 5369-5378.
[657]A. Butscher, M. Bohner, N. Doebelin, S. Hofmann, R. Müller, New depowdering-friendly designs for three-dimensional printing of calcium phosphate bone substitutes, Acta Biomater. 9(11) (2013) 9149-9158.
[658]A. Butscher, M. Bohner, C. Roth, A. Ernstberger, R. Heuberger, N. Doebelin, P.R. Von Rohr, R. Müller, Printability of calcium phosphate powders for three-dimensional printing of tissue engineering scaffolds, Acta Biomater. 8(1) (2012) 373-385.
[659]L. Fiocco, B. Michielsen, E. Bernardo, Silica-bonded apatite scaffolds from calcite-filled preceramic polymers, J. Eur. Ceram. Soc. 36(13) (2016) 3211-3218.
[660]J.-S. Lee, Y.-J. Seol, M. Sung, W. Moon, S.W. Kim, J.-H. Oh, D.-W. Cho, Development and analysis of three-dimensional (3D) printed biomimetic ceramic, International Journal of Precision Engineering and Manufacturing 17(12) (2016) 1711-1719.
[661]S. Lei, M.C. Frank, D.D. Anderson, T.D. Brown, A method to represent heterogeneous materials for rapid prototyping: the Matryoshka approach, Rapid Prototyping Journal (2014).
[662]P. Miranda, A. Pajares, E. Saiz, A.P. Tomsia, F. Guiberteau, Mechanical properties of calcium phosphate scaffolds fabricated by robocasting, Journal of Biomedical Materials Research Part A: An Official Journal of The Society for Biomaterials, The Japanese Society for Biomaterials, and The Australian Society for Biomaterials and the Korean Society for Biomaterials 85(1) (2008) 218-227.
[663]H. Seitz, W. Rieder, S. Irsen, B. Leukers, C. Tille, Three-dimensional printing of porous ceramic scaffolds for bone tissue engineering, Journal of Biomedical Materials Research Part B: Applied Biomaterials: An Official Journal of The Society for Biomaterials, The Japanese Society for Biomaterials, and The Australian Society for Biomaterials and the Korean Society for Biomaterials 74(2) (2005) 782-788.
[664]S. Tarafder, V.K. Balla, N.M. Davies, A. Bandyopadhyay, S. Bose, Microwave-sintered 3D printed tricalcium phosphate scaffolds for bone tissue engineering, J. Tissue Eng. Regen. Med. 7(8) (2013) 631-641.
[665]S. Tarafder, N.M. Davies, A. Bandyopadhyay, S. Bose, 3D printed tricalcium phosphate bone tissue engineering scaffolds: effect of SrO and MgO doping on in vivo osteogenesis in a rat distal femoral defect model, Biomaterials Science 1(12) (2013) 1250-1259.
[666]E. Vorndran, M. Klarner, U. Klammert, L.M. Grover, S. Patel, J.E. Barralet, U. Gbureck, 3D powder printing of β-tricalcium phosphate ceramics using different strategies, Adv. Eng. Mater. 10(12) (2008) B67-B71.
[667]H. Wang, G. Wu, J. Zhang, K. Zhou, B. Yin, X. Su, G. Qiu, G. Yang, X. Zhang, G. Zhou, Osteogenic effect of controlled released rhBMP-2 in 3D printed porous hydroxyapatite scaffold, Colloids Surf. B. Biointerfaces 141 (2016) 491-498.
[668]P.H. Warnke, H. Seitz, F. Warnke, S.T. Becker, S. Sivananthan, E. Sherry, Q. Liu, J. Wiltfang, T. Douglas, Ceramic scaffolds produced by computer-assisted 3D printing and sintering: Characterization and biocompatibility investigations, Journal of Biomedical Materials Research Part B: Applied Biomaterials: An Official Journal of The Society for Biomaterials, The Japanese Society for Biomaterials, and The Australian Society for Biomaterials and the Korean Society for Biomaterials 93(1) (2010) 212-217.
[669]E. Bernardo, L. Fiocco, G. Parcianello, E. Storti, P. Colombo, Advanced ceramics from preceramic polymers modified at the nano-scale: A review, Materials 7(3) (2014) 1927-1956.
[670]Z.C. Eckel, C. Zhou, J.H. Martin, A.J. Jacobsen, W.B. Carter, T.A. Schaedler, Additive manufacturing of polymer-derived ceramics, Science 351(6268) (2016) 58-62.
[671]H. Elsayed, P. Colombo, E. Bernardo, Direct ink writing of wollastonite-diopside glass-ceramic scaffolds from a silicone resin and engineered fillers, J. Eur. Ceram. Soc. 37(13) (2017) 4187-4195.
[672]H. Shao, X. Ke, A. Liu, M. Sun, Y. He, X. Yang, J. Fu, Y. Liu, L. Zhang, G. Yang, Bone regeneration in 3D printing bioactive ceramic scaffolds with improved tissue/material interface pore architecture in thin-wall bone defect, Biofabrication 9(2) (2017) 025003.

[673]J. Xie, H. Shao, D. He, X. Yang, C. Yao, J. Ye, Y. He, J. Fu, Z. Gou, Ultrahigh strength of three-dimensional printed diluted magnesium doping wollastonite porous scaffolds, Mrs Communications 5(4) (2015) 631-639.

[674]A. Zocca, H. Elsayed, E. Bernardo, C. Gomes, M. Lopez-Heredia, C. Knabe, P. Colombo, J. Günster, 3D-printed silicate porous bioceramics using a non-sacrificial preceramic polymer binder, Biofabrication 7(2) (2015) 025008.

[675]S. Cao, X.-F. Wei, Z.-J. Sun, H.-H. Zhang, Investigation on urea-formaldehyde resin as an in-powder adhesive for the fabrication of Al2O3/borosilicate–glass composite parts by three dimensional printing (3DP), J. Mater. Process. Technol. 217 (2015) 241-252.

[676]M. Faes, J. Vleugels, F. Vogeler, E. Ferraris, Extrusion-based additive manufacturing of ZrO2 using photoinitiated polymerization, CIRP Journal of Manufacturing Science and Technology 14 (2016) 28-34.

[677]E. Feilden, E.G.-T. Blanca, F. Giuliani, E. Saiz, L. Vandeperre, Robocasting of structural ceramic parts with hydrogel inks, J. Eur. Ceram. Soc. 36(10) (2016) 2525-2533.

[678]Y.-y. Li, L.-t. Li, B. Li, Direct write printing of three-dimensional ZrO2 biological scaffolds, Materials & Design 72 (2015) 16-20.

[679]F.-H. Liu, C.-Y. Lin, Y.-H. Liu, Y.-S. Liao, A Study on the Manufacturing of Through-Hole Al2O3 Scaffolds with Ceramic Powders in Different Grain Diameters, International Journal of Engineering and Technology 7(1) (2015) 55.

[680]H. Shao, D. Zhao, T. Lin, J. He, J. Wu, 3D gel-printing of zirconia ceramic parts, Ceram. Int. 43(16) (2017) 13938-13942.

[681]W. Zhang, R. Melcher, N. Travitzky, R.K. Bordia, P. Greil, Three-dimensional printing of complex-shaped alumina/glass composites, Adv. Eng. Mater. 11(12) (2009) 1039-1043.

[682]H. Zhao, C. Ye, Z. Fan, C. Wang, 3D printing of CaO-based ceramic core using nanozirconia suspension as a binder, J. Eur. Ceram. Soc. 37(15) (2017) 5119-5125.

[683]R. Detsch, S. Schaefer, U. Deisinger, G. Ziegler, H. Seitz, B. Leukers, In vitro-osteoclastic activity studies on surfaces of 3D printed calcium phosphate scaffolds, J. Biomater. Appl. 26(3) (2011) 359-380.

[684]C. Bergmann, M. Lindner, W. Zhang, K. Koczur, A. Kirsten, R. Telle, H. Fischer, 3D printing of bone substitute implants using calcium phosphate and bioactive glasses, J. Eur. Ceram. Soc. 30(12) (2010) 2563-2567.

[685]J. Dávila, M. Freitas, P. Inforçatti Neto, Z. Silveira, J. Silva, M. d'Ávila, Fabrication of PCL/β-TCP scaffolds by 3D mini-screw extrusion printing, J. Appl. Polym. Sci. 133(15) (2016).

[686]A. Malayeri, C. Gabbott, G. Reilly, E. Ghassemieh, P. Hatton, F. Claeyssens, Feasibility of 3D printing and stereolithography for fabrication of custom-shaped poly (lactic acid): hydroxyapatite composite biomaterial scaffolds, J. Tissue Eng. Regen. Med., WILEY-BLACKWELL 111 RIVER ST, HOBOKEN 07030-5774, NJ USA, 2012, pp. 367-367.

[687]W. Bian, D. Li, Q. Lian, X. Li, W. Zhang, K. Wang, Z. Jin, Fabrication of a bio-inspired beta-Tricalcium phosphate/collagen scaffold based on ceramic stereolithography and gel casting for osteochondral tissue engineering, Rapid Prototyping Journal (2012).

[688]S. Wüst, M.E. Godla, R. Müller, S. Hofmann, Tunable hydrogel composite with two-step processing in combination with innovative hardware upgrade for cell-based three-dimensional bioprinting, Acta Biomater. 10(2) (2014) 630-640.

[689]J. Weichhold, U. Gbureck, F. Goetz-Neunhoeffer, K. Hurle, Setting mechanism of a CDHA forming α-TCP cement modified with sodium phytate for improved injectability, Materials 12(13) (2019) 2098.

[690]S.V. Dorozhkin, Calcium orthophosphate cements and concretes, Materials 2(1) (2009) 221-291.

[691]S. Pina, J. Ferreira, Injectability of brushite-forming Mg-substituted and Sr-substituted α-TCP bone cements, J. Mater. Sci. Mater. Med. 21(2) (2010) 431-438.

[692]P. Jamshidi, R.H. Bridson, A.J. Wright, L.M. Grover, Brushite cement additives inhibit attachment to cell culture beads, Biotechnology and Bioengineering 110(5) (2013) 1487-1494.

[693]B. Kanter, M. Geffers, A. Ignatius, U. Gbureck, Control of in vivo mineral bone cement degradation, Acta Biomater. 10(7) (2014) 3279-3287.

[694]K. Hurle, J. Weichhold, M. Brueckner, U. Gbureck, T. Brueckner, F. Goetz-Neunhoeffer, Hydration mechanism of a calcium phosphate cement modified with phytic acid, Acta Biomater. 80 (2018) 378-389.

[695]P. Leamy, P. Brown, K. TenHuisen, C. Randall, Fluoride uptake by hydroxyapatite formed by the hydrolysis of α-tricalcium phosphate, Journal of Biomedical Materials Research: An Official Journal of The Society for Biomaterials, The Japanese Society for Biomaterials, and the Australian Society for Biomaterials 42(3) (1998) 458-464.

[696]K. Hurle, J. Neubauer, M. Bohner, N. Doebelin, F. Goetz-Neunhoeffer, Effect of amorphous phases during the hydraulic conversion of α-TCP into calcium-deficient hydroxyapatite, Acta Biomater. 10(9) (2014) 3931-3941.

[697]W.L. Lindsay, Chemical equilibria in soils, John Wiley and Sons Ltd.1979.
[698]D.R. Taves, Similarity of octacalcium phosphate and hydroxyapatite structures, Nature 200(4913) (1963) 1312-1313.
[699]W. Brown, N. Eidelman, B. Tomazic, Octacalcium phosphate as a precursor in biomineral formation, Advances in Dental Research 1(2) (1987) 306-313.
[700]A. Rodrigues, A. Lebugle, Behavior in wet atmosphere of an amorphous calcium phosphate with an atomic Ca/P ratio of 1.33, J. Solid State Chem. 148(2) (1999) 308-315.
[701]O. Suzuki, S. Kamakura, T. Katagiri, M. Nakamura, B. Zhao, Y. Honda, R. Kamijo, Bone formation enhanced by implanted octacalcium phosphate involving conversion into Ca-deficient hydroxyapatite, Biomaterials 27(13) (2006) 2671-2681.
[702]K. Hurle, T. Christel, U. Gbureck, C. Moseke, J. Neubauer, F. Goetz-Neunhoeffer, Reaction kinetics of dual setting α-tricalcium phosphate cements, J. Mater. Sci. Mater. Med. 27(1) (2016) 1.
[703]T. Konishi, M. Mizumoto, M. Honda, Y. Horiguchi, K. Oribe, H. Morisue, K. Ishii, Y. Toyama, M. Matsumoto, M. Aizawa, Fabrication of novel biodegradable α-tricalcium phosphate cement set by chelating capability of inositol phosphate and its biocompatibility, Journal of Nanomaterials 2013 (2013) 4.
[704]E. Graf, J.W. Eaton, Antioxidant functions of phytic acid, Free Radical Biology and Medicine 8(1) (1990) 61-69.
[705]I. Ajaxon, C. Öhman, C. Persson, Long-term in vitro degradation of a high-strength brushite cement in water, PBS, and serum solution, BioMed Research International 2015 (2015).
[706]F. Tamimi, Z. Sheikh, J. Barralet, Dicalcium phosphate cements: Brushite and monetite, Acta Biomater. 8(2) (2012) 474-487.
[707]Z. Sheikh, M. Geffers, T. Christel, J.E. Barralet, U. Gbureck, Chelate setting of alkali ion substituted calcium phosphates, Ceram. Int. 41(8) (2015) 10010-10017.
[708]M. Hofmann, A. Mohammed, Y. Perrie, U. Gbureck, J. Barralet, High-strength resorbable brushite bone cement with controlled drug-releasing capabilities, Acta Biomater. 5(1) (2009) 43-49.
[709]L.M. Grover, U. Gbureck, A.J. Wright, J.E. Barralet, Cement formulations in the calcium phosphate H2O–H3PO4–H4P2O7 system, J. Am. Ceram. Soc. 88(11) (2005) 3096-3103.
[710]C. Oliveira, A. Ferreira, F. Rocha, Dicalcium phosphate dihydrate precipitation: characterization and crystal growth, Chem. Eng. Res. Des. 85(12) (2007) 1655-1661.
[711]T. Christel, S. Christ, J.E. Barralet, J. Groll, U. Gbureck, Chelate bonding mechanism in a novel magnesium phosphate bone cement, J. Am. Ceram. Soc. 98(3) (2015) 694-697.
[712]P.W. Atkins, J. De Paula, Physical chemistry, Oxford university press, Oxford UK1998.
[713]P.A.H. Wyatt, A thermodynamic bypass goto log k, CRC Press1982.
[714]M. Bohner, H. Merkle, t.J. Lemai, In vitro aging of a calcium phosphate cement, J. Mater. Sci. Mater. Med. 11(3) (2000) 155-162.
[715]I. Ajaxon, C. Persson, Mechanical properties of brushite calcium phosphate cements, (2017).
[716]J. Weichhold, F. Goetz-Neunhoeffer, K. Hurle, U. Gbureck, Pyrophosphate ions inhibit calcium phosphate cement reaction and enable storage of premixed pastes with a controlled activation by orthophosphate addition, Ceram. Int. 48(11) (2022) 15390-15404.
[717]S. Heinemann, S. Rössler, M. Lemm, M. Ruhnow, B. Nies, Properties of injectable ready-to-use calcium phosphate cement based on water-immiscible liquid, Acta Biomater. 9(4) (2013) 6199-6207.
[718]E. Ooms, J. Wolke, J. Van Der Waerden, J. Jansen, Trabecular bone response to injectable calcium phosphate (Ca-P) cement, Journal of Biomedical Materials Research: An Official Journal of The Society for Biomaterials, The Japanese Society for Biomaterials, and The Australian Society for Biomaterials and the Korean Society for Biomaterials 61(1) (2002) 9-18.
[719]M.-P. Ginebra, E. Fernandez, E. De Maeyer, R. Verbeeck, M. Boltong, J. Ginebra, F. Driessens, J. Planell, Setting reaction and hardening of an apatitic calcium phosphate cement, J. Dent. Res. 76(4) (1997) 905-912.
[720]H. Monma, Effect of additives on hydration and hardening of tricalcium phosphate, Gypsum and lime 188 (1984) 11-16.
[721]M. Bohner, H. Tiainen, P. Michel, N. Döbelin, Design of an inorganic dual-paste apatite cement using cation exchange, J. Mater. Sci. Mater. Med. 26(2) (2015) 63.
[722]Z. Pan, Y. Wang, Q. Wei, X. Chen, F. Jiao, W. Qin, Effect of sodium pyrophosphate on the flotation separation of calcite from apatite, Sep. Purif. Technol. 242 (2020) 116408.
[723]W. Qin, Q. Wei, F. Jiao, N. Li, P. Wang, L. Ke, Effect of sodium pyrophosphate on the flotation separation of chalcopyrite from galena, International Journal of Mining Science and Technology 22(3) (2012) 345-349.
[724]L. Changgen, L. Yongxin, Selective flotation of scheelite from calcium minerals with sodium oleate as a collector and phosphates as modifiers. II. The mechanism of the interaction between phosphate modifiers and minerals, Int. J. Miner. Process. 10(3) (1983) 219-235.

[725]L.M. Grover, A.J. Wright, U. Gbureck, A. Bolarinwa, J. Song, Y. Liu, D.F. Farrar, G. Howling, J. Rose, J.E. Barralet, The effect of amorphous pyrophosphate on calcium phosphate cement resorption and bone generation, Biomaterials 34(28) (2013) 6631-6637.
[726]P. Van Cappellen, L. Charlet, W. Stumm, P. Wersin, A surface complexation model of the carbonate mineral-aqueous solution interface, Geochim. Cosmochim. Acta 57(15) (1993) 3505-3518.
[727]M. Habib, J.M. Bockris, Specific adsorption of ions, Comprehensive Treatise of Electrochemistry, Springer1980, pp. 135-219.
[728]F. Hingston, R. Atkinson, A. Posner, J. Quirk, Specific adsorption of anions, Nature 215(5109) (1967) 1459-1461.
[729]O. Stern, Zur theorie der elektrolytischen doppelschicht, Zeitschrift für Elektrochemie und angewandte physikalische Chemie 30(21-22) (1924) 508-516.
[730]C. Labbez, A. Nonat, I. Pochard, B. Jönsson, Experimental and theoretical evidence of overcharging of calcium silicate hydrate, Journal of Colloid and Interface Science 309(2) (2007) 303-307.
[731]A. Garg, C.A. Cartier, K.J. Bishop, D. Velegol, Particle zeta potentials remain finite in saturated salt solutions, Langmuir 32(45) (2016) 11837-11844.
[732]M. Neuman, W. Neuman, F. Burton, On the possible role of crystals in the origins of life, II. The adsorption of Amino Acids by apatite crystals, Biosystems 3(1) (1969) 69-73.
[733]J. Christoffersen, M.R. Christoffersen, Kinetics of dissolution of calcium hydroxyapatite: IV. The effect of some biologically important inhibitors, J. Cryst. Growth 53(1) (1981) 42-54.
[734]Y. Chen, Q. Feng, G. Zhang, D. Liu, R. Liu, Effect of sodium pyrophosphate on the reverse flotation of dolomite from apatite, Minerals 8(7) (2018) 278.
[735]K. Hurle, J. Neubauer, M. Bohner, N. Doebelin, F. Goetz-Neunhoeffer, Calorimetry investigations of milled α-tricalcium phosphate (α-TCP) powders to determine the formation enthalpies of α-TCP and X-ray amorphous tricalcium phosphate, Acta Biomater. 23 (2015) 338-346.
[736]X. Chen, S. Wu, J. Zhou, Influence of porosity on compressive and tensile strength of cement mortar, Construction and Building Materials 40 (2013) 869-874.
[737]D.-M. Liu, Influence of porosity and pore size on the compressive strength of porous hydroxyapatite ceramic, Ceram. Int. 23(2) (1997) 135-139.
[738]M. Pfeiffle, Fabrikation und Optimierung von lagerstabilen, wasserbasierten Zementformulierungen aus α-TCP und Hyaluronsäure zur Herstellung von dreidimensionalen Scaffolds als Knochenersatzmaterial via 3d-Extrusionsdruck, Fakultät für Chemie und Pharmazie, Julius-Maximilians-Universität Würzburg, 2021.
[739]V. Steinacker, Analyse der Biokompatibilität von Calzium- und Magnesiumphosphatzement mit verschiedenen Additiva, Julius-Maximilians-Universität Würzburg, not yet published.
[740]K. Chatterjee, T.K. Ghosh, 3D printing of textiles: potential roadmap to printing with fibers, Adv. Mater. 32(4) (2020) 1902086.
[741]S. Ford, T. Minshall, Invited review article: Where and how 3D printing is used in teaching and education, Additive Manufacturing 25 (2019) 131-150.
[742]W. Gao, Y. Zhang, D. Ramanujan, K. Ramani, Y. Chen, C.B. Williams, C.C. Wang, Y.C. Shin, S. Zhang, P.D. Zavattieri, The status, challenges, and future of additive manufacturing in engineering, Computer-Aided Design 69 (2015) 65-89.
[743]P. Li, Y. Zhang, Z. Zheng, Polymer-assisted metal deposition (PAMD) for flexible and wearable electronics: principle, materials, printing, and devices, Adv. Mater. 31(37) (2019) 1902987.
[744]F.P. Melchels, M.A. Domingos, T.J. Klein, J. Malda, P.J. Bartolo, D.W. Hutmacher, Additive manufacturing of tissues and organs, Prog. Polym. Sci. 37(8) (2012) 1079-1104.
[745]N. Nachal, J. Moses, P. Karthik, C. Anandharamakrishnan, Applications of 3D printing in food processing, Food Engineering Reviews 11(3) (2019) 123-141.
[746]T.D. Ngo, A. Kashani, G. Imbalzano, K.T. Nguyen, D. Hui, Additive manufacturing (3D printing): A review of materials, methods, applications and challenges, Composites Part B: Engineering 143 (2018) 172-196.
[747]E. Abelseth, L. Abelseth, L. De la Vega, S.T. Beyer, S.J. Wadsworth, S.M. Willerth, 3D printing of neural tissues derived from human induced pluripotent stem cells using a fibrin-based bioink, ACS Biomaterials Science & Engineering 5(1) (2018) 234-243.
[748]L.E. Bertassoni, J.C. Cardoso, V. Manoharan, A.L. Cristino, N.S. Bhise, W.A. Araujo, P. Zorlutuna, N.E. Vrana, A.M. Ghaemmaghami, M.R. Dokmeci, Direct-write bioprinting of cell-laden methacrylated gelatin hydrogels, Biofabrication 6(2) (2014) 024105.
[749]T. Billiet, E. Gevaert, T. De Schryver, M. Cornelissen, P. Dubruel, The 3D printing of gelatin methacrylamide cell-laden tissue-engineered constructs with high cell viability, Biomaterials 35(1) (2014) 49-62.

[750]T.T. Demirtaş, G. Irmak, M. Gümüşderelioğlu, A bioprintable form of chitosan hydrogel for bone tissue engineering, Biofabrication 9(3) (2017) 035003.
[751]N. Diamantides, C. Dugopolski, E. Blahut, S. Kennedy, L.J. Bonassar, High density cell seeding affects the rheology and printability of collagen bioinks, Biofabrication 11(4) (2019) 045016.
[752]R. Gaetani, D.A. Feyen, V. Verhage, R. Slaats, E. Messina, K.L. Christman, A. Giacomello, P.A. Doevendans, J.P. Sluijter, Epicardial application of cardiac progenitor cells in a 3D-printed gelatin/hyaluronic acid patch preserves cardiac function after myocardial infarction, Biomaterials 61 (2015) 339-348.
[753]G. Griffanti, E. Rezabeigi, J. Li, M. Murshed, S.N. Nazhat, Rapid biofabrication of printable dense collagen bioinks of tunable properties, Adv. Funct. Mater. 30(4) (2020) 1903874.
[754]J. Jia, D.J. Richards, S. Pollard, Y. Tan, J. Rodriguez, R.P. Visconti, T.C. Trusk, M.J. Yost, H. Yao, R.R. Markwald, Engineering alginate as bioink for bioprinting, Acta Biomater. 10(10) (2014) 4323-4331.
[755]N.C. Negrini, N. Celikkin, P. Tarsini, S. Farè, W. Święszkowski, Three-dimensional printing of chemically crosslinked gelatin hydrogels for adipose tissue engineering, Biofabrication 12(2) (2020) 025001.
[756]D. Petta, U. D'amora, L. Ambrosio, D. Grijpma, D. Eglin, M. D'este, Hyaluronic acid as a bioink for extrusion-based 3D printing, Biofabrication 12(3) (2020) 032001.
[757]P. Rastogi, B. Kandasubramanian, Review of alginate-based hydrogel bioprinting for application in tissue engineering, Biofabrication 11(4) (2019) 042001.
[758]A.G. Tabriz, M.A. Hermida, N.R. Leslie, W. Shu, Three-dimensional bioprinting of complex cell laden alginate hydrogel structures, Biofabrication 7(4) (2015) 045012.
[759]Q. Wang, Q. Xia, Y. Wu, X. Zhang, F. Wen, X. Chen, S. Zhang, B.C. Heng, Y. He, H.W. Ouyang, 3D-printed atsttrin-incorporated alginate/hydroxyapatite scaffold promotes bone defect regeneration with TNF/TNFR signaling involvement, Advanced Healthcare Materials 4(11) (2015) 1701-1708.
[760]Q. Wu, D. Therriault, M.-C. Heuzey, Processing and properties of chitosan inks for 3D printing of hydrogel microstructures, ACS Biomaterials Science & Engineering 4(7) (2018) 2643-2652.
[761]M. Yeo, J.-S. Lee, W. Chun, G.H. Kim, An innovative collagen-based cell-printing method for obtaining human adipose stem cell-laden structures consisting of core–sheath structures for tissue engineering, Biomacromolecules 17(4) (2016) 1365-1375.
[762]J.P. Armstrong, M. Burke, B.M. Carter, S.A. Davis, A.W. Perriman, 3D bioprinting using a templated porous bioink, Advanced Healthcare Materials 5(14) (2016) 1724-1730.
[763]A. Chiappone, E. Fantino, I. Roppolo, M. Lorusso, D. Manfredi, P. Fino, C.F. Pirri, F. Calignano, 3D printed PEG-based hybrid nanocomposites obtained by sol–gel technique, ACS applied materials & interfaces 8(8) (2016) 5627-5633.
[764]G. Gao, T. Yonezawa, K. Hubbell, G. Dai, X. Cui, Inkjet-bioprinted acrylated peptides and PEG hydrogel with human mesenchymal stem cells promote robust bone and cartilage formation with minimal printhead clogging, Biotechnol. J. 10(10) (2015) 1568-1577.
[765]A. Grémare, V. Guduric, R. Bareille, V. Heroguez, S. Latour, N. L'heureux, J.C. Fricain, S. Catros, D. Le Nihouannen, Characterization of printed PLA scaffolds for bone tissue engineering, Journal of Biomedical Materials Research Part A 106(4) (2018) 887-894.
[766]M. Hospodiuk, M. Dey, D. Sosnoski, I.T. Ozbolat, The bioink: A comprehensive review on bioprintable materials, Biotechnol. Adv. 35(2) (2017) 217-239.
[767]J. Lee, S. Chae, H. Lee, G.H. Kim, A 3D printing strategy for fabricating in situ topographical scaffolds using pluronic F-127, Additive Manufacturing 32 (2020) 101023.
[768]A.D. Olubamiji, Z. Izadifar, J.L. Si, D.M. Cooper, B.F. Eames, D.X. Chen, Modulating mechanical behaviour of 3D-printed cartilage-mimetic PCL scaffolds: influence of molecular weight and pore geometry, Biofabrication 8(2) (2016) 025020.
[769]H. Seo, S.G. Heo, H. Lee, H. Yoon, Preparation of PEG materials for constructing complex structures by stereolithographic 3D printing, RSC advances 7(46) (2017) 28684-28688.
[770]L. Shor, S. Güçeri, R. Chang, J. Gordon, Q. Kang, L. Hartsock, Y. An, W. Sun, Precision extruding deposition (PED) fabrication of polycaprolactone (PCL) scaffolds for bone tissue engineering, Biofabrication 1(1) (2009) 015003.
[771]P. Wang, B. Zou, H. Xiao, S. Ding, C. Huang, Effects of printing parameters of fused deposition modeling on mechanical properties, surface quality, and microstructure of PEEK, J. Mater. Process. Technol. 271 (2019) 62-74.
[772]J. Won, C. Park, J. Bae, G. Ahn, C. Kim, D. Lim, D. Cho, W. Yun, J. Shim, J. Huh, Evaluation of 3D printed PCL/PLGA/β-TCP versus collagen membranes for guided bone regeneration in a beagle implant model, Biomedical Materials 11(5) (2016) 055013.
[773]S. Xin, D. Chimene, J.E. Garza, A.K. Gaharwar, D.L. Alge, Clickable PEG hydrogel microspheres as building blocks for 3D bioprinting, Biomaterials Science 7(3) (2019) 1179-1187.

[774]C. Yang, X. Tian, D. Li, Y. Cao, F. Zhao, C. Shi, Influence of thermal processing conditions in 3D printing on the crystallinity and mechanical properties of PEEK material, J. Mater. Process. Technol. 248 (2017) 1-7.
[775]K. Zhang, Q. Fu, J. Yoo, X. Chen, P. Chandra, X. Mo, L. Song, A. Atala, W. Zhao, 3D bioprinting of urethra with PCL/PLCL blend and dual autologous cells in fibrin hydrogel: An in vitro evaluation of biomimetic mechanical property and cell growth environment, Acta Biomater. 50 (2017) 154-164.
[776]G. Brunello, S. Sivolella, R. Meneghello, L. Ferroni, C. Gardin, A. Piattelli, B. Zavan, E. Bressan, Powder-based 3D printing for bone tissue engineering, Biotechnol. Adv. 34(5) (2016) 740-753.
[777]B. Zhang, X. Pei, P. Song, H. Sun, H. Li, Y. Fan, Q. Jiang, C. Zhou, X. Zhang, Porous bioceramics produced by inkjet 3D printing: effect of printing ink formulation on the ceramic macro and micro porous architectures control, Composites Part B: Engineering 155 (2018) 112-121.
[778]J. Babilotte, V. Guduric, D. Le Nihouannen, A. Naveau, J.C. Fricain, S. Catros, 3D printed polymer–mineral composite biomaterials for bone tissue engineering: fabrication and characterization, Journal of Biomedical Materials Research Part B: Applied Biomaterials 107(8) (2019) 2579-2595.
[779]N. Beheshtizadeh, M. Azami, H. Abbasi, A. Farzin, Applying extrusion-based 3D printing technique accelerates fabricating complex biphasic calcium phosphate-based scaffolds for bone tissue regeneration, Journal of Advanced Research (2021).
[780]Z. Ding, X. Wang, J. Sanjayan, P.X. Zou, Z.-K. Ding, A feasibility study on HPMC-improved sulphoaluminate cement for 3D printing, Materials 11(12) (2018) 2415.
[781]C. Kelder, A.D. Bakker, J. Klein-Nulend, D. Wismeijer, The 3D printing of calcium phosphate with K-carrageenan under conditions permitting the incorporation of biological components—a method, Journal of Functional Biomaterials 9(4) (2018) 57.
[782]R. Trombetta, J.A. Inzana, E.M. Schwarz, S.L. Kates, H.A. Awad, 3D printing of calcium phosphate ceramics for bone tissue engineering and drug delivery, Ann. Biomed. Eng. 45(1) (2017) 23-44.
[783]D. Jansen, C. Stabler, F. Goetz-Neunhoeffer, S. Dittrich, J. Neubauer, Does Ordinary Portland Cement contain amorphous phase? A quantitative study using an external standard method, Powder Diffr. 26(1) (2011) 31-38.
[784]M. Yashima, A. Sakai, High-temperature neutron powder diffraction study of the structural phase transition between α and α' phases in tricalcium phosphate Ca3 (PO4) 2, Chem. Phys. Lett. 372(5-6) (2003) 779-783.
[785]M. Yashima, A. Sakai, T. Kamiyama, A. Hoshikawa, Crystal structure analysis of β-tricalcium phosphate Ca3 (PO4) 2 by neutron powder diffraction, J. Solid State Chem. 175(2) (2003) 272-277.
[786]K. Sudarsanan, R. Young, Significant precision in crystal structural details. Holly Springs hydroxyapatite, Acta Crystallographica Section B: Structural Crystallography and Crystal Chemistry 25(8) (1969) 1534-1543.
[787]D. Ectors, F. Goetz-Neunhoeffer, J. Neubauer, A generalized geometric approach to anisotropic peak broadening due to domain morphology, J. Appl. Crystallogr. 48(1) (2015) 189-194.
[788]C. Calvo, Crystal structure of. alpha.-calcium pyrophosphate, Inorganic Chemistry 7(7) (1968) 1345-1351.
[789]L. Schroeder, E. Prince, B. Dickens, Hydrogen bonding in Ca (H2PO4) 2. H2O as determined by neutron diffraction, Acta Crystallographica Section B: Structural Crystallography and Crystal Chemistry 31(1) (1975) 9-12.
[790]M. Catti, G. Ferraris, A. Filhol, Hydrogen bonding in the crystalline state. CaHPO4 (monetite), P\overline {1} or P1? A novel neutron diffraction study, Acta Crystallographica Section B: Structural Crystallography and Crystal Chemistry 33(4) (1977) 1223-1229.
[791]P.E. International Union for Crystallography, International Tables for Crystallography, Volume C. Mathematical Physical and Chemical Tables, third edition, Wiley, 2004.
[792]S. Bergold, F. Goetz-Neunhoeffer, J. Neubauer, Mechanically activated alite: New insights into alite hydration, Cem. Concr. Res. 76 (2015) 202-211.
[793]M. Mathew, W. Brown, L. Schroeder, B. Dickens, Crystal structure of octacalcium bis (hydrogenphosphate) tetrakis (phosphate) pentahydrate, Ca 8 (HP0 4) 2 (PO 4) 4· 5H 2 O, Journal of Crystallographic and Spectroscopic Research 18(3) (1988) 235-250.
[794]S. Bergold, F. Goetz-Neunhoeffer, J. Neubauer, Quantitative analysis of C-S-H in hydrating alite pastes by in-situ XRD, Cem. Concr. Res. 53 (2013) 119-126.
[795]S. Bergold, F. Goetz-Neunhoeffer, J. Neubauer, Quantitative analysis of C–S–H in hydrating alite pastes by in-situ XRD, Cem. Concr. Res. 53 (2013) 119-126.
[796]D. Ectors, F. Goetz-Neunhoeffer, W.-D. Hergeth, U. Dietrich, J. Neubauer, In situ H-1-TD-NMR: Quantification and microstructure development during the early hydration of alite and OPC, Cem. Concr. Res. 79 (2016) 366-372.

[797]G. Berger, C. Ullner, G. Neumann, H. Marx, New characterization of setting times of alkali containing calcium phosphate cements by using an automatically working device according to Gillmore needle test, Key Eng. Mater., Trans Tech Publ, 2006, pp. 825-828.
[798]E.W. Washburn, Note on a method of determining the distribution of pore sizes in a porous material, Proceedings of the National Academy of Sciences of the United States of America 7(4) (1921) 115.
[799]C. Böhm, P. Stahlhut, J. Weichhold, A. Hrynevich, J. Teßmar, P.D. Dalton, The Multiweek Thermal Stability of Medical-Grade Poly (ε-caprolactone) During Melt Electrowriting, Small 18(3) (2022) 2104193.
[800]A. Seifert, J. Groll, J. Weichhold, A.V. Boehm, F.A. Müller, U. Gbureck, Phase Conversion of Ice-Templated α-Tricalcium Phosphate Scaffolds into Low-Temperature Calcium Phosphates with Anisotropic Open Porosity, Adv. Eng. Mater. 23(5) (2021) 2001417.
[801]F. Kaiser, L. Schröter, S. Stein, B. Krüger, J. Weichhold, P. Stahlhut, A. Ignatius, U. Gbureck, Accelerated bone regeneration through rational design of magnesium phosphate cements, Acta Biomater. (2022).
[802]C. Blum, J. Weichhold, G. Hochleitner, V. Stepanenko, F. Würthner, J. Groll, T. Jungst, Controlling Topography and Crystallinity of Melt Electrowritten Poly (ε-Caprolactone) Fibers, 3D Printing and Additive Manufacturing (2021).
[803]J. Kade, B. Tandon, J. Weichhold, D. Pisignano, L. Persano, R. Luxenhofer, P. Dalton, Melt Electrowriting of Poly (vinylidene fluoride-co-trifluoroethylene), (2021).
[804]I. Holzmeister, J. Weichhold, J. Groll, H. Zreiqat, U. Gbureck, Hydraulic reactivity and cement formation of baghdadite, J. Am. Ceram. Soc. 104(7) (2021) 3554-3561.